

Immunoregulatory function for the autophagy protein ATG16L1 in myeloid cells

Dissertation
zur Erlangung des Doktorgrades
der Mathematisch-Naturwissenschaftlichen Fakultät
der Christian-Albrechts-Universität zu Kiel

vorgelegt von

Anne Luzius

2016
Kiel, Deutschland

1st Examiner: Prof. Dr. Philip Rosenstiel

2nd Examiner: Prof. Dr. Thomas Roeder

Date of oral examination: 20. Juli 2016

Approved for print on: 20. Juli 2016

Approved by: gez. Prof. Dr. Wolfgang J. Duschl

Parts of this dissertation are contained in the following manuscript:

Anne Luzius, Maren Falk-Paulsen, Jan W. P. Kuiper, Stamatia Papoutsopoulou, Hang Thi Thu Nguyen, Marlene Jentsch, Robert Häsler, Nicolas Gisch, Wolfram Klapper, Stefan Schreiber, Nicolas Barnich, Werner Müller, Philip Rosenstiel.

Autophagy is a critical mechanism for temporal control of NF- κ B signaling in myeloid cells.

TABLE OF CONTENT

Table of content	5
1 Introduction	9
1.1 Autophagy – a bulk degradation pathway.....	9
1.2 Macroautophagy.....	10
1.2.1 The molecular core machinery.....	10
1.2.2 Selective autophagy by specific cargo receptors.....	12
1.2.3 Autophagy and its physiological functions.....	12
1.3 The autophagy protein ATG16L1.....	13
1.3.1 Role of ATG16L1 in immune responses.....	14
1.4 Inflammation.....	15
1.4.1 Sepsis.....	16
1.5 Myeloid cells - the first line of defense.....	17
1.5.1 Neutrophils.....	18
1.5.2 Monocytes and macrophages.....	19
1.6 Toll-like receptors in innate immune responses.....	20
1.6.1 Toll-like receptor 4 (TLR4) signaling.....	23
1.6.2 Negative regulation of TLR4 signaling.....	24
2 Aims of the study	26
3 Material and Methods	27
3.1 Material.....	27
3.2 Methods.....	27
3.2.1 Animal-Housing.....	27
3.2.2 Generation of <i>Atg16l1</i> conditional knock-out mice.....	27
3.2.3 Genotyping of <i>Atg16l1LysM</i> mice.....	28
3.2.4 Animal experiments.....	30
3.2.4.1 Anakinra therapy.....	30
3.2.4.2 Sublethal Endotoxin-induced sepsis.....	30
3.2.4.3 Antibiotic treatment.....	30
3.2.4.4 Preventive antibiotic treatment.....	31
3.2.5 Bacterial DNA extraction from mouse feces.....	31
3.2.6 16SrDNA sequencing for bacterial identification.....	31
3.2.7 Sequence analysis for taxonomic classification of identified bacteria.....	32
3.2.8 Isolation and cultivation of cells.....	33
3.2.8.1 Isolation of lamina propria and intestinal epithelial fractions from the small intestine.....	33
3.2.8.2 Magnetic-activated cell sorting (MACS) for isolation of CD11b ⁺ cells derived from the lamina propria.....	33
3.2.8.3 Isolation and differentiation of bone marrow-derived macrophages.....	34

3.2.8.4	MACS for isolation of hematopoietic stem cells from spleen.....	34
3.2.9	Protein extraction and protein assay	34
3.2.10	Sodium dodecyl sulfate polyacrylamide gel electrophoresis	35
3.2.11	Western blot and protein detection.....	35
3.2.12	Total RNA isolation	37
3.2.13	Reverse transcription (RT)-PCR.....	38
3.2.14	Semi-quantitative end-point PCR.....	38
3.2.15	Quantitative real-time PCR (qPCR)	39
3.2.16	Immunofluorescence.....	41
3.2.17	Immunohistochemistry.....	41
3.2.17.1	Tissue processing.....	41
3.2.17.2	Hematoxylin and eosin (H&E) staining.....	41
3.2.17.3	3,3'-Diaminobenzidine (DAB) staining.....	42
3.2.17.4	Terminal deoxynucleotidyl transferase dUTP nick end labeling (TUNEL).....	42
3.2.18	Immunoassays	43
3.2.18.1	Enzyme linked immunosorbent assay (ELISA)	43
3.2.18.2	Multiplex technology	43
3.2.19	Flow cytometry Analysis	43
3.2.19.1	Flow cytometry analysis of tissue and macrophages.....	45
3.2.19.2	Flow cytometry analysis of blood.....	46
3.2.19.3	FITC-Dextran Endocytosis assay	46
3.2.19.4	Receptor internalization assay	46
3.2.20	Statistical analysis	46
4	Results	47
4.1	Proof of the tissue-specific ATG16L1 deletion in <i>Atg16l1LysM</i> mice.....	47
4.1.1	CD11b ⁺ lamina propria cells.....	47
4.1.2	Bone marrow-derived macrophages (BMDMs).....	47
4.2	Loss of <i>Atg16l1</i> leads to impaired autophagy in bone marrow-derived macrophages.....	49
4.3	Characterization of the <i>Atg16l1LysM</i> mouse model	50
4.3.1	<i>Atg16l1LysM</i> mice develop a multifaceted spontaneous phenotype.....	50
4.3.2	Increased extramedullary hematopoiesis in the spleen of <i>Atg16l1LysM</i> mice ..	53
4.3.3	Loss of <i>Atg16l1</i> in myeloid cells alters composition of splenocytes.....	55
4.3.4	Myeloid derived-suppressor cell (MDSC)-like phenotype in the spleen of <i>Atg16l1LysM</i> mice	57
4.3.5	Expression of cytokines in the spleen of <i>Atg16l1LysM</i> mice.....	58
4.3.6	Splenic phenotype of <i>Atg16l1LysM</i> mice is not driven by bacterial invasion	59
4.3.7	Enhanced protein level of pro-IL1 β but not TLR4 components in the spleen of <i>Atg16l1LysM</i> mice	60
4.3.8	Expression of inflammasome components in the spleen of <i>Atg16l1LysM</i> mice.....	60
4.3.9	Myeloid cell infiltration affects multiple organs but not the brain of <i>Atg16l1LysM</i> mice	61

4.3.10	Neutrophilia in the blood of <i>Atg16l1LysM</i> mice	63
4.3.11	Cytokine levels in untreated <i>Atg16l1LysM</i> mice	64
4.4	Impact of IL1R inhibition on the basal phenotype of <i>Atg16l1LysM</i> mice	65
4.5	Role of ATG16L1 in TLR4 signaling.....	69
4.5.1	Hyper-secretion of cytokines is transcriptionally regulated in LPS-stimulated <i>Atg16l1LysM</i> BMDMs	69
4.5.2	Cytokine expression and secretion is modulated by constitutive NF- κ B and p38 MAPK activation in <i>Atg16l1LysM</i> BMDMs.....	71
4.5.3	Impaired autophagy does not result in accumulation of TLR4 signaling components but p62	74
4.5.4	<i>Atg16l1</i> -deficient macrophages display an intact endocytotic machinery	76
4.5.5	<i>Atg16l1</i> deficiency influences protein levels of the TLR4 negative regulator A20 but not CYLD upon LPS stimulation	78
4.5.6	Reactive oxygen species amplify but do not cause LPS-induced hyper-activation in <i>Atg16l1LysM</i> BMDMs	80
4.5.7	Constitutive NF- κ B activation occurs independent of IL1R signaling in <i>Atg16l1LysM</i> BMDMs	82
4.6	Role of ATG16L1 in TLR4 signaling <i>in vivo</i> using the endotoxin shock model.....	83
4.7	Impact of microbiota on the basal <i>Atg16l1LysM</i> phenotype	84
5	Discussion.....	92
5.1	Characterization of the <i>Atg16l1LysM</i> mouse model	92
5.1.1	Spontaneous systemic inflammation in <i>Atg16l1LysM</i> mice	92
5.1.2	Myeloid-derived suppressor cell-like cell population in <i>Atg16l1LysM</i> mice.....	93
5.1.3	A pivotal role for the commensal microbiota in the development of the inflammatory <i>Atg16l1LysM</i> phenotype	94
5.1.4	Dispensable role for IL1 cytokines in the development of the inflammatory phenotype in <i>Atg16l1LysM</i> mice and BMDMs	96
5.2	Autophagy as a negative regulator of TLR4 signaling	99
5.2.1	Loss of <i>Atg16l1</i> leads to increased TLR4-mediated NF- κ B signaling.....	99
5.2.2	ATG16L1 orchestrates in first line MyD88- but not TRIF-mediated signaling	100
5.2.3	Crosstalk between p38 MAPK and NF- κ B signaling.....	101
5.2.4	The autophagy receptor p62 as a putative central mediator of NF- κ B signaling in autophagy-deficient cells	101
5.2.5	Impaired autophagosomal-lysosomal degradation of A20 is associated with sustained NF- κ B signaling	105
5.3	Future prospects	108
6	Summary.....	110
7	Zusammenfassung.....	112
8	Appendix.....	114
8.1	Buffers and media.....	114
8.2	Kits	115
8.3	Reagents.....	116

8.4	Devices.....	120
8.5	Consumables.....	121
9	References.....	123
10	Supplements.....	146
10.1	List of Abbreviations.....	146
10.2	List of Figures.....	151
10.3	List of Tables.....	154
10.4	Acknowledgement.....	155
10.5	Curriculum Vitae.....	156
10.6	Eidesstattliche Erklärung.....	158

1 INTRODUCTION

1.1 AUTOPHAGY – A BULK DEGRADATION PATHWAY

Even though eukaryotic cells are constantly exposed to changing environmental conditions, a dynamic turnover of protein and organelle synthesis, degradation and recycling enables the maintenance of their cellular homeostasis. To adjust the level of intracellular material, eukaryotic cells developed two major degradation pathways. The ubiquitin-proteasome system controls degradation of cytoplasmic short-lived proteins [1]. In contrast, degradation and recycling of long-term proteins and organelles is regulated by a bulk degradation process called autophagy (Greek: *auto-*, "self" and *phagein*, "to eat") by which the cytosolic cargo is delivered to lysosomes for degradation [2]. Both pathways result in the release of the macromolecular breakdown products back into the cytoplasm in order to restore the cellular homeostasis.

Unlike the ubiquitin-proteasome system, the term autophagy refers to a collection of distinct self-eating processes (Figure 1-1). Based on the molecular pathways, autophagy is classified in three groups: (I) chaperone-mediated autophagy, (II) microautophagy and (III) macroautophagy.

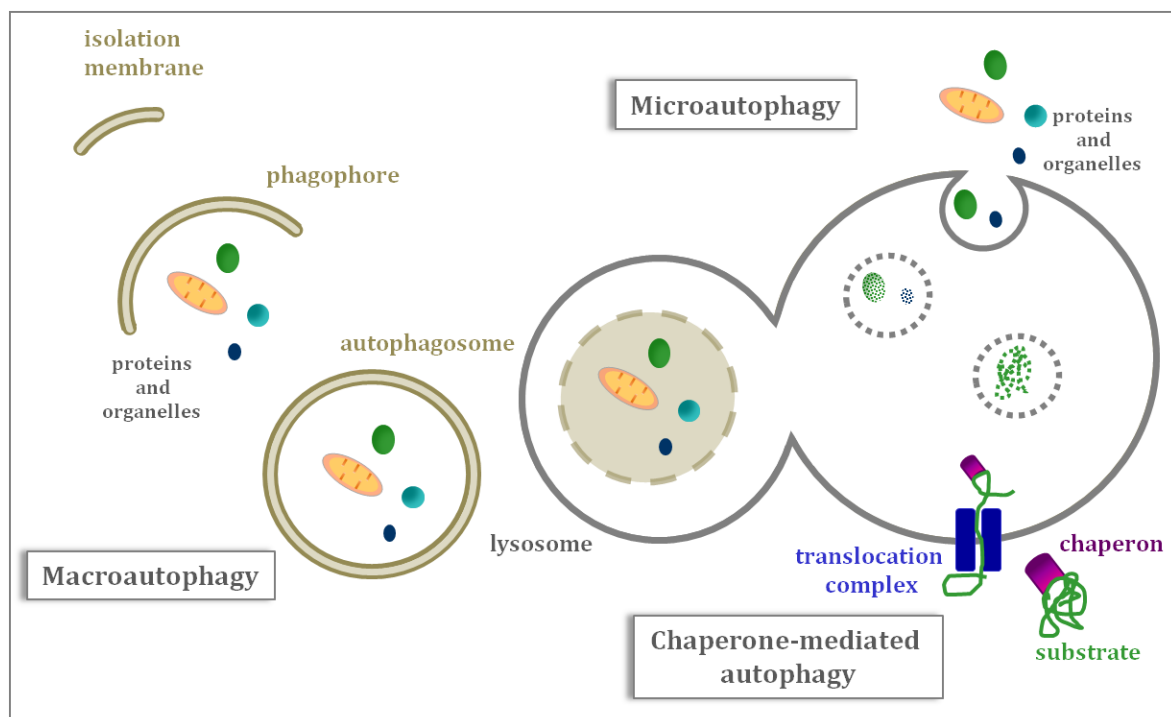


FIGURE 1-1: SCHEMATIC DEPICTION OF MAIN TYPES OF AUTOPHAGY (MODIFIED FROM [3])

Autophagy represents a tightly regulated catabolic process targeting cytoplasmic content to lysosomes for degradation. Due to distinct molecular mechanisms, autophagy can be broadly classified in three classes: macroautophagy, chaperone-mediated autophagy and microautophagy. See text for more details.

Lysosomal delivery through chaperone-mediated autophagy occurs independently of vesicle formation [4]. Substrate proteins, containing a KFERQ-like pentapeptide motif, are selectively recognized by the heat shock-cognate protein of 70 kDa (Hsc70)-containing chaperone-complex and targeted to the lysosomal membrane. Substrate-mediated multimerization of the lysosome-associated membrane protein type 2A (LAMP-2A) facilitates the substrate translocation into the lysosomal lumen for its degradation.

Cytoplasmic content is also trapped in vesicles which are directly formed through the invagination of the lysosomal membrane [5]. This non-selective degradation pathway, called microautophagy, represents the least understood type of autophagy.

In contrast, macroautophagy is the most prevalent form of autophagy in eukaryotic cells and was intensively studied during the last two decades [6, 7]. A membrane sac, called isolation membrane, initially sequesters the cytoplasmic constituents. Further elongation of the isolation membrane generates the phagophore. The phagophore ultimately closes and results in a double-membraned compartment called autophagosome. Fusion with lysosomes to autolysosomes finally enables lysosomal degradation of the autophagic content.

1.2 MACROAUTOPHAGY

The present study focuses on mammalian macroautophagy, which is hereafter referred as autophagy, and reviews the molecular mechanism as well as the physiological function of autophagy in more detail.

1.2.1 THE MOLECULAR CORE MACHINERY

Deciphering of the molecular mechanisms underlying autophagy was primarily based on the discovery of autophagy-related (*ATG*) genes in yeast and mammals.

Focusing on mammalian homologues, an essential subset of ATG proteins regulates the initial steps of autophagosome formation and is thus referred as the molecular core machinery [8].

Upon amino acid deprivation, as classical stimulus for canonical autophagy, distinct multimeric protein complexes mediate the initiation of autophagosome formation. Besides the UNC51-like kinase (ULK) and class III phosphatidylinositol 3-kinase (PI3P) complexes [9, 10], two ubiquitin-like conjugation systems were discovered to be essentially required for elongation of the pre-autophagosomal membrane (Figure 1-2).

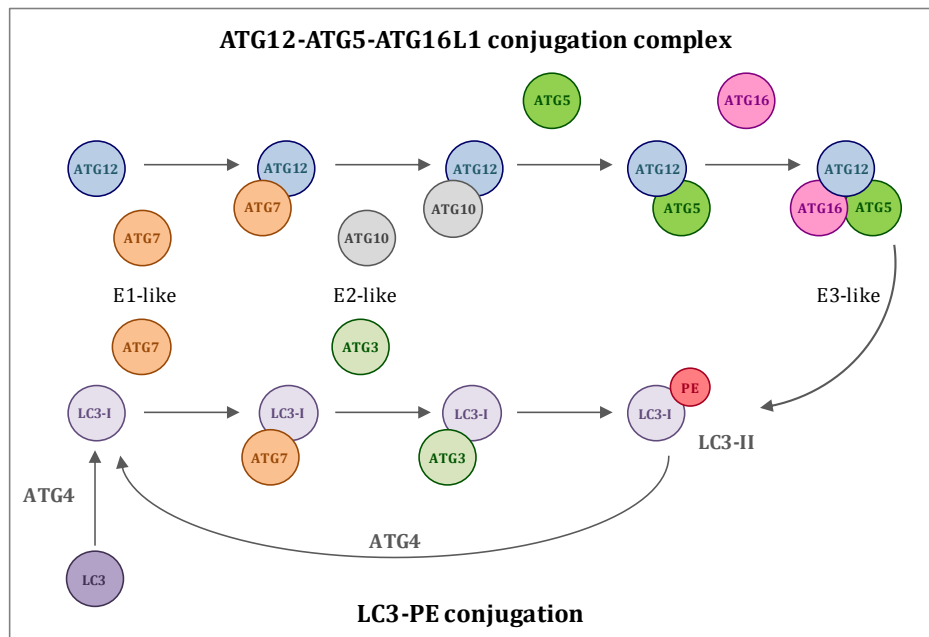


FIGURE 1-2: UBIQUITIN-LIKE CONJUGATION SYSTEMS INVOLVED IN AUTOPHAGOSOME BIOGENESIS (MODIFIED FROM [11])

Elongation of the autophagic isolation membrane requires two ubiquitin-like conjugation systems, the ATG12-ATG5-ATG16L1 conjugation complex and the LC3-PE conjugation system. See text for more details. ATG - autophagy-related protein, LC3 - microtubule-associated protein 1 light chain 3, PE - phosphatidylethanolamine

At first, localization of the ATG12-ATG5-ATG16L1 complex to the isolation membrane participates in autophagosome formation [12]. In detail, ATG7-dependent activation of the ubiquitin-like protein ATG12 subsequently leads to the transfer of ATG12 to the E2 ubiquitin conjugating enzyme-like protein ATG10 [13]. This mechanism facilitates the covalent binding of ATG12 to ATG5, which finally conjugates with the autophagy-related protein 16 like 1 (*S. cerevisiae*) (ATG16L1) to form an 800-kDa multimeric complex [12, 14]. Recently it was reported that recruitment of this multimeric complex to the isolation membrane is obtained by the direct binding of ATG16L1 to the WD-repeat phosphatidylinositol 3-phosphate effector protein 2b (WIPI2b) [15]. Acting in an E3 ubiquitin ligase-like manner, the ATG12-ATG5-ATG16L1 complex subsequently defines the site of conjugation for the second ubiquitin-like conjugation system by promoting lipidation of the microtubule-associated protein 1 light chain 3 (LC3) [16]. Synthesized as precursor, LC3 is proteolytically cleaved by ATG4 into its cytosolic form, namely LC3-I [17]. Similar to ATG12, LC3-I is activated by the E1 ubiquitin activating enzyme-like protein ATG7 and transferred to an E2 ubiquitin conjugating enzyme-like protein, in this case ATG3 [18]. Finally, LC3-I is conjugated to phosphatidylethanolamine (PE) and thus converted in its membrane-bound form LC3-II which specifically localizes to the autophagosomal double-membrane [19]. Depletion of either ATG7 or one of the components of the ATG12-ATG5-ATG16L1 complex results in an impaired conversion of LC3 meaning a strong accumulation of LC3-I with a concurrent absence of LC3-II [20-22].

Upon completion of the autophagosome formation, the ATG12-ATG5-ATG16L1 complex and the outer-membrane associated LC3-II dissociates from the autophagic membrane [12, 19]. However, following the autophagosome-lysosome fusion, lysosomal hydrolytic enzymes degrade intra-autophagosomal LC3-II. Thus, the turnover over of LC3-I to LC3-II is a well-established marker to investigate the autophagic flux in mammalian cells [23].

1.2.2 SELECTIVE AUTOPHAGY BY SPECIFIC CARGO RECEPTORS

Whereas autophagy, in response to nutrient deprivation, is a non-selective bulk degradation of cytosolic material, several forms of selective autophagy have been identified upon other stresses like removal of aggregated proteins (aggrephagy), damaged organelles e.g. mitochondria (mitophagy) or invading bacteria e.g. *Salmonella enterica* (xenophagy) [24].

Autophagic selectivity is conferred by autophagy cargo receptors which bind the cargo earmarked with degradation signals [25]. In mammals, Lys⁶³-linked poly-ubiquitination is the most prevalent degradation signal and can be bound by the ubiquitin-binding domain (UBD) of the cargo receptors [26]. Additionally, these receptors commonly possess a LC3 interacting region (LIR) to bridge the captured cargo, targeted for degradation, to the autophagosomal membrane. Sequestosome-1 (SQSTM1, hereafter referred as p62) was the first identified adaptor protein which directly binds LC3 to facilitate degradation of ubiquitinated protein aggregates [27]. Importantly, p62 also has other functions (see 5.2.4). Following the discovery of p62, several other selective autophagy receptors such as neighbor of BRCA1 gene 1 protein (NBR1) [28] and nuclear dot protein 52 kDa (NDP52) [29] were discovered. As reported for p62^{-/-} mice, absence of autophagy cargo receptors results in hyper-accumulation of insoluble Lys⁶³-ubiquitinated proteins [30].

Most of the autophagic receptors undergo constant degradation even in an unloaded state. Activation of these receptors is mainly regulated on transcriptional level. Besides amino acid depletion, activation of TLR4 and TLR2/6, for example, strongly induces the expression of p62 [31, 32]. On the other hand, cellular localization and spatial organization have an impact on their activation. In this case, oligomerization of p62 and NBR1 triggers sequestration and clustering of the autophagic cargo [28, 33]. Although autophagic receptors lack a unique specialization, cooperation between them is important for the selectivity of a specific cargo.

1.2.3 AUTOPHAGY AND ITS PHYSIOLOGICAL FUNCTIONS

Based on its various cellular functions in adaptive responses to starvation, quality control of proteins and organelles as well as elimination of invading pathogens, impaired autophagy has been implicated in a wide range of human diseases [34]. In this context, *in vivo* studies in mice

enlightened the multifaceted functions of autophagy in physiological processes and gave first insights in the complex phenotypic consequences caused by the impairment of autophagy.

Mice deficient in components of the ULK or PI3P complex, initiated upstream of the two ubiquitin-like conjugation systems in autophagosome biogenesis, die early in embryogenesis [35, 36]. Interestingly, mouse models harboring a constitutive homozygous knock-out of essential autophagy-related genes, such as *Atg7*, *Atg5* or *Atg16l1*, were born at the expected Mendelian frequency [20-22]. However, neonatal lethality of these mice demonstrated the physiological relevance of autophagy during the early neonatal starvation period. In contrast, mice deficient in *Lc3b*, one of the two isoforms of *Lc3*, did not show any phenotypic abnormalities [37].

Conditional mouse models lacking *Atg* genes in the particular tissue revealed a crucial role for autophagy in cell differentiation. Besides increased mortality at the age of 8-14 weeks and a severe anemia, mice with a conditional depletion of *Atg7* in hematopoietic cells showed a significant decrease in T and B lymphocyte counts [38]. T cell-specific knock-out of either *Atg5* or *Atg7* resulted in reduced numbers of peripheral T cells and enhanced apoptosis of mature T lymphocytes presumably based on impaired mitophagy [39, 40]. Similarly, studies in mice lacking *Atg5* in B cells displayed a role for autophagy in B cell development in the bone marrow and B cell survival in the periphery [41].

Studies in mice deficient for *Atg* genes in terminally differentiated cell types additionally implied a substantial role for autophagy in tissue homeostasis. Tissue-specific ablation of *Atg5* or *Atg7* e.g. in liver and brain caused severe phenotypes characterized by hepatic dysfunctions [21, 42] and neurodegeneration associated with accumulation of ubiquitinated proteins [43, 44], respectively. Within the intestinal epithelium, homeostasis of particularly Paneth cells is strongly dependent on an intact autophagic machinery [45].

In accordance with the intracellular removal of invading pathogens via the autophagosomal pathway, mice particularly lacking *Atg5* or *Atg7* in myeloid cells showed an increased susceptibility to infections with *Mycobacterium tuberculosis* [46, 47] but also *Candida albicans* [48] or *Toxoplasma gondii* [49].

1.3 THE AUTOPHAGY PROTEIN ATG16L1

The *Atg16l1* gene (human: 3411base pairs (bp), RefSeq.NM_030803; mouse: 3149bp, RefSeq.NM_029846) is located on chromosome 2 on position 37.1. The encoding protein was originally obtained in a yeast-two hybrid screen as a potential interaction partner of yeast *atg12* [50]. However, detailed studies demonstrated that yeast *atg16* (previously known as *apg16*) directly interacts with *atg5* via its N-terminal coiled-coil domain being indirectly associated with *atg12*. Absence of *atg16* hinders the recruitment of the *atg12-atg5* conjugate

to the autophagic isolation membrane. Studies in mammalian cells further showed that formation of this multimeric complex is essentially involved in autophagosome biogenesis from yeast to mice and men [12, 51, 52].

Named after the weak but significant homology in its N-terminal region with yeast *atg16*, the mammalian ATG16 like 1 protein (ATG16L1) contains an N-terminal ATG5-binding region and a coiled-coil domain required for self-oligomerization [12, 53, 54]. Additionally, the C-terminal region consists of seven tryptophan-aspartic acid (WD) repeats exhibiting a β -propeller structure. WD repeats are protein interaction domains found in functionally diverse proteins [55] suggesting that there might be undiscovered binding partners of ATG16L1 that interact with this region. Recent reports also suggested a protein-binding region for autophagy components, e.g. focal adhesion kinase family-interacting protein of 200 kD (FIP200) and WIPI2b, in between the coiled-coil and WD40 domains without affecting the integrity of the ATG12-ATG5-ATG16L1 complex [15, 56, 57].

Generated by alternative splicing, multiple isoforms of ATG16L1 were identified. Whereas at least four isoforms were reported for human *ATG16L1* [53], Mizushima *et al.* confirmed that the murine *Atg16l1* gene encodes for at least three isoforms [12]. Interestingly, although ATG16L1 is ubiquitously expressed in murine tissue, ATG16L1 α (lacking exon 8 and 9, appr. 63 kDa) and ATG16L1 β (lacking exon 9, appr. 71 kDa) were preferentially expressed in liver, kidney, spleen, thymus and testes. The third murine isoform ATG16L1 γ (complete sequence of exon 8 and 9, 75 kDa) was mainly expressed in the brain. Mouse ATG16L1 β and human ATG16L1-1 share 90 % identity and 93 % similarity of their amino acid sequence showing a high degree of homology. The cellular functions of these isoforms are hardly investigated. However, findings of a recently published study indicate that the distinct isoforms of ATG16L1 might contribute to different autophagic properties [58].

1.3.1 ROLE OF ATG16L1 IN IMMUNE RESPONSES

Besides xenophagy [46, 59], autophagy has also been reported to play a diverse role in other immunological processes, e.g. in modulation of signal transduction [60, 61] and regulation of cytokine secretion [22, 62, 63]. In this context, one of the best functionally studied disease-associated single nucleotide polymorphisms (SNPs) is rs2241880 in the human *ATG16L1* gene, which is highly associated with Crohn's disease, a chronic inflammatory disorder of the gastrointestinal tract [64, 65]. This SNP results in an exchange from threonine to alanine in the amino acid sequence of ATG16L1 at position 300 and is thus called T300A allelic variant. Studies in mice showing an impaired expression of *Atg16l1* in the intestinal epithelium, due to conditional depletion or hypomorphic expression, exhibit abnormalities in the ultrastructure of Paneth cells with an altered architecture of secretory vesicles loaded

with antimicrobial peptides such as lysozyme and defensins [66, 67]. This finding was confirmed in Crohn's patients harboring the homozygous *ATG16L1* risk allele T300A. Importantly, work by Murthy and colleagues demonstrated that the T300A variant of *ATG16L1* represents a hypomorphic allele [68]. Using knock-in mouse models bearing either the human (T300A) or murine (T316A) missense variant Murthy *et al.* showed an increased sensitivity to caspase-3-dependent cleavage leading to a defective autophagic capacity and augmented pro-inflammatory cytokine production in the ileum. In this context, *ATG16L1*-deficient cells showed *in vitro* an increased replication of the Crohn's disease-associated adherent-invasive *Escherichia coli* strain LF82 [69]. Human peripheral blood mononuclear cells (PBMCs) bearing the T300A allele showed increased production of IL1 β upon muramyl dipeptide (MDP) stimulation [70]. Similar findings were obtained in macrophages derived from *Atg16l1* chimeric mice in response to LPS [22]. The latest links assume a variety of molecular mechanisms, by which *ATG16L1* and autophagy may modulate inflammasome-dependent IL1 β secretion, e.g. due to impaired degradation of the inflammasome itself [71] or a regulatory function of damaged mitochondria activating the inflammasome via production of reactive oxygen species (ROS) [72]. Interestingly, *ATG16L1* was also identified as regulator of IL1 receptor signaling in fibroblasts by modulating IL1 β -induced MAPK and NF- κ B activation pointing to a potential immunomodulatory function independent of inflammasome activation [60].

Elucidation of the molecular mechanisms of *ATG16L1* might deepen the understanding of its regulatory capacity in immunomodulatory processes and its role within human diseases.

1.4 INFLAMMATION

The World Health Organization defines health as “a state of complete physical, mental and social well-being and not merely the absence of disease or infirmity” [73]. From the biological point of view an organism's health is stated as the dynamic physiological homeostasis of all biological systems resisting environmental changes and thus preserving life [74].

Within this complex network, the host's immunity is a major component maintaining the healthy state. Besides the continuous control of steady-state conditions ensuring the host's cellular and molecular functionality, the immune system patrols physical barriers preventing the invasion of foreign agents. In case of noxious stimuli or conditions like infections or injury the immune system immediately initiates a protective immune reaction called inflammation (Latin: *inflammare*, “to set on fire”).

Inflammation is traditionally defined by its five cardinal signs: redness (*rubor*), increased heat (*calor*), swelling (*tumor*), pain (*dolor*) and loss of function (*functio laesa*). The aim of the induced inflammatory cascade is in first line the elimination of the initial cause and the

ensuing restoration of tissue homeostasis. Inflammation can be classified in two subtypes: acute and chronic inflammation.

Acute inflammation is typified by a rapid onset and a short duration lasting from a few minutes to a couple of days. The pathophysiological mechanisms are well understood and represent a controlled and self-limiting inflammatory cascade [75, 76]. At first, blood flow increases through vasodilation. As a consequence, increased vascular permeability facilitates on the one hand the leakage of plasma proteins and on the other hand the migration of leukocytes, mainly neutrophils, to the site of inflammation. The release of pro-inflammatory mediators, like cytokines and chemokines, activates recruited leukocytes and finally induces the elimination of the noxious agent followed by a resolution and a repair phase. A dysregulation of this preprogrammed inflammatory cascade, due to a failed elimination of the invading agent or a malfunction of the affected tissue, results in persisting inflammatory conditions, called chronic inflammation [75, 76].

In contrast to an acute inflammation, chronic inflammation lasts from weeks to years. Representing the switch from the innate to the adaptive immunity, the predominantly invading leukocytes shift from neutrophils to mononuclear cells, mainly macrophages and lymphocytes causing characteristic tissue damage based on their continuous secretion of pro-inflammatory mediators. Tissue repair involves the processes of new blood vessel formation (angiogenesis) and fibrosis.

Importantly, inflammation is critical for the development of a variety of complex human diseases including metabolic disorders [77], cardiovascular diseases [78], neurodegenerative diseases [79], autoimmune diseases [80], intestinal diseases [81] but also cancer [82]. Thus, a profound knowledge about the initiation and the molecular mechanisms of (chronic) inflammation is of central interest in numerous clinical disciplines.

1.4.1 SEPSIS

One of the oldest inflammatory symptoms in human medicine can be traced back until the age of the Ancient Greeks (4th century B.C.). Hippocrates observed a phenomenon by which flesh rots and wounds fester, called sepsis (Greek: *σηπω*, “to rot”) [83]. Until the 19th century, sepsis was claimed as a result of the invasion of pathogenic organisms spreading into the host’s blood stream and thus was often described as “blood poisoning” [84]. Nowadays, immunopathogenesis of sepsis is assumed to be caused by an over-activation of the host’s innate immune system and the following pro-inflammatory cascade. In 1992 and 2003, an international consensus panel defined sepsis as “systemic inflammatory response to infection” [85, 86]. Septic patients might manifest several symptoms including increased or decreased body temperature, elevated blood cell count, increased heart rate, rapid

respiratory rate but also an altered mental status. However, clinical manifestations of sepsis exhibit great interindividual variations depending on patient factors like age, gender, underlying health state and genetic predisposition [84, 87]. On the other hand, load and virulence of the causative organism but also the initial site of infection play a decisive role in the course of disease. Sepsis complicated by acute organ dysfunction and finally multiple organ dysfunction is further clinically classified as severe sepsis and septic shock, respectively [85, 86].

Even after centuries of research, sepsis remains worldwide the leading cause of death in critically ill patients [84-86]. The overall mortality rate varies from 30 % up to 50 % in elderly patients [88]. In Germany, a prevalence of 12.4 % for sepsis and 11.0 % for severe sepsis was determined in intensive care units [89]. In 2010, the worldwide incidence was estimated up to 19 million cases per year emphasizing the immense medical and health economic burden due to sepsis [90].

The most common infectious diseases causing sepsis are pneumonia followed by intra-abdominal and urinary tract infections as well as primary infections of the blood stream [88]. Moreover, clinical data demonstrate a number of long-term consequences for survivors of (severe) sepsis [91, 92]. Besides cognitive and physical impairments, survivors also show an increased susceptibility to sequelae like ischemic stroke and myocardial infarction [93].

As discussed in the following chapters, investigations of initiating microbial components, the regulatory role of innate immune cells and their secreted inflammatory mediators as well as underlying molecular mechanisms of innate immune receptor signaling achieved great advances in the understanding of the immunopathogenesis of sepsis. However, sepsis still remains a major challenge in medicine and the development of new effective therapeutical approaches is necessary to increase the survival rate following (severe) sepsis.

1.5 MYELOID CELLS - THE FIRST LINE OF DEFENSE

In adult mammals, the bone marrow acts as the predominant reservoir of hematopoietic stem cells (HSCs) giving continuously rise to all types of blood cells: erythrocytes, leukocytes and platelets [94]. Classification of leukocytes is typically based on their hematopoietic lineage (Figure 1-3). Natural killer (NK) cells as well as T and B lymphocytes derive from a common lymphoid progenitor (CLP) [95]. Myeloid cells arise from a common myeloid progenitor (CMP) [96] and comprise granulocytes, monocytes, macrophages and dendritic cells [97].

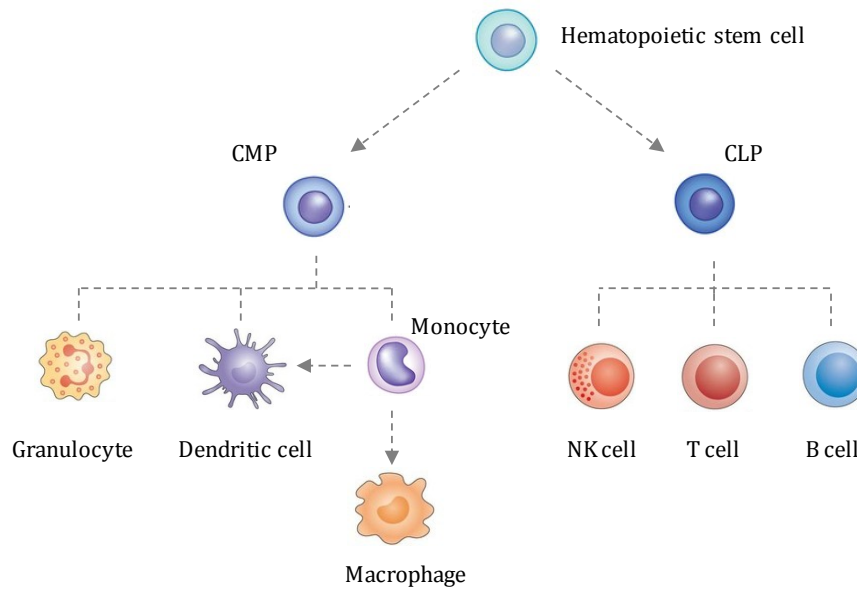


FIGURE 1-3: SCHEMATIC STEPS OF LEUKOCYTE DIFFERENTIATION (MODIFIED FROM [98, 99])

Leukocytes derived from hematopoietic stem cells of the bone marrow are generated by either common myeloid progenitor (CMP) cells or common lymphoid progenitor (CLP) cells. See text for more details.

Once released from the bone marrow, myeloid cells circulate through blood and the lymphatic system and are rapidly recruited to the site of tissue damage or infection. Myeloid cells are not only distinguished by their morphology but also by their recruitment kinetics and cellular functions during infection and inflammation.

1.5.1 NEUTROPHILS

Granulocytes are morphologically distinguishable from other myeloid cells due to their segmented nucleus and characteristic cytoplasmic granules. Besides macrophages, granulocytes were first discovered as “microphages” by Ilya Metchnikoff in the 19th century and were later on categorized by Paul Ehrlich in basophilic, neutrophilic and eosinophilic polymorphonuclear cells due to their distinct staining characteristics [100]. Whereas basophils and eosinophils are mainly involved in the pathogenesis of allergic disease, neutrophils represent the first myeloid cell population during tissue damage or infection.

Neutrophils are well-characterized terminally differentiated myeloid cells with a short half-life of 6-12 hours and are the most abundant myeloid cell type [101]. During inflammatory processes neutrophils migrate in response to chemo-attractants, like interleukin-8 (IL8), to the site of inflammation [102, 103]. Using flow cytometry, neutrophils can be identified by their specific cell surface co-expression of CD11b and Ly6G [104]. As phagocytic cells, the general function of neutrophils relies in first line on the engulfment of extracellular pathogens and agents and its ensuing intracellular clearance (phagocytosis). Besides phagocytosis, neutrophils possess a variety of extracellular microbicidal mechanisms

to eliminate bacteria [101, 105]. The major pool of antimicrobial substances is captured in cytoplasmic granules which are secreted upon neutrophil activation and can be classified in two major subtypes: primary or azurophilic granules and secondary or specific granules [106]. Azurophilic granules are the major storage site of the myeloperoxidase (MPO) and other cytotoxic molecules like serine proteases and defensins. Among other components, peroxidase-negative secondary granules mainly contain lysozyme and lactoferrin. Besides the degranulation response, neutrophils exhibit a second extracellular destruction process called neutrophil respiratory burst. By increasing the consumption of oxygen during phagocytosis, neutrophils generate ROS with a high antimicrobial potential [107]. Additionally, neutrophil-derived cytokines, like macrophage inflammatory protein-1 α (MIP1 α) [108], make an important contribution to activation, differentiation and recruitment of other myeloid cells like macrophages and dendritic cells [101, 109]. Recent findings further implicate a role for neutrophils in the resolution of inflammation as neutrophils also secrete anti-inflammatory cytokines like interleukin-10 (IL10) [110]. Additionally, a subset of neutrophils, called myeloid-derived suppressor cells (MDSCs), mediates immune suppression by inhibiting T cell response during systemic inflammatory conditions [111].

1.5.2 MONOCYTES AND MACROPHAGES

Monocytes are directly generated from myeloid progenitor cells in the bone marrow and afterwards released in the blood circulation where they represent 4-10 % of the peripheral leukocytes. In 1968, van Furth and colleagues established the mononuclear phagocyte system by which monocytes serve as precursor of tissue-resident macrophages under steady-state conditions [112]. Distinguished by their cell surface markers, these so called classical monocytes exclusively express CD14 in humans and are defined as Ly6C^{high} myeloid cells in mice [113, 114]. In the meantime, it is known that two independent systems evolved to renew myeloid cells. Classical monocytes mainly serve as systemic reservoir for macrophages and dendritic cells under inflammatory conditions [115]. In contrast, embryonic myeloid precursors are the resource of tissue-resident macrophages in various organs, like brain, liver and epidermis, enabling a continuous self-renewal within the native tissue [116, 117].

Tissue macrophages reside in most lymphoid and non-lymphoid organs where they are involved in steady-state tissue homeostasis via clearance of apoptotic cells and production of growth hormones [118]. Among others, tissue-resident macrophages include alveolar macrophages in the lung, osteoclasts in the bone, Kupffer cells in the liver and microglia in the brain. However, according to the variable microenvironment of the local milieu, there is a high demand on functional specificity for resident macrophages to maintain tissue homeostasis. Intestinal macrophages, for example, are constantly exposed to changing

environmental and microbial conditions by food uptake. To avoid an over-reaction to the host's commensal gut flora under healthy conditions, intestinal macrophages, in contrast to splenic macrophages, spontaneously produce high amounts of the anti-inflammatory cytokine IL10 mediating a hypo-responsiveness towards bacterial and viral components and in turn an impaired production of pro-inflammatory cytokines like IL12 [119].

First discovered by Ilya Metchnikoff, macrophages are traditionally defined as phagocytic cells [100]. Their broad range of immune receptors on the plasma membrane and in the cytoplasm facilitates an early and efficient recognition and ingestion of a wide array of bacterial, viral and fungal pathogens ([120], see also chapter 1.6). Upon engulfment of the extracellular pathogens in (phago-) lysosomes, immunogenic peptides were immediately processed and loaded on major histocompatibility complex II (MHCII) molecules [121]. The ensuing MHCII-mediated antigen presentation at the cell surface of activated macrophages finally drives naïve T cells into T helper cells. In this way, macrophages are able to communicate the nature of the invading pathogen to the adaptive immune system mediating a long-lasting antigen-specific response. Simultaneously, activated macrophages secrete pro-inflammatory cytokines like tumor necrosis factor-alpha (TNF α) [122], interleukin 12 (IL12) [123] as well as IL8/CXCL1 [124, 125] initiating the recruitment of additional innate and adaptive immune cells to the site of local infection [103, 126]. Besides MHCII expression at the cell surface as classical activation marker [127], expression of CD95/Fas is upregulated on activated macrophages [128]. Although it is best known for its role as death receptor inducing apoptosis [129], CD95/Fas is able to promote secretion of pro-inflammatory cytokines like CXCL1. Especially upon activation through lipopolysaccharide, a constituent of the outer layer of the outer membrane of gram-negative bacteria, macrophages increase CD14, an accessory protein of the Toll-like receptor 4 (TLR4), at their cell surface [130-132] (see also chapter 1.6.1).

Besides their crucial role within the initiation of the appropriate immune response, macrophages are also essentially involved in the resolution of inflammation by eliminating apoptotic cells and regulate wound healing [133, 134].

1.6 TOLL-LIKE RECEPTORS IN INNATE IMMUNE RESPONSES

In 1989, Janeway revolutionized the research field of immunology, proposing a concept by which innate immune cells sense conserved microbial structures, so called pathogen-associated molecular patterns (PAMPs), by a limited number of pattern recognition receptors (PRRs) [135]. After several decades of intensive studies in a variety of model organisms and humans, it is nowadays well-known how myeloid cells use PRRs as sophisticated tool to protect the host against an enormous diversity of microbial classes such

as viruses, bacteria and fungi. Besides specific tissue expression patterns and distinct cellular localizations, PRRs recognize a broad spectrum of ligands subsequently inducing specific intracellular signaling pathways and downstream gene expression to initiate an appropriate immune response.

One of the major subfamilies of PRRs is represented by mammalian Toll-like receptors (TLRs). However, the first Toll protein was originally discovered in 1985 by the group of Christiane Nüsslein-Vollhard who reported the involvement of Toll in the dorsoventral polarity of the developing *Drosophila melanogaster* embryo [136]. Although the homology between the cytosolic domain of Toll and the human interleukin 1 receptor (IL1R) was already predicted in 1991 [137], the impact of *Drosophila* Toll in host defense was still unsolved as the molecular mechanism by which the IL1R presumably signals was still unclear. One of the important steps in this research field was the characterization of the plant N protein in 1994 [138]. Besides an N-terminal domain homolog to the cytosolic Toll and IL1R domain, the plant N protein was described to mediate the resistance against the tobacco mosaic virus. This finding provided one of the first evidences for a crucial role of proteins containing the evolutionarily conserved Toll-IL1 receptor (TIR) domain in host defense. Due to their structural relation, the mammalian Toll homologues were called Toll-like receptors [139]. In the meantime, ten *TLR* genes in humans (*TLR1-10*) and 12 murine *Tlr* genes (*Tlr1-9, Tlr11-13*) were identified [140].

Mammalian TLRs have now been studied for over 20 years and their complex signaling network is well-understood [140-142] (Figure 1-4). Mammalian TLRs are type I transmembrane receptors exhibiting an extracellular domain containing leucine-rich repeats (LRRs), a single membrane-spanning segment and the above mentioned intracellular TIR domain [143]. They can be broadly subdivided by their cellular localization. TLR1, TLR2, TLR4, TLR5, TLR6 and TLR11 are exclusively expressed at the cell surface and mainly recognize bacterial components like flagellin [144] and bacterial lipopeptides [145, 146]. On the other hand, TLR3, TLR7, TLR8, TLR9 and TLR13 are located in endosomes sensing non-self nucleic acids like double-stranded (ds) and single-stranded (ss) viral RNA [147, 148] but also CpG-rich hypomethylated bacterial DNA [149]. Neither a ligand nor a role for TLR10 has been reported so far [141, 150]. Activation of mammalian TLRs is initiated by ligand binding to their ectodomain followed by the formation of homo- or hetero-dimers [151]. The rearranged TIR domains subsequently act as scaffold for the recruitment of TIR domain-containing signaling adaptors that bridge TLRs to proteins of the downstream signaling cascades. Interestingly, TLRs as well as members of the IL1R family signal in part through identical components like the adaptor molecule myeloid differentiation primary-response protein 88 (MyD88) [152], the downstream activated interleukin 1 receptor-

associated kinases (IRAKs) [153] and the E3 ubiquitin protein ligase TNF receptor-associated factor 6 (TRAF6) [154] (see also chapter 1.6.1.)

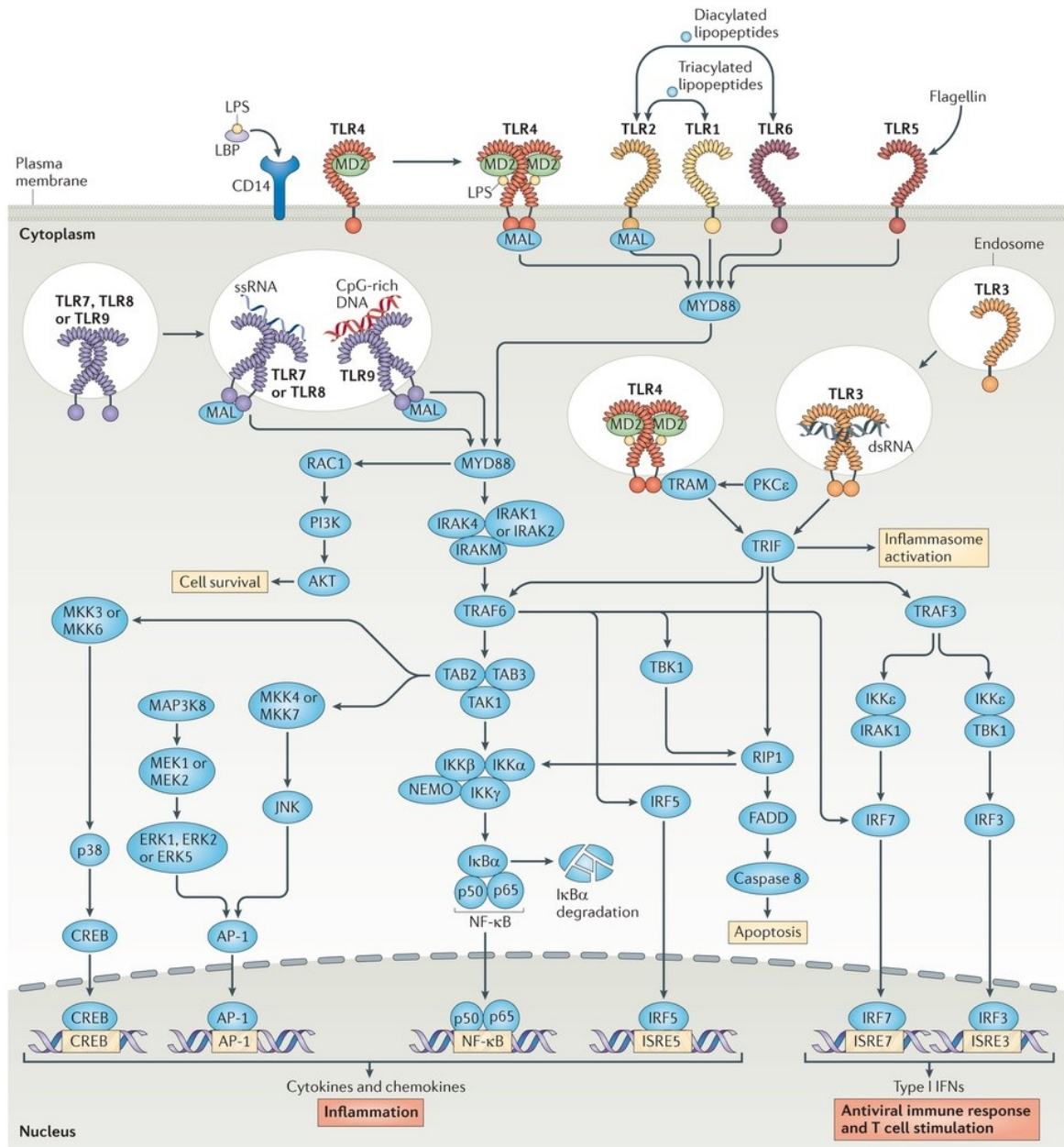


FIGURE 1-4: MAMMALIAN TOLL-LIKE RECEPTOR (TLR) SIGNALING (TAKEN FROM [142])

Mammalian TLRs possess distinct ligand specificities and cellular localizations. However, TLR-induced signaling pathways share common features like the TIR-domain containing adaptor molecules MyD88 and TRIF but also the downstream activation of transcription factors like NF- κ B and IRF3/7. See text for more details. IRF3/7: interferon regulatory factor 3/7; MyD88: myeloid differentiation primary-response protein 88; NF- κ B: nuclear factor 'kappa-light-chain-enhancer' of activated B-cells; TRIF: TIR-domain-containing adapter-inducing interferon- β

As one of the major PRR families, TLRs are key regulators of innate immune responses. Thus, an appropriate (de-)activation of TLR signaling is of prime importance and dysregulation of the signaling leads to several infectious and inflammatory diseases in humans like tuberculosis [155], arteriosclerosis [156], inflammatory bowel disease [157] and sepsis [158, 159].

1.6.1 TOLL-LIKE RECEPTOR 4 (TLR4) SIGNALING

TLR4, originally named hToll, was the first identified human homologue of *Drosophila* Toll [160]. Within the family of mammalian TLRs, TLR4 adopts an exceptional position due to the unique ligand recognition and cellular translocation that is directly linked to the replacement of adaptor molecules and the activation of individual signaling pathways.

The first and best-characterized ligand of TLR4 is LPS [161-163]. However, during the last decades it was demonstrated that recognition of LPS by TLR4 is complex and involves additional non-TLR components. In detail, detection of LPS is mainly mediated by a stable hetero-dimer of TLR4 and its essential co-receptor myeloid differentiation factor 2 (MD2) [164, 165]. The accessory proteins CD14 and LPS-binding protein (LBP) further enhance LPS detection by direct binding and ensuing presentation of LPS to TLR4-MD2 complexes [166-168].

Unlike the majority of TLRs which directly signal through the adaptor molecule MyD88, TLR4-MyD88 interaction is indirectly mediated by the bridging adaptor TIR domain-containing adaptor protein (TIRAP, also known as Mal) (Figure 1-4). LPS-induced TLR4 dimerization initially triggers the assembly of a submembrane signaling complex consisting of MyD88-Mal and IRAKs. In brief, recruitment of IRAK4 to MyD88-Mal mediates the (auto-)phosphorylation of IRAK1/2 through its intrinsic kinase activity [169-171]. Based on its hyper-phosphorylation, IRAK1 dissociates from the initial receptor complex and associates with the E3 ubiquitin ligase TRAF6 [172, 173]. Upon activation, self-oligomerized TRAF6 joins a complex with the Lys⁶³-specific E2 conjugation enzymes Ubc13 and Uev1A enabling the attachment of non-degradative Lys⁶³-linked ubiquitin chains to TRAF6 substrates and TRAF6 itself [174]. In turn, poly-ubiquitinated TRAF6 dictates the recruitment of the transforming growth factor β -activated kinase 1 (TAK1) and the TAK1 binding proteins 1/2/3 (TAB1/2/3) [175, 176]. The TRAF6-TAB-TAK1 complex formation culminates in the phosphorylation and thus activation of TAK1 [175, 177].

Upon activation, TAK1 acts as kinase which phosphorylates and activates the I κ B kinase (IKK) and MAPK kinases (MKKs) pathway [175]. MKKs induce downstream kinases like p38, c-Jun N-terminal kinase (JNK) and extracellular signal-regulated protein kinases (ERK) which finally regulate the activity of transcription factors like the activator protein-1 (AP-1) [175].

On the other hand, the activated IKK complex, consisting of the subunits IKK α , IKK β and IKK γ (also known as NEMO), induces the transcriptional activation of transcription factors of the nuclear factor 'kappa-light-chain-enhancer' of activated B-cells (NF- κ B) family [178, 179]. In brief, nuclear factor of kappa light polypeptide gene enhancer in B-cells inhibitor (I κ B) proteins are phosphorylated by the activated IKK complex which is directly associated with the ubiquitination and proteasomal degradation of I κ B proteins [180, 181]. Under

physiological conditions, NF- κ B transcription factors are bound in their inactive form by I κ B proteins retaining them in the cytoplasm [182]. The induced degradation of I κ B proteins finally enables the translocation of NF- κ B dimers into the nucleus. In mammals, the NF- κ B family includes five members: p50, p52, p65 (RelA), RelB and c-Rel, [183]. The most abundant NF- κ B heterodimer is p65-p50 which is primarily targeted by I κ B α [184]. The nuclear transcriptional activity of NF- κ B can be further influenced by posttranslational modifications such as phosphorylation and acetylation. In case of LPS-induced NF- κ B activation, it is known that IKK-dependent phosphorylation at serine 536 plays a crucial role for the transactivation potential of p65 [185]. Due to the complexity of heterodimers and posttranslational modifications, the NF- κ B transcription factor family is able to induce the expression of a broad range of genes in response to the appropriate stimuli. LPS stimulation, for example, induces the NF- κ B-controlled expression of pro-inflammatory cytokines like *Il8/Cxcl1* [160]. Upon internalization of TLR4 from the plasma membrane into the early endosomal compartment (Figure 1-4), a second adaptor molecule, namely TIR-domain-containing adapter-inducing interferon- β (TRIF), is recruited [186, 187]. Similar to Mal, the TRIF-related adaptor molecule (TRAM) bridges TLR4 and TRIF. The newly formed receptor complex initiates the recruitment of the downstream E3 ubiquitin ligase TNF receptor-associated factor 3 (TRAF3) [188]. Ubc13-mediated Lys⁶³-polyubiquitination of TRAF3 orchestrates the activation of the downstream IKK-related kinases TRAF-associated NF- κ B activator (TANK)-binding kinase-1 (TBK1) and IKK ϵ [188, 189]. TBK1 and IKK ϵ then phosphorylate the interferon-regulatory transcription factors (IRF) IRF3 and IRF7 leading to their nuclear translocation which finally stimulates the transcription of type I interferons (IFN), such as *IFNB* [190-192]. Additionally, TRIF directly engages TRAF6 to activate canonical NF- κ B and MAPK signaling in a MyD88-independent manner [187, 193] (Figure 1-4). Since *MyD88*-deficient cells revealed a delayed activation kinetic of NF- κ B and MAPK signaling, the TRIF-dependent activation cascade is called 'late phase activation' [187].

1.6.2 NEGATIVE REGULATION OF TLR4 SIGNALING

TLR signaling is tightly controlled by comprehensive negative regulation to prevent an overwhelming of the host's immune response. For this reason, numerous inhibitory mechanisms, ranging from extracellular decoy receptors to intracellular inhibitors, contribute to a complex regulatory network in the surveillance of TLR-mediated signal transduction. The following chapter introduces a small excerpt of the broad mechanistic repertoire of the cell to shut down TLR4-induced signaling on distinct hierarchical levels.

As an extracellular decoy receptor, the naturally occurring soluble form of the TLR4 enables the binding of LPS and thus inhibits NF- κ B signaling [194]. *In vivo* studies in mice

demonstrated that the observed effect is even more pronounced in a combinational treatment of the recombinant soluble forms of TLR4 and MD2 [195]. Scavenger receptors such as macrophage scavenger receptor 1 (MSR1) also co-operate in the recognition of LPS and thus suppress TLR4 signaling [196].

Further, TLR4 signaling can be shut down by intracellular dominant-negative signaling factors. One of these factors is an LPS-inducible splice variant of MyD88 (MyD88s) which abrogates the interaction of MyD88 and IRAK4 due to a lacking intermediate domain [197, 198]. Similarly, expression of the inactive IRAK homologue IRAK-M is initiated upon LPS stimulation and avoids the IRAK-TRAF6 complex formation [199].

Lys⁶³-linked poly-ubiquitination is a critical step within the signaling cascade of either NF- κ B or IRF activation (see chapter 1.6.1). Therefore, deubiquitinase enzymes (DUBs) play a crucial role in the negative regulation of TLR4 signaling. One of the best studied DUBs is the TNF α -induced protein 3 (TNFAIP3, hereafter referred as A20) [200]. Among others, the deubiquitinase activity of A20 targets IKK activators like TRAF6 and IKK γ [201, 202]. As the expression of A20 is directly controlled by NF- κ B [203], A20 constitutes a characteristic example for an autoregulative pathway. Cyldromatosis (turban tumor syndrome) (CYLD) is a second DUB attenuating NF- κ B signaling by deubiquitinating a range of signaling mediators like TRAF6 and TAK1 [204, 205].

Another negative feedback loop takes place in the nucleus and is initiated by the NF- κ B dependent gene expression of its inhibitory binding partner *I κ B α* [206]. After entering the nucleus, newly synthesized I κ B α abrogates the NF- κ B-DNA binding and, due to its nuclear-export sequence, exports NF- κ B back into the cytoplasm [207].

Although the down-regulation of TLR4 signaling is ensured by a wide range of negative regulators on distinct levels of the signal transduction cascade, the absence of one of these principles often has far-reaching consequences. Deficiency of e.g. *A20* or *I κ B α* in mice causes lethal inflammation [208, 209]. Similarly, single-nucleotide polymorphisms (SNPs) in human genes encoding for anti-inflammatory signaling molecules such as *IRAKM* and *A20* are associated with the pathogenesis of autoimmune and inflammatory diseases [210, 211].

2 AIMS OF THE STUDY

Autophagy is involved in various fundamental processes like survival during nutrient-deprivation, intracellular quality control of proteins and organelles but also immunoregulatory functions such as bacterial defense and cytokine secretion.

Specifically for the autophagy protein ATG16L1, recent *in vivo* studies implicated a regulatory role in secretory pathways. Deletion of *Atg16l1* in the intestinal epithelium resulted in a disrupted formation of lysozyme-containing granula in Paneth cells as well as a diminished production of antimicrobial peptides which might point to a disturbed secretion in Paneth cells [67]. On the other hand, ATG16L1 was suggested as negative regulator of inflammasome-mediated IL1 β and IL18 secretion [22]. However, little is known about the exact molecular mechanisms by which ATG16L1 affects inflammatory responses.

The aim of the present study was to investigate the role of ATG16L1 in the secretory pathway of myeloid cells, particularly of macrophages. Using a conditional mouse model lacking *Atg16l1* in myeloid cells (*Atg16l1LysM*), which includes deletion in granulocytes, macrophages and dendritic cells, the following major questions were addressed:

I) Does the loss of *Atg16l1* affect secretory pathways of myeloid cells under baseline conditions?

To verify the role of ATG16L1 in myeloid cells under baseline conditions, the present study characterized the basal phenotype of *Atg16l1LysM* mice, particularly of the immune relevant organs. Based on the literature, the IL1 cytokine family and IL1 receptor signaling represented the starting point for the investigation.

II) Does ATG16L1 have an impact on secretory pathways of myeloid cells under inflammatory conditions?

Bone marrow-derived macrophages from *Atg16l1LysM* mice were used for *in vitro* studies. The present study investigated a putative role of ATG16L1 in secretory pathways in macrophages under inflammatory conditions, notably upon LPS stimulation. The *in vivo* relevance was examined in *Atg16l1LysM* mice using an endotoxin shock model.

3 MATERIAL AND METHODS

3.1 MATERIAL

All materials used including buffers, media, kits, reagents, devices and consumables are listed in the appendix (chapter 8). Antibodies and primers are listed in the appropriate methodological chapters.

3.2 METHODS

3.2.1 ANIMAL-HOUSING

Mice were housed under specific-pathogen-free (SPF) conditions in individual ventilated cages (IVCs) under a 12 h light-dark cycle. Food and water were provided *ad libitum* and environmental conditions were maintained at 21 °C ± 2 °C with 60 % ± 5 % humidity.

3.2.2 GENERATION OF *ATG16L1* CONDITIONAL KNOCK-OUT MICE

The conditional *Atg16l1* knock-out mouse line was generated in collaboration with GenOway (Lyon, France) using the Cre/lox technology [67]. Briefly, the Cre/lox system is based on a recombination mechanism in P1 bacteriophages with two components: (i) a Cre recombinase and (ii) *loxP* sites [212]. *LoxP* sites are specific 34 bp sequences flanking the gene region in which the Cre-mediated recombination takes place. The tissue-specific knock-out is achieved by expressing the Cre recombinase under the control of a tissue-specific promoter.

The generated conditional *Atg16l1* knock-out mouse line includes a single distal *loxP* site upstream of the first exon, within the promoter region of the *Atg16l1* gene as well as a *loxP* site together with an FRT flanked neomycin selection cassette within intron 1 (Figure 3-1). Breeding with deleter-mice constitutively expressing the Flp recombinase removed the neomycin selection cassette and consequently generated the conditional *Atg16l1* knock-out mouse line in which exon 1 of the *Atg16l1* gene is flanked by *loxP* sites (*Atg16l1^{fl/fl}*). Translation of all isoforms of the *Atg16l1* gene is disrupted by a Cre-mediated excision of exon 1. To obtain a specific *Atg16l1* knock-out model in myeloid cells means macrophages and granulocytes (*Atg16l1^{fl/fl}LysM*), *Atg16l1^{fl/fl}* mice, backcrossed onto C57BL/6J mice (Jackson Laboratory, Bar Harbour, USA), were bred with *LysMcre* mice (B6.129P2-*Lyz2^{tm1(cre)Jfo}/J*; Jackson Laboratory, Bar Harbour, USA) expressing the Cre recombinase under the control of the endogenous *Lysozyme 2* (*Lyz2*) promoter [213].

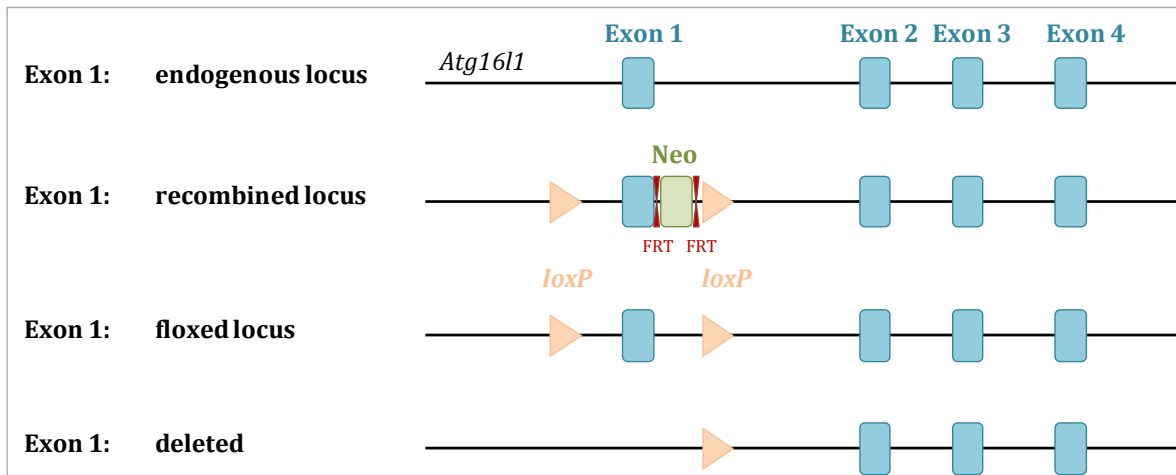


FIGURE 3-1: TARGETING STRATEGY FOR THE CONDITIONAL *ATG16L1* MOUSE LINE

For the deletion of *Atg16l1* a targeting vector containing exon 1 flanked by *loxP* sites and a neomycin selection cassette were inserted into murine blastocysts. Breeding with Flp deleter-mice removed the neomycin cassette and created an *Atg16l1* floxed mouse line (*Atg16l1^{fl/fl}*). Mating of *Atg16l1^{fl/fl}* mice with mice possessing a Cre recombinase under the control of the *Lyz2* promoter revealed a myeloid-specific knock-out of *Atg16l1* (*Atg16l1^{LysM}*).

3.2.3 GENOTYPING OF *ATG16L1^{LysM}* MICE

Isolation of genomic DNA of ear or tail biopsies was performed in 150 μ L of 50 mM NaOH solution for 1 h at 94 $^{\circ}$ C. Samples were centrifuged for 1 min at 1,000 x g and the DNA containing supernatant was transferred into a fresh tube and stored at -20 $^{\circ}$ C. Insertion of *loxP* sites within the *Atg16l1* gene as well as the *LysMcre* (*LysM*) transgene were validated using specific primer pairs (Table 1).

TABLE 1: PRIMER SEQUENCES FOR GENOTYPING OF *ATG16L1^{FL/FL}* AND *ATG16L1^{ΔMΦ}* MICE

Primer	Sequence (5' \rightarrow 3')	Product size
<i>Atg16l1</i> (for)	CAGAATAATTTCCGGCAGAGACCGG	floxed: 537 bp wild type: 444 bp
<i>Atg16l1</i> (rev)	AGCCAAAGAAGGAAGGTAAGCAACGAA	
<i>LysM</i> + (for)	CCCAGAAATGCCAGATTACG	700 bp
<i>LysM</i> + (rev)	CTTGGGCTGCCAGAATTTCTC	
<i>LysM</i> - (for)	CTTGGGCTGCCAGAATTTCTC	350 bp
<i>LysM</i> - (rev)	TTACAGTCGGCCAGGCTGAC	

For amplification by means of a polymerase-chain reaction (PCR), 0.5 μ L of the isolated DNA was added to the following standard PCR mixture:

- 13 μ L nuclease-free water (Qiagen, Hilden, Germany)
- 4 μ L 5X Green GoTaq[®] Reaction Buffer (Promega, Mannheim, Germany)
- 0.5 μ L deoxynucleotide triphosphates (dNTPs) (Thermo Scientific, Darmstadt, Germany)
- 0.5 μ L primer pair (10 μ M each)

- 0.5 µL DreamTaq DNA polymerase (Thermo Scientific, Darmstadt, Germany)

Following an optimal annealing temperature and different amplicon sizes per primer pair, different PCR programs were used for genotype assessment using the GeneAmp PCR System 9700 (Applied Biosystems, Darmstadt, Germany) (Table 2).

TABLE 2: PCR PROGRAMS FOR GENOTYPING OF *ATG16L1^{FL/FL}* AND *ATG16L1 Δ M Φ* MICE

Step	Temperature	Duration	Cycles
Denaturation	95 °C	4 min	1
Denaturation	95 °C	30 sec	
Annealing			
- <i>Atg16l1</i>	63 °C	30 sec	38
- <i>LysM +/-</i>	62 °C	1 min	35
Elongation	72 °C		
- <i>Atg16l1</i>		5 min	
- <i>LysM +/-</i>		1 min	
Extension	72 °C	8 min	1

For visualization, the DNA amplicons were loaded onto a 1 % (w/v) agarose gel in 100 mL 0.5 x Tris-acetate (TAE) buffer supplemented with 10 x SYBR® Safe DNA gel stain (Life Technologies, Darmstadt, Germany). Gel electrophoresis was carried out at 100 V for 30 to 60 min. Using the ChemiDoc XRS system (Bio-Rad, Munich, Germany) and the associated QuantityOne® 1-D Analysis Software (Version 4.6.8, Bio-Rad, Munich Germany) the amplified DNA was visualized with UV-light and documented (Figure 3-2).

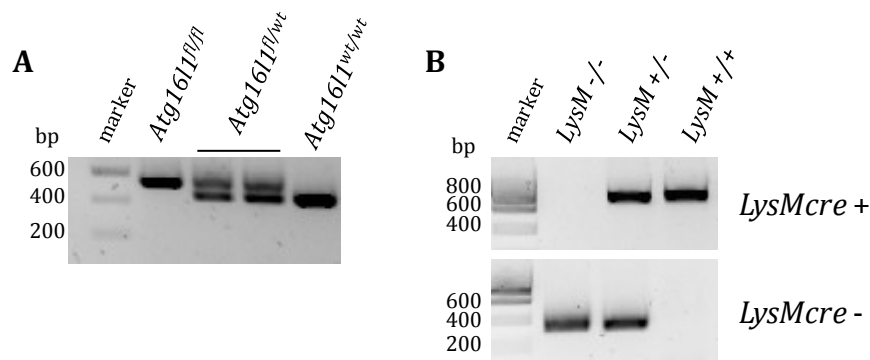


FIGURE 3-2: AGAROSE GEL ELECTROPHORESIS OF GENOTYPING PCRS FOR *ATG16L1^{FL/FL}* AND *ATG16L1^{LysM}*
 Genomic DNA was isolated from mouse tissue and specific sequences were amplified by PCR. Based on the amplicon size, *loxP* sites (A), the *LysMcre* transgene (*LysM -/-* = wild type, *LysM +/+* = *LysMcre*) were identified. PCR products are shown as black/white inverted images.

3.2.4 ANIMAL EXPERIMENTS

All animal experiments were approved by the Animal Investigation Committee of the University Hospital Schleswig-Holstein (Campus Kiel, Germany) (acceptance no.: V 242-7224.121-33 (125-9/13)). Gender-matched mice between 8 and 14 weeks of age were used. Mice were sacrificed by cervical dislocation or, in case of cardiac puncture for collection of serum, mice were intraperitoneally injected with a narcotic mixture of 100 mg/kg body weight ketamine and 16 mg/kg body weight xylazine. For RNA and protein extraction, tissues were snap-frozen in liquid nitrogen and stored at - 80 °C. For immunohistochemistry, tissues were fixed in 10 % formalin at 4 °C for at least 24 h.

3.2.4.1 ANAKINRA THERAPY

For a duration of 14 days, gender-matched *Atg16l1^{fl/fl}* and *Atg16l1LysM* mice (n=8 per genotype) at the age of 9-13 weeks received a daily intraperitoneal injection of 200 µg Anakinra (Kineret®, Swedish Orphan Biovitrum AB, Stockholm, Sweden), a recombinant human interleukin-1 receptor antagonist (IL1Ra), which was shown to interact with the murine interleukin-1 receptor [214]. Control mice (n=4-5 per genotype) received a daily injection of 200 µL 0.9 % (w/v) NaCl (Fresenius Kabi Deutschland GmbH, Bad Homburg, Germany). Body weight was monitored every second day. After 14 d mice were sacrificed. Organs and cells were collected and subsequently analyzed or stored at - 80 °C.

3.2.4.2 SUBLETHAL ENDOTOXIN-INDUCED SEPSIS

Ultrapure lipopolysaccharide (LPS) from *Escherichia coli* (KPM53) was a generous gift by Dr. Nicolas Gisch (Research Center Borstel, Borstel, Germany). Endotoxin-induced sepsis in gender-matched *Atg16l1^{fl/fl}* and *Atg16l1LysM* mice at the age of 9-14 weeks was achieved by an intraperitoneal injection of 5 mg/kg body weight ultrapure LPS for the indicated duration of 1, 3, 6, 24 or 72 h (n=5-7 per genotype). Control mice (n=5-7 per genotype) received an intraperitoneal injection of 5 µL/g body weight PBS (Gibco, Darmstadt, Germany). Loss of body weight was monitored every 8 h as an index of disease progression. Animals were excluded from the experiment as soon as the weight loss exceeded 20 % of the initial body weight or if animals showed a severely impaired general state of health, e.g. apathy and horrent coat. Mice were sacrificed after the indicated time point. Serum and organs were collected for further analyses and stored at - 80 °C.

3.2.4.3 ANTIBIOTIC TREATMENT

Within the age of 8-11 weeks, gender-matched *Atg16l1^{fl/fl}* and *Atg16l1LysM* mice (n=5 per genotype) were treated for 4 weeks with an antibiotic cocktail of 1 g/L ampicillin (Sigma Aldrich, Munich, Germany), 0.5 g/L vancomycin (Hikma Pharma GmbH, Gräfelfing, Germany), 1 g/L neomycin (Sigma Aldrich, Munich, Germany) and 1 g/L metronidazole (Sigma Aldrich,

Munich, Germany) diluted in sterile filtered drinking water [215]. Neomycin was removed from the antibiotic cocktail at day 7. Antibiotic water was refreshed every 4-5 days due to the half-life of the diluted antibiotics. Control animals (n = 3 per genotype) obtained untreated drinking water. Body weight was recorded daily. Feces were collected on day 0, 1, 3, 5, 7, 14, 21 and 28 to analyze the composition and decrease of microbiota (see chapter 3.2.5). Collected feces were stored at - 80 °C. After 4 weeks mice were sacrificed. Serum and organs were collected and stored at - 80 °C for further analysis.

3.2.4.4 PREVENTIVE ANTIBIOTIC TREATMENT

Atg16l1^{fl/fl} and *Atg16l1^{LysM}* breeding pairs and offsprings were treated with a broad-spectrum antibiotic cocktail consisting of 1 g/L ampicillin (Sigma Aldrich, Munich, Germany), 0.5 g/L vancomycin (Hikma Pharma GmbH, Gräfelfing, Germany), 200 mg/L Ciprofloxacin (Fresenius Kabi Deutschland GmbH, Bad Homburg, Germany) and 1 g/L metronidazole (Sigma Aldrich, Munich, Germany) supplemented with 2 % (w/v) sucrose (Roth, Karlsruhe, Germany) [216]. The control groups received solely 2 % (w/v) sucrose in the drinking water. Drinking water was refreshed every third day. Antibiotic treatment persisted until weaning of the offsprings. Offsprings were sacrificed at the age of 3-4 weeks. Serum, organs and feces were collected and stored at - 80 °C for further analysis.

3.2.5 BACTERIAL DNA EXTRACTION FROM MOUSE FECES

Bacterial DNA extraction from mouse feces was performed applying a modified protocol of the PowerSoil® DNA Isolation Kit (MoBio, Carlsbad, USA). Feces were pulverized with a mortar, transferred into PowerBead Tubes and incubated in 60 µL Solution C1 and 20 µL Proteinase K for 2 h at 50 °C in a heating block rotating at 400 U/min. Further extraction steps were performed according to manufacturer's instruction. Extracted DNA was quantified using the Quant-iT PicoGreen dsDNA Assay Kit (Invitrogen, Darmstadt, Germany).

3.2.6 16SRDNA SEQUENCING FOR BACTERIAL IDENTIFICATION

Sequencing, preparation and amplification of the bacterial DNA was performed in our in-house sequencing platform. After isolation of the bacterial DNA, the variable regions V3 and V4 of the *16S rRNA* gene were amplified using dual indexed primers. The forward primer consisted of a 5' illumina adaptor (5'-AATGATACGGCGACCACCGAGATCTACAC-3'), an index (5'-XXXXXXXX-3'), a forward primer pad (5'-TATGGTAATT-3'), a linker (5'-GT-3') and a *16S rRNA* specific primer (5'-GTGCCAGCMGCCGCGGTAA-3'). The reverse primer included the reverse complement of the 3' illumina adaptor (5'-CAAGCAGAAGACGGCATACGAGAT-3'), an index (5'-XXXXXXXXXXXX-3'), a reverse primer pad (5'-AGTCAGTCAG-3'), a linker (5'-CC-3')

and the *16S rRNA* specific reverse primer (5'-GGACTACHVGGGTWTCTAAT-3'). Amplification was performed in duplicates with the Phusion HotStart Flex 2 Master Mix (New England Biolabs GmbH, Frankfurt a.M., Germany) using the cycling conditions listed in Table 3 in a GeneAmp PCR System 9700 (Applied Biosystems, Darmstadt, Germany).

TABLE 3: PCR PROGRAM FOR THE AMPLIFICATION OF THE VARIABLE REGIONS V3 AND V4 OF THE *16S rRNA* GENE

Step	Temperature	Duration	Cycles
Denaturation	98 °C	3 min	1
Denaturation	98 °C	10 sec	30
Annealing	50 °C	30 sec	
Elongation	72 °C	30 sec	
Extension	72 °C	10 min	1

PCR products were run on a 2 % agarose gel to assess the amplicon size and amplification performance. Quantities of the amplicons were normalized with the SequelPrep™ Normalization Plate Kit (Invitrogen, Darmstadt, Germany). Purification of the specific amplicon bands was performed using the QIAquick Gel Extraction Kit (Qiagen, Hilden, Germany) and concentration of the purified PCR products was measured with the Quant-iT™ PicoGreen® dsDNA Assay Kit (Invitrogen). Equal amount of the PCR products was mixed in a single tube and sequenced using the MiSeq sequencer (Illumina, San Diego, USA) and the MiSeq Reagent Kit v3 (Illumina, San Diego, USA) for 2 x 300 bp, which allowed the generation of paired end reads with overlapping regions.

3.2.7 SEQUENCE ANALYSIS FOR TAXONOMIC CLASSIFICATION OF IDENTIFIED BACTERIA

Sequence analysis was kindly performed by Dr. Ateequr Rehman. In brief, sequenced reads were primarily processed for quality control using the software MOTHUR (http://www.mothur.org/wiki/Download_mothur, version 1.32.1). Forward and reverse reads were assembled to form contigs. In the present study, sequences with more than 450 bases in length as well as sequences having any ambiguous base or more than six homopolymers were excluded from the downstream analysis. Sequences passing these quality control parameters were subjected to the alignment against the *16S rRNA* gene of the Silva reference data base [217] obtained from the MOTHUR website. Sequences, which were not aligned to the target region of the *16S rRNA* gene, were discarded from the analysis. Furthermore, chimeric sequences were detected with the Uchime algorithm as implemented in MOTHUR and were removed from the analysis. Classification of the sequences was achieved using MOTHUR curated green genes training sets taxonomy database (release August 2013, containing 202,421 bacterial and archaeal sequences). Sequence classification

was performed in MOTHUR with the following parameters: method = Wang, k-mer size = 8, iteration = 100 and cutoff = 60. Sequences deemed to be originated from eukaryotes, chloroplasts or mitochondria were excluded from subsequent phylotype based analysis. Good quality classified bacterial sequences were binned in genus level phylotypes (label = 1). In order to display shared and unique phylotypes in samples and groups, MOTHUR based *make.shared* command was implemented to generate a count table. This table contained the number of sequences of each phylotype in a given sample. Diversity of the microbial populations was assessed using the non-parametric Shannon's index.

3.2.8 ISOLATION AND CULTIVATION OF CELLS

3.2.8.1 ISOLATION OF LAMINA PROPRIA AND INTESTINAL EPITHELIAL FRACTIONS FROM THE SMALL INTESTINE

Lamina propria cells and intestinal epithelial cells were isolated using the Lamina Propria Dissociation Kit for mouse (Miltenyi BioTech, Bergisch Gladbach, Germany). Preparation of the small intestine and isolation of the two distinct cell fractions was performed according to the manufacturer's protocol. In brief, intestinal epithelial cells were isolated by disruption of the structural integrity of the epithelium using ethylenediaminetetraacetic acid (EDTA) and dithiothreitol (DTT). Beside mechanical disruption the remaining lamina propria tissue was further enzymatically dissociated into a single cell suspension using collagenase.

3.2.8.2 MAGNETIC-ACTIVATED CELL SORTING (MACS) FOR ISOLATION OF CD11B⁺ CELLS DERIVED FROM THE LAMINA PROPRIA

The positive selection of CD11b⁺ from the lamina propria fraction of the small intestine was performed using CD11b MicroBeads (human and mouse) from Miltenyi BioTec (Bergisch Gladbach, Germany). Briefly, the principle of this method relies on a specific separation of CD11b⁺ cells by magnetic beads labelled with antibodies against CD11b. By loading the cell suspension in a magnetic field, the magnetically labeled CD11b⁺ cells were retained in the magnetic column and can be separately eluted. In this study, a total number of 0.4-1 x 10⁶ cells were used for the isolation of CD11b⁺ cells using a 30 µm pre-separation filter followed by a magnetic MS column. To increase the purity of isolated CD11b⁺ cells the labeled fraction was again passed over a second magnetic MS column. Purity of isolated CD11b⁺ cells was analyzed by flow cytometry (see 3.2.19).

3.2.8.3 ISOLATION AND DIFFERENTIATION OF BONE MARROW-DERIVED MACROPHAGES

All *ex vivo* experiments were performed with littermates at the age of 7-26 weeks. Mice were sacrificed by cervical dislocation. Femur and tibia were removed and temporarily stored in ice-cold DMEM medium (Invitrogen, Darmstadt, Germany). Bones were opened under sterile conditions. Bone marrow was flushed out with ice-cold BMDM medium (see chapter 8.1) using a syringe and a 26G needle. After disaggregation of the cells by gently pipetting several times within a 50 mL tube, cells were additionally passed through a 70 μ m cell strainer. Finally, bone marrow cells were placed in a 15 cm petri dish in a total volume of 30 mL BMDM medium supplemented with 20 ng/mL macrophage colony-stimulating factor (mCSF) and cultured at 37 °C with 5 % (w/v) CO₂ and 100 % (w/v) humidity for seven days. Additional 15 mL BMDM medium supplemented with 20 ng/mL mCSF were added on day four. As differentiated bone marrow-derived macrophages (BMDMs) attach to the petri dish undifferentiated cells were gently removed with warm PBS (Gibco, Darmstadt, Germany) and further cultivated in a 10 mL petri dish in BMDM medium. On day seven, differentiated BMDMs were scraped off with ice-cold PBS and transferred into a 50 mL tube. After centrifugation at 300 x g for 10 min at 4 °C, the supernatant was discarded and cells were resuspended in 5 mL BMDM medium. Cells were counted using an automatic cell counter (Cellometer Auto T4 Plus, PeqLab, Erlangen, Germany) and plated on either 6-well plates (1 x 10⁶ cells/well), 12-well plates (0.5 x 10⁶ cells/well), 96-well flat-bottom plates (2.5-4 x 10⁴ cells/well) or 10 mL petri dishes (3-5 x 10⁶ cells/well).

3.2.8.4 MACS FOR ISOLATION OF HEMATOPOIETIC STEM CELLS FROM SPLEEN

Spleens of *Atg16l1^{fl/fl}* and *Atg16l1^{LysM}* mice (n=5) were collected and temporarily stored in DMEM medium (Invitrogen, Darmstadt, Germany) on ice. To obtain cell suspensions each spleen was carefully grinded through a 40 μ m cell strainer and splenocytes were counted as described in chapter 3.2.8.3. Differentiated splenocytes were removed using the Lineage Cell Depletion kit for mouse (Miltenyi BioTec, Bergisch Gladbach, Germany). Lineage negative (lin⁻) cells were stained for specific stem cell markers and analyzed by flow cytometry (see 3.2.19).

3.2.9 PROTEIN EXTRACTION AND PROTEIN ASSAY

0.5-1 x 10⁶ BMDMs were washed once with PBS (Gibco, Darmstadt, Germany) and lysed with 30-40 μ L 1 x denaturing lysis buffer (DLB) freshly supplemented with protease and phosphatase inhibitor (Thermo Scientific, Darmstadt, Germany). Cell lysis was performed by heating the samples at 95 °C for 5 min followed by sonication for 5 sec. Lysates were centrifuged at 16,000 x g for 10 min at 4 °C and the protein containing supernatant was

transferred into a new 1.5 mL tube. Protein concentrations were determined using DC™ Protein Assay (Bio-Rad, Munich, Germany) according to the manufacturer's protocol. Briefly, the colorimetric assay is based on the Lowry method [218]. Hereby, proteins first react with copper in an alkaline medium following an immediate reduction by Folin reagent by the copper-treated-proteins. Absorbance was measured at 750 nm using the microplate reader Infinite M200 Pro (Tecan, Männedorf, Switzerland) and the associated software i-control™ 1.9 (Tecan, Männedorf, Switzerland). Protein lysates were stored at -80 °C.

3.2.10 SODIUM DODECYL SULFATE POLYACRYLAMIDE GEL ELECTROPHORESIS

For protein analysis, 10 - 15 µg of total protein was used. Lysates were supplemented with 5 X SDS loading dye and heated at 95 °C for 5 min. Proteins were separated using a 3 % stacking gel and a 10 %, 12 % or 15 % separation gel (Table 4). Electrophoresis was performed in 1 x Tris/Glycine/SDS (TGS) buffer and carried out at 15 mA for 30 min and at 30 mA for additional 60 min.

TABLE 4: COMPOSITION OF STACKING AND SEPARATION GEL FOR PROTEIN SEPARATION BY SDS-PAGE

Components of separation gel	10 % separation gel	12 % separation gel	15 % separation gel	Components of stacking gel	3 % stacking gel
Distilled water	4.15 mL	3.5 mL	2.5 mL	Distilled water	1.95 mL
Separation buffer	2.5 mL	2.5 mL	2.5 mL	Stacking buffer	0.75 mL
30 % Bis-acrylamide (35.7:1)	3.35 mL	4 mL	5 mL	30 % Bis-acrylamide (35.7:1)	0.3 mL
TEMED	10 µL			TEMED	3 µL
10 % (w/v) APS	100 µL			10 % (w/v) APS	30 µL

3.2.11 WESTERN BLOT AND PROTEIN DETECTION

For further analysis, separated proteins were transferred onto a polyvinylidene difluoride (PVDF) membrane using a semi-dry immunoblotting technique with a discontinuous buffer system of one cathode buffer and two anode buffers at 0.1 A for 45 min. After blocking the

membrane for 1 h at room temperature with 5 % (w/v) blotting grade blocker (non-fat dry milk) from Bio-Rad (Munich, Germany) or bovine serum albumin (BSA) in 1 X Tris-buffered saline (TBS) supplemented with 0.1 % (v/v) Tween 20 (TTBS), membranes were incubated with specific primary antibodies over night at 4 °C (Table 5).

TABLE 5: LIST OF PRIMARY ANTIBODIES USED FOR IMMUNOBLOTTING

Primary antibody	Host species	Working dilution	Company	Article number
A20	rabbit	1:500	Cell Signaling Technology (Leiden, The Netherlands)	#5630
ATG16L1	mouse	1:500	MBL International (Woburn, USA)	M150-3
CYLD	rabbit	1:500	Cell Signaling Technology (Leiden, The Netherlands)	#8462
LC3BI/II	rabbit	1:1,000	Novus Biologicals (Cambridge, United Kingdom)	NB100-2331
MSR1	goat	1:1,000	R&D Systems (Abingdon, United Kingdom)	AF1797
MyD88	rabbit	1:500	Cell Signaling Technology (Leiden, The Netherlands)	#4283
p38	rabbit	1:1,000	Cell Signaling Technology (Leiden, The Netherlands)	#9212
p65	rabbit	1:1,000	Cell Signaling Technology (Leiden, The Netherlands)	#3031
p62	guinea pig	1:1,000	Progen Biotechnik (Heidelberg, Germany)	GP62-C
phospho-ERK1/2	rabbit	1:1,000	Cell Signaling Technology (Leiden, The Netherlands)	#4370
phospho-IκBα	rabbit	1:500	Cell Signaling Technology (Leiden, The Netherlands)	#2859
phospho-p38	rabbit	1:1,000	Cell Signaling Technology (Leiden, The Netherlands)	#9211
phosho-p65	rabbit	1:1,000	Cell Signaling Technology (Leiden, The Netherlands)	#3031
pro-IL1β	goat	1:500	R&D Systems (Abingdon, United Kingdom)	AF401-NA
RIP1	rabbit	1:1,000	Cell Signaling Technology (Leiden, The Netherlands)	#3493
TLR4	mouse	1:250	Novus Biologicals (Cambridge, United Kingdom)	NB100-56566
TRAF6	rabbit	1:500	Santa Cruz Biotechnology (Heidelberg, Germany)	sc-7221

Primary antibody	Host species	Working dilution	Company	Article number
TRIF	rabbit	1:500	Abcam (Cambridge, United Kingdom)	ab13810
β -Actin	mouse	1:10,000	Sigma (Munich, Germany)	A-5441

Membranes were washed with TTBS and probed with appropriate horseradish peroxidase (HRP)-conjugated secondary antibodies for 1 h at room temperature (Table 6).

TABLE 6: LIST OF HORSE RADISH PEROXIDASE (HRP)-CONJUGATED SECONDARY ANTIBODIES USED FOR IMMUNOBLOTTING

Secondary antibody	Host species	Working dilution	Company	Article number
Goat-HRP	donkey	1:3,000	Abcam (Cambridge, United Kingdom)	ab6884
Guinea pig-HRP	rabbit	1:3,000	Abcam (Cambridge, United Kingdom)	ab 6771
Mouse-HRP	sheep	1:3,000	GE Healthcare (Hamburg, Germany)	NA931V
Rabbit-HRP	sheep	1:3,000	GE Healthcare (Hamburg, Germany)	NA934V

Following additional washing steps with TTBS, protein bands were visualized by chemiluminescence with ECL™ Western Blotting Detection Reagents (GE Healthcare, Hamburg, Germany) or Pierce ECL™ Plus Western Blotting Substrate (Thermo Scientific, Darmstadt, Germany) and X-Ray films (GE Healthcare, Hamburg, Germany). Films were developed using the automatic developer machine Curix 60 (Agfa, Mortsels, Belgium). Stripping was performed in 50 mL stripping buffer supplemented with 0.6 % (v/v) β -mercaptoethanol for 20-30 min at 55 °C. Alternatively, HRP inactivation was achieved by incubation with 15 % H₂O₂ for 1 h at room temperature.

3.2.12 TOTAL RNA ISOLATION

RNA extracts of tissues and BMDMs were prepared using the RNeasy kit (Qiagen, Hilden, Germany) following manufacturer's instructions. Liquid nitrogen frozen tissues were first pulverized with a mortar and approximately 50 mg of the particular tissues were lysed in

350 µL RLT buffer. Alternatively, BMDMs were washed once with warm PBS (Gibco, Darmstadt, Germany) and directly lysed in RLT buffer (Qiagen, Hilden, Germany). Homogenization of lysates was performed using the QIAshredder system (Qiagen, Hilden, Germany). RNA concentrations were measured using the NanoDrop spectrometer ND1000 (PeqLab, Erlangen, Germany).

3.2.13 REVERSE TRANSCRIPTION (RT)-PCR

For further analysis, 200 – 1000 ng total RNA was transcribed into complementary DNA (cDNA) by reverse transcription. Therefore, the Maxima H Minus First Strand cDNA Synthesis kit (Thermo Scientific, Darmstadt, Germany) was used according to the manufacturer's protocol.

3.2.14 SEMI-QUANTITATIVE END-POINT PCR

Amplification of the targeted cDNA was performed by semi-quantitative endpoint PCR. A standard PCR reaction was set up in a final volume of 20 µl. Table 7 contains the pipetting scheme for the reaction.

TABLE 7: PIPETTING SCHEME FOR STANDARD PCR REACTION

	µL
PCR H ₂ O	12.5
5 x GoTaq Puffer	4.0
dNTPs (10 µM each)	0.5
GoTaq Polymerase	0.5
Primer-Mix (10 µM each)	0.5
cDNA	2.0

Exon-exon spanning primer pairs were designed to prevent amplification of genomic DNA. The following primer pairs were used for semi-quantitative end-point PCR (Table 8).

TABLE 8: LIST OF PRIMERS USED FOR THE SEMI-QUANTITATIVE END-POINT PCR

Gene	Primer sequence forward (5' → 3')	Primer sequence reverse (5' → 3')
<i>Gapdh</i>	CCGGGGCTGGCATTGCTCTCA	CTTGCTCAGTGTCTTGGCTGGGG
<i>iNOS</i>	GTCAACTGCAAGAGAACGGA	GCCCCAGTTTTTGATCCTCA

The used standard PCR program is shown in Table 9. In case of *iNOS* amplification a Touchdown PCR was performed to avoid the amplification of non-specific sequences (Table 10).

TABLE 9: STANDARD PCR PROGRAM

Cycles	Time	Temp [°C]
1	4 min	95
30	30 sec	95
	30 sec	54
	45 sec	72
1	5 min	72

TABLE 10: TOUCHDOWN PCR PROGRAM

Cycles	Time	Temp [°C]
1	4 min	95
10	30 sec	95
	30 sec	65-55 (reduce 1 °C each cycle)
	30 sec	72
35	30 sec	95
	30 sec	55
	30 sec	72
1	5 min	72

3.2.15 QUANTITATIVE REAL-TIME PCR (qPCR)

Amplification and simultaneous quantification of the targeted cDNA was achieved by quantitative real-time PCR (qPCR). Specific exon-exon spanning primers were designed based on transcript models of the NCBI database (<http://www.ncbi.nlm.nih.gov/nuccore/>, July 2014) with a length of 20-25 bases, an optimal annealing temperature of 60 °C and an amplicon size of 200-400 bp (Table 11). Primers were synthesized by Microsynth (Lindau, Germany).

TABLE 11: LIST OF PRIMERS USED FOR THE QUANTITATIVE REAL-TIME PCR

Gene	Primer sequence forward (5' → 3')	Primer sequence reverse (5' → 3')
<i>A20</i>	CGATACACGCTGGAGATGTT	CTGATGCCATTTTGACCAAG
<i>Asc</i>	AACTGCGAGAAGGCTATGGG	TGGTCCACAAAGTGTCTGT
<i>Cd11b</i>	GTTTCTACTGTCCCCAGCA	TTTTTGTCTCTCCATTTCAGC
<i>Cd11c</i>	GTCTCCAAGTTGCTCAGAGCCTGCT	TGGTGGCATCTTGCCGAGCTC
<i>Cd19</i>	ACCAGTTGGCAGGATGATGG	CCCATGCTGGTTCTAGGTCG
<i>Cd3e</i>	AAGTAATGAGCTGGCTGCGT	TCGTCACTGTCTAGAGGGCA
<i>Cd4</i>	CGTGCTGGGTGGCTCCTTCG	AGAGCAGAAGGCCGGAGGCA
<i>Cxcl1</i>	GCTGGGATTCACCTCAAGAA	TGGGGACACCTT TTAGCA TC
<i>Gapdh</i>	CCGGGGCTGGCATTGCTCTCA	CTTGCTCAGTGTCTTGGCTGGGG
<i>Ifng</i>	ACTGGCAAAGGATGGTGACA	TCATTGAATGCTTGGCGCTG
<i>Il10</i>	TGCTATGCTGCCTGCTCTTA	TTTTCACAGGGGAGAAATCG
<i>Il1a</i>	CGCTTGAGTCGGCAAAGAAAT	AAGGTGCTGATCTGGGTTGG
<i>Il1b</i>	GGCTGTCTGATGAGAGCAT	TGTTTATCTCGGAGCCTGTA
<i>Il2</i>	GGAACCTGAAACTCCCCAGG	TGTGTTGTCAGAGCCCTTTAGT
<i>Il4</i>	TCACTGACGGCACAGAGCTA	CTGTGGTGTCTTTCGTTGCTG
<i>Il6</i>	GAC AAC TTT GGC ATT GTG G	ATG CAG GGA TGA TGT TCT G
<i>Nlrp3</i>	AGCCAGAGTGGAAATGACACG	CGTGTAGCGACTGTTGAGGT
<i>pro-Casp1</i>	AGAAACGCCATGGCTGACAA	TCCTGCCAGGTAGCAGTCTT

Gene	Primer sequence forward (5'→3')	Primer sequence reverse (5'→3')
<i>S100a8</i>	GTCCTCAGTTTGTGCAGAATATAAA	GCCAGAAGCTCTGCTACTCC
<i>S100a9</i>	CTGTGACTCTTTAGCCTTGAGCA	GTTGCCAACTGTGCTTCCAC
<i>Tnfa</i>	TCACACTCAGATCATCTTCTC	AGACTCCTCCCAGGTATATG

All qPCR experiments were carried out on the 7900HT Fast Real Time PCR System (Applied Biosystems, Darmstadt, Germany). Samples were run in duplicates on 384-well plates. The PCR mixture contained 5-10 ng cDNA and 0.5 µL of specific primer pairs (5 µM each) or 0.5 µL of the specific TaqMan® gene expression assay (Table 12). Standardized PCR program was performed according to the SYBR® Select Master Mix protocol (Applied Biosystems, Darmstadt, Germany) or TaqMan Gene Expression Master Mix protocol (Applied Biosystems, Darmstadt, Germany). Cycle threshold (Ct) values of the target genes were normalized to the respective gene expression of *Gapdh* or *b-Actin*.

TABLE 12: LIST OF TAQMAN ASSAYS USED FOR QUANTITATIVE REAL-TIME PCR

Gene	Company	TaqMan Assay ID
<i>Actb</i>	Life Technologies (Darmstadt, Germany)	00607939
<i>Atg16l1</i>	Life Technologies (Darmstadt, Germany)	00513085
<i>Gapdh</i>	Life Technologies (Darmstadt, Germany)	99999915
<i>Ifnb</i>	Life Technologies (Darmstadt, Germany)	439552
<i>Ifng</i>	Life Technologies (Darmstadt, Germany)	1168134
<i>Il1b</i>	Life Technologies (Darmstadt, Germany)	01336189
<i>Il18</i>	Life Technologies (Darmstadt, Germany)	00434225
<i>Mpo</i>	Life Technologies (Darmstadt, Germany)	01298424

For quantification of bacteria in murine tissues, detection and amplification of eukaryotic bacterial DNA was performed by a designed TaqMan Assay listed in Table 13.

TABLE 13: DESIGNED TAQMAN ASSAY USED FOR EUKARYOTIC BACTERIAL DNA QUANTIFICATION BY QUANTITATIVE REAL-TIME PCR

Probe sequence	Primer sequence for (5'→3')	Primer sequence rev (5'→3')
TGCCAGCAGCCGCGTAATAC	CCTACGGGNGGCWGCAG	GGACTACHVGGGTWTCTAAT

3.2.16 IMMUNOFLUORESCENCE

BMDMs were seeded on cover slips overnight. Following a washing step with PBS, cells were fixed in 4 % (w/v) paraformaldehyde for 30 min at room temperature. Cells were washed three times with PBS and permeabilized for 3 min at room temperature using 1 % (v/v) Triton X-100 in PBS supplemented with 5 % (w/v) BSA. Unspecific binding sites were blocked with 5 % (v/v) goat serum for at least 60 min at room temperature. Incubation with the primary antibody against p62 (also see Table 5) was performed using a dilution of 1:500 over night at 4 °C. Following three washing steps with PBS, incubation with the second antibody goat anti-guinea pig conjugated with Alexa Fluor-488 (Life Technologies, Darmstadt, Germany, #A-11073) for 45 min at room temperature. Cells were washed for three times with PBS following a washing step with aqua dest and subsequently embedded in mounting medium (Roth, Karlsruhe, Germany). Stainings were analyzed using the confocal laser scanning microscope TCS SP5 (Leica, Wetzlar, Germany) and the appropriate software Leica Application Suite Advanced Fluorescence (Leica, Wetzlar, Germany).

3.2.17 IMMUNOHISTOCHEMISTRY

3.2.17.1 TISSUE PROCESSING

Murine tissues were directly fixed in 10 % (w/v) formalin for at least 24 h at 4 °C. In terms of bones a decalcification step was performed in cooperation with the Prof. Wolfram Klapper's laboratory (Department of Pathology, Haematopathology Section and Lymph Node Registry, University Hospital Schleswig-Holstein, Campus Kiel, Germany). Dehydration was achieved by incubation in ascending ethanol and xylene series. Tissues were embedded in paraffin and dissected in 3.5 - 4.5 µm sections using the RM2255 microtome (Leica, Wetzlar, Germany).

3.2.17.2 HEMATOXYLIN AND EOSIN (H&E) STAINING

Samples were rehydrated in decreasing xylene and ethanol series following additional washing steps with distilled water. Slides were stained for 2 - 5 min in hematoxylin. Nuclei were blue-up by incubation for approximately 10 min under running water. Counterstaining of the cytoplasm was performed using 1 % (v/v) eosin solution for 2 min. For further analysis, slides were again dehydrated and embedded in Roti-Histokitt mounting medium (Roth, Karlsruhe, Germany). Slides were analyzed with a transmitted light microscope (Axio Imager Z1, ZEISS, Oberkochen, Germany) and the AxioVision Rel 4.9 software (ZEISS, Oberkochen, Germany).

3.2.17.3 3,3'-DIAMINOBENZIDINE (DAB) STAINING

Rehydration of the slides and slide analysis was performed as described in chapter 3.2.17.2. Antigen retrieval was achieved by boiling slides for up to 20 min in citrate buffer (pH 6.0). Blocking of unspecific binding sites and inactivation of naturally occurring peroxidases was achieved using 5 % (v/v) goat serum in PBS and 3 % hydrogen peroxide treatment, respectively. Incubation times were individually adapted with respect to the primary antibody. Antibody incubation and DAB staining was performed according to the manufacturer's protocol of the Vectastain Elite ABC Kit (Vector Labs, Peterborough, United Kingdom). In brief, primary antibody signaling was maximized by incubation with a biotinylated second antibody. Colorimetric reaction of 3,3'-Diaminobenzidine (DAB) was achieved by a second incubation step using a horseradish peroxidase-conjugated streptavidin antibody, which allows DAB to get oxidized and gives a dark-brown color. Used antibodies and working dilutions are listed in Table 14.

TABLE 14: LIST OF ANTIBODIES USED FOR IMMUNOHISTOCHEMISTRY

Antibody	Working dilution	Company	Article number
Ki67	1:500	BD Biosciences (Heidelberg, Germany)	556003
IBA-1	1:1000	Abcam (Cambridge, United Kingdom)	ab107159
MPO	not diluted	GeneTex (Irvine, USA)	Gtx15484
p62	1:500	Progen Biotechnik (Heidelberg, Germany)	GP62-C

3.2.17.4 TERMINAL DEOXYNUCLEOTIDYL TRANSFERASE dUTP NICK END LABELING (TUNEL)

Slides were rehydrated as described in chapter 3.2.17.2. Apoptotic cells were stained using the ApopTag® Plus Peroxidase *In Situ* Apoptosis Detection Kit (Merck Millipore, Darmstadt, Germany) according to the manufacturer's protocol. In brief, terminal deoxynucleotidyl transferase dUTP nick end labeling (TUNEL) is an enzymatic reaction to detect apoptotic cells by labeling terminal ends of DNA fragments. Stained slides were analyzed as described in chapter 3.2.17.2.

3.2.18 IMMUNOASSAYS

3.2.18.1 ENZYME LINKED IMMUNOSORBENT ASSAY (ELISA)

Detection of cytokine and chemokine levels in serum or cell culture supernatants was achieved with enzyme linked immunosorbent assays (ELISA). All ELISA used in this study were performed according to the manufacturer's protocol (Table 15). Absorbance was measured using the microplate reader Infinite M200 Pro (Tecan, Männedorf, Switzerland) and the associated software i-control™ 1.9 (Tecan, Männedorf, Switzerland).

TABLE 15: LIST OF ANTIBODY PAIRS USED FOR ENZYME LINKED IMMUNOSORBENT ASSAYS

Cytokine	Company	Article number
murine CXCL1	R&D Systems (Abingdon, United Kingdom)	DY453
murine IFN β	PBL Assay Science (New Jersey, USA)	#42400
murine IL18	MBL International (Woburn, USA)	CMC3013

3.2.18.2 MULTIPLEX TECHNOLOGY

Similar to the ELISA technique the multiplex technology is an antibody-based detection method for cytokines, chemokines and other inflammatory mediators. In brief, specific capture antibodies are coupled to magnetic beads. Fluorochrome-labeled detection antibodies enable the analysis by flow cytometry. In this study, the Bio-Plex Pro™ Mouse Cytokine 23-plex Assay (Bio-Rad, Munich, Germany) was used and measurement was performed in cooperation with Bioglobe Service (Hamburg, Germany). Median of the particular cytokine and chemokine concentration was calculated and values were z-score normalized. Results were depicted in heat-maps using the software Spotfire Integromics Biomarker Discovery 5.5 (Tibco Software Inc., Palo Alto, USA).

3.2.19 FLOW CYTOMETRY ANALYSIS

For all measurements, 10,000 cells were analyzed with a FACSCalibur™ (BD Biosciences, Heidelberg, Germany) and the associated software CellQuest™ Pro (Version 5.2, BD Biosciences, Heidelberg, Germany). In all experiments, dead cells and cell debris were excluded using by gating in forward scatter vs. sideward scatter dot plots (R1, see also Figure 4-11). Used fluorochrome-conjugated antibodies and working dilutions as well as isotype controls are listed in Table 16 and Table 17, respectively.

TABLE 16: LIST OF USED FLUOROCHROME-LABELED ANTIBODIES FOR FLOW CYTOMETRY ANALYSIS

Antibody	Fluorochrome	Isotype	Working dilution	Company	Article number
CD11b	APC	Rat IgG2b κ	1:100	eBioscience (Frankfurt a. M., Gemany)	17-0112
CD11b	PE	Rat IgG2b	1:100	eBioscience (Frankfurt a. M., Gemany)	12-0112
CD11c	APC	Armenian hamster IgG	1:8	eBioscience (Frankfurt a. M., Gemany)	17-0114
CD14	FITC	Rat IgG2a κ	1:5	eBioscience (Frankfurt a. M., Gemany)	11-0141
CD19	FITC	Rat IgG2a κ	1:4	Immunotools (Friesoythe, Germany)	22220193
CD25	FITC	Rat IgG1	1:6	Immunotools (Friesoythe, Germany)	22150253
CD3	PE	Armenian hamster IgG	1:50	eBioscience (Frankfurt a. M., Gemany)	12-0031
CD95	PE	Armenian hamster IgG2, λ 2	1:6	BD Biosciences (Heidelberg, Germany)	554258
c-Kit	FITC	Rat IgG2b κ	1:10	eBioscience (Frankfurt a. M., Gemany)	11-1171
Ly6G	FITC	Rat IgG2b κ	1:100	eBioscience (Frankfurt a. M., Gemany)	11-5931
MHCII	PE	Rat IgG2b	1:100	eBioscience (Frankfurt a. M., Gemany)	12-5322
Sca-1	PE	Rat IgG2a κ	1:8	eBioscience (Frankfurt a. M., Gemany)	12-5981

TABLE 17: LIST OF ISOTYPE CONTROLS USED FOR FLOW CYTOMETRY ANALYSIS

Isotype control	Fluorochrome	Working dilution	Company	Article number
Armenian hamster IgG	APC	1:8	BD Biosciences (Heidelberg, Germany)	553956
Armenian hamster IgG	PE	1:50	eBioscience (Frankfurt a. M., Gemany)	12-4888
Rat IgG1	FITC	1:6	BioLegend (Fell, Germany)	400406
Rat IgG2a κ	FITC	1:4	BioLegend (Fell, Germany)	400506
Rat IgG2a κ	PE	1:8	BD Biosciences (Heidelberg, Germany)	12-4321

Isotype control	Fluorochrome	Working dilution	Company	Article number
Rat IgG2a κ	FITC	1:6	Immunotools (Friesoythe, Germany)	22225033
Rat IgG2b	PE	1:100	eBioscience (Frankfurt a. M., Germany)	12-4031
Rat IgG2b κ	APC	1:100	eBioscience (Frankfurt a. M., Germany)	17-4031
Rat IgG2b κ	FITC	1:10 or 1:100	eBioscience (Frankfurt a. M., Germany)	11-4031

Used unconjugated primary antibodies and isotype controls as well as fluorochrome-labeled secondary antibodies are listed in Table 18 and Table 19, respectively.

TABLE 18: LIST OF UNCONJUGATED ANTIBODIES AND ISOTYPE CONTROLS FOR FLOW CYTOMETRY ANALYSIS

Primary antibody	Isotype	Working dilution	Company	Article number
TLR4	mouse IgG2b κ	1:40	Abcam (Cambridge, United Kingdom)	ab22048
	mouse IgG2b κ	1:40	MBL International (Woburn, USA)	M077.3

TABLE 19: LIST OF SECONDARY ANTIBODIES FOR FLOW CYTOMETRY ANALYSIS

Secondary antibody	Fluorochrome	Isotype	Working dilution	Company	Article number
Goat anti-mouse	Alexa Fluor 488	Rat IgG2b κ	1:40	Applied Biosystems (Darmstadt, Germany)	A11029

3.2.19.1 FLOW CYTOMETRY ANALYSIS OF TISSUE AND MACROPHAGES

For flow cytometry analysis, 2.5×10^4 cells per well were seeded in a 96-well V-bottom plate, washed with FACS washing buffer (FWB) and centrifuged at $300 \times g$ for 5 min at room temperature. The supernatant was discarded and in case of monocytes and macrophages an unspecific antibody binding was prevented by blocking the Fc-receptor with anti-CD16/32 for 15 min on ice. Incubation with the fluorochrome-labeled antibodies (Table 16), unconjugated primary antibodies (Table 18) and particular isotype control combination (Table 17, Table 18) was performed at 4°C for 1 h. In case of staining with unconjugated primary antibodies, following three additional washing steps incubation with fluorochrome-labeled secondary antibodies was performed for 30 min at 4°C . Cells were washed two times with $100 \mu\text{L}$ FWB and afterwards resuspended in $80 \mu\text{L}$ FWB. Measurement was performed using flow cytometry.

3.2.19.2 FLOW CYTOMETRY ANALYSIS OF BLOOD

Blood was stored in EDTA tubes at room temperature. A mixture of 7 μL of the indicated fluorochrome-labeled antibody combination as well as the particular isotype control was prepared in a 96-well V-bottom plate. Avoiding direct light, 15 μL of the collected blood was added and incubated for 10 min at room temperature. For lysis of the red blood cells, 200 μL 1 x BD FACS Lysing Solution (BD Biosciences, Heidelberg, Germany) was added. Following a 15 min incubation at room temperature, cells were centrifuged at 300 x g for 5 min. The washing step was performed in 150 μL FWB and followed by an additional centrifugation at 300 x g for 5 min. Stained cells were resuspended in 80 μL FWB and directly analyzed by flow cytometry.

3.2.19.3 FITC-DEXTRAN ENDOCYTOSIS ASSAY

Endocytosis assay was performed by incubating 2.5×10^4 cells per well seeded in a 12-well plate with 1 mg/mL FITC-Dextran (Sigma Aldrich, Munich, Germany) for 60 min by 37 °C. Following three washing steps with 1 mL ice-cold PBS (Gibco, Darmstadt, Germany), cells were finally resuspended in 100 μL FWB and analyzed by flow cytometry.

3.2.19.4 RECEPTOR INTERNALIZATION ASSAY

For internalization assays 2.5×10^4 cells per well were seeded in a 12-well plate and grown over night. Cells were stimulated with either 100 ng/mL LPS (*E.coli* F515) or 1 $\mu\text{g}/\text{mL}$ CD95 Ligand (BD Biosciences, Heidelberg, Germany) for the indicated time points. Receptor internalization was stopped by washing with 1 mL ice-cold PBS (Gibco, Darmstadt, Germany). Staining of the remaining receptors at the cell surface was performed as described in chapter 3.2.19.1.

3.2.20 STATISTICAL ANALYSIS

All data were analyzed with a two-tailed unpaired or paired Student's *t*-test [219] using the software GraphPad Prism 5 (GraphPad Software). Data are shown as mean \pm standard deviation (S.D.). Statistical significance of the survival analysis was performed by a log-rank test. A p-value of < 0.05 was considered as significant (*) whereas a p-value of < 0.01 was considered as strongly significant (**), a p-value of < 0.001 as highly significant (***) and a p-value of < 0.0001 as extremely significant (****).

4 RESULTS

4.1 PROOF OF THE TISSUE-SPECIFIC ATG16L1 DELETION IN *ATG16L1**LYSM* MICE

4.1.1 CD11B⁺ LAMINA PROPRIA CELLS

Deletion of floxed genes in the *LysMcre* mouse model is described to be exclusively restricted to myeloid cells [213]. Tissue-specificity in the *Atg16l1LysM* mouse model was determined by isolation of distinct cell populations of the small intestine utilizing the magnetic-activated cell sorting (MACS) technology (Figure 4-1). CD11b⁺ immune cells derived from the lamina propria served as a positive control for the specific *Atg16l1* deletion in myeloid cells. Non-CD11b cells derived from the lamina propria as well as intestinal epithelial cells (IECs) were used as negative controls representing two distinct non-myeloid cell populations.

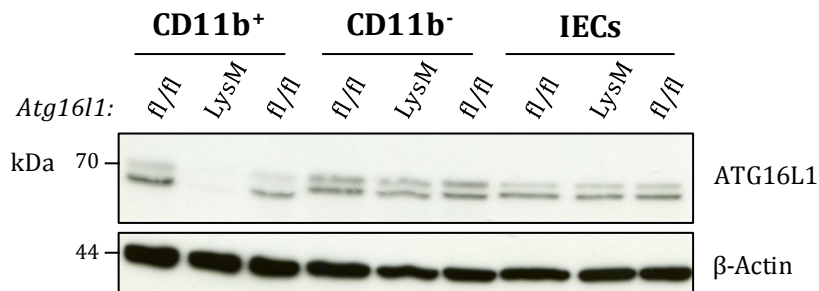


FIGURE 4-1: TISSUE-SPECIFIC KNOCK-OUT OF ATG16L1 IN CD11B⁺ MYELOID CELLS

Small intestine of *Atg16l1^{fl/fl}* and *Atg16l1LysM* mice was dissociated in lamina propria cells and intestinal epithelial cells (IECs) using the Lamina Propria Dissociation Kit for mouse. Additionally, CD11b⁺ and CD11b⁻ cell populations were isolated from the lamina propria fraction by magnetic-activated cell sorting (MACS). Protein levels of ATG16L1 were verified by immunoblot. Levels of β -Actin served as loading control.

Atg16l1^{fl/fl} mice showed a uniform protein expression of ATG16L1 in all three cell types. As expected, the same was observed for CD11b⁻ and IEC populations of *Atg16l1LysM* mice. In contrast, ATG16L1 was completely absent in CD11b⁺ myeloid cells of *Atg16l1LysM* mice demonstrating a specific deletion of *Atg16l1*.

4.1.2 BONE MARROW-DERIVED MACROPHAGES (BMDMs)

Bone marrow-derived macrophages (BMDMs) were used as *ex vivo* model. Due to the fact that bone marrow is the major source of hematopoietic stem cells and therefore harbors all three classes of blood cells (leukocytes, erythrocytes and platelets), efficiency of mCSF-mediated BMDM differentiation was verified on day seven by flow cytometry (Figure 4-2). In this study, differentiated BMDMs were defined by cell surface expression of CD11b. Cells were separated by their size indicated by the forward scatter (FSC) and their granularity

indicated by the sideward scatter (SSC) (Figure 4-2). Cell debris and dead cells were excluded from the analysis by gating (Figure 4-2, left panel, black frame). Independent of the genetic background mCSF-mediated differentiation of bone marrow cells revealed more than 95 % macrophages specified as CD11b⁺ cells (Figure 4-2, right panel) demonstrating an efficient and specific differentiation.

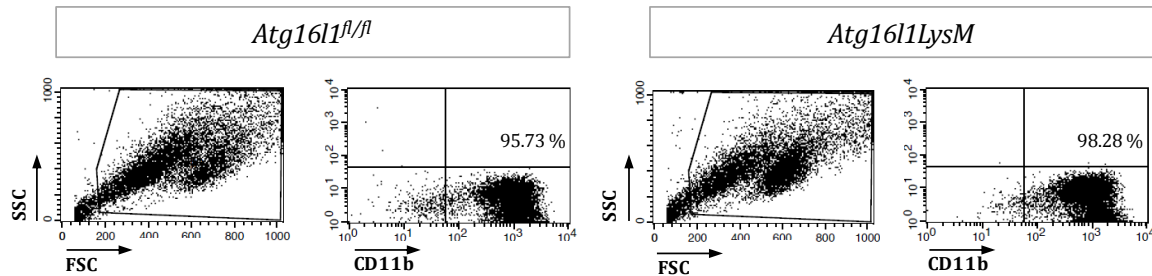


FIGURE 4-2: CD11B EXPRESSION ON EX VIVO DIFFERENTIATED BMDMS OF *ATG16L1^{FL/FL}* AND *ATG16L1^{LYSM}* MICE
 Bone marrow cells of *Atg16l1^{fl/fl}* and *Atg16l1^{LysM}* mice were isolated under sterile conditions and differentiated for at least seven days in presence of 20 ng/mL mCSF into macrophages. Purity of the differentiated BMDMs was verified measuring the macrophage-specific cell surface expression of CD11b by flow cytometry. FSC: forward scatter; SSC: sideward scatter

To verify the efficiency of the conditional knock-out in BMDMs of *Atg16l1^{LysM}* mice expression of *Atg16l1* on RNA (Figure 4-3 A) and protein level (Figure 4-3 B) was evaluated compared to the expression in BMDMs of *Atg16l1^{fl/fl}* littermates. *Atg16l1^{LysM}* BMDMs showed a significantly reduced expression of *Atg16l1* on mRNA level. Similarly, an exceedingly decreased protein level of ATG16L1 was observed in *Atg16l1^{LysM}* BMDMs.

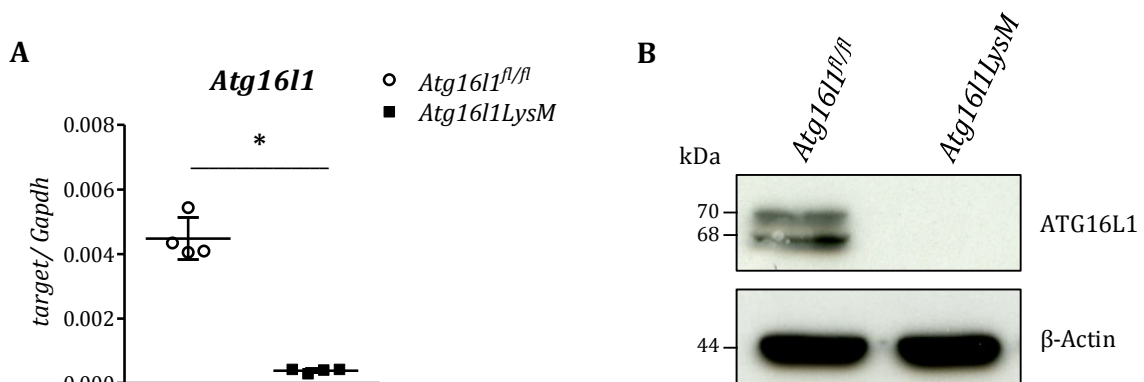


FIGURE 4-3: SUCCESSFUL KNOCK-OUT OF *ATG16L1* IN *ATG16L1^{LYSM}* BMDMS
 RNA and proteins were extracted from untreated BMDMs of *Atg16l1^{fl/fl}* and *Atg16l1^{LysM}* mice (n=4). RNA was transcribed into cDNA and expression of *Atg16l1* was determined using a TaqMan Assay for all murine isoforms of *Atg16l1* (A). TaqMan data represent mean \pm S.D. and statistical significance was evaluated by an unpaired Student's *t*-test. **** *p* < 0.0001 Protein levels of ATG16L1 were analyzed by immunoblot with β -Actin serving as loading control (B).

4.2 LOSS OF *ATG16L1* LEADS TO IMPAIRED AUTOPHAGY IN BONE MARROW-DERIVED MACROPHAGES

ATG16L1 is described to promote the elongation of the autophagosomal isolation membrane and is an essential component within autophagosome formation in yeast and mammalian cells [12, 51]. For this reason, the autophagic flux was biochemically studied in *Atg16l1*-deficient macrophages by determining the conversion of LC3BI to its phosphatidylethanolamine-conjugated form LC3BII (Figure 4-4) which is an established marker for autophagosome formation [220]. Besides investigating basal autophagy in untreated cells, autophagy was induced by nutrient starvation with Hank's Balanced Salt Solution and chemically by stimulation with the mTOR inhibitor rapamycin.

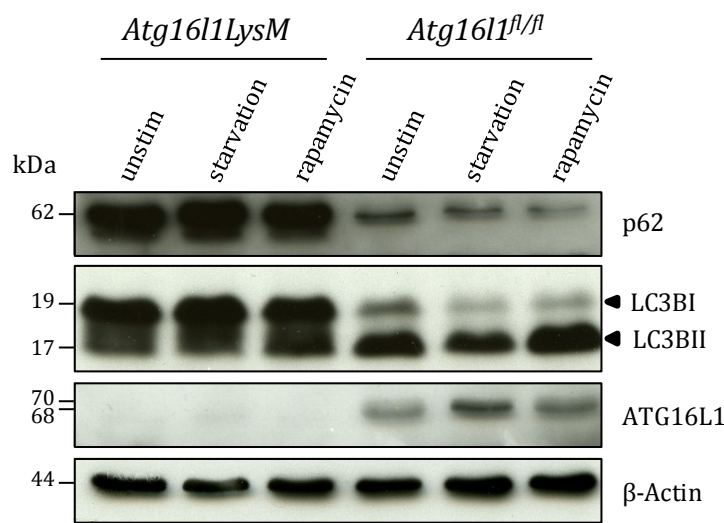


FIGURE 4-4: IMPAIRED AUTOPHAGY IN *ATG16L1LysM* BMDMs

Atg16l1^{fl/fl} and *Atg16l1LysM* BMDMs were nutrient-starved with HBSS for 3 h, stimulated with rapamycin (50 μ g/mL) for 20 min or were left unstimulated. Protein lysates were probed by immunoblot for levels of the indicated proteins. β -Actin served as a loading control. Immunoblot represents results of three independent experiments. HBSS: Hank's Balanced Salt Solution, unstim: unstimulated

Untreated *Atg16l1^{fl/fl}* BMDMs showed both forms of LC3B indicating an intact basal autophagic activity. Induction of autophagy by both, starvation and rapamycin treatment, led to a subsequent decrease in LC3BI and a simultaneously increase in LC3BII. However, in *Atg16l1LysM* BMDMs an accumulation of LC3BI was detected under all three conditions, whereas the lipidation of LC3BII did not occur. Further, lysosomal degradation of the autophagosomal content was monitored by degradation of the selective autophagy receptor sequestosome 1 (Sqstm1, also known as p62) (Figure 4-4). Starvation-induced as well as rapamycin-induced autophagy decreased the protein levels of p62 in *Atg16l1^{fl/fl}* BMDMs. In contrast, already in unstimulated *Atg16l1LysM* macrophages p62 was remarkably accumulated compared to *Atg16l1^{fl/fl}* BMDMs, while induction of autophagy even increased p62 levels in these cells. These results point to a loss of function as a result of the *Atg16l1* deletion.

4.3 CHARACTERIZATION OF THE *ATG16L1LYSM* MOUSE MODEL

4.3.1 *ATG16L1LYSM* MICE DEVELOP A MULTIFACETED SPONTANEOUS PHENOTYPE

After confirmation of the successful tissue-specific knock-out of *Atg16l1*, the basal phenotype of the *Atg16l1LysM* mouse model was studied.

Atg16l1LysM mice were born viable and at the expected Mendelian 1:2:1 ratio (Table 1).

TABLE 20: NUMBER OF MICE OF VARIOUS GENOTYPES OBTAINED BY THE *ATG16L1^{FL}/LysM* INTERCROSS

	<i>Atg16l1^{fl/fl}</i>	<i>Atg16l1^{fl/LysM}</i>	<i>Atg16l1LysM</i>
Observed number of mice	93	181	99
Expected number of mice (ratio 1:2:1)	93.25	186.5	93.25

Analysis of the body weight did not reveal differences between *Atg16l1LysM* and *Atg16l1^{fl/fl}* littermates (Figure 4-5 A).

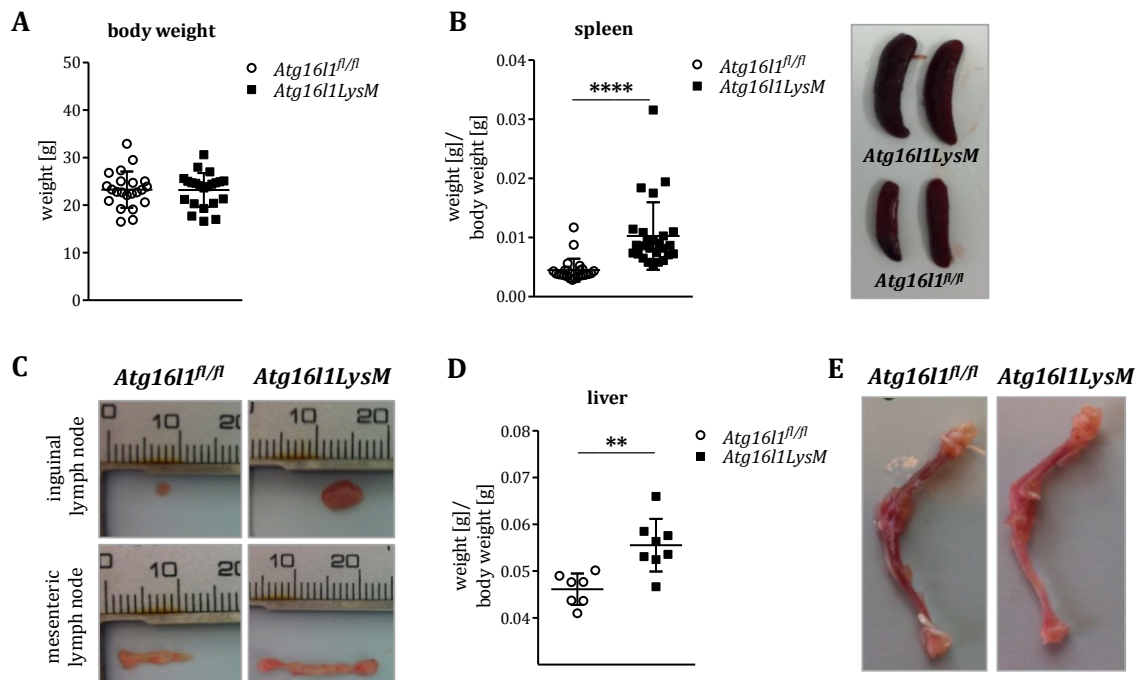


FIGURE 4-5: BASAL PHENOTYPE OF HEMATOPOIETIC ORGANS OF THE *ATG16L1LYSM* MOUSE MODEL

Body weight (A, n=22), spleen weight (B, n=24-26), lymph node size (C), liver weight (D, n=7-8) and bones (E) of *Atg16l1LysM* mice at the age of 7-26 weeks were compared to *Atg16l1^{fl/fl}* littermates. Data are shown as mean \pm S.D. and statistical significance was evaluated with an unpaired Student's *t*-test. ** $p < 0.01$, **** $p < 0.0001$

In contrast, gross examination of the tissues of untreated *Atg16l1LysM* mice showed a spontaneous increase in spleen (splenomegaly, Figure 4-5 B), lymph nodes (lymphadenopathy, Figure 4-5 C) and liver size (hepatomegaly, Figure 4-5 D). Further, the bones were characteristically brighter in *Atg16l1LysM* mice than in *Atg16l1^{fl/fl}* animals (Figure 4-5 E). Quantification of the gastrointestinal tract revealed a significant elongation of the small intestine (Figure 4-6 A) whereas colon length and caecum weight were unaltered (Figure 4-6 B and C).

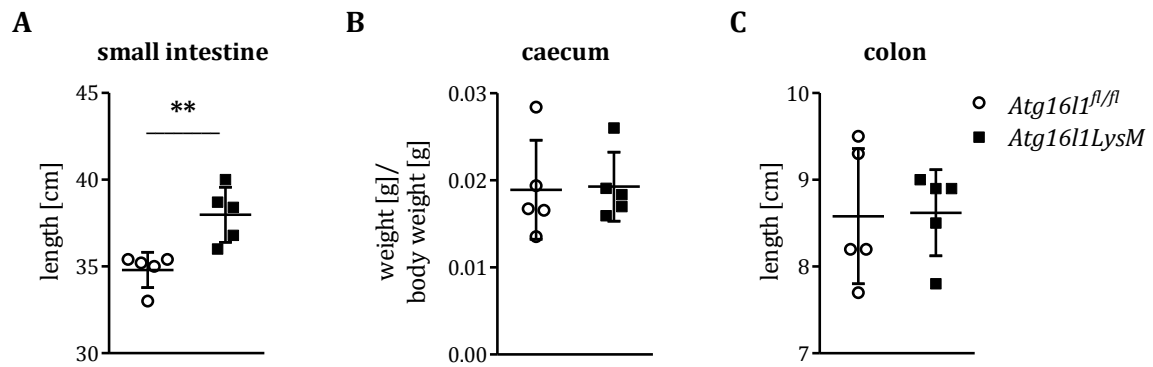


FIGURE 4-6: BASAL PHENOTYPE OF THE GASTROINTESTINAL TRACT IN THE *ATG16L1LysM* MICE

The gastrointestinal tract of *Atg16l1^{fl/fl}* and *Atg16l1LysM* littermates (n=5) was investigated. Length of small intestine (A) and colon (C) as well as caecum weight (B) are graphically depicted. Statistical significance was tested by an unpaired Student's *t*-test. * $p < 0.05$

Next, the affected tissues of *Atg16l1LysM* mice were analyzed by histology. Liver and lung showed a spontaneous infiltration of immune cells (Figure 4-5). Spleen and mesenteric lymph nodes (MLNs) displayed a disordered architectural structure, which was characterized by the loss of a clear differentiation between the red and white pulp as well as the germinal center (gc) and corona (c) (Figure 4-5). Dissection of the small intestine revealed an augmented size and number of aggregated lymphoid nodules, called Peyer's patches (pp), in the submucosa of *Atg16l1LysM* mice compared to *Atg16l1^{fl/fl}* mice (Figure 4-5 ileum). No obvious abnormalities were seen in the morphology of the colon (data not shown).

In summary, the basal phenotype of *Atg16l1LysM* mice is characterized by the development of a spontaneous hepatosplenomegaly, lymphadenopathy and elongated small intestine accompanied by a massive immune cell infiltration in distinct tissues like spleen, lymph nodes, liver and lung compared to *Atg16l1^{fl/fl}* littermates.

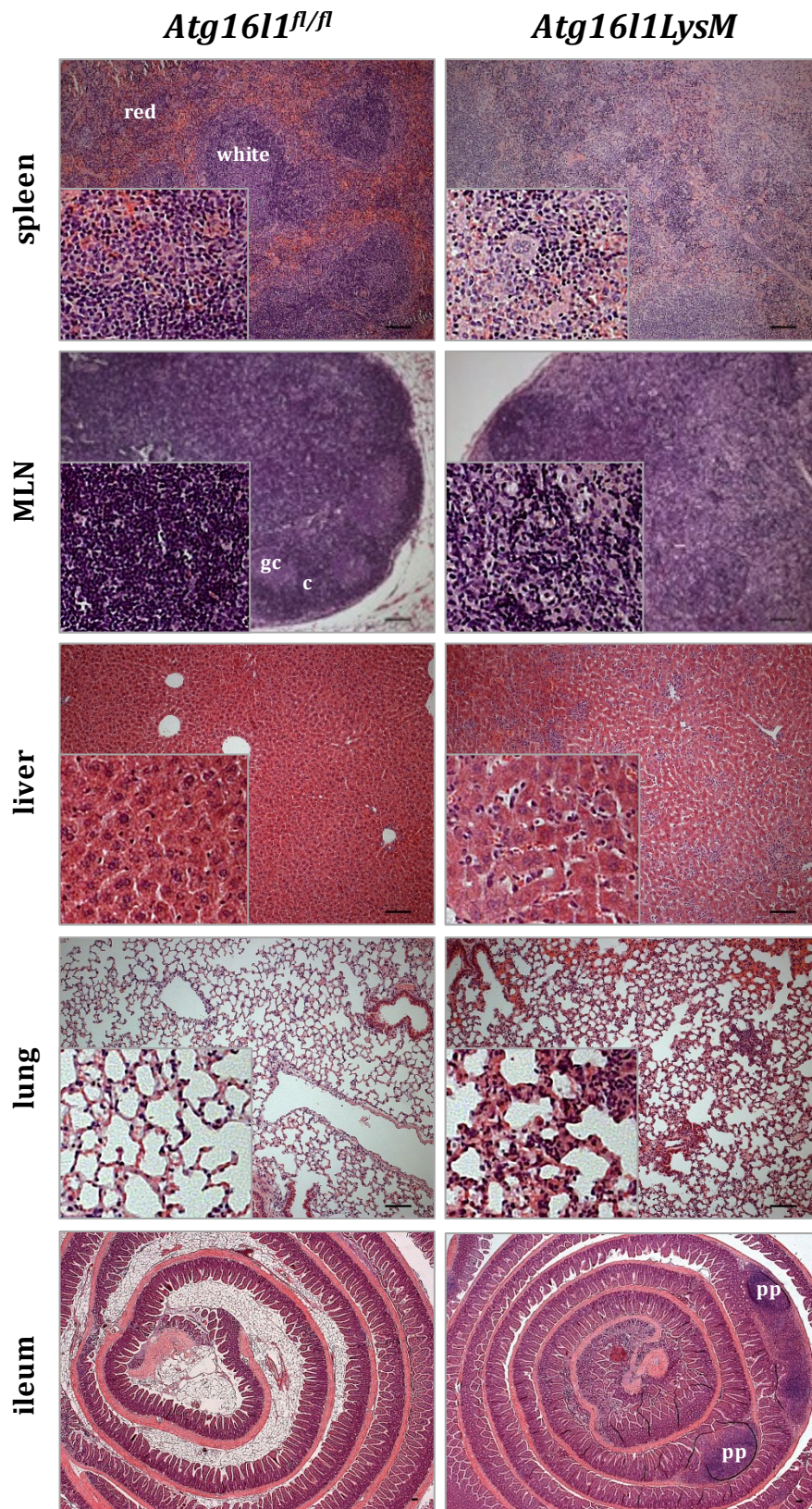


FIGURE 4-7: SPONTANEOUS IMMUNE CELL INFILTRATION IN VARIOUS TISSUES OF *ATG16L1^{LysM}* MICE

Formalin-fixed and paraffin-embedded tissues were dissected in 3.5 – 4.5µm sections and stained with H&E. Indicated tissues were analyzed by transmission light microscopy. Scale bars represent 100 µm. Images are representative for at least three mice. MLN: mesenteric lymph node, red: red pulp, white: white pulp, gc: germinal center, c: corona, pp: Peyer's patch

4.3.2 INCREASED EXTRAMEDULLARY HEMATOPOIESIS IN THE SPLEEN OF *ATG16L1LYSM* MICE

To analyze the splenomegaly in *Atg16l1LysM* animals in more detail the number of hematopoietic stem cells (HSCs) within the spleen was analyzed (Figure 4-8). Differentiated splenocytes were depleted by cell type-specific lineage antigens. Remaining lineage negative cells (lin^-) were stained for the HSC markers stem cell antigen-1 (Sca-1) and proto-oncogene c-Kit (c-Kit) (Figure 4-8 A, fourth panel). To verify the purity of depletion remaining differentiated splenocytes were analyzed by flow cytometry (Figure 4-8 A, second and third panel). After lineage depletion slight contaminations of 5.85 % \pm 1.13 of CD3⁺ and 8.1 % \pm 2.14 of CD19⁺ cells were detected. Staining of CD11b⁺ cells revealed 7.58 % \pm 1.5 in the lin^- population (Figure 4-8 A, third panel). Since these contaminations were detected in lin^- splenic cells of *Atg16l1^{fl/fl}* and *Atg16l1LysM* mice, analysis of HSC markers was still comparable between both genotypes.

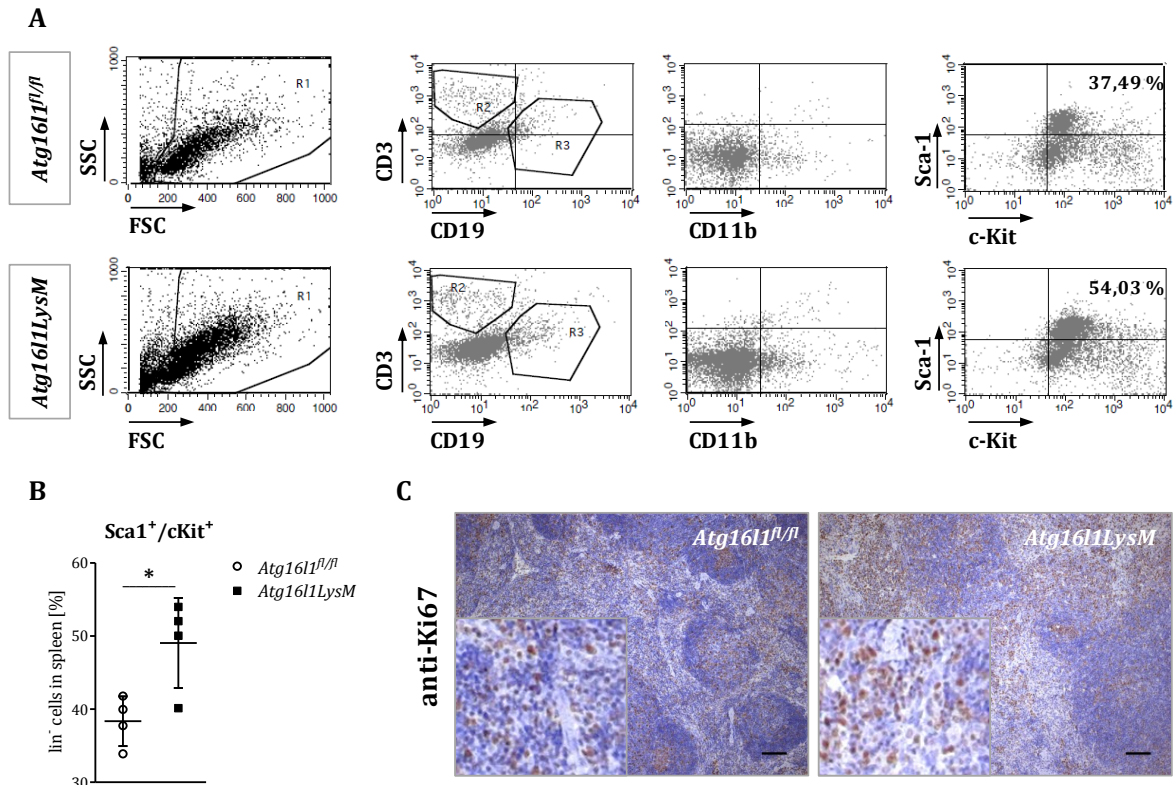


FIGURE 4-8: INCREASED NUMBER OF HEMATOPOIETIC STEM CELLS IN THE SPLEEN OF *ATG16L1LYSM* MICE

Cell type-specific lineage depletion of splenocytes was performed using the Lineage Cell Depletion kit for mouse. Splenic lin^- cells of *Atg16l1^{fl/fl}* and *Atg16l1LysM* mice (n=4) were stained for cell type-specific antigens and HSC markers and were analyzed by flow cytometry. The gating strategy is shown by dot plots (A). R1 – gate on living cells, R2 – gate on CD3⁺ cells, R3 – gate on CD19⁺ cells. Percentage of Sca-1⁺/c-Kit⁺ cells were corrected for the isotype controls and are graphically displayed (B). Data are shown as mean \pm S.D. Statistical significance was calculated by an unpaired Student's *t*-test. * *p* < 0.05 Formalin-fixed and paraffin-embedded histological sections of the spleen were stained for the proliferation marker Ki67 (brown) (C). Images were analyzed by transmission light microscopy and are representative for three mice. Scale bars represent 100 μ m. FSC: forward scatter, SSC: sideward scatter

After gating on living cells (R1), analysis of HSCs showed a significant increase in Sca-1⁺/c-Kit⁺ cells in the spleen of *Atg16l1LysM* mice compared to *Atg16l1^{fl/fl}* mice (Figure 4-8 B). Histological staining of the proliferation marker Ki67 revealed an augmented number of proliferative cells in the spleen of *Atg16l1LysM* mice (Figure 4-8 C).

To investigate whether the increased proliferation rate also resulted in an increased turnover, apoptotic cells were immunohistochemically analyzed (Figure 4-9). Microscopic analysis of TUNEL⁺ cells revealed no differences in the number of apoptotic splenic cells between both, *Atg16l1^{fl/fl}* and *Atg16l1LysM* animals.

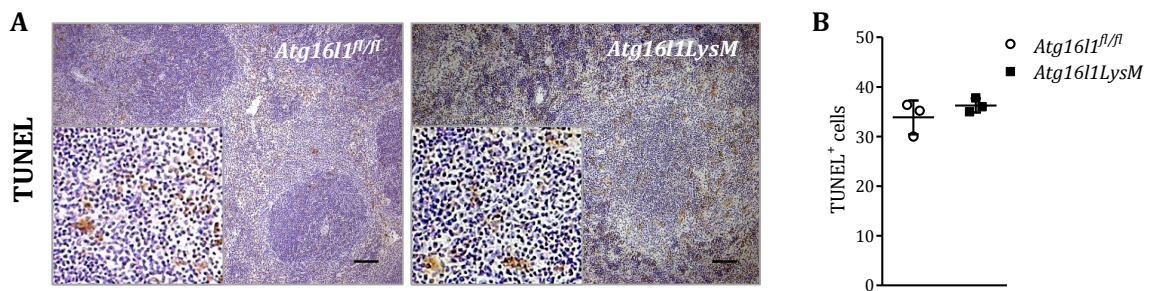


FIGURE 4-9: EQUAL NUMBERS OF APOPTOTIC TUNEL⁺ CELLS IN THE SPLEEN OF *ATG16L1^{FL/FL}* AND *ATG16L1LYSM* MICE

Formalin-fixed and paraffin-embedded splenic sections of *Atg16l1^{fl/fl}* and *Atg16l1LysM* littermates (n=3) were stained for apoptotic cells with ApopTag® Plus Peroxidase *In Situ* Apoptosis Detection Kit (Merck Millipore, Darmstadt, Germany) (A). Scale bars represent 100 µm. Images were analyzed by transmission light microscopy. Counting of TUNEL⁺ cells (brown) was performed in a blinded fashion with 5 images per mouse. Mean ± S.D. of TUNEL positive cells is graphically depicted (B). Statistical significance was calculated using an unpaired Student's *t*-test.

Bone marrow was microscopically analyzed, because *Atg16l1LysM* mice showed a splenic expansion of extramedullary hematopoiesis which is characterized by an increased number of HSCs and proliferative cells. In contrast, bone marrow of *Atg16l1LysM* mice was slightly hyperplastic compared to C57BL/6J wild type mice but did not show any indications for a hematologic disorder or specific inflammatory alteration (Figure 4-10).

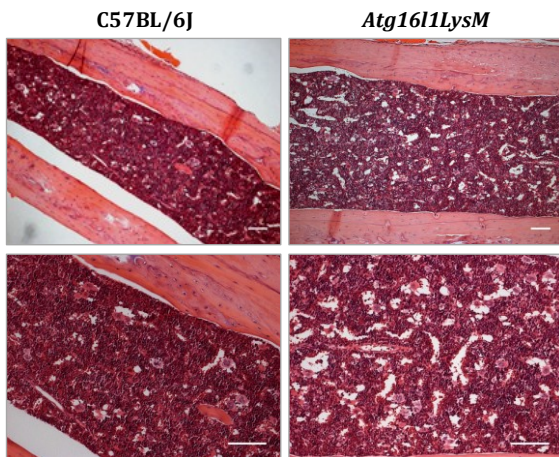


FIGURE 4-10: INTACT HEMATOPOIESIS IN BONE MARROW OF *ATG16L1LYSM* MICE

Formalin-fixed bones of *Atg16l1LysM* and C57BL/6J wild type mice (n=2) were decalcified and afterwards paraffin-embedded. Sections were stained for H&E and analyzed by transmission light microscopy. Scale bars represent 100 µm.

4.3.3 LOSS OF *ATG16L1* IN MYELOID CELLS ALTERS COMPOSITION OF SPLENOCYTES

Since the spleen was the most affected organ in *Atg16l1LysM* mice this study first focused on the splenic immune cell composition. Flow cytometry analysis included stainings for CD3⁺ T cells, CD19⁺ B cells, CD11c⁺ dendritic cells, CD11b⁺ macrophages as well as CD11b⁺/Ly6G⁺ neutrophils and dot plots are representatively depicted in Figure 4-11.

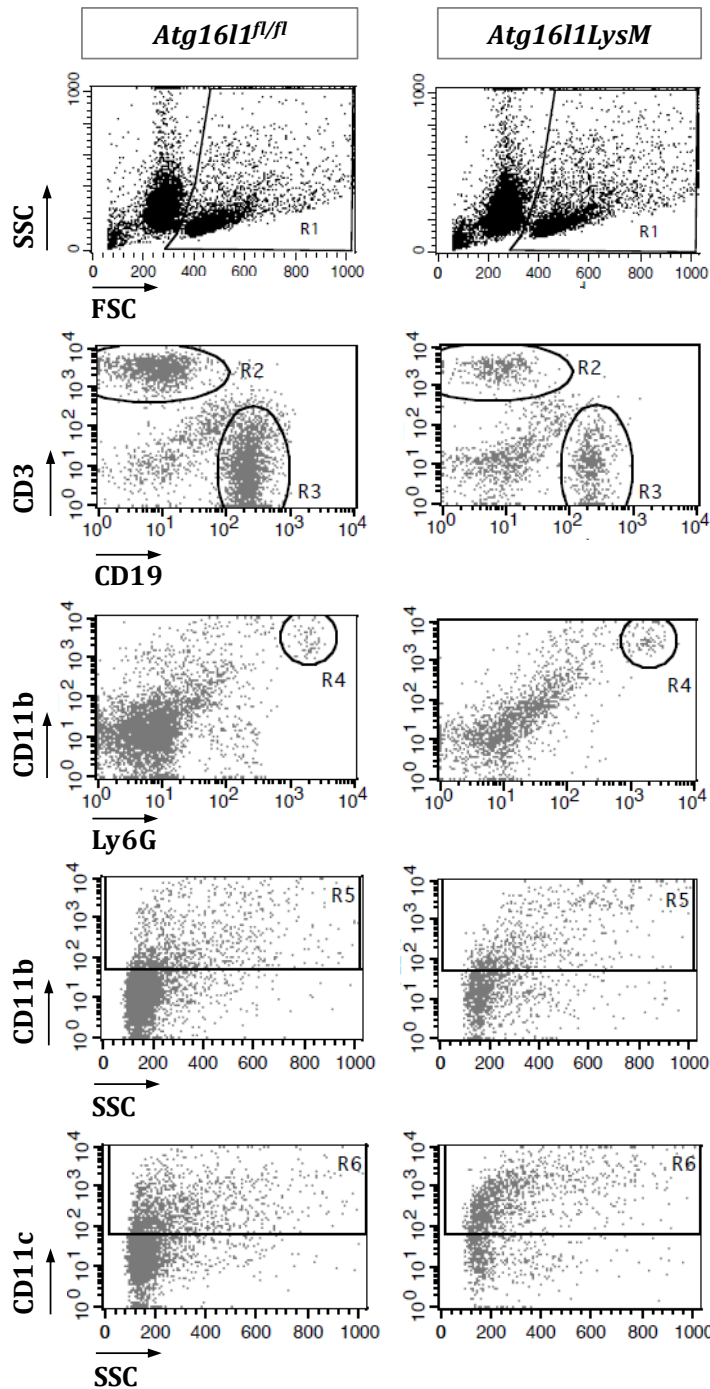


FIGURE 4-11: GATING STRATEGY OF IMMUNE CELL POPULATIONS IN THE SPLEEN OF *ATG16L1LysM* MICE

Dot plots depicting forward scatter (FSC) and sideward scatter (SSC) were used to exclude dead cells and erythrocytes by gating. Analysis of CD3⁺ T cells (R2), CD19⁺ B cells (R3), CD11b⁺/Ly6G⁺ neutrophils (R4), CD11b⁺ macrophages (R5) and CD11c⁺ dendritic cells (R6) are exemplarily shown in dot plots.

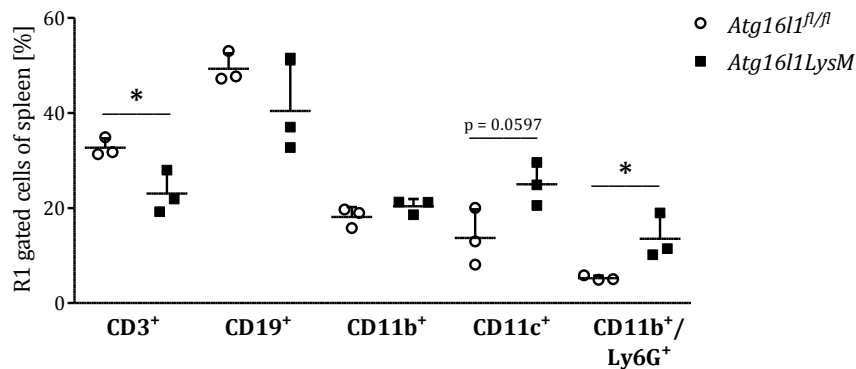


FIGURE 4-12: ALTERED IMMUNE CELL COMPOSITION IN THE SPLEEN OF *ATG16L1*LysM MICE

Splenocytes were isolated from *Atg16l1^{fl/fl}* and *Atg16l1LysM* littermates (n=3) and stained for the indicated cell type-specific antigens and the particular isotype control combinations and analyzed by flow cytometry. Percentage of the individual cell population was corrected for the particular isotype control. Data are shown as mean \pm S.D. Statistical significance was calculated by an unpaired Student's *t*-test. * $p < 0.05$

Dead cells, cell debris and red blood cells were excluded from further analysis by gating (Figure 4-11, R1). *Atg16l1LysM* mice showed a significantly decreased number of CD3⁺ T cells whereas CD11b⁺/Ly6G⁺ neutrophils were significantly elevated compared to *Atg16l1^{fl/fl}* animals (Figure 4-12). CD19⁺ B cells were slightly decreased whereas the number of CD11c⁺ dendritic cells was markedly upregulated. CD11b⁺ macrophages were only slightly increased in the spleen of *Atg16l1LysM* mice. In line, expression analysis of cell type-specific antigens in the spleen of *Atg16l1LysM* and *Atg16l1^{fl/fl}* mice showed significantly diminished mRNA expression of *Cd3e* and *Cd4* for T cells as well as *Cd19* for B cells (Figure 4-13) which further strengthened the observed reduction of adaptive immune cells within the spleen of *Atg16l1LysM* mice compared to *Atg16l1^{fl/fl}* animals (Figure 4-12). Moreover, flow cytometry analysis detected upregulation of CD11b⁺ splenocytes could be confirmed on mRNA expression level (Figure 4-13). Expression of *Cd11c* did not show differences between *Atg16l1LysM* and *Atg16l1^{fl/fl}* mice (Figure 4-13).

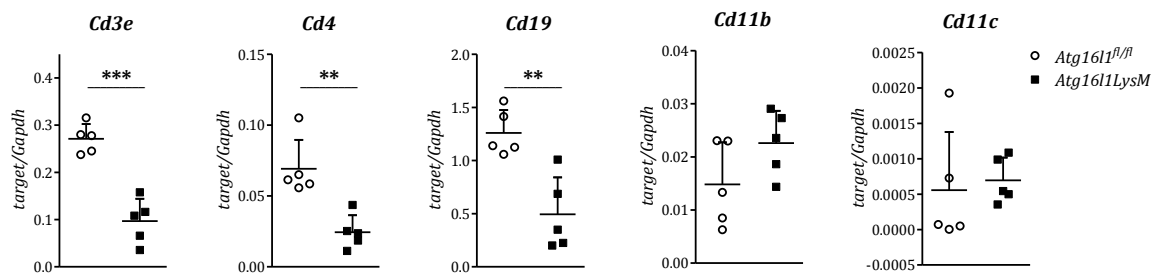


FIGURE 4-13: CHANGED EXPRESSION OF CELL TYPE-SPECIFIC MARKERS IN THE SPLEEN OF *ATG16L1*LysM MICE

Spleens of *Atg16l1^{fl/fl}* and *Atg16l1LysM* mice (n=5) were frozen in liquid nitrogen and mortared. RNA extracts were reverse transcribed into cDNA. Expression levels of the indicated cell-type specific genes were analyzed by SYBR® green qPCR and normalized to *Gapdh*. Data are shown as mean \pm S.D. and statistical significance was calculated with an unpaired Student's *t*-test. ** $p < 0.01$, *** $p < 0.001$

Thus, splenomegaly in *Atg16l1LysM* mice was associated with an increased number of innate immune cells whereby adaptive immune cells are significantly downregulated. Next, the activation status of adaptive and innate immune cells was investigated by flow cytometry (Figure 4-14).

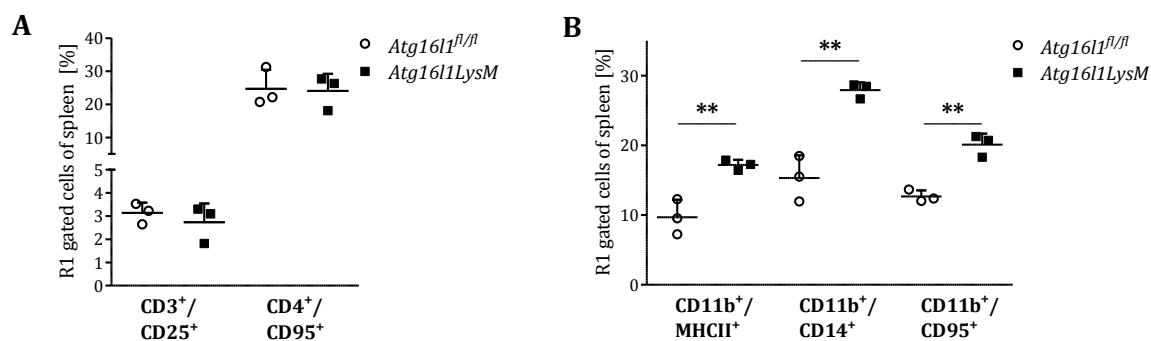


FIGURE 4-14: INCREASED NUMBER OF ACTIVATED MYELOID CELLS BUT NOT T CELLS IN *ATG16L1LysM* SPLEEN
Splenocytes were isolated from *Atg16l1^{fl/fl}* and *Atg16l1LysM* littermates (n=3) and stained for the indicated antigen combinations or particular isotype controls and analyzed by flow cytometry. Percentage of activated T cells (A) or macrophages (B) was corrected for the particular isotype control. Data are shown as mean ± S.D. An unpaired Student's *t*-test was performed to evaluate the statistical significance. ** *p* < 0.01

Equal numbers of CD3⁺/CD25⁺ and CD4⁺/CD95⁺ T cells were observed in the spleen of *Atg16l1LysM* and *Atg16l1^{fl/fl}* mice (Figure 4-14 A) whereas the number of activated CD11b⁺ myeloid cells characterized by MHCII, CD14 and CD95 was significantly higher in *Atg16l1LysM* animals compared to *Atg16l1^{fl/fl}* littermates (Figure 4-14 B).

4.3.4 MYELOID DERIVED-SUPPRESSOR CELL (MDSC)-LIKE PHENOTYPE IN THE SPLEEN OF *ATG16L1LysM* MICE

Myeloid derived suppressor cells (MDSCs) are described to exert a high immunosuppressive function on T cell proliferation and response [221]. Thus, the spleen of *Atg16l1^{fl/fl}* and *Atg16l1LysM* mice was analyzed for specific MDSC markers (Figure 4-15). *Atg16l1LysM* mice displayed a prominent expression of *inducible nitric oxide synthase* (iNOS), a hall mark of MDSC expansion [221], which was completely absent in the spleen of *Atg16l1^{fl/fl}* mice (Figure 4-15 A). Moreover, significantly increased mRNA expression levels of *myeloperoxidase* (*Mpo*), *S100 calcium binding protein A8* (*S100a8*) and *S100 calcium binding protein A9* (*S100a9*) were detected in spleens of *Atg16l1LysM* mice when compared to *Atg16l1^{fl/fl}* mice (Figure 4-15B). In agreement with these results histological spleen sections of *Atg16l1LysM* mice, showed markedly elevated numbers of clustered MPO⁺ cells compared to *Atg16l1^{fl/fl}* mice (Figure 4-13 C) which further supports the findings of an increased CD11b⁺/Ly6G⁺ population detected by flow cytometry (Figure 4-12).

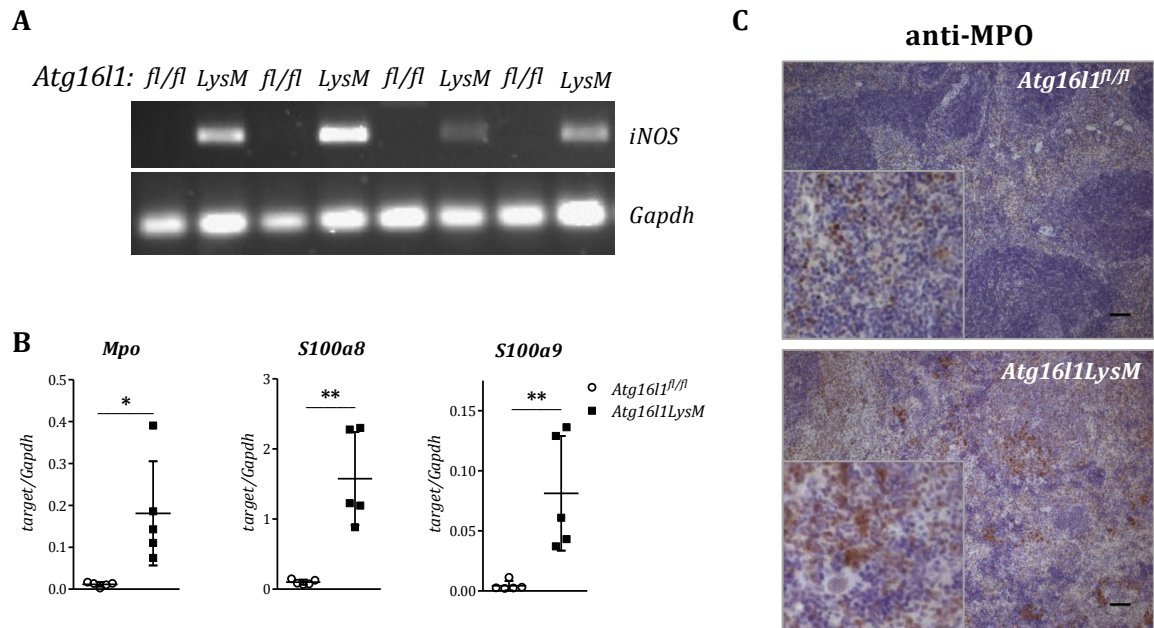


FIGURE 4-15: IDENTIFICATION OF MDSC ATTRIBUTES IN THE SPLEEN OF *ATG16L1LYSM* MICE

Snap frozen spleens of *Atg16l1^{fl/fl}* and *Atg16l1^{LysM}* mice were mortared and RNA was extracted. cDNA synthesis was performed. Splenic levels of *iNOS* were determined by end-point PCR in four littermate pairs (**A**). *Gapdh* level served as loading control. Splenic levels of *Mpo* as well as *S100a8* and *S100a9* were determined in five littermate pairs by TaqMan Assay and SYBR® green qPCR, respectively (**B**). Expression of the indicated targets was normalized to *Gapdh*. Formalin-fixed and paraffin-embedded splenic sections (n=3) were stained for MPO (brown) and analyzed by transmission light microscopy (**C**). Scale bars represent 100 μ m. iNOS: inducible nitric oxide synthase, MPO: myeloperoxidase

4.3.5 EXPRESSION OF CYTOKINES IN THE SPLEEN OF *ATG16L1LYSM* MICE

To further investigate whether the observed increase in myeloid cells and their hyper-activation influences the cytokine profile in the spleen of *Atg16l1^{LysM}* mice, mRNA expression analysis of distinct cytokines and chemokines was performed (Figure 4-16). Expression levels of the pro-inflammatory cytokines *interleukin 1 beta* (*Il1b*), *Il6* and *tumor necrosis factor alpha* (*Tnfa*) as well as the anti-inflammatory cytokines *Il10* and *Il4* were equally determined in *Atg16l1^{fl/fl}* and *Atg16l1^{LysM}* mice. In contrast, the pro-inflammatory cytokines *Il1a* and *interferon gamma* (*Ifng*) revealed a slight upregulation on mRNA level in *Atg16l1^{LysM}* mice. The pro-inflammatory neutrophil attracting chemokine (*C-X-C motif*) *ligand 1* (*Cxcl1*) was significantly increased whereas expression of the pro-inflammatory cytokine *Il18* and the autocrine T cell-mediated cytokine *Il2* was significantly diminished.

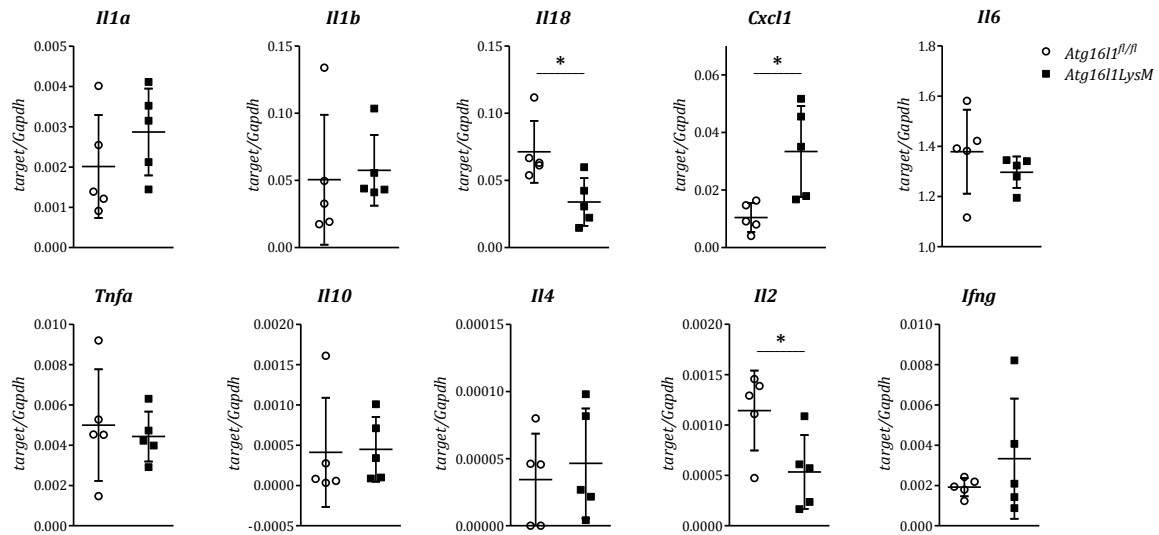


FIGURE 4-16: ALTERED EXPRESSION OF MYELOID- AND T CELL-SPECIFIC CYTOKINES AND CHEMOKINES IN THE SPLEEN OF *ATG16L1*LysM MICE

Spleens of *Atg16l1^{fl/fl}* and *Atg16l1LysM* mice (n=5) were snap frozen in liquid nitrogen. RNA extraction and cDNA synthesis were performed; expression of the indicated targets was analyzed by means of SYBR® green qPCR and normalized to *Gapdh*. Expression of *Il1b* and *Il18* was analyzed by TaqMan Assay. Data show mean ± S.D. Statistical significance was calculated with an unpaired Student's *t*-test. * *p* < 0.05

Taken together, the cytokine profile in the spleen of *Atg16l1LysM* mice reflected in particular the naïve status of T cells and the hyper-activation of myeloid cells.

4.3.6 SPLENIC PHENOTYPE OF *ATG16L1*LysM MICE IS NOT DRIVEN BY BACTERIAL INVASION

Clearance of invading bacteria is one of the main functions of the spleen. Since the observed splenomegaly in *Atg16l1LysM* mice was accompanied by an increased number of hyper-activated CD11b⁺ splenocytes, a putative barrier dysfunction was investigated by means of a PCR for eukaryotic bacteria (Figure 4-17).

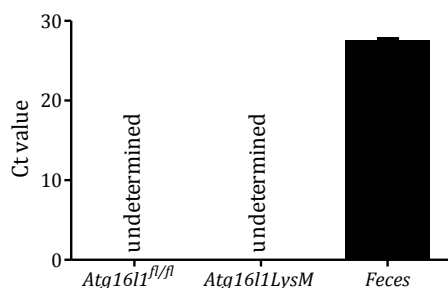


FIGURE 4-17: NO BACTERIAL INVASION IN THE SPLEEN OF *ATG16L1*LysM MICE

Spleens of *Atg16l1^{fl/fl}* and *Atg16l1LysM* mice (n=9) were directly frozen in liquid nitrogen and mortared. After DNA extraction, DNA of eukaryotic bacteria was detected using a specific TaqMan assay. Murine feces were used as positive control. Data are shown as mean ± S.D.

However, bacterial DNA was neither observed in the spleen of *Atg16l1^{fl/fl}* mice nor their *Atg16l1LysM* littermates. In conclusion, a bacterial invasion did not explain the observed hyper-activation of CD11b⁺ myeloid cells in the spleen of *Atg16l1LysM* mice.

4.3.7 ENHANCED PROTEIN LEVEL OF PRO-IL1B BUT NOT TLR4 COMPONENTS IN THE SPLEEN OF *ATG16L1LYSM* MICE

Recent studies have indicated a pivotal role for autophagy in IL1 cytokine production based on increased secretion of IL1 β after activation of TLR4 signaling [22]. To analyze this phenomenon in *Atg16l1^{fl/fl}* and *Atg16l1LysM* mice, protein levels of IL1 β were determined in the spleen (Figure 4-18).

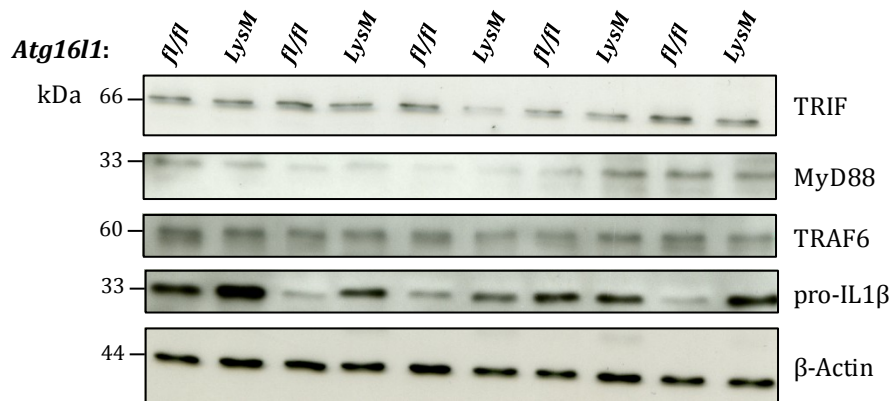


FIGURE 4-18: PRO-IL1B BUT NOT TLR4 SIGNALING MOLECULES ACCUMULATE IN THE SPLEEN OF *ATG16L1LYSM* MICE

Snap frozen spleens of *Atg16l1^{fl/fl}* and *Atg16l1LysM* mice (n=5) were mortared. Proteins were extracted and lysates were probed by immunoblot for the indicated proteins with β -Actin serving as loading control.

In four out of five littermate pairs the full-length inactive form of IL1 β (pro-IL1 β) was markedly enhanced in *Atg16l1LysM* mice compared to *Atg16l1^{fl/fl}* mice. To determine if this observation is due to a defective degradation machinery of TLR4 signaling components, protein levels of MyD88, TRIF and TRAF6 were analyzed. However, none of the investigated proteins showed elevated levels when comparing both genotypes.

4.3.8 EXPRESSION OF INFLAMMASOME COMPONENTS IN THE SPLEEN OF *ATG16L1LYSM* MICE

Autophagy was further described to modulate IL1 β production through regulation of the NOD-like receptor family, Pyrin domain containing 3 (NLRP3) inflammasome [222]. Thus, mRNA levels of inflammasome components were investigated (Figure 4-19). Activation of the inflammasome depends on the formation of a multimeric protein complex of the enzymatically inactive pro-Caspase-1 (pro-Casp1), Pyrin domain of apoptosis-associated speck-like protein containing a CARD (ASC) and the NOD-like receptor family, Pyrin domain containing protein 3 (NLRP3). Among both genotypes mRNA expression analysis of the three mentioned inflammasome components did not reveal any differences (Figure 4-19).

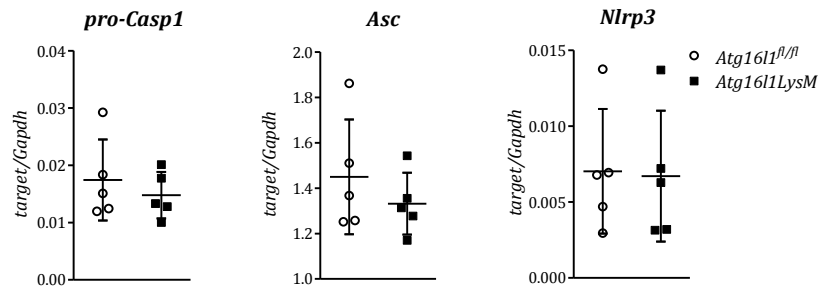


FIGURE 4-19: UNALTERED EXPRESSION ON NLRP3 INFLAMMASOME COMPONENTS IN *ATG16L1LYSM* SPLEENS

Spleens of *Atg16l1^{fl/fl}* and *Atg16l1LysM* mice (n=5) were subsequently frozen in liquid nitrogen and mortared. Extracted RNA was reverse transcribed into cDNA and expression analysis was performed by means of SYBR® green qPCR. Expression levels of the indicated target genes were normalized to *Gapdh*. Data are shown as mean ± S.D. and the statistical significance was calculated using an unpaired Student's *t*-test.

Summing up, the detected accumulation of pro-IL1 β in the spleens of *Atg16l1LysM* animals could be traced back neither to elevated protein levels of Toll-like receptor 4 signaling molecules nor to increased mRNA expression levels of NLRP3 inflammasome components.

4.3.9 MYELOID CELL INFILTRATION AFFECTS MULTIPLE ORGANS BUT NOT THE BRAIN OF *ATG16L1LYSM* MICE

Given that innate immune cells, especially neutrophils, seem to play a crucial role in the splenic phenotype of *Atg16l1LysM* mice, additionally affected organs like mesenteric lymph nodes, liver and lung were analyzed by immunohistochemistry (Figure 4-20). Mesenteric lymph nodes (MLNs) of *Atg16l1LysM* mice showed cluster of MPO⁺ cells which was completely absent in MLNs of *Atg16l1^{fl/fl}* mice. Similar results were observed for liver and lung of *Atg16l1LysM* mice when compared to their *Atg16l1^{fl/fl}* littermates. However, not every cluster of infiltrated immune cells in the liver of *Atg16l1LysM* mice consisted of MPO⁺ cells suggesting a second infiltrating cell type (Figure 4-20, liver).

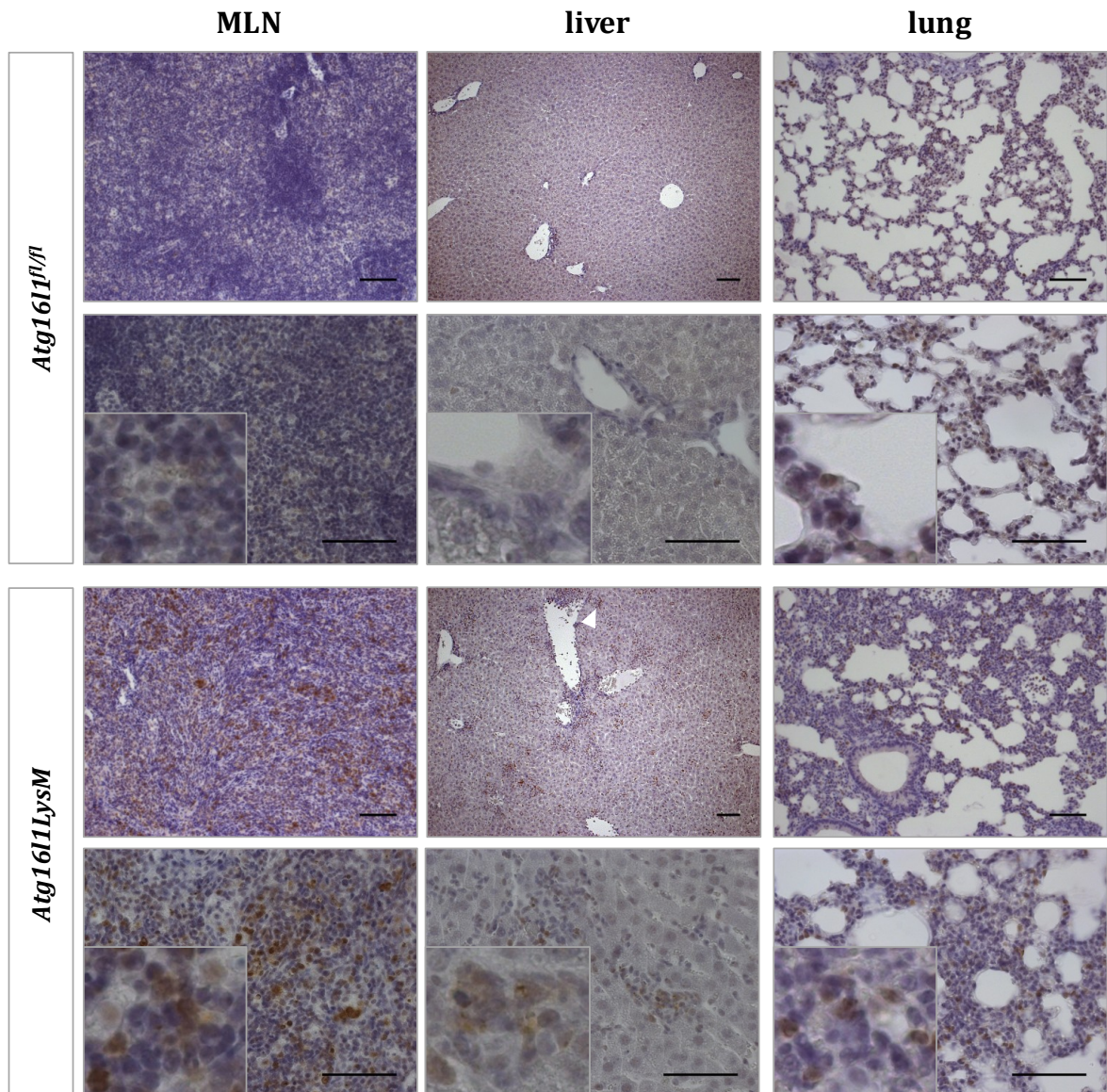


FIGURE 4-20: INCREASED NUMBER OF MPO⁺ CELLS IN MLN, LIVER AND LUNG OF *ATG16L1^{LysM}* MICE

Tissues of *Atg16l1^{fl/fl}* and *Atg16l1^{LysM}* mice (n=3) were formalin-fixed and paraffin-embedded. Sections of MLN, liver and lung were stained for MPO (brown) and analyzed by transmission light microscopy. White arrows exemplarily indicate MPO⁺ cells. Scale bars represent 50 μ m. MLN: mesenteric lymph node; MPO: myeloperoxidase

In line, staining of macrophages using the pan-macrophage marker ionized calcium-binding adapter molecule 1 (IBA-1) [223] showed an increased infiltration of IBA-1⁺ macrophages in MLN and liver of *Atg16l1^{LysM}* mice compared to their *Atg16l1^{fl/fl}* littermates (Figure 4-21). Besides an elevated number, *Atg16l1^{LysM}* mice revealed larger irregularly shaped IBA-1⁺ cells suggesting an increased pseudopodia formation and thus activation of IBA-1⁺ cells in the liver [224, 225]. In contrast, similar numbers of IBA-1⁺ microglia were observed in brain sections of *Atg16l1^{LysM}* and *Atg16l1^{fl/fl}* mice. IBA-1⁺ microglia exhibited the characteristic ramified shape pointing to quiescent microglia populations and thus an intact blood-brain barrier in both genotypes [226].

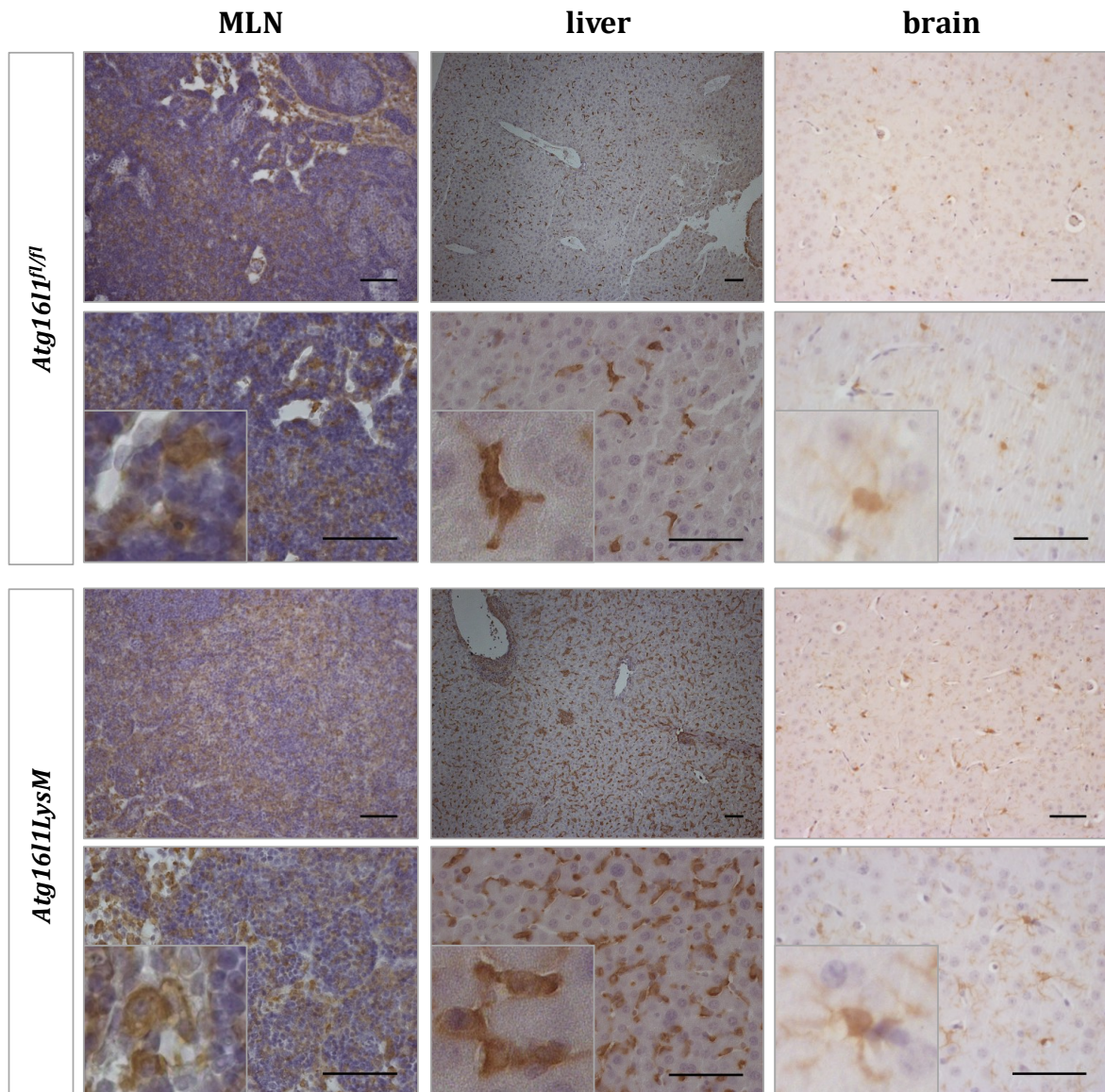


FIGURE 4-21: ELEVATED INFILTRATION OF IBA-1+ MACROPHAGES IN MLN, LIVER AND BRAIN OF *ATG16L1LYSM* MICE

MLN, liver and brain tissues of *Atg1611^{fl/fl}* and *Atg1611LysM* mice (n=3) were formalin-fixed and paraffin-embedded. Sections were stained for IBA-1 (brown) and analyzed by transmission light microscopy. Scale bars represent 50 μ m. IBA-1: ionized calcium-binding adapter molecule 1; MLN: mesenteric lymph node

4.3.10 NEUTROPHILIA IN THE BLOOD OF *ATG16L1LYSM* MICE

In order to study whether the phenotype of CD11b⁺ cells is restricted to tissue-resident macrophages of the spleen, leukocyte populations in the blood of *Atg1611LysM* mice were analyzed using flow cytometry (Figure 4-22).

Dead cells and cell debris were excluded similarly as described for splenic cells (Figure 4-11, R1). No alterations were observed in the distribution of CD3⁺ and CD19⁺ immune cells, whereas CD11b⁺ and CD11c⁺ cells were slightly elevated in the blood of *Atg1611LysM* mice compared to *Atg1611^{fl/fl}* littermates (Figure 4-22 A). *Atg1611LysM* mice showed a significantly increased CD11b⁺/Ly6G⁺ population as seen in the spleen (see chapter 4.3.3). In addition,

analysis of the number of activated CD11b⁺ cells revealed a significant increase in the blood of *Atg16l1LysM* mice compared to *Atg16l1^{fl/fl}* mice (Figure 4-22 B). In accordance with results seen in the spleen (see chapter 4.3.3) numbers of activated T cells in the blood of *Atg16l1LysM* mice were not altered.

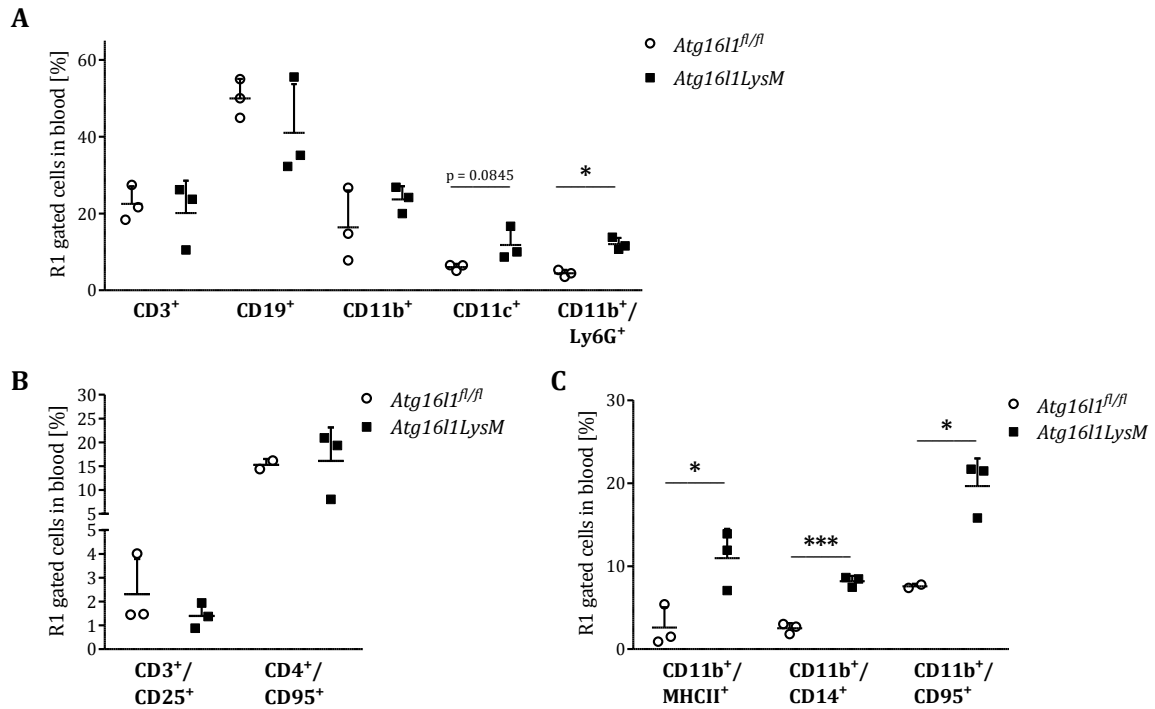


FIGURE 4-22: PROPORTION OF LEUKOCYTES IN THE BLOOD OF *ATG16L1LYSM* MICE

Blood of *Atg16l1^{fl/fl}* and *Atg16l1LysM* littermates (n=3) was collected in EDTA tubes. After staining for the indicated antigens or particular isotype controls, red blood cells were lysed with 1 x BD FACS Lysing Solution and remaining cells were analyzed by flow cytometry. Percentage of the indicated cell populations (A) as well as activated T cells (B) or macrophages (C) was corrected for the particular isotype control. Data are shown as mean \pm S.D. An unpaired Student's *t*-test was performed to evaluate the statistical significance. * $p < 0.05$, *** $p < 0.001$

4.3.11 CYTOKINE LEVELS IN UNTREATED *ATG16L1LYSM* MICE

Since *Atg16l1LysM* mice showed a multifaceted inflammatory phenotype in various organs, serum cytokine and chemokine levels were analyzed in untreated *Atg16l1^{fl/fl}* and *Atg16l1LysM* littermates (Figure 4-23). The multiplex-based screening revealed elevated cytokine levels under basal conditions in *Atg16l1LysM* mice compared to *Atg16l1^{fl/fl}* animals.

In detail, significant increase was observed for IL12p40 and p70, IL18, TNF α and IL10 as well as the myeloid-related chemokines macrophage inflammatory protein 1 alpha (MIP1 α) and beta (MIP1 β). No alterations were observed for IL1 α and IL1 β as well as for IL2, IL3, IL4, IL5, IL6, IL9, IL13, IL17, granulocyte-colony stimulating factor (G-CSF), granulocyte-macrophage stimulating factor (GM-CSF), IFN γ , monocyte chemotactic protein 1 (MCP1) and the chemokine regulated on activation, normal T cell expressed and secreted (RANTES) (data not shown).

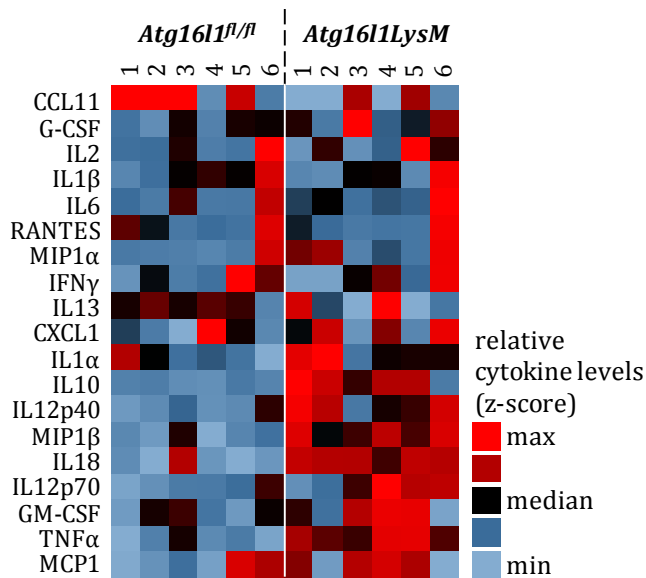


FIGURE 4-23: INCREASED CYTOKINE AND CHEMOKINE LEVELS IN THE SERUM OF *ATG16L1LYSM* MICE

Blood from *Atg16l1^{fl/fl}* and *Atg16l1LysM* littermates (n=6) was collected in lithium-heparin tubes. Cytokine and chemokine levels in the serum were measured using the Bio-Plex Pro™ Mouse Cytokine 23-plex Assay (BioRad). Levels of IL18 were measured by ELISA. Results are displayed in a heat-map. For better readability, concentration values were z-score normalized.

4.4 IMPACT OF IL1R INHIBITION ON THE BASAL PHENOTYPE OF *ATG16L1LYSM* MICE

Recent studies implicated a role for autophagy in secretion of pro-inflammatory cytokines of the IL1-family [22, 46, 62, 227]. With regard to increased IL1 cytokines levels in spleen and serum of mice lacking *Atg16l1* in the myeloid lineage, the *in vivo* role of IL1R signaling was studied. *Atg16l1^{fl/fl}* and *Atg16l1LysM* mice were daily treated with 200 µg of the human interleukin-1 receptor (IL1R) antagonist Anakinra (Kineret®, Swedish Orphan Biovitrum AB) for a period of two weeks in order to inhibit IL1R signaling ([214], [228]).

During this period of Anakinra treatment, body weight of *Atg16l1^{fl/fl}* as well as *Atg16l1LysM* mice did not alter compared to sodium chloride (NaCl)-treated control mice (Figure 4-24 A). Analysis of the body weight revealed no effect of the IL1R antagonist on the spontaneous splenomegaly (Figure 4-24 B) and hepatomegaly (Figure 4-24 E) of *Atg16l1LysM* mice.

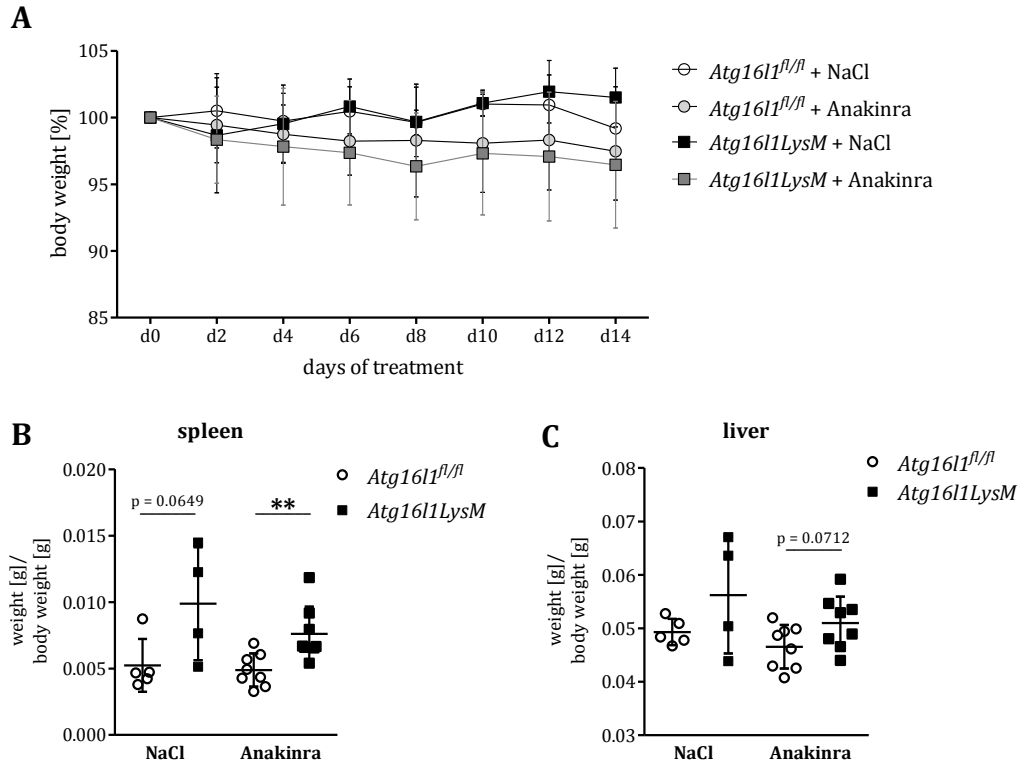


FIGURE 4-24: BODY AND ORGAN WEIGHT OF *ATG16L1^{FL/FL}* AND *ATG16L1LYSM* MICE AFTER ANAKINRA THERAPY
Atg16l1^{fl/fl} and *Atg16l1LysM* mice were daily treated with 200 µg Anakinra (n=8) or 200 µL NaCl (n=4-5) for 14 d. Body weight loss was daily recorded (A). After a two week period of treatment, spleen (B) and liver weight (C) were assessed. Data represent mean ± S.D. and statistical significance was calculated with an unpaired Student's *t*-test. ** *p* < 0.01

Histological analysis of the spleen of Anakinra-treated *Atg16l1^{fl/fl}* and *Atg16l1LysM* mice did not show differences in the morphology compared to appropriate NaCl-treated control mice (Figure 4-25). Thus, inhibition of IL1R signaling did not restore the architectural disorder in the spleen of *Atg16l1LysM* mice.

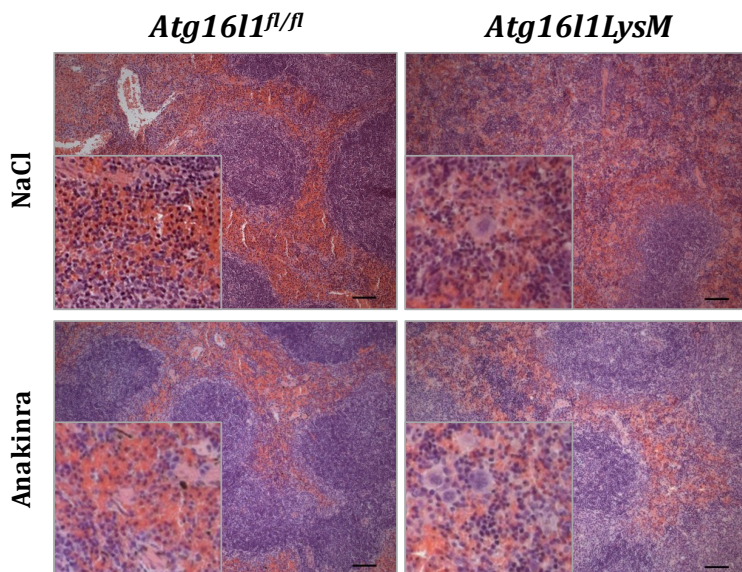


FIGURE 4-25: HISTOLOGICAL ANALYSIS OF THE SPLENIC MORPHOLOGY IN *ATG16L1LYSM* MICE AFTER ANAKINRA TREATMENT

After the two weeks treatment of 200 µg Anakinra (n=8) or 200 µL NaCl (n=4-5) per day, spleens of *Atg16l1^{fl/fl}* and *Atg16l1LysM* mice were formalin-fixed and paraffin-embedded. Splenic sections were stained with H&E and analyzed by transmission light microscopy. Scale bars represent 100 µm.

The impact of the IL1 cytokine family was further determined on cellular and molecular levels analyzing the cellular composition and activation status in the spleen of Anakinra-treated *Atg16l1^{fl/fl}* and *Atg16l1LysM* mice (Figure 4-26).

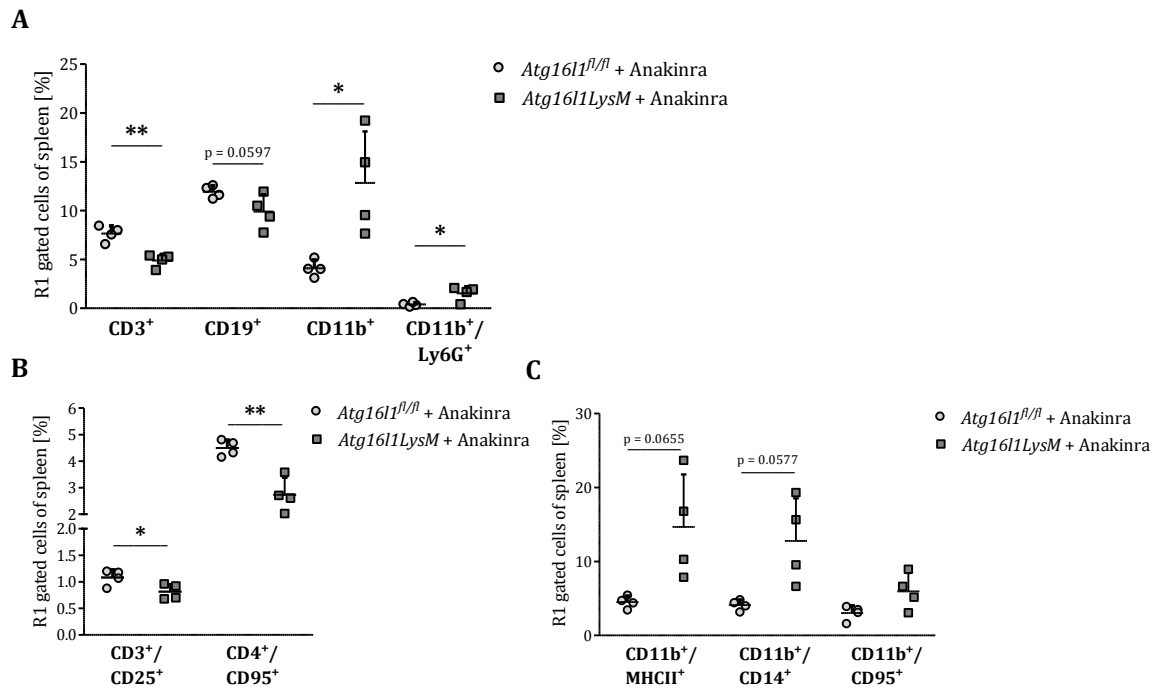


FIGURE 4-26: INHIBITION OF IL1R SIGNALING DID NOT RESCUE THE ALTERED LEUKOCYTE COMPOSITION IN THE SPLEEN OF *ATG16L1LYSM* MICE

Atg16l1^{fl/fl} and *Atg16l1LysM* mice (n=4) were daily administered with 200 µg Anakinra for 14 d. Splenocytes were stained with the indicated antibodies or appropriate isotype controls and analyzed by flow cytometry. Cellular composition (A) as well as numbers of activated T cells (B) and macrophages (C) were depicted as percentage of leukocytes corrected for the particular isotype control. Data are shown as mean ± S.D. Evaluation of statistical significance was performed with an unpaired Student's *t*-test. * *p* < 0.05, ** *p* < 0.01

After 14 d of Anakinra treatment, *Atg16l1LysM* mice still showed a significant decrease of CD3⁺ T cells and CD19⁺ B cells whereas CD11b⁺ macrophages and CD11b⁺/Ly6G⁺ neutrophils were significantly upregulated compared to Anakinra-treated *Atg16l1^{fl/fl}* mice (Figure 4-26 A). Splenic T cells of *Atg16l1LysM* mice demonstrated a diminished cell surface expression of CD25 and CD95 compared to *Atg16l1^{fl/fl}* mice (Figure 4-26 B). As expected from these results, CD11b⁺ splenocytes of Anakinra-treated *Atg16l1LysM* mice still displayed an enhanced cell surface expression of the activation markers MHCII, CD14 and CD95 (Figure 4-26 C).

To determine whether IL1R inhibition has an influence on the altered cytokine expression in the spleen of *Atg16l1LysM* mice, mRNA expression analysis were performed (Figure 4-27). Inhibition of IL1R signaling did neither change expression of the IL1 family members *Il1a* and *Il1b* nor *Tnfa*, *Il10* and *Il6*. In contrast, a slight decrease in *Il18* expression was seen in Anakinra-treated *Atg16l1^{fl/fl}* and *Atg16l1LysM* mice compared to the appropriate NaCl-treated

control mice. Significantly enhanced mRNA expression of *Cxcl1* in *Atg16l1LysM* mice persisted after treatment with Anakinra indicating an IL1R signaling independent mechanism.

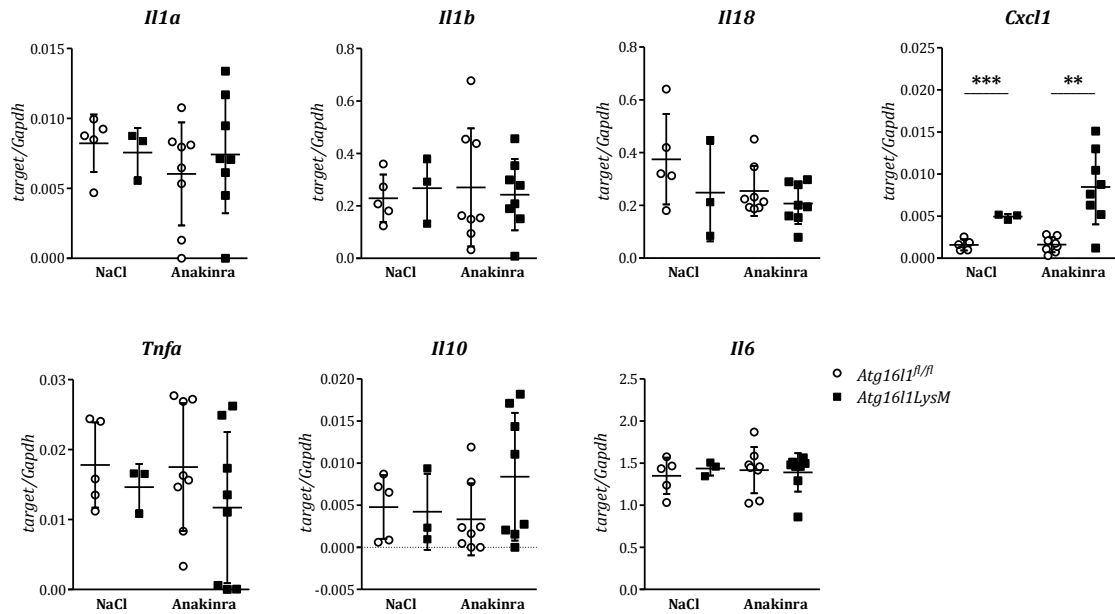


FIGURE 4-27: ANAKINRA TREATMENT DID NOT ALTER DIFFERENCES IN CYTOKINE EXPRESSION OF *ATG16L1^{FL/FL}* AND *ATG16L1^{LysM}* MICE

Atg16l1^{FL/FL} and *Atg16l1LysM* mice received a daily intraperitoneal injection of 200 µg Anakinra (n=8) or 200µL NaCl (n=4-5) as control. RNA from liquid nitrogen frozen spleens was extracted and transcribed into cDNA. Expression levels of the indicated chemokines and cytokines were measured by SYBR® green qPCR and normalized to *Gapdh*. Data represent mean ± S.D. and statistical analysis was performed with an unpaired Student’s *t*-test. ** *p* < 0.01, *** *p* < 0.001

For verification of unaffected cytokine levels, serum cytokine and chemokine levels of Anakinra-treated *Atg16l1^{FL/FL}* and *Atg16l1LysM* mice were measured (Figure 4-28). Inhibition of IL1R signaling did not result in alterations of one of the 24 investigated cytokines which is exemplarily shown for IL18 and IL12p40 in Figure 4-28.

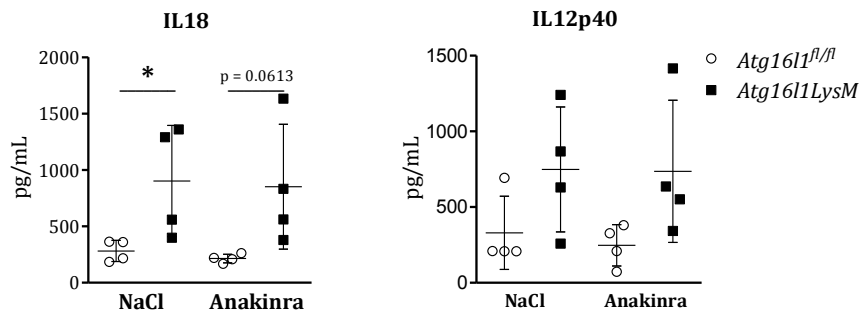


FIGURE 4-28: UNALTERED CYTOKINE CONCENTRATIONS IN THE SERUM AFTER ANAKINRA TREATMENT

Blood from *Atg16l1^{FL/FL}* and *Atg16l1LysM* mice was collected in lithium-heparin tubes after a two-week period of Anakinra treatment (200µg/day, n=8) or NaCl (200µL/day) n=4-5) as control. Concentrations of IL18 were measured by ELISA. IL12p40 levels were analyzed using the Bio-Plex Pro™ Mouse Cytokine 23-plex Assay (BioRad). Data are represented as mean ± S.D. and statistical significance was evaluated by an unpaired Student’s *t*-test. * *p* < 0.05

Taken together, the observed phenotype of *Atg1611LysM* mice could not be reverted by pharmacological IL1R signaling inhibition suggesting that IL1R signaling and the IL1 cytokine family does not mediate the complex inflammatory phenotype of the conditional *Atg1611LysM* knock-out mouse model.

4.5 ROLE OF ATG16L1 IN TLR4 SIGNALING

4.5.1 HYPER-SECRETION OF CYTOKINES IS TRANSCRIPTIONALLY REGULATED IN LPS-STIMULATED *ATG16L1LYSM* BMDMS

To investigate the hyper-activation of *Atg1611*-deficient CD11b⁺ cells in more detail, the functional role of ATG16L1 was further analyzed using bone marrow-derived macrophages (BMDMs) as *ex vivo* model. Since recently published studies implicated a role for autophagy and ATG16L1 in cytokine [22, 62, 227] and hormone secretion [229], the functional impact of ATG16L1 on exocytotic secretory pathways was studied. In a preliminary experiment, secretion of CXCL1 upon stimulation with several bacterial and viral stimuli was screened in *Atg1611LysM* and *Atg1611^{fl/fl}* BMDMs (Figure 4-29).

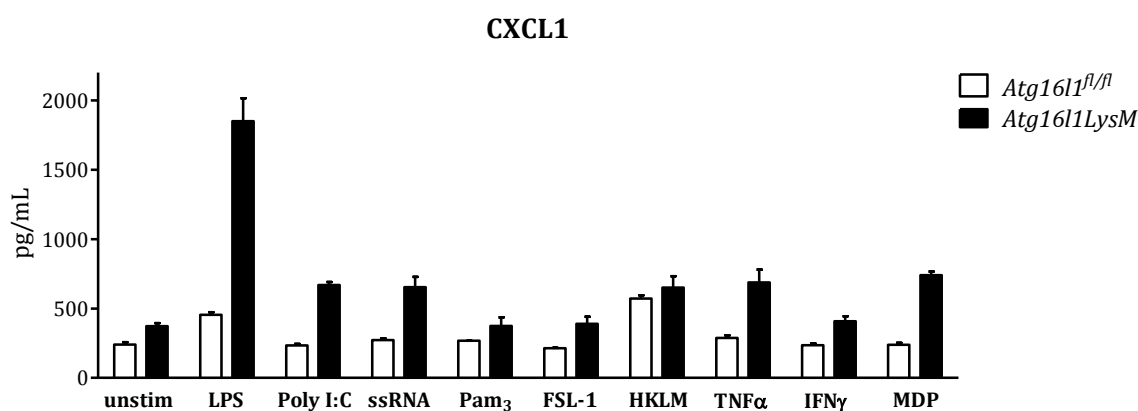


FIGURE 4-29: INCREASED CXCL1 SECRETION IN *ATG16L1LYSM* BMDMS UPON TLR4 STIMULATION

Atg1611^{fl/fl} and *Atg1611LysM* BMDMs (n=1) were either left unstimulated or stimulated with 100 ng/mL LPS (*E. coli* F515), 1 μ g/mL Poly I:C, 1 μ g/mL ssRNA40 (ssRNA), 100 ng/mL Pam₃CSK₄ (Pam₃), 100 ng/mL FSL-1, 100 bacteria/cell heat-killed *Listeria monocytogenes* (HKLM), 25 ng/mL TNF α , 25 ng/mL IFN γ or 10 ng/mL MDP for 24 h. Cell culture supernatants were collected and concentrations of CXCL1 were measured by ELISA. Data are shown as mean of the measured triplicates \pm S.D.

Already untreated *Atg1611LysM* BMDMs showed a slightly increased CXCL1 secretion compared to *Atg1611^{fl/fl}* BMDMs. Stimulation with lipopolysaccharide (LPS), polyinosinic:polycytidylic acid (Poly I:C), single-stranded RNA (ssRNA), TNF α or muramyl dipeptide (MDP) even resulted in a much stronger increase of CXCL1 release of *Atg1611LysM* BMDMs whereas LPS treatment by far showed the strongest difference. Only slight differences were detected upon stimulation with the synthetic lipoproteins Pam₃CSK₄ and

FSL-1 as well as upon stimulation with heat-killed *Listeria monocytogenes* (HKLM) and IFN γ . For this reason, the present study and any further experiments focused on the role of ATG16L1 in TLR4 signaling.

To address if the observed results represent a general effect of ATG16L1 on cytokine secretion, supernatants of untreated and LPS-treated BMDMs were analyzed for several cytokines and chemokines. No differences were observed between *Atg161LysM* and *Atg1611^{fl/fl}* BMDMs under basal conditions (data not shown) whereas stimulation with LPS induced cytokine and chemokine secretion in both genotypes (Figure 4-30). However, *Atg161LysM* macrophages showed an augmented LPS-induced cytokine production compared to LPS-treated *Atg1611^{fl/fl}* BMDMs. Out of the 23 studied cytokines and chemokines IL1 α and CXCL1 were significantly upregulated in *Atg161LysM* BMDMs. No changes were observed for the release of IL3, IL4, IL5, IL9, IL17, MCP1, RANTES and IFN γ (data not shown).

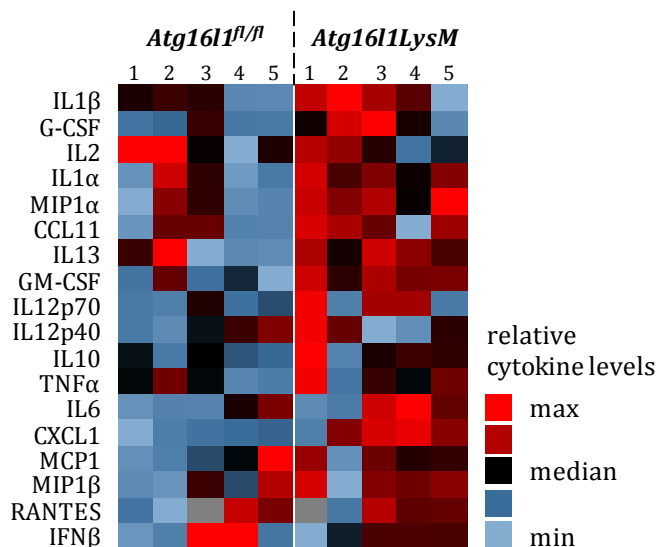


FIGURE 4-30: TLR4-MEDIATED HYPER-SECRETION OF CYTOKINES AND CHEMOKINES IN *ATG16L1LysM* BMDMs
Atg1611^{fl/fl} and *Atg161LysM* BMDMs (n=5) were stimulated with 25 ng/mL LPS (*E. coli* F515) for 24 h. Cell culture supernatants were collected and concentrations of cytokines and chemokines were measured in duplicates using the Bio-Plex Pro™ Mouse Cytokine 23-plex Assay (BioRad) or ELISA. For better readability, concentration values were z-score normalized.

To define whether the loss of *Atg1611* affects cytokine secretion directly by influencing the release or indirectly by regulating the expression, mRNA expression levels of pro- and anti-inflammatory cytokines and chemokines were determined (Figure 4-31). Although untreated *Atg1611*-deficient BMDMs did not show altered cytokine levels in the supernatant (data not shown), mRNA expression analysis revealed significantly upregulated expression of *Cxcl1* and *Ifng* as well as significantly diminished expression of *interleukin-18* (*Il18*) compared to *Atg1611^{fl/fl}* macrophages. Stimulation with LPS for 24 h resulted in significantly increased mRNA expression levels of *Il1a*, *Il1b* and *Cxcl1* validating the observed significant differences in IL1 α and CXCL1 secretion after LPS treatment (Figure 4-30). LPS-treated *Atg161LysM* BMDMs also exhibited significantly increased expression of *Ifng* in response to LPS. No alterations were observed for *Il6* and *Il10* as well as the type I interferon *Ifnb*, whereas expression of *Tnfa* and *Il18* was slightly reduced in *Atg161LysM* macrophages compared to *Atg1611^{fl/fl}* BMDMs after LPS stimulation.

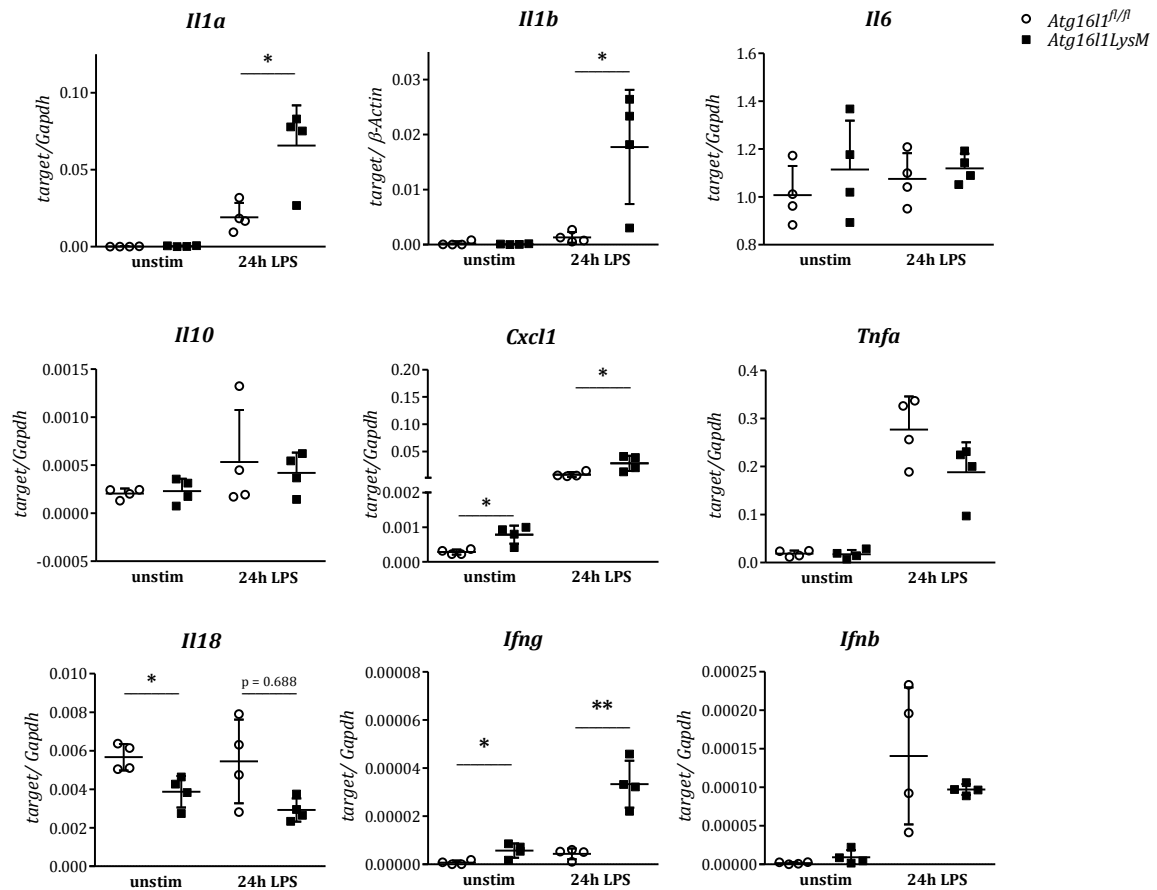


FIGURE 4-31: *Atg16l1*-DEFICIENCY LEADS TO AN ALTERED GENE EXPRESSION OF CYTOKINES AND CHEMOKINES AFTER LPS STIMULATION

In three independent experiments *Atg16l1^{fl/fl}* and *Atg16l1^{LysM}* BMDMs (n=4) were stimulated with 25 ng/mL LPS (*E. coli* F515) for 24 h or left unstimulated. Expression levels of *Il1a*, *Il6*, *Il10*, *Cxcl1* and *Tnfa* were analyzed by SYBR green qPCR. *Il1b*, *Il18*, *Ifng* and *Ifnb* expression analysis were performed using TaqMan assays. Expression levels of the indicated targets were normalized to *Gapdh* or β -*Actin*. Data are shown as mean \pm S.D. and were tested for statistical significance using an unpaired Student's *t*-test. * $p < 0.05$, ** $p < 0.01$

4.5.2 CYTOKINE EXPRESSION AND SECRETION IS MODULATED BY CONSTITUTIVE NF- κ B AND P38 MAPK ACTIVATION IN *ATG16L1LYSM* BMDMs

LPS-triggered TLR4 activation results in various signaling cascades initiating the activation of transcription factors like NF- κ B, AP-1 and IRFs, which in turn leads to expression of cytokines and chemokines. In this scenario, NF- κ B controls expression of pro- and anti-inflammatory cytokines whereas IRFs specifically induce expression of type I interferons like IFN β . Given that expression of the upregulated cytokines *Il1a*, *Il1b*, *Cxcl1* and *Ifng* is mainly controlled by NF- κ B [230-234], phosphorylation of the NF- κ B subunit p65 at Ser536 was investigated in a time course of LPS stimulation (Figure 4-32).

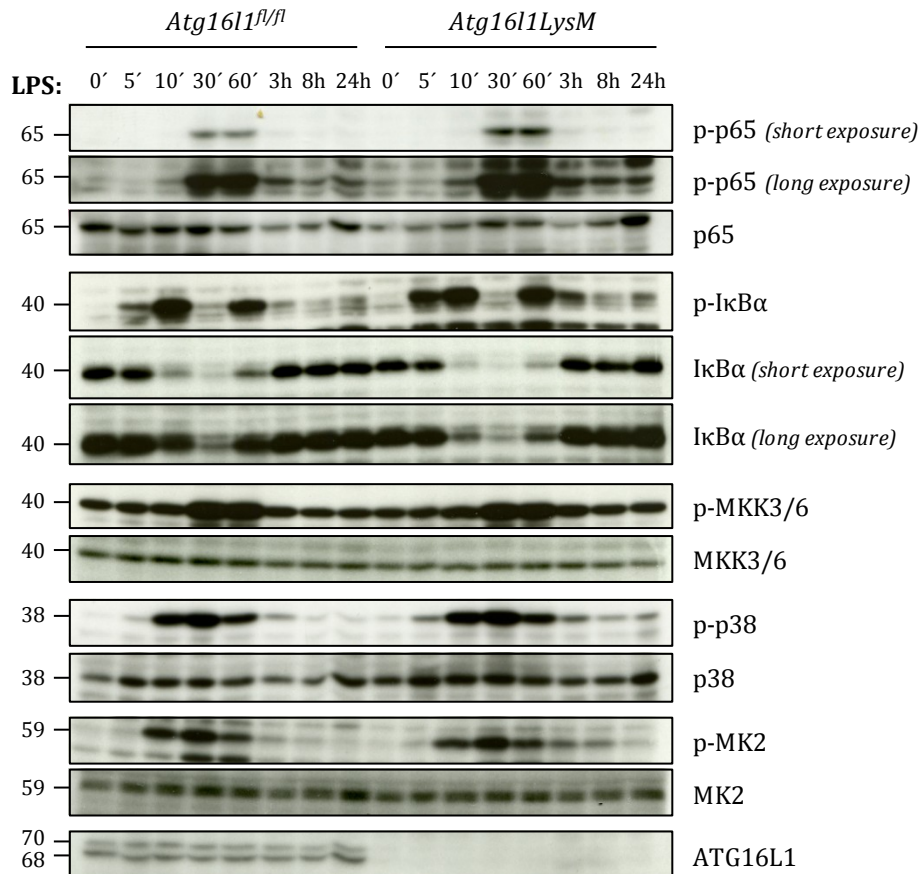


FIGURE 4-32: INCREASED AND PROLONGED PHOSPHORYLATION OF CANONICAL P65 AND P38 MAPK SIGNALING IN *ATG16L1^{LysM}* MACROPHAGES UPON LPS STIMULATION

Atg16l1^{fl/fl} and *Atg16l1^{LysM}* BMDMs were stimulated with 25 ng/mL LPS (*E. coli* F515) for the indicated time points or left unstimulated. Proteins were extracted and immunoblotted. Protein levels were evaluated using the indicated antibodies. Unphosphorylated proteins served as loading control. One representative immunoblot out of at least three individual experiments is shown.

Loss of *Atg16l1* resulted in an earlier and stronger activation of canonical NF-κB signaling by showing increased phosphorylation of the NF-κB subunit p65 and IκBα already after 30 min and 5 min of LPS stimulation, respectively (Figure 4-32). As expected, the augmented IκBα phosphorylation subsequently resulted in increased degradation of IκBα in *Atg16l1^{LysM}* BMDMs in response to LPS. Further, p65 activation was prolonged for up to 24 h in *Atg16l1*-deficient macrophages when compared to *Atg16l1^{fl/fl}* littermate BMDMs. Similar results were observed for the canonical p38 MAPK signaling [235]. Phosphorylation and thus activation of MKK3/6 was stronger induced in *Atg16l1^{LysM}* BMDMs already 10 min after LPS treatment. As canonical downstream targets, MKK3/6 phosphorylation mediated an earlier and stronger phosphorylation of p38 MAPK directly initiating the phosphorylation of MK2. In line with the canonical NF-κB signaling, MKK3/6, p38 and MK2 as components of the canonical p38 MAPK pathway demonstrated an enhanced and sustained activation for up to 24 h after LPS treatment. None of the indicated signaling molecules showed an accumulation of its basal unphosphorylated protein levels excluding a deregulated protein homeostasis of these molecules due to the lack of autophagy.

Beside canonical NF- κ B activation via phosphorylation of I κ B α and its subsequent proteasomal degradation [236] several studies reported a substantial role for p38 MAPK in NF- κ B activation [237, 238]. To investigate a putative crosstalk between p38 MAPK signaling and the canonical NF- κ B pathway BMDMs derived from *Atg16l1^{fl/fl}* and *Atg16l1^{LysM}* mice were challenged with either LPS or the selective p38 activity inhibitor SB202190 (ip38) alone or a combination of both stimuli (Figure 4-33).

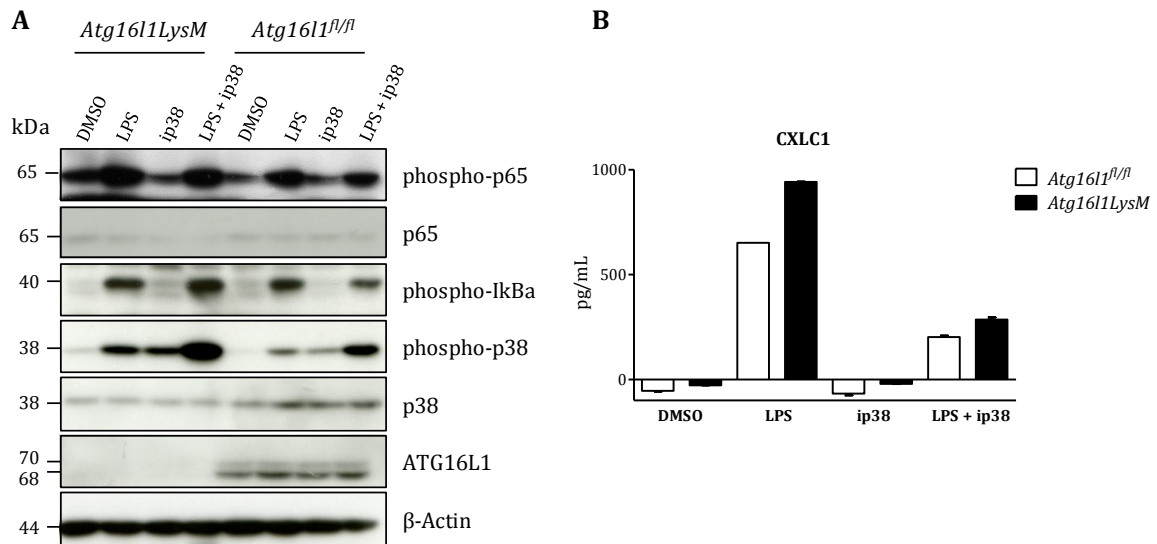


FIGURE 4-33: CONSTITUTIVE ACTIVATION OF P65 OCCURRED INDEPENDENT OF P38 MAPK ACTIVITY
Atg16l1^{fl/fl} and *Atg16l1^{LysM}* BMDMs were stimulated for 6 h with DMSO as control or 25 ng/mL LPS (*E.coli* F515) in absence or presence of 10 μ M p38 activity inhibitor SB202190 (ip38). Stimulation with ip38 was performed 1 h prior to DMSO or LPS. Protein lysates were immunoblotted and protein levels were analyzed using the indicated antibodies (A). β -Actin and unphosphorylated proteins served as loading controls. One representative immunoblot out of 3 individual experiments is shown. CXCL1 concentrations were determined in the appropriate supernatant by ELISA (B). ELISA results are representatives for at least three independent experiments. Data represent mean \pm S.D. of technical duplicates.

Stimulation with ip38 alone resulted in elevated phospho-p38 levels compared to the appropriate DMSO-treated controls but had no effect on phospho-I κ B α or phospho-p65 levels in BMDMs of both genotypes. In addition, blocked p38 activity during LPS treatment further increased phospho-p38 but hardly reduced phospho-I κ B α and phospho-p65 levels and did not diminish the observed differences in LPS-treated *Atg16l1^{LysM}* BMDMs compared to *Atg16l1^{fl/fl}* BMDMs. Following downstream events of NF- κ B activation, CXCL1 secretion was analyzed as a hallmark of the *ex vivo* phenotype in *Atg16l1*-deficient macrophages (Figure 4-33 B). Inhibition of p38 activity combined with LPS treatment led to a decrease in CXCL1 secretion. However, the relative differences between *Atg16l1^{LysM}* and *Atg16l1^{fl/fl}* BMDMs persisted even during inhibition of p38 MAPK activity.

4.5.3 IMPAIRED AUTOPHAGY DOES NOT RESULT IN ACCUMULATION OF TLR4 SIGNALING COMPONENTS BUT P62

Recent studies implicated a role for autophagy in regulation of TLR4 signaling by degrading TLR4 components and complexes [239, 240]. For this reason, protein levels of TLR4 signaling molecules upstream of the canonical NF- κ B and p38 MAPK signaling pathways were studied (Figure 4-34).

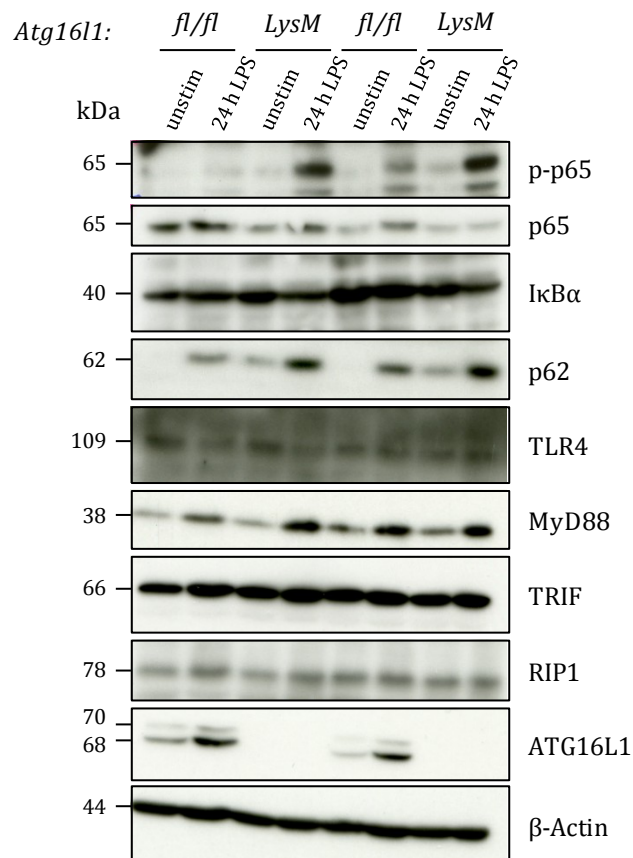


FIGURE 4-34: PROTEIN LEVELS OF TLR4 SIGNALING MOLECULES IN ABSENCE AND PRESENCE OF LPS

Atg16l1^{fl/fl} and *Atg16l1*^{LysM} BMDMs were left unstimulated or stimulated with 25 ng/mL LPS (*E. coli* F515) for 24 h. Proteins were extracted and immunoblotted. Protein levels were analyzed using the indicated antibodies. β -Actin and unphosphorylated proteins served as loading controls.

Atg16l1^{fl/fl} and *Atg16l1*^{LysM} BMDMs showed similar levels of the TLR4 receptor and its adaptor molecules MyD88, TRIF and receptor-interacting serine/threonine-protein kinase 1 (RIP1) in presence and absence of LPS. In contrast, p62 levels increased in BMDMs of both genotypes in response to LPS. The observed relative differences seen in unstimulated cells persisted after LPS stimulation in *Atg16l1*^{LysM} BMDMs. Coinciding with the immunoblot results, immunofluorescence analysis determined increased cytoplasmic level of p62 in untreated *Atg16l1*^{LysM} BMDMs compared to *Atg16l1*^{fl/fl} macrophages (Figure 4-35 A). Whereas *Atg16l1*^{fl/fl} BMDMs demonstrated a uniform cytosolic distribution of p62, endogenous p62 in *Atg16l1*-deficient BMDMs was primarily localized in cytosolic aggregates. This phenomenon was also observed in cells of the red pulp in the spleen of *Atg16l1*^{LysM} mice under basal conditions whereas it was completely absent in *Atg16l1*^{fl/fl} mice (Figure 4-35 B). Stimulation with LPS at first provoked the formation of large p62 aggregates in

Atg16l1^{fl/fl} BMDMs while a further accumulation of p62 was observed in *Atg16l1LysM* macrophages compared to the appropriate untreated cells (Figure 4-35 A). The initially detected differences in p62 levels of untreated *Atg16l1^{fl/fl}* and *Atg16l1LysM* macrophages were preserved in presence of LPS supporting the findings on protein levels determined by immunoblot (Figure 4-34) which might point to a physiological role of p62 aggregate formation in response to LPS.

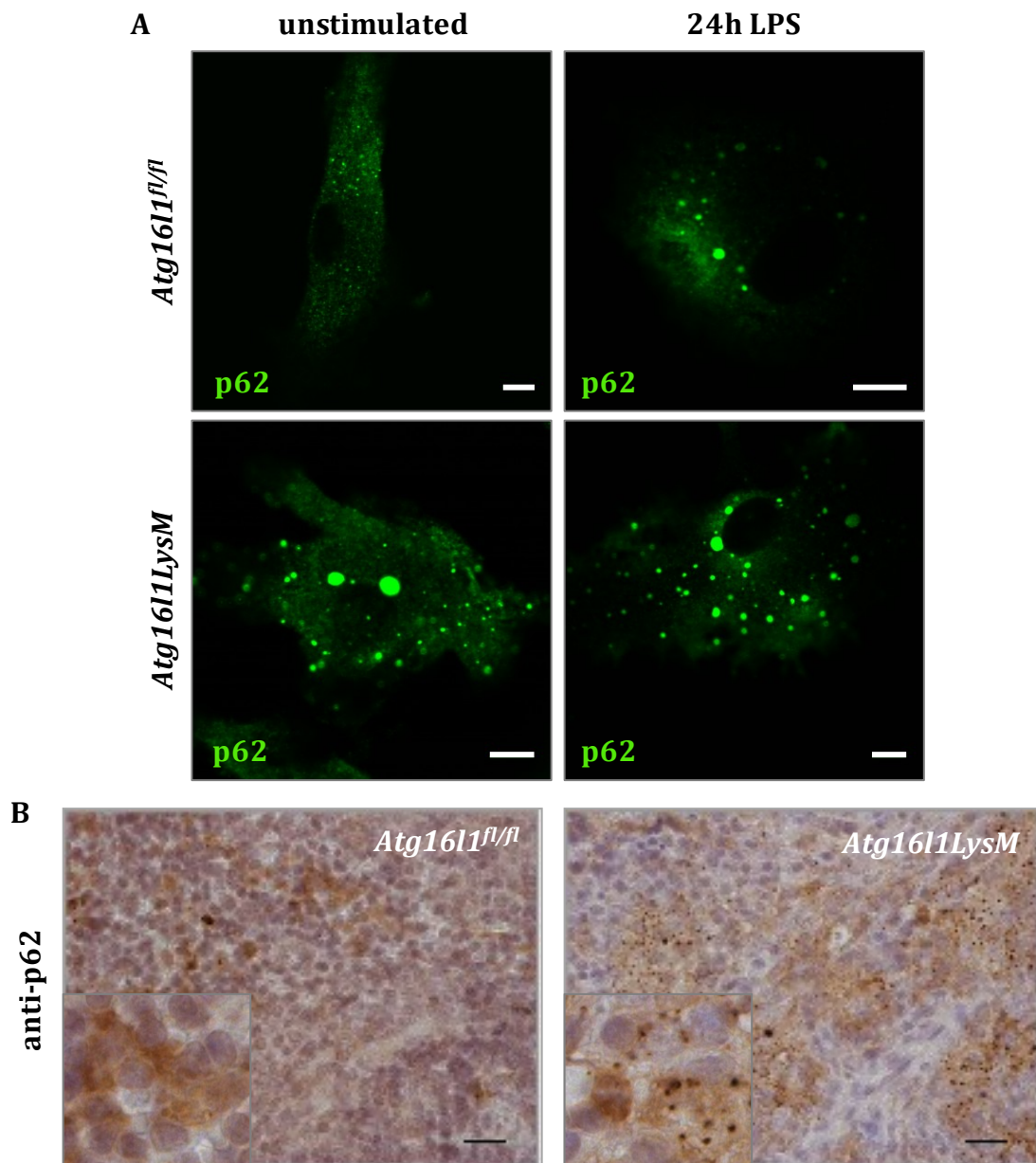


FIGURE 4-35: IN VITRO AND IN VIVO AGGREGATES OF P62 IN ATG16L1-DEFICIENT MACROPHAGES
 BMDMs derived from *Atg16l1^{fl/fl}* and *Atg16l1LysM* mice were left unstimulated or treated with 25 ng/mL LPS (*E.coli* F515) for 24 h and stained for p62 (green) using the immunofluorescence technique (A). Scale bars represent 5 μ m. Representative images from at least 3 independent experiments are shown. Splenic sections from *Atg16l1^{fl/fl}* and *Atg16l1LysM* mice were immunohistochemically stained for p62 (brown) (B). Scale bars represent 100 μ m. Images are representative for four independent littermate pairs.

4.5.4 *ATG16L1*-DEFICIENT MACROPHAGES DISPLAY AN INTACT ENDOCYTOTIC MACHINERY

Since TLR4 internalization emerged as a crucial step in TRIF-dependent late NF- κ B signaling [241] and *Atg16l1*-deficient BMDMs showed a LPS-induced prolonged NF- κ B activation, endocytosis was next investigated. To first analyze a putative general effect of *Atg16l1*-deficiency on the endocytotic machinery, pinocytosis was measured by FITC-Dextran uptake (Figure 4-36).

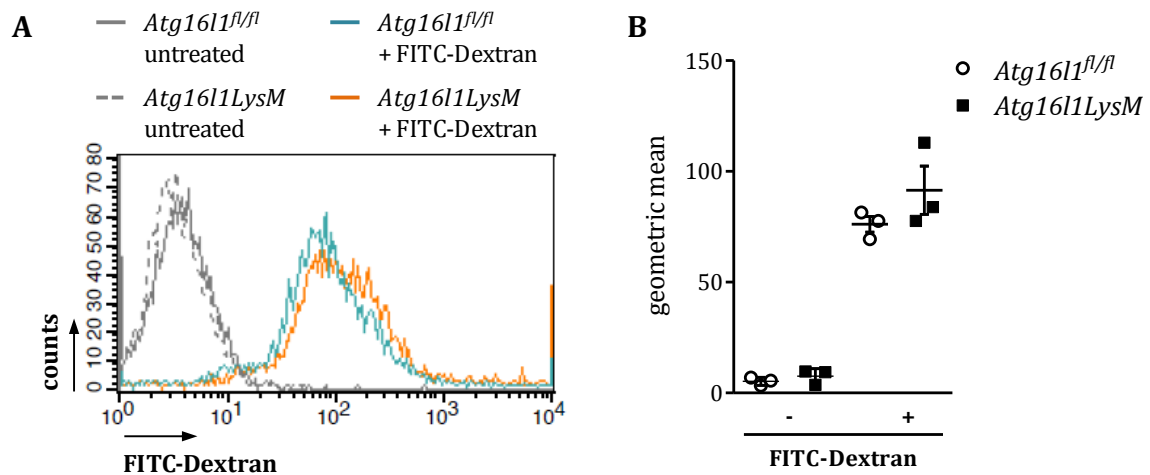


FIGURE 4-36: INTACT PINOCYTOSIS IN *ATG16L1*-DEFICIENT BMDMS

Atg16l1^{fl/fl} and *Atg16l1LysM* BMDMs (n=3) were incubated with 1 mg/mL FITC-Dextran or left untreated for 60 min. Fluorescence intensity was measured by flow cytometry and depicted as a representative histogram (A). Geometric means of fluorescence intensity (n=3) are displayed in a graph as mean \pm S.D. and statistical significance was tested using an unpaired Student's *t*-test (B).

Atg16l1^{fl/fl} and *Atg16l1LysM* BMDMs showed no differences in FITC-Dextran uptake. However, endocytosis is not exclusively subclassified in pinocytosis, phagocytosis and receptor-mediated endocytosis by the up taken particles but also by their invagination mechanisms. A general defect in receptor internalization could explain the increased TLR4 signaling (Figure 4-32) as well as the upregulated activation markers on *Atg16l1*-deficient CD11b⁺ myeloid cells *in vivo* (Figure 4-14). Stimulation-induced receptor internalization of CD95, one of the significantly upregulated activation markers on CD11b⁺ cells in spleen and blood (Figure 4-14, Figure 4-22), was analyzed by flow cytometry (Figure 4-37).

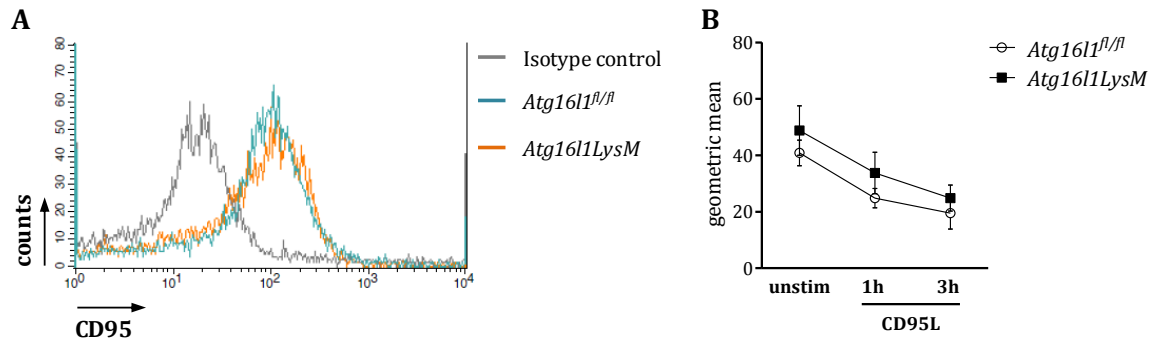


FIGURE 4-37: SIMILAR INTERNALIZATION CAPACITY OF CD95 ON *ATG16L1^{FL/FL}* AND *ATG16L1^{LysM}* BMDMs

Cell surface expression of CD95 was analyzed on untreated *Atg16l1^{FL/FL}* and *Atg16l1^{LysM}* BMDMs (n=4) by flow cytometry (A). Representative histogram of the fluorescence intensity is depicted. Internalization rate of CD95 was analyzed in *Atg16l1^{FL/FL}* and *Atg16l1^{LysM}* BMDMs (n=4) after treatment with 1µg/mL CD95L for the indicated time points (B). Graph displays geometric means of the fluorescence intensity ± S.D. Statistical significance was evaluated using an unpaired Student's *t*-test. CD95L: CD95 Ligand

Although not expected from the *in vivo* results, similar cell surface expression of CD95 was determined on untreated *Atg16l1^{FL/FL}* and *Atg16l1^{LysM}* BMDMs (Figure 4-37 A). Following stimulation with anti-CD95 as ligand (CD95L) for up to 3 h, BMDMs of both genotypes showed a similar internalization capacity of the CD95 receptor (Figure 4-37 B). Moreover, neither TLR4 nor macrophage scavenger receptor 1 (MSR1) showed differences in cell surface expression and on protein levels, respectively (Figure 4-38).

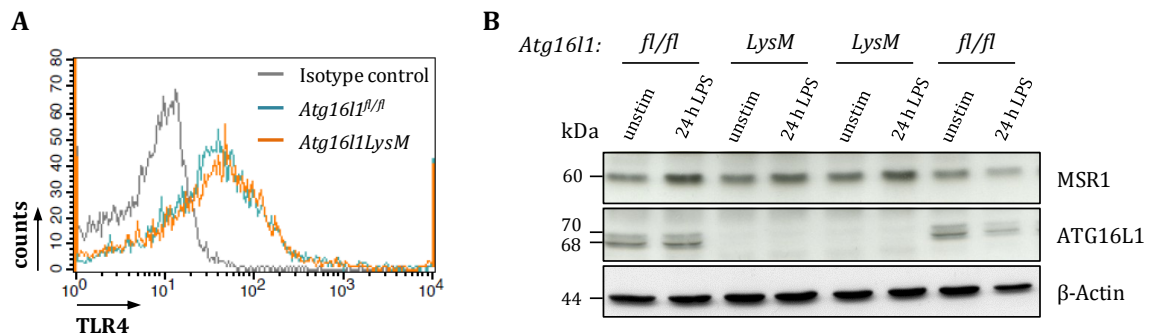


FIGURE 4-38: EQUAL EXPRESSION OF LPS-BINDING RECEPTORS IN *ATG16L1^{FL/FL}* AND *ATG16L1^{LysM}* BMDMs

TLR4 surface expression was analyzed by flow cytometry on untreated *Atg16l1^{FL/FL}* and *Atg16l1^{LysM}* BMDMs (A). Histogram is representative for at least three independent experiments. Protein levels of MSR1 in untreated and LPS-stimulated (*E.coli*, F515) *Atg16l1^{FL/FL}* and *Atg16l1^{LysM}* BMDMs (n=2) were analyzed by immunoblot. β-Actin served as loading control. MSR1: macrophage scavenger receptor 1

Summing up, *Atg16l1* deficiency did not result in a general endocytotic dysfunction as determined by FITC-Dextran uptake and CD95 internalization.

4.5.5 *ATG16L1* DEFICIENCY INFLUENCES PROTEIN LEVELS OF THE TLR4 NEGATIVE REGULATOR A20 BUT NOT CYLD UPON LPS STIMULATION

Protein levels of MyD88, TRIF and RIP1 were not affected and thus did not explain the prolonged activation of p38 and p65 in *Atg16l1LysM* BMDMs. Thus, the present study next focused on negative feedback loops as a regulatory mechanism of TLR4 signaling.

NF- κ B activation is controlled by a variety of negative feedback loops ensuring the downregulation of the TLR4 signaling cascade, e.g. *tumor necrosis factor, alpha-induced protein 3* (*Tnfaip3*, also known as *A20*) and *cylindromatosis (turban tumor syndrome)* (*Cyld*) [242]. No alterations on protein levels of A20 and CYLD were observed in unstimulated *Atg16l1LysM* BMDMs when compared to *Atg16l1^{fl/fl}* BMDMs (Figure 4-39). Challenging BMDMs for 6 h with LPS equally decreased the levels of CYLD in both, *Atg16l1LysM* and *Atg16l1^{fl/fl}* macrophages. In contrast, protein levels of A20 were increased upon LPS stimulation in BMDMs of both genotypes. However, *Atg16l1LysM* macrophages showed a much stronger increase of A20 after LPS stimulation, which did not persist after inhibition of protein biosynthesis by cycloheximide (CHX). This result showed an LPS-mediated *de novo* synthesis of A20 which is amplified due to *Atg16l1* deficiency.

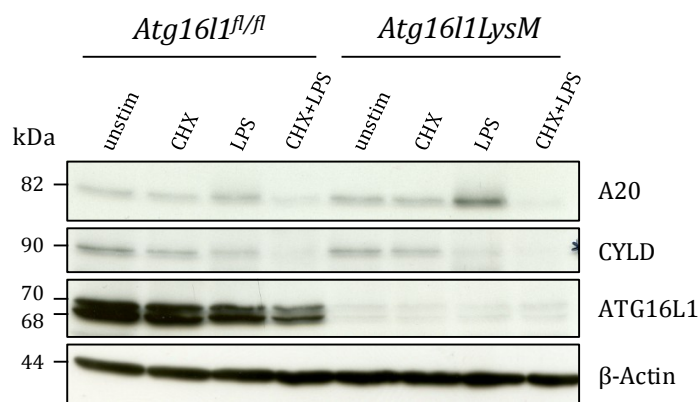


FIGURE 4-39: *ATG16L1* DEFICIENCY AFFECTS A20 BUT NOT CYLD LEVELS

Atg16l1^{fl/fl} and *Atg16l1LysM* BMDMs were left unstimulated or stimulated for 6 h with 25 ng/mL LPS (*E.coli* F515) in absence or presence of 1 μ g/mL CHX (1 h prior to LPS). CHX or LPS alone served as controls. Protein extracts were immunoblotted. Using the indicated antibodies, proteins levels were detected. β -Actin served as loading control. CHX: cycloheximide

To determine whether the elevated A20 levels directly resulted from the observed sustained p65 phosphorylation in *Atg16l1LysM* BMDMs mRNA expression levels of *A20* were analyzed (Figure 4-40). In contrast to the detected differences in NF- κ B-dependent cytokine expression (Figure 4-31), loss of *Atg16l1* did not differentially modulate *A20* expression compared to *Atg16l1^{fl/fl}* BMDMs neither in absence nor in presence of LPS, which pointed to a regulatory function of ATG16L1 on the post-translational level of A20.

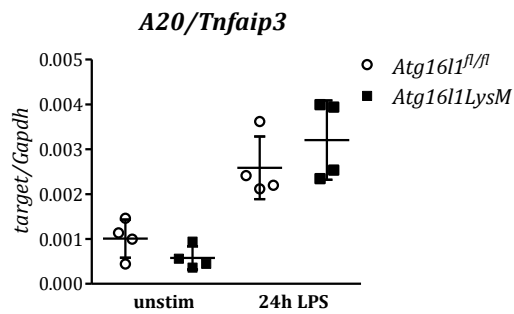


FIGURE 4-40: SIMILAR MRNA EXPRESSION OF A20 UPON LPS STIMULATION IN *ATG16L1^{LysM}* AND *ATG16L1^{FL/FL}* MACROPHAGES

Using SYBR green qPCR mRNA expression of *A20/Tnfaip3* was measured after RNA extraction of untreated or LPS-treated (25 ng/mL, *E.coli* F515) *Atg16l1^{fl/fl}* and *Atg16l1^{LysM}* BMDMs (n=4 per genotype). *A20/Tnfaip3* expression was normalized to *Gapdh*. Data represent mean ± S.D. Statistical significance was evaluated using an unpaired Student's *t*-test.

This finding leads back to the hypothesis of a role for ATG16L1 in protein homeostasis. For this reason, protein degradation and trafficking was chemically inhibited during LPS stimulation in *Atg16l1^{fl/fl}* and *Atg16l1^{LysM}* macrophages (Figure 4-41 A). Inhibition of protein trafficking from the Golgi apparatus to the plasma membrane by Brefeldin A (BrefA) during LPS treatment did neither affect phosphorylation of p65 and p38 nor levels of A20. Inhibition of the proteasome using MG132 further increased LPS-induced phospho-p38 levels whereas phospho-p65 and A20 levels were only slightly enhanced compared to LPS-treated cells of both genotypes. In contrast, inhibition of lysosomal protein degradation means by treatment with Bafilomycin A (BafA) resulted in the opposite effect showing increased LPS-induced phospho-p65 and A20 levels but not phospho-p38 levels. Treatment with BafA and LPS further coincides with an increased CXCL1 secretion whereas LPS-induced CXCL1 secretion was slightly reduced by blocking proteasomal degradation (Figure 4-41 B).

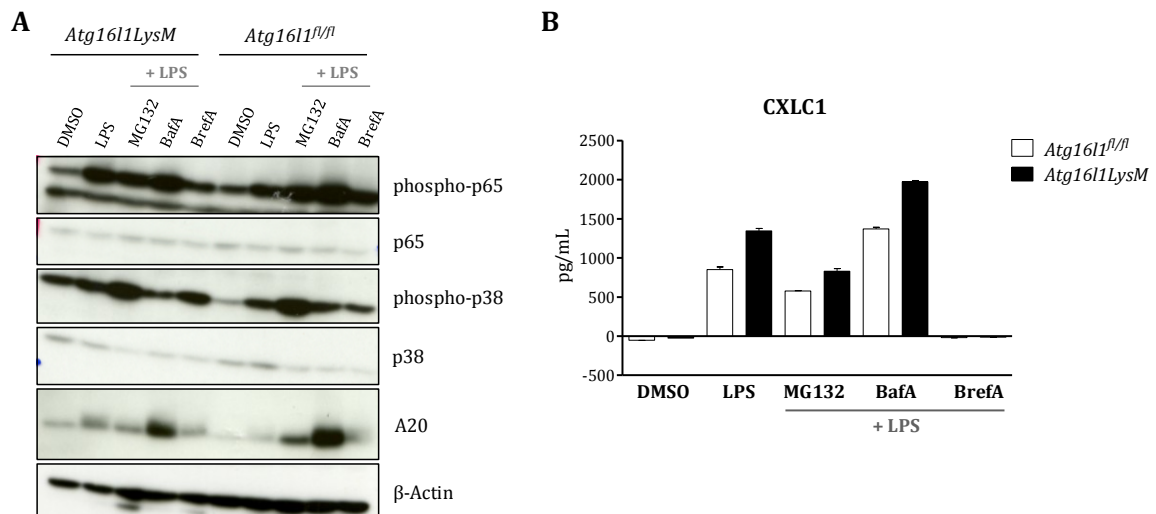


FIGURE 4-41: INHIBITION OF LYSOSOMAL DEGRADATION DURING LPS STIMULATION LEADS TO A20 ACCUMULATION *Atg16l1^{fl/fl}* and *Atg16l1^{LysM}* BMDMs were stimulated for 8 h with DMSO as control, 25 ng/mL LPS (*E.coli* F515) alone or in combination with either 1 nM MG132, 100 nM BafA or 5 µg/mL BrefA 1h prior to LPS. Proteins were extracted and immunoblotted. Protein levels were detected using the indicated antibodies (A). β-Actin and unphosphorylated proteins served as loading controls. One representative immunoblot out of 3 individual experiments is shown. CXCL1 levels were determined in the appropriate supernatant by ELISA (B). ELISA results are representatives for at least three independent experiments. Data represent mean ± S.D. of technical duplicates.

4.5.6 REACTIVE OXYGEN SPECIES AMPLIFY BUT DO NOT CAUSE LPS-INDUCED HYPER-ACTIVATION IN *ATG16L1*LysM BMDMS

Recent studies suggested an immunoregulatory role for autophagy in NLRP3 activation via reactive oxygen species (ROS) due to impaired clearance of damaged mitochondria [22, 72, 227]. For this reason, the impact of *Atg16l1* deficiency in macrophages on ROS production and a putative role in the observed LPS-mediated hyper-activation was investigated.

Analysis of Mitotracker staining using flow cytometry revealed a similar membrane potential of mitochondria in *Atg16l1*LysM BMDMs compared to *Atg16l1*^{fl/fl} BMDMs (Figure 4-42 A). Similar results were also seen for ROS production under basal conditions (Figure 4-42 B).

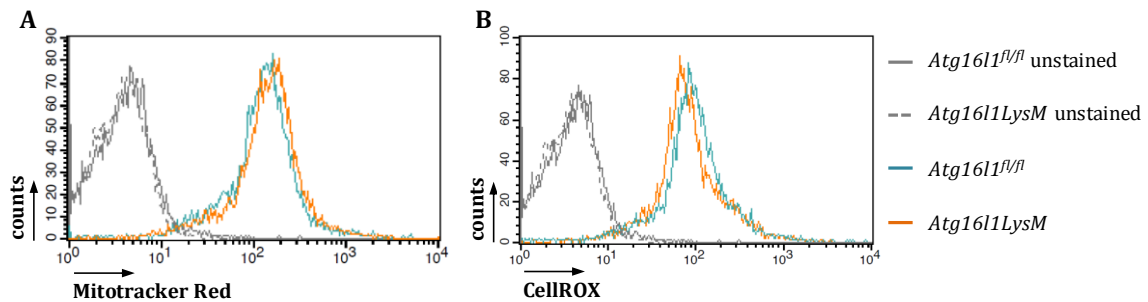


FIGURE 4-42: *ATG16L1* DEFICIENCY DOES NOT ALTER MITOCHONDRIAL MEMBRANE POTENTIAL AND ROS PRODUCTION IN MACROPHAGES

Untreated *Atg16l1*^{fl/fl} and *Atg16l1*LysM BMDMs were stained with either 1 μ M Mitotracker Red (A) or 5 μ M CellROX Deep Red (B) for 30 min at 37 $^{\circ}$ C and analyzed using flow cytometry. Representative histograms out of three independent experiments are displayed.

To investigate whether increased ROS production might be responsible for the observed phenotype in macrophages lacking *Atg16l1* BMDMs were stimulated with LPS alone or in combination with the ROS inhibitor diphenyleneiodonium (DPI) [243]. First, inhibitory properties of DPI regarding LPS-mediated ROS production was confirmed by flow cytometry (Figure 4-43).

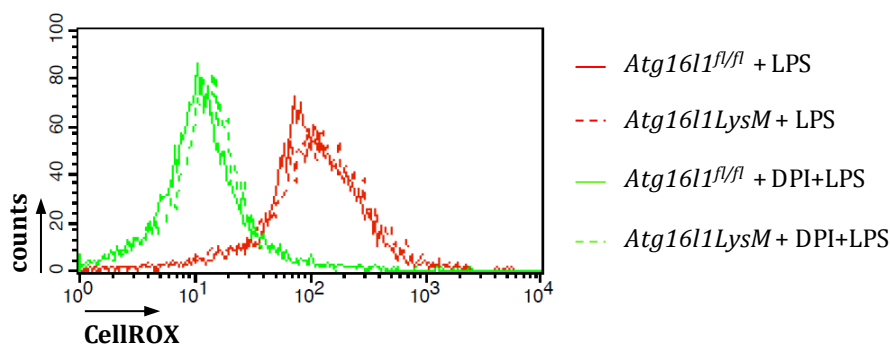


FIGURE 4-43: INHIBITION OF LPS-INDUCED PRODUCTION OF REACTIVE OXYGEN SPECIES IN BMDMS

Atg16l1^{fl/fl} and *Atg16l1*LysM BMDMs were treated for 24 h with 25 ng/mL LPS (*E.coli* F515) alone or in combination with 2 μ M DPI that was administered 1 h prior to LPS. Cells were stained with 5 μ M CellROX Deep Red for 30 min at 37 $^{\circ}$ C and analyzed by flow cytometry. Representative histogram out of three independent experiments is depicted. DPI: Diphenyleneiodonium

DPI specifically blocked LPS-induced ROS production in both, *Atg16l1^{fl/fl}* and *Atg16l1LysM* BMDMs. Next, the functional impact of ROS within the LPS-mediated phenotype of *Atg16l1LysM* macrophages was analyzed on protein level (Figure 4-44 A). Stimulation with DPI alone does not result in altered protein levels. In contrast, inhibition of LPS-induced ROS production markedly decreased phosphorylation of p38 and p65 in *Atg16l1^{fl/fl}* as well as *Atg16l1LysM* BMDMs. However, the observed differences in phospho-p38 and phospho-p65 as well as on pro-IL1 β levels persisted between *Atg16l1LysM* BMDMs compared to *Atg16l1^{fl/fl}* cells suggesting an amplifying but not initial role for ROS within TLR4-mediated hyper-activation in *Atg16l1LysM* BMDMs. Interestingly, this phenomenon was not observed for A20 indicating a ROS-independent mechanism of regulating A20 levels. In agreement with the remaining differences in phosphorylation of p65, analysis of CXCL1 concentrations in the supernatant of BMDMs treated with LPS and DPI showed a diminished CXCL1 secretion compared to LPS-treated BMDMs with lasting differences between *Atg16l1LysM* and *Atg16l1^{fl/fl}* BMDMs (Figure 4-44 B).

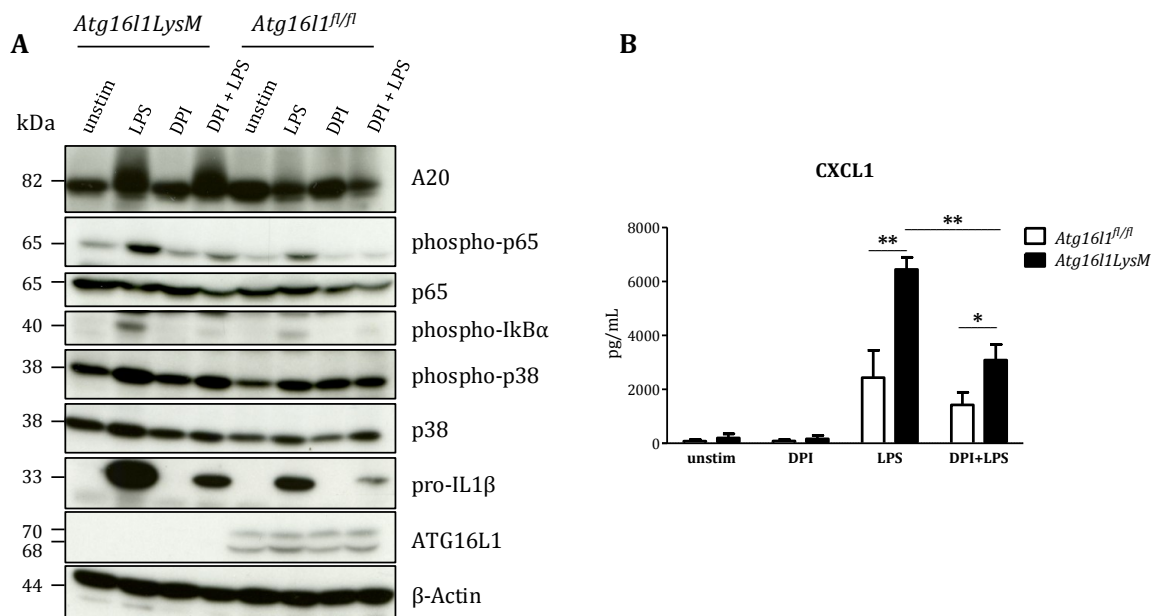


FIGURE 4-44: INHIBITION OF REACTIVE OXYGEN SPECIES AMELIORATES THE LPS-MEDIATED PHENOTYPE IN *Atg16l1LysM* BMDMs

Atg16l1^{fl/fl} and *Atg16l1LysM* BMDMs were left unstimulated for 24 h or stimulated with either 25 ng/mL LPS (*E.coli* F515) or 2 μ M DPI or in combination by administer DPI 1 h prior to LPS. Proteins were extracted; immunoblotted and indicated proteins were analyzed using the indicated antibodies (A). Unphosphorylated levels of the appropriate phosphorylated proteins as well as β -Actin served as loading controls. One representative immunoblot out of three independent experiments is displayed. CXCL1 concentrations were determined in the appropriate supernatant (n=3) by ELISA (B). Data represent mean \pm S.D. and statistical significance was evaluated using an unpaired Student's *t*-test. * $p < 0.05$, ** $p < 0.01$, DPI: Diphenyleneiodonium

4.5.7 CONSTITUTIVE NF- κ B ACTIVATION OCCURS INDEPENDENT OF IL1R SIGNALING IN *ATG16L1**LysM* BMDMS

Since pro-IL1 β was stronger induced after LPS stimulation in *Atg16l1LysM* BMDMs compared to *Atg16l1^{fl/fl}* BMDMs (Figure 4-44 A), a positive feedback loop of IL1 β on long-term NF- κ B activation was investigated using the IL1R antagonist Anakinra which was previously used in the *in vivo* study (Figure 4-45).

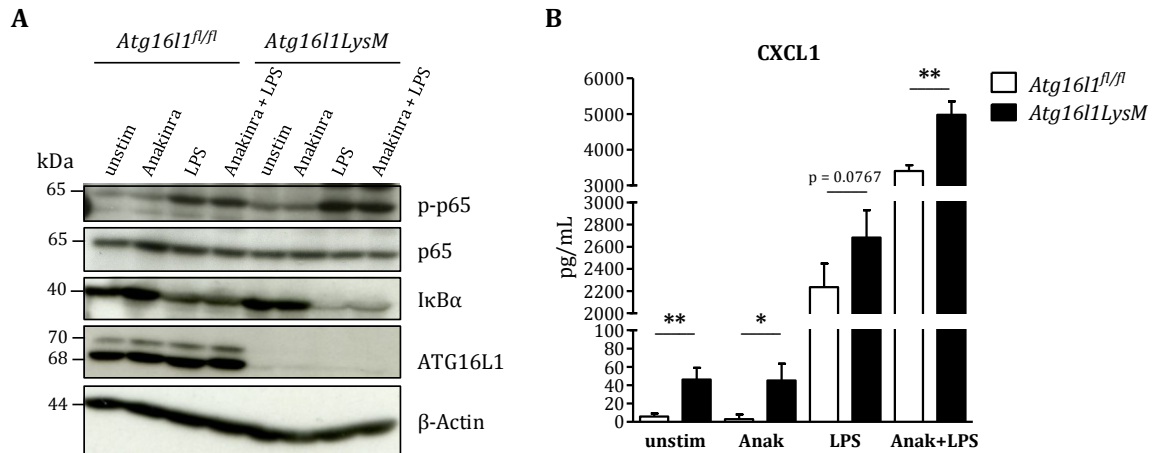


FIGURE 4-45: INHIBITION OF IL1R SIGNALING DOES NOT AFFECT LPS-INDUCED NF- κ B ACTIVATION
Atg16l1^{fl/fl} and *Atg16l1LysM* BMDMs were left unstimulated for 24 h or stimulated with either 25 ng/mL LPS (*E.coli* F515) or 1 μ g/mL Anakinra or in combination by administer Anakinra 1 h prior to LPS. Proteins were extracted; immunoblotted and indicated proteins were analyzed using the indicated antibodies (A). Unphosphorylated levels of p65 as well as β -Actin served as loading controls. One representative immunoblot out of three independent experiments is shown. CXCL1 concentrations were determined in the appropriate supernatant (n=3) by ELISA (B). Data represent mean \pm S.D. and statistical significance was evaluated using an unpaired Student's *t*-test. * $p < 0.05$, ** $p < 0.01$, Anak: Anakinra

Anakinra treatment neither attenuated the basal nor the LPS-induced differences in p65 phosphorylation and I κ B α degradation between *Atg16l1^{fl/fl}* and *Atg16l1LysM* BMDMs (Figure 4-45 A). Corroborating these observations, augmented CXCL1 production of *Atg16l1LysM* BMDMs compared to *Atg16l1^{fl/fl}* BMDMs persisted after treatment with the IL1R antagonist in presence and absence of LPS (Figure 4-45 B). Additionally, inhibition of IL1R signaling prior to LPS stimulation further increased the production of CXCL1.

Taken together, these findings exclude a putative feedback loop of pro-IL1 β on the constitutive LPS-induced activation of NF- κ B signaling.

4.6 ROLE OF ATG16L1 IN TLR4 SIGNALING *IN VIVO* USING THE ENDOTOXIN SHOCK MODEL

The *in vivo* impact of *Atg16l1*-deficiency on TLR4 signaling was further analyzed by challenging *Atg16l1^{fl/fl}* and *Atg16l1LysM* mice with a sublethal dosage of LPS (*E. coli* KPM53) for 72 h. In this setting, four out of seven *Atg16l1LysM* mice died within the first 24 h of LPS treatment whereas all *Atg16l1^{fl/fl}* mice survived (Figure 4-46).

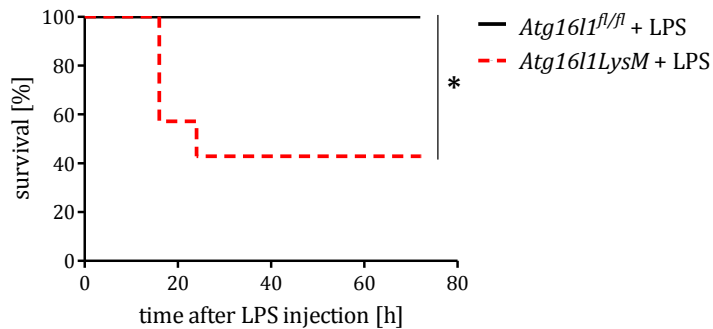


FIGURE 4-46: SURVIVAL CURVE DURING SUBLETHAL ENDOTOXIN SHOCK
Atg16l1^{fl/fl} and *Atg16l1LysM* mice (n=7) received an intraperitoneal injection of 5 mg/kg LPS (*E. coli* KPM53) or 5 μ L/g PBS as control. Survival was monitored for 72 h and depicted in a Kaplan-Meier curve. Statistical significance was calculated using a log-rank test. * p < 0.05

Validation of the organ weight after 72 h of LPS administration revealed a hepatosplenomegaly in *Atg16l1^{fl/fl}* mice comparable to PBS- or LPS-treated *Atg16l1LysM* mice (Figure 4-47 A and B). Spleen and liver weight of *Atg16l1LysM* mice did not increase further by LPS treatment.

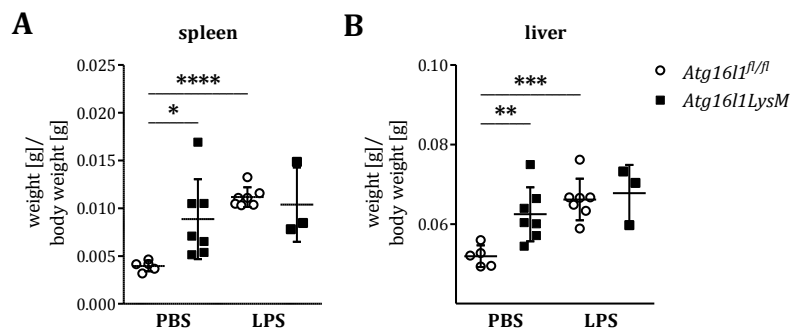


FIGURE 4-47: ORGAN WEIGHT AFTER 72 HOURS OF AN ENDOTOXIN-INDUCED SEPTIC SHOCK

Spleen weight (A) and liver weight (B) of *Atg16l1^{fl/fl}* and *Atg16l1LysM* mice (n=3-7) were assessed 72 h after an intraperitoneal injection of a sublethal dose of 5 mg/kg LPS (*E. coli* KPM53) or 5 μ L/g PBS as a control. Data represents mean \pm S.D. and statistical significance was evaluated using an unpaired Student's *t*-test. * p < 0.05, ** p < 0.01, *** p < 0.001, **** p < 0.0001

Analysis of the cytokine response within the first 6 h of LPS treatment showed markedly elevated levels of pro-inflammatory cytokines in the serum of *Atg16l1LysM* mice when compared to *Atg16l1^{fl/fl}* mice (Figure 4-48).

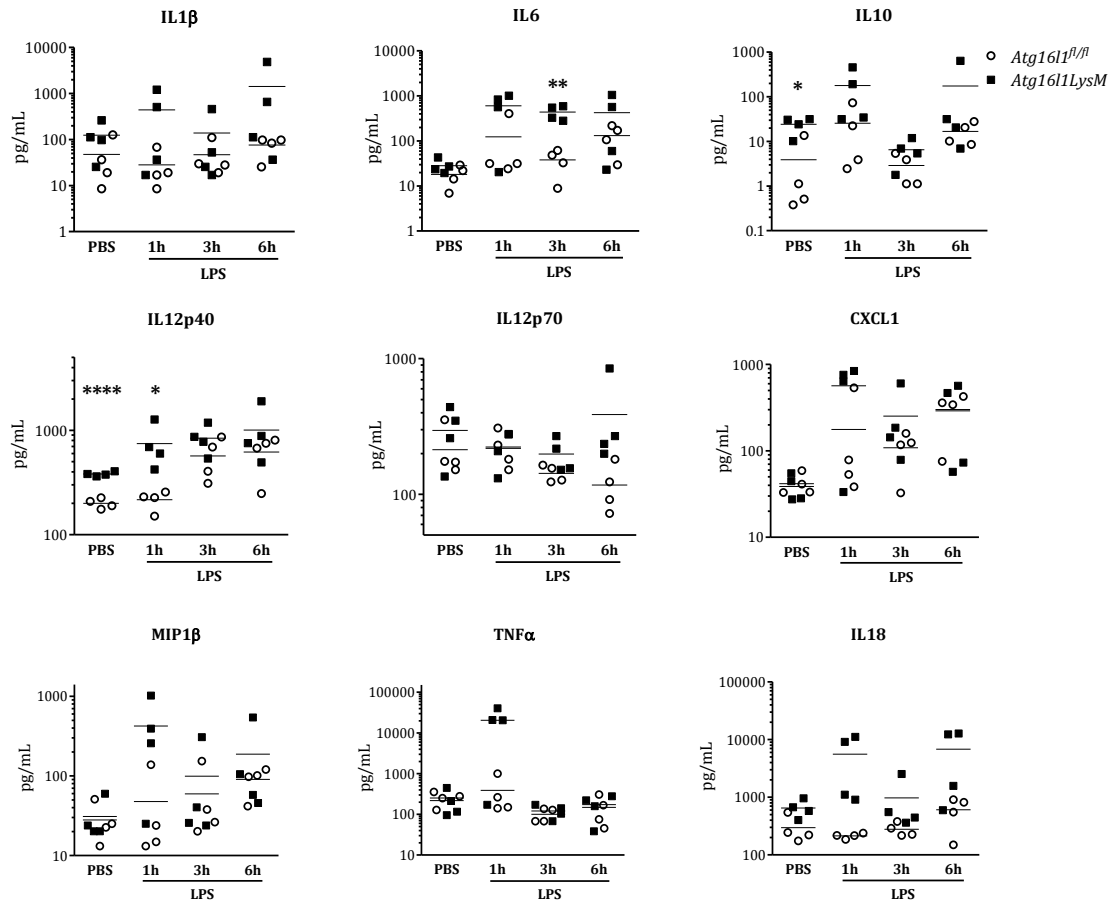


FIGURE 4-48: CYTOKINE AND CHEMOKINE LEVELS DURING ENDOTOXIN-INDUCED SEPSIS
Atg16l1^{fl/fl} and *Atg16l1^{LysM}* mice (n=4) were injected with a sublethal dosis of 5 mg/kg LPS (*E.coli* KPM53) for the indicated time points or with 5 μ L/g PBS as control. Blood was collected in lithium-heparin tubes and serum was analyzed using the Bio-Plex Pro™ Mouse Cytokine 23-plex Assay (BioRad) or ELISA. Data are depicted as mean. Statistical significance was calculated using an unpaired Student's *t*-test. * $p < 0.05$, ** $p < 0.01$, *** $p < 0.001$

Consistent with the mortality rate, approximately 50 % of *Atg16l1^{LysM}* mice showed highly upregulated cytokines, e.g. IL1 β , MIP1 β , TNF α or IL18.

These results provide *in vivo* evidence that *Atg16l1* deletion in the myeloid lineage increases sensitivity and severity to a sublethal LPS-induced septic shock resulting in an elevated cytokine production of pro-inflammatory cytokines.

4.7 IMPACT OF MICROBIOTA ON THE BASAL *ATG16L1^{LysM}* PHENOTYPE

To gain further insights into the *in vivo* relevance of the observed LPS hyper-sensitivity, the role of gut resident microbiota, as a natural source of endotoxin, was investigated with respect to the manifestation of the *Atg16l1^{LysM}* phenotype. Adult *Atg16l1^{fl/fl}* and *Atg16l1^{LysM}* mice were treated with an antibiotic cocktail in order to deplete the intestinal microflora. Both, antibiotic-treated *Atg16l1^{fl/fl}* and *Atg16l1^{LysM}* mice, lost weight within the first week but recovered after removal of neomycin from the antibiotic cocktail (Figure 4-49).

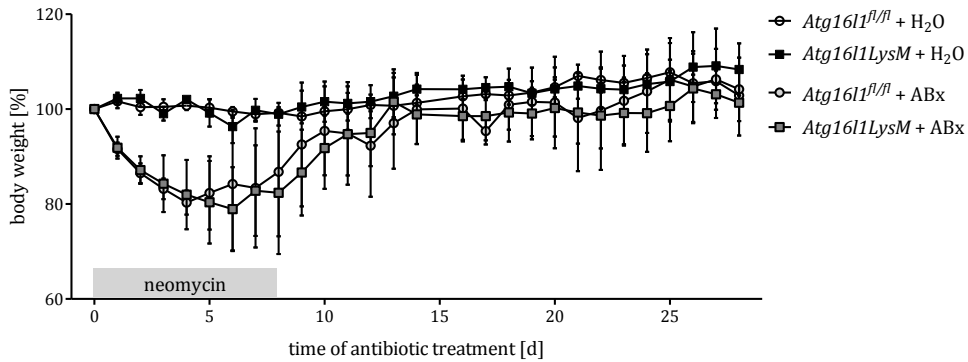


FIGURE 4-49: BODY WEIGHT LOSS DURING ANTIBIOTIC TREATMENT

8-12 week-old *Atg16l1^{fl/fl}* and *Atg16l1LysM* mice (n=5) were treated with an antibiotic cocktail administered via drinking water for 4 weeks. The control groups (n=3) received water without treatment. Neomycin was removed from the antibiotic cocktail at day 7. Body weight was monitored every day and is depicted in a graph as mean \pm S.D. ABx: antibiotics

Fecal microbial populations were analyzed using the non-parametric index of Shannon diversity that takes presence and absence as well as bacterial abundance into account (Figure 4-50). Microbial populations were diminished from day 7 up to day 28 in the feces of both, *Atg16l1^{fl/fl}* and *Atg16l1LysM* mice indicating a successful microbial depletion.

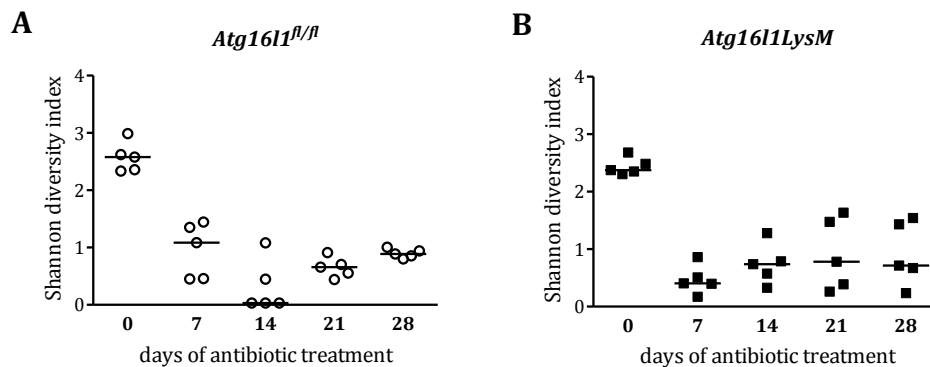


FIGURE 4-50: SUCCESSFUL MICROBIAL DEPLETION IN THE FECES OF ANTIBIOTIC-TREATED MICE

An antibiotic cocktail was administered via drinking water to *Atg16l1^{fl/fl}* and *Atg16l1LysM* mice (n=5) over a period of 4 weeks. Feces were collected every 7 days. Bacterial DNA was isolated and 16SrDNA sequencing was performed using the MiSeq sequencer (Illumina, San Diego, USA). Diversity of microbial populations in feces of *Atg16l1^{fl/fl}* mice (A) and *Atg16l1LysM* mice (B) was assessed using the non-parametric Shannon's index.

Organ weight of *Atg16l1^{fl/fl}* and *Atg16l1LysM* mice was analyzed after 4 weeks of antibiotic treatment (Figure 4-51). As described, pathological indicators appear as a result of a diminished intestinal microbial community [244]. Thus, antibiotic treatment resulted in reduced spleen weight and enlarged ceca in mice of both genotypes (Figure 4-51 A and B).

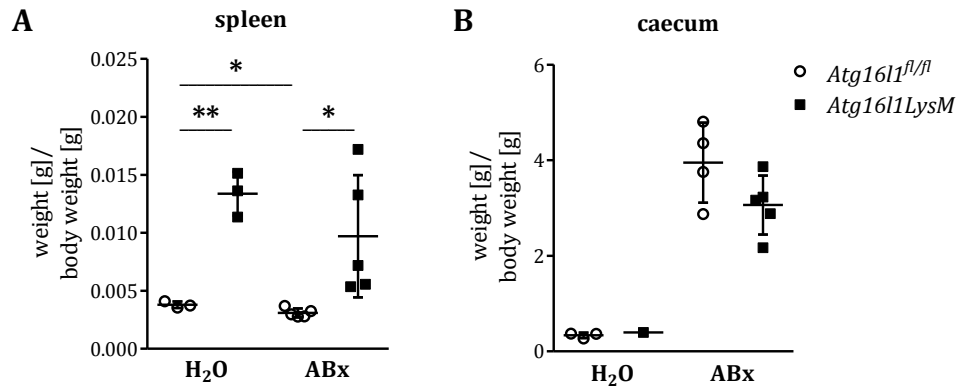


FIGURE 4-51: SPLEEN AND CAECUM WEIGHT AFTER ANTIBIOTIC TREATMENT

Spleen (A) and caecum weight (B) of adult *Atg16l1^{fl/fl}* and *Atg16l1^{LysM}* mice (n=1-5) were analyzed after 4 weeks of antibiotic treatment. Data are shown as mean \pm S.D. and statistical significance was evaluated by an unpaired Student's *t*-test. * $p < 0.05$, ** $p < 0.01$, ABx: antibiotics

Whereas all *Atg16l1^{fl/fl}* mice showed a reduced spleen weight, only three out of five *Atg16l1^{LysM}* mice demonstrated a decrease in spleen weight after antibiotic treatment compared to untreated *Atg16l1^{LysM}* mice (Figure 4-51 A). However, these two mice do not match with the once having a higher microbial diversity from day 21 on (Figure 4-50 B).

Measurements of cytokine concentrations in serum revealed no changes in antibiotic-treated *Atg16l1^{fl/fl}* mice compared to untreated mice (Figure 4-52). *Atg16l1^{LysM}* mice showed significantly reduced IL18 levels after the antibiotic cocktail. IL12p40 was not affected and MIP1 β was even increased.

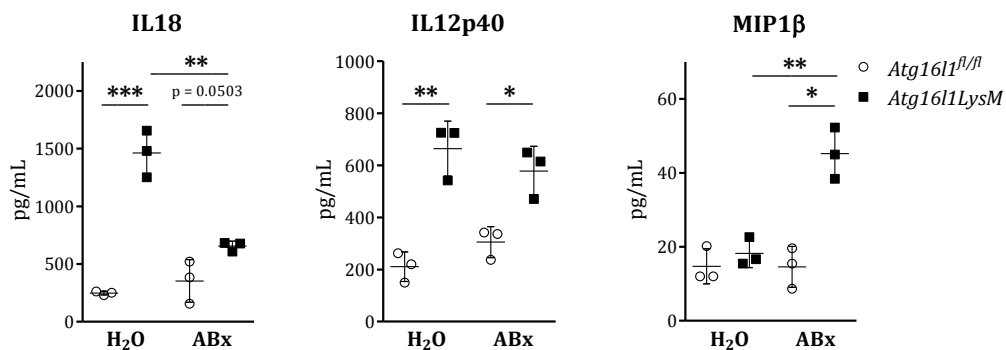


FIGURE 4-52: CYTOKINE LEVELS IN SERUM OF ANTIBIOTIC-TREATED *ATG16L1^{LysM}* AND *ATG16L1^{FL/FL}* MICE

Blood from untreated and antibiotic-treated *Atg16l1^{fl/fl}* and *Atg16l1^{LysM}* mice (n=3) was collected in lithium-heparin tubes and analyzed using the Bio-Plex Pro™ Mouse Cytokine 23-plex Assay (BioRad) or ELISA. Data represent mean \pm S.D. Results were tested for statistical significance using an unpaired Student's *t*-test. * $p < 0.05$, ** $p < 0.01$, *** $p < 0.001$, ABx: antibiotics

Expression analysis of cell type-specific markers still displayed a reduced expression of *Cd3e* and *Cd19* in the spleen of antibiotic-treated *Atg16l1^{LysM}* mice compared to *Atg16l1^{fl/fl}* mice (Figure 4-53).

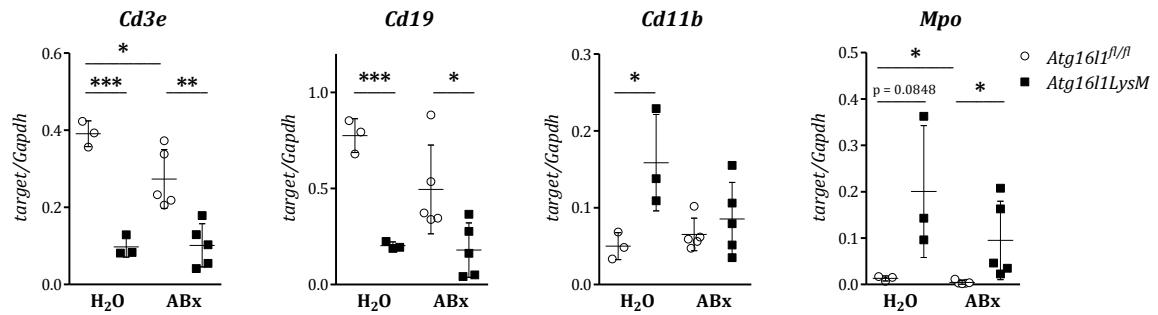


FIGURE 4-53: EXPRESSION OF CELL TYPE SPECIFIC MARKERS IN THE SPLEEN AFTER ANTIBIOTIC TREATMENT

Atg16l1^{fl/fl} and *Atg16l1LysM* mice were left untreated (n=3) or treated for 4 weeks with an antibiotic cocktail (n=5). RNA from liquid nitrogen frozen spleens was extracted and transcribed into cDNA. Expression levels of the indicated cell type specific markers were measured by SYBR® green qPCR and normalized to *Gapdh*. Expression of *Mpo* was measured by TaqMan Assay. Data represent mean \pm S.D. and statistical analysis was performed with an unpaired Student's *t*-test. * $p < 0.05$, ** $p < 0.01$, *** $p < 0.001$, ABx: antibiotics

On the other hand, microbial depletion normalized *Cd11b* expression in *Atg16l1LysM* to expression levels in untreated as well as antibiotic-treated *Atg16l1^{fl/fl}* mice. Antibiotic treatment resulted in diminished expression of the neutrophil marker *Mpo* in the spleens of both, *Atg16l1^{fl/fl}* and *Atg16l1LysM* mice, which was further confirmed by immunohistochemistry (Figure 4-54).

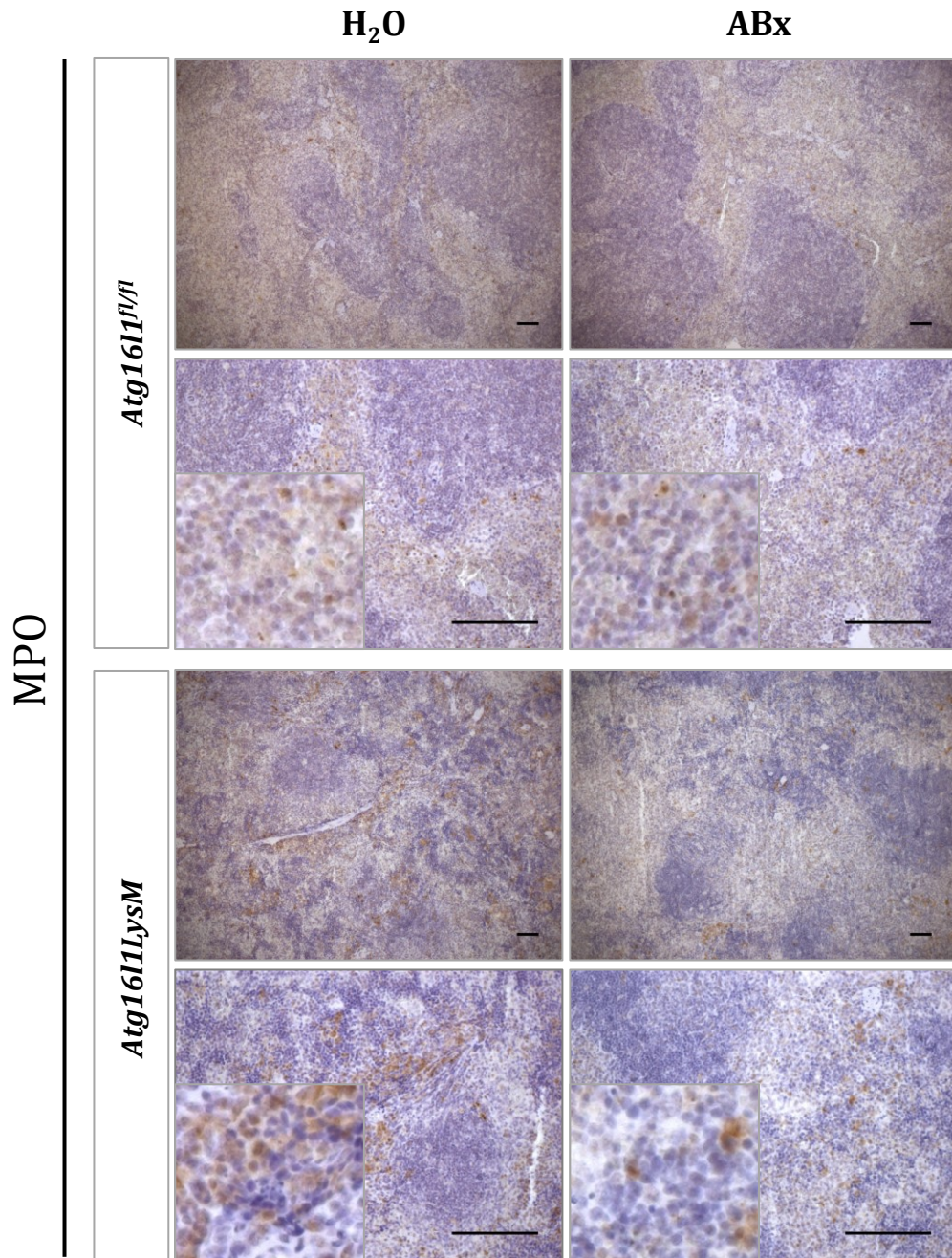


FIGURE 4-54: MICROBIAL DEPLETION RESULTS IN REDUCED NUMBERS OF SPLENIC MPO+ CELLS IN *ATG1611LYSM* MICE

Atg1611^{fl/fl} and *Atg1611LysM* mice were left untreated (n=3) or treated with an antibiotic cocktail for 4 weeks (n=5). Spleens were formalin-fixed and paraffin-embedded and stained for MPO+ cells. Representative images analyzed by transmission light microscopy are shown. Scale bars represent 50 μ m. MPO: myeloperoxidase

As the spleen weight of untreated *Atg1611LysM* mice varied from two to ten times larger when compared to their *Atg1611^{fl/fl}* littermates (Figure 4-5 B), interpretation whether the spleen weight was specifically reduced based on the use of antibiotics remains speculative. Suggesting that adult *Atg1611LysM* mice with an age of 8-12 weeks already developed a very prominent phenotype, a second preventive antibiotic treatment was performed starting during the prenatal phase until the age of 3 weeks.

Gross examination of *Atg1611LysM* mice at the age of 3 weeks showed neither an increased small intestine length nor liver weight compared to *Atg1611^{f/f}* mice (Figure 4-55). However, even at the age of 3 weeks *Atg1611LysM* mice developed a significant splenomegaly, which was completely rescued by inhibition of the microbial colonization after birth. A successful microbial depletion was determined by the significantly increased caecum weight serving as a pathological indicator in antibiotic-treated mice [244].

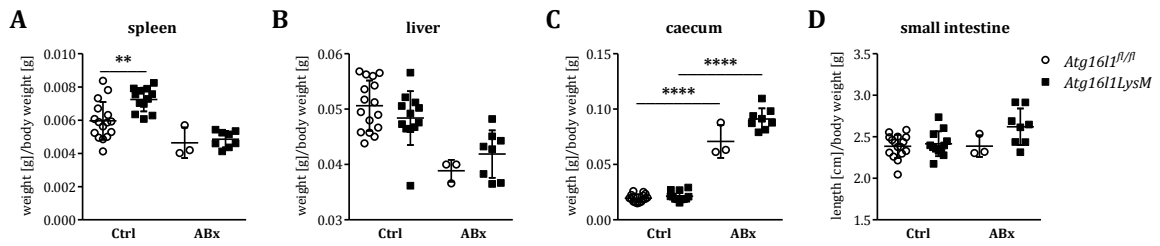


FIGURE 4-55: ORGAN WEIGHT AND LENGTH AFTER PREVENTIVE ANTIBIOTIC TREATMENT

Spleen (A), liver (B) and caecum weight (C) as well as small intestine length (D) were analyzed after control sucrose treatment (n=12-16) and preventive antibiotic treatment (n=3-8) of 3-week old *Atg1611^{f/f}* and *Atg1611LysM* mice. Data are shown as mean \pm S.D. and statistical significance was evaluated by an unpaired Student's *t*-test. * p < 0.05, **** p < 0.0001, ABx: antibiotics, Ctrl: control

Analysis of the splenic cell composition revealed an attenuated T cell population in *Atg1611LysM* mice after preventive antibiotic treatment (Figure 4-56 A).

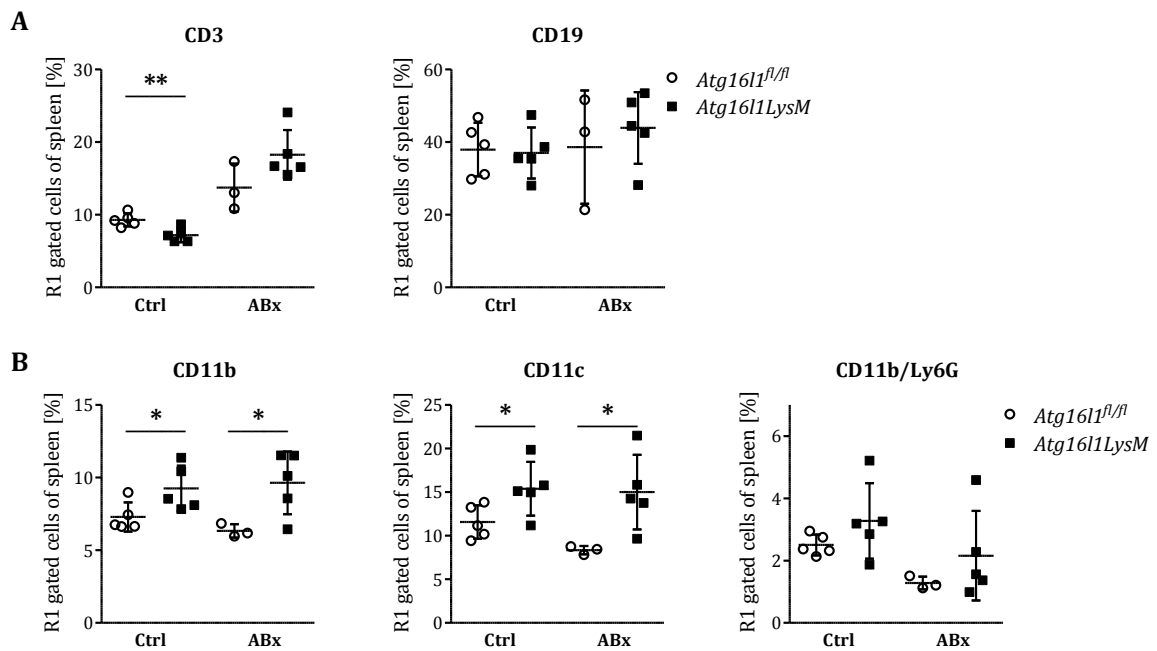


FIGURE 4-56: SPLENIC CELL COMPOSITION AFTER PREVENTIVE ANTIBIOTIC TREATMENT

Splenic cell composition of 3 week old *Atg1611^{f/f}* and *Atg1611LysM* mice preventively treated with an antibiotic cocktail (n=3-5) or 2 % sucrose (n=5) as control was analyzed by flow cytometry. Percentage of the individual adaptive (A) and innate (B) immune cell population was corrected for the particular isotype control. Data are shown as mean \pm S.D. Statistical significance was calculated by an unpaired Student's *t*-test. * p < 0.05, ** p < 0.01, ABx: antibiotics, Ctrl: control

Although increased populations of CD11b⁺ and CD11c⁺ cells persisted in *Atg16l1LysM* mice, the number of CD11b⁺/Ly6G⁺ cells was markedly decreased in both, antibiotic-treated *Atg16l1^{fl/fl}* and *Atg16l1LysM* mice (Figure 4-56 B). A similar pattern was observed for the activation status of innate and adaptive immune cells (Figure 4-57). Whereas the decreased T cell activation was restored in *Atg16l1LysM* mice after microbial depletion (Figure 4-57 A), CD11b⁺ cells of *Atg16l1LysM* mice continuously expressed increased activation markers at their cell surface compared to antibiotic-treated *Atg16l1^{fl/fl}* mice (Figure 4-57 B).

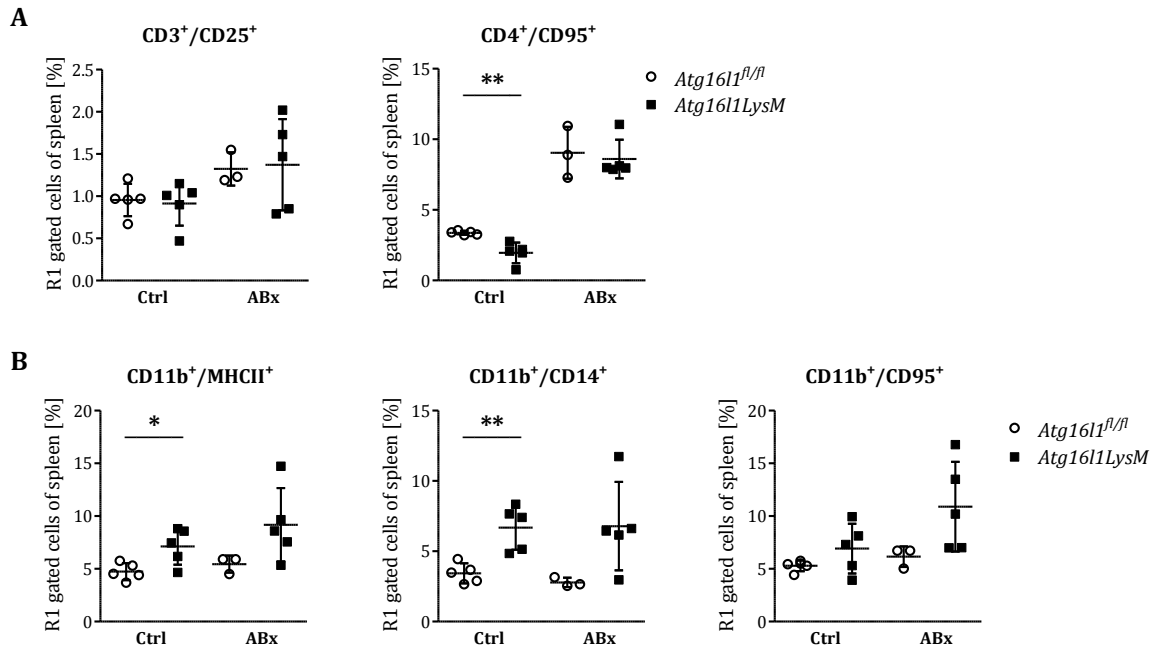


FIGURE 4-57: ACTIVATION STATUS OF SPLENIC IMMUNE CELLS AFTER PREVENTIVE ANTIBIOTIC TREATMENT
Atg16l1^{fl/fl} and *Atg16l1LysM* mice were preventively treated with an antibiotic cocktail (n=3-5) or 2% sucrose (n=5) as control. Splenocytes were isolated and stained for the indicated antigen combinations or particular isotype controls and analyzed by flow cytometry. Percentage of the indicated T cell activation markers (A) or myeloid cell activation markers (B) was corrected for the particular isotype control. Data are shown as mean ± S.D. An unpaired Student's *t*-test was performed to evaluate statistical significance. * $p < 0.05$, ** $p < 0.01$, ABx: antibiotics, Ctrl: control

Since preventive antibiotic treatment ameliorated the suppressed T cell phenotype of *Atg16l1LysM* mice, expression of MDSC-associated genes was analyzed (Figure 4-58). Antibiotic-treated *Atg16l1LysM* mice demonstrated a significant reduction of *Mpo*, *S100a8* and *S100a9* expression in the spleen compared to the appropriate control group.

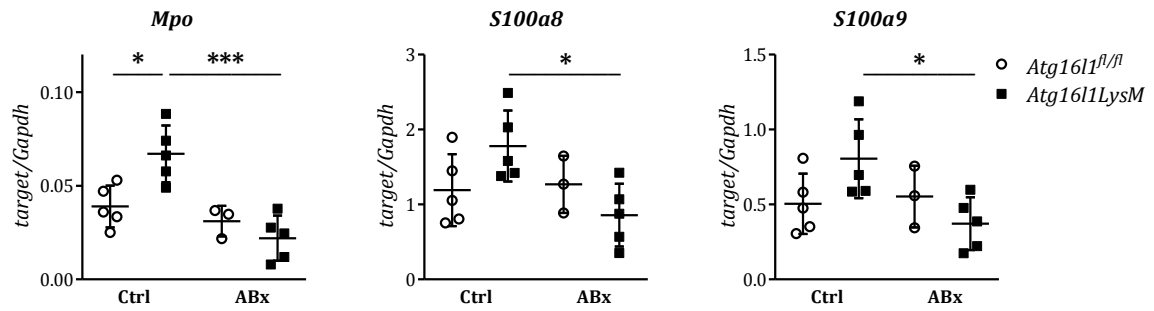


FIGURE 4-58: ATTENUATED EXPRESSION OF MDSC-ASSOCIATED GENES IN THE SPLEEN OF *Atg16l1LysM* MICE AFTER PREVENTIVE ANTIBIOTIC TREATMENT

Spleens of *Atg16l1^{fl/fl}* and *Atg16l1LysM* mice preventively treated with an antibiotic cocktail (n=3-5) or 2% sucrose as control were snap frozen and mortared. RNA extraction and cDNA synthesis were performed. Expression of the indicated targets was analyzed by SYBR® green qPCR and normalized to *Gapdh*. Expression of *Mpo* was analyzed by TaqMan Assay. Data show mean \pm S.D. Statistical significance was calculated with an unpaired Student's *t*-test. * $p < 0.05$, *** $p < 0.001$, ABx: antibiotics, Ctrl: control, Mpo: myeloperoxidase

Taken together, inhibition of the colonization of the commensal microbial community in *Atg16l1LysM* mice partially attenuated the spontaneous phenotype by rescuing the splenomegaly as well as the suppressed T cell phenotype.

5 DISCUSSION

Autophagy plays a decisive role in maintaining the cellular homeostasis of eukaryotic cells through degradation and recycling of proteins and organelles [6]. Imbalance of this sensitive homeostasis as a result of genetic variants in autophagy-related genes is associated with numerous human diseases like inflammatory bowel disease [64], asthma [245] and various types of cancer [246-249]. For this reason, molecular functions of the individual autophagic components in inflammatory processes were intensively studied during the last years but still remain incompletely understood. Because macrophages represent the first line of defense in the immune response, the aim of the present study was to investigate the impact of ATG16L1 on inflammatory signaling pathways and cytokine production in myeloid cells. Using a myeloid-specific knock-out mouse model the results obtained in the study presented here combines for the first time *in vivo* as well as *ex vivo* data showing a vital role for ATG16L1 in immunoregulatory processes.

5.1 CHARACTERIZATION OF THE *ATG16L1LYSM* MOUSE MODEL

5.1.1 SPONTANEOUS SYSTEMIC INFLAMMATION IN *ATG16L1LYSM* MICE

In contrast to *Atg16l1* chimeric mice [22], the present study demonstrated that mice lacking *Atg16l1* in the myeloid lineage develop a multifaceted spontaneous phenotype characterized by systemic inflammatory symptoms. Gross examination of *Atg16l1LysM* mice displayed a hepatosplenomegaly and lymphadenopathy. In detail, *Atg16l1LysM* mice showed an extensive extramedullary hematopoiesis in the spleen accompanied by increased numbers of myeloid cells in spleen, lymph nodes, liver and peripheral blood. Although these abnormalities at first sight resemble clinical symptoms of a chronic myeloid leukemia (CML) in humans [250], bone marrow of *Atg16l1LysM* mice did not reveal any histological anomalies in myeloid differentiation. These findings exclude CML as cause of the spontaneous phenotype seen in *Atg16l1LysM* mice. Similarly, an equal numbers of myeloid cells were detected in the bone marrow of *Atg5LysM* and *Atg5^{fl/fl}* control mice [46]. However, *Atg16l1LysM* mice exhibited significantly elevated serum levels of pro-inflammatory cytokines and significantly upregulated numbers of activated CD11b⁺ myeloid cells in the peripheral blood and lymphoid organs.

Surprisingly, the basal inflammatory phenotype of mice lacking other *Atg* genes in the myeloid lineage appears less prominent. Both, *Atg5LysM* and *Atg7LysM* mice solely develop a spontaneous inflammation in the lung [46, 251, 252]. Similar to the cytokine expression profile observed in the spleen of *Atg16l1LysM* mice, *Atg5LysM* and *Atg7LysM* mice show

increased pulmonary expression levels of various pro-inflammatory cytokines like *Il1a* and *Tnfa*. Further, increased mRNA levels of the neutrophil-attracting chemokine *Cxcl1* coincides with a substantial infiltration of CD11b⁺/Ly6G⁺ neutrophils in the lung of *Atg5LysM* and *Atg7LysM* mice recapitulating the observed inflammatory characteristics in the spleen of *Atg16l1LysM* mice. In line with the presented findings in *Atg16l1*-deficient CD11b⁺ cells of the spleen, untreated *Atg5*-deficient alveolar macrophages demonstrated an inflammatory phenotype characterized by upregulation of activation markers like MHCII [46]. In contrast to *Atg7*-deficient macrophages showing an increased cell surface expression of inflammation inhibitory receptors such as macrophage scavenger receptor 1 (MSR1), protein levels of MSR1 were comparable between BMDMs of *Atg16l1LysM* and *Atg16l1^{fl/fl}* mice. Bonilla and colleagues reported a less efficient depletion of *Atg7* in splenic macrophages corresponding with a less prominent phenotype in *Atg7LysM* mice which could explain the distinct phenotypes in autophagy-deficient mouse models [47].

Summing up, loss of *Atg16l1* in the myeloid lineage leads to a complex inflammatory phenotype in mice under physiological conditions whose individual aspects are discussed in more detail below.

5.1.2 MYELOID-DERIVED SUPPRESSOR CELL-LIKE CELL POPULATION IN *ATG16L1LYSM* MICE

CD11b⁺/Ly6G⁺ cells account for less than 5 % in the spleen under healthy conditions and are absent in lymph nodes [253]. However, *Atg16l1LysM* mice showed significantly increased numbers of CD11b⁺/Ly6G⁺ myeloid cells in the spleen and the peripheral blood. Beside differentiated neutrophils, a second cell type, namely myeloid-derived suppressor cells (MDSCs), are described to co-express CD11b and Ly6G [254] and exhibit a potent immunosuppressive function on T cells [221]. MDSCs expand in blood, spleen and lymph nodes under pathological conditions, e.g. infections, inflammation and cancer [221]. Although myeloid cells of *Atg16l1LysM* mice demonstrated a strong inflammatory phenotype, the overall number of T cells was significantly diminished. In line with the proposed immunosuppressive function of CD11b⁺/Ly6G⁺ myeloid cells on T cells, the number of activated CD3⁺/CD25⁺ and CD4⁺/CD95⁺ T cells remained unaffected in *Atg16l1LysM* mice.

The inhibitory capacity of MDSCs is mainly mediated by two mechanisms: (I) depletion of the conditionally essential amino acid L-arginine from the extracellular environment by arginase-1 and (II) production of nitric oxide (NO) and reactive oxygen species (ROS) by inducible nitric oxide synthase (iNOS) [221, 255]. Indeed, *iNOS* was strongly upregulated in the spleen of *Atg16l1LysM* mice suggesting that iNOS could contribute to T cell suppression in these mice. Increased MPO levels are another hallmark of MDSCs [256] but MPO is also stored

in large amounts in azurophilic granules of neutrophils that are released after neutrophil activation as part of the antimicrobial system [257]. *Atg16l1LysM* mice obtained increased numbers of MPO⁺ cells in spleen, lymph nodes, liver and lung determined by immunohistochemistry. However, it needs to be further investigated whether the differences in MPO observed in *Atg16l1LysM* mice results from increased numbers of neutrophils or the development of a MDSC-like cell population. Further, it has been reported that IL1 β and the antimicrobial peptides S100A8/A9, both upregulated in the spleen of *Atg16l1LysM* mice, play an important role in activation and expansion of MDSCs promoting an autocrine feedback loop [258, 259]. Yet, it must be emphasized that so far unequivocal markers of MDSCs are not defined as most of the described principles are also hallmarks of inflammation.

Taken together, CD11b⁺/Ly6G⁺ cell populations in lymphoid organs and the peripheral blood of *Atg16l1LysM* mice putatively represent a MDSC-like population that in turn may drive suppression of the T cell activation profile and expansion in these mice. However, a direct immunosuppressive capability of CD11b⁺/Ly6G⁺ cells of *Atg16l1LysM* mice on T cells needs to be demonstrated.

5.1.3 A PIVOTAL ROLE FOR THE COMMENSAL MICROBIOTA IN THE DEVELOPMENT OF THE INFLAMMATORY *ATG16L1LYSM* PHENOTYPE

Depletion of the intestinal microbiota using antibiotics was accompanied by a slightly ameliorated spleen size and a diminished infiltration of splenic MPO⁺ myeloid cells in adult *Atg16l1LysM* mice. These observations lead to the hypothesis of a decisive role for the commensal microbial community in the manifestation of the spontaneous *Atg16l1LysM* phenotype. This was even more pronounced by the inhibition of intestinal microbial colonization through a preventive administration of antibiotics which completely rescued the splenomegaly and significantly diminished the expression of *Mpo* as well as *S100a8/9* in *Atg16l1LysM* mice. Coinciding with the normalization of these supposed MDSC-like characteristics, the diminished numbers of CD3⁺ T cells and CD4⁺/CD95⁺ activated T cells in the spleen was entirely restored. In a study investigating MDSC induction in tumor-bearing mice the phenomenon was also abrogated after depletion of commensal bacteria [260]. These findings point towards a regulatory function of the commensal microbiota on MDSC development in different pathological conditions in mice (Figure 5-1).

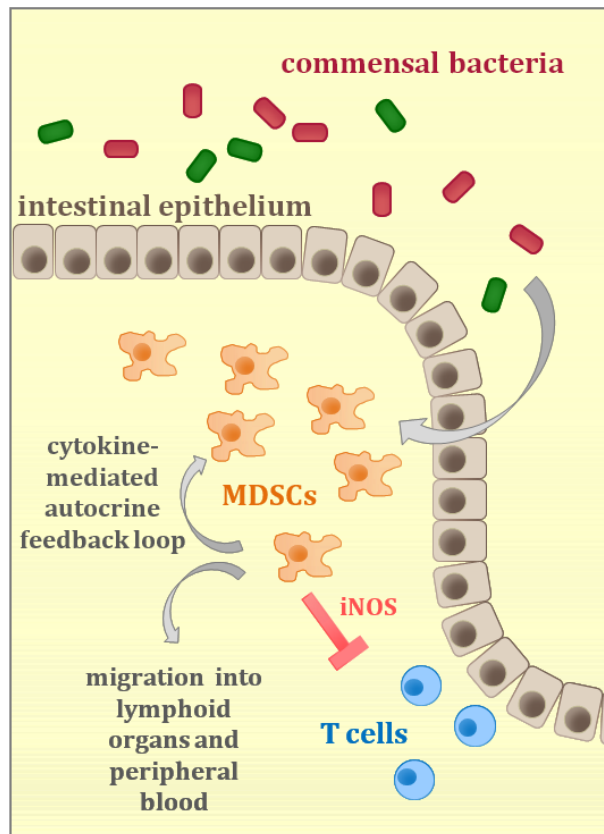


FIGURE 5-1: PROPOSED MECHANISM FOR THE IMPACT OF THE COMMENSAL MICROBIOTA ON THE MANIFESTATION OF THE *ATG16L1LysM* PHENOTYPE

Loss of *Atg16l1* in the myeloid lineage results in an inflammatory conditions partially mediated by the hyper-sensitivity to the commensal intestinal microbiota. Postnatal colonization of the commensal microbiota might be involved in the appearance and activation of a myeloid-derived suppressor cell (MDSC)-like cell population. Subsequent MDSC-dependent cytokine production triggers the expansion and migration of MDSC-like cells into lymphoid organs and the peripheral blood and thus facilitates the T cell suppression via the expression of inducible nitric oxide synthase (iNOS).

In line with findings in *Atg16l1LysM* mice presented here, a one-week intranasal antibiotic therapy of 2 week-old *Atg7LysM* mice reduced the levels of pro-inflammatory cytokines as well as neutrophil infiltration in the lung [251]. Moreover, preventive antibiotic treatment from prenatal stage to 3 weeks of age rescued the lung phenotype of *Atg7LysM* mice [251]. Thus, the postnatal microflora seems to act as crucial trigger for the spontaneous inflammation in mouse models lacking autophagy-related genes in the myeloid lineage.

However, *Atg5LysM* and *Atg7LysM* mice as well as *Atg16l1* chimeric mice demonstrated increased numbers of CD4⁺ T cells and regulatory T cells [22, 46, 251]. A conceivable explanation for the distinct phenotypes, might be the individual cellular functions of *Atg* proteins in various autophagy-independent processes like secretion of hormones and cytokines [261]. On the other hand, differences within microbial communities might give reason for dissimilarities in the presence of MDSC-like cell populations and T cell numbers in autophagy-deficient mouse models. Recent studies reported the capability of bacterial components, like the TLR-ligands LPS [262] and Flagellin [263], to elicit MDSCs. In this context, analysis of the microbial composition would enable the identification of specific MDSC-associated microbial communities. However, the research field of MDSC development, mobilization and expansion is still poorly understood and controversially discussed. Thus, further analysis is required and subject of ongoing studies.

On the other hand, (activated) CD11b⁺ myeloid cells did not show reduced numbers after prenatal antibiotic treatment. Since antibiotic treatment strongly decreases but do not

completely abolish intestinal microbes, this phenomenon might reflect the hyper-sensitivity of CD11b⁺ myeloid cells towards the remaining microbes. Moreover, it is noteworthy that an effect of the antibiotics itself on the phenotype cannot be fully ruled out. Rederivation of the *Atg16l1LysM* mouse model into germ-free conditions could exclude antibiotics as an influencing factor and might probably normalize the hyper-activation state of CD11b⁺ myeloid cells. This might finally elucidate the role of the commensal microbiota in the manifestation of the systemic inflammatory phenotype in *Atg16l1LysM* mice.

5.1.4 DISPENSABLE ROLE FOR IL1 CYTOKINES IN THE DEVELOPMENT OF THE INFLAMMATORY PHENOTYPE IN *ATG16L1LYSM* MICE AND BMDMS

A noteworthy *in vivo* observation in *Atg16l1LysM* mice comprised an upregulation of interleukin-1 (IL1) family members. In line with this observation, untreated *Atg5LysM* mice and *Atg7LysM* mice also showed augmented pulmonary expression of *Il1a* and *Il1b*, respectively, suggesting a crucial role for IL1 cytokines in the development of inflammation in autophagy-deficient mice [46, 252]. Moreover, *Atg16l1*-deficient macrophages showed significantly upregulated *Il1a* and *Il1b* mRNA expression resulting in higher intracellular levels of pro-IL1 β and significantly increased IL1 α secretion in response to LPS compared to wild type BMDMs. Accordingly, previous studies implicated a role for autophagy and ATG16L1 as regulator of interleukin-1 receptor (IL1R) signaling [60] and effector of IL1 cytokine production [22, 46, 72, 227].

However, the spontaneous inflammatory phenotype of *Atg16l1LysM* mice still persisted after a 2-week-treatment with the competitive IL1R inhibitor Anakinra. Interestingly, spontaneous inflammation in the lung of *Atg7LysM* mice did also not attenuate in response to subcutaneous Anakinra administration [252]. These results weaken the hypothesis of IL1 α and IL1 β as central mediators of the spontaneous inflammatory phenotype in autophagy-deficient mice. Moreover, inhibition of IL1R signaling by Anakinra in *ex vivo* differentiated *Atg16l1LysM* BMDMs did neither diminish LPS-induced prolonged NF- κ B signaling nor increased CXCL1 production. For this reason, TLR4-mediated IL1 α / β production can be excluded as amplifying feedback loop in *Atg16l1*-deficient macrophages.

Although several studies used a comparable experimental setup of a daily Anakinra injection [228, 252], it is worth mentioning that the terminal half-life of Anakinra ranges from 4 to 6 hours [264]. This fact might speak against an efficient inhibition of IL1 α and IL1 β activity by a single daily dose. Contradicting this argument, pharmacokinetics of Anakinra in mice, receiving a single dosage regime comparable to the concentration used in the presented study, indeed showed a half-life of the IL1R antagonist of approximately 6 hours in serum but a prolonged accumulation for up to 12 hours in liver and kidney [214]. Moreover, a single

daily dose of Anakinra resulted in a less severe chemically-induced colitis after 5 days [265] indicative for a sufficient inhibition of IL1R signaling already after a short duration treatment. Maturation of the inactive IL1 β precursor into its active form is restricted to proteolytic cleavage by caspase-1 [266]. As part of the inflammasome, caspase-1 activation is initiated through the formation of a multimeric complex consisting of an eponymous sensor molecule like NLRP3, the adaptor molecule ASC and the immature pro-form of caspase-1 [267]. The NLRP3 inflammasome is a well-characterized multiprotein complex and its activation can be triggered by mitochondrial ROS production [72]. However, under basal conditions, loss of *Atg16l1* in macrophages neither affected mitochondrial membrane potential and thus mitochondrial homeostasis nor intracellular ROS production and pro-IL1 β level in the presented study.

With respect to the reported role of autophagy in IL1 cytokine production and/or secretion [22, 46, 72, 227], *Atg16l1LysM* BMDMs unexpectedly demonstrated similar ROS levels compared to *Atg16l1^{fl/fl}* BMDMs in response to LPS. In contrast, a significant upregulation of *Il1b* on transcriptional levels was observed. These results corresponded with a stronger increase of pro-IL1 β protein levels. Interestingly, the increased levels of pro-IL1 β in *Atg16l1LysM* BMDMs correlated with increased phospho-p65 and phospho-p38 levels which are crucial signaling mediators of the IL1R/TLR superfamily [268]. In agreement with the described *ex vivo* data, spleens of *Atg16l1LysM* mice revealed elevated levels of pro-IL1 β but not *pro-Casp1*, *Nlrp3* or *Asc*, at least on transcriptional level. This finding suggests an NLRP3-independent regulation of pro-IL1 β in the absence of *Atg16l1*. In contrast to the presented *ex vivo* findings, studies in *Atg16l1*-deficient fetal liver-derived macrophages showed an elevated ROS-dependent IL1 β secretion but not transcription [22]. Additionally, Saitoh and colleagues did neither observe an increased activation of NF- κ B nor IRF3 or p38 MAPK implicating a regulatory role for ATG16L1 in IL1 β secretion exclusively via the NLRP3 inflammasome. The major reason for the different study outcomes might be the initial conditions. Whereas macrophages in Saitoh's study were derived from the fetal liver of a phenotypically inconspicuous constitutive knock-out model of *Atg16l1* [22], *Atg16l1LysM* macrophages originated from the bone marrow of tissue-specific knock-out mice already showing a very prominent inflammatory phenotype. In addition, differentiation of BMDMs in the presented study was achieved with mCSF treatment. In contrast, *Atg16l1*-deficient fetal liver-derived macrophages were *ex vivo* differentiated using the granulocyte macrophage colony-stimulating factor (gmCSF) which mainly facilitates the differentiation of dendritic cells [269]. Thus, different pathological conditions could also affect the *ex vivo* phenotype of *Atg16l1*-deficient macrophages in response to LPS.

Inhibition of NAD(P)H oxidase-derived ROS using DPI [243] markedly reduced LPS-induced pro-IL1 β levels in *Atg16l1^{fl/fl}* and *Atg16l1LysM* BMDMs and was associated with decreased

levels of phosphorylated p65, I κ B α and p38. Nevertheless the observed differences in phospho-p65, phospho-p38 and pro-IL1 β persisted in *Atg16l1LysM* BMDMs coinciding with a lasting elevated CXCL1 secretion. Recent studies linked an impaired autophagic machinery to ROS-dependent inflammasome activation mediated by calpain activation, defective mitophagy and/or disrupted elimination of the inflammasome itself [46, 71, 72, 227]. However, the findings presented here point to mitochondrial ROS production as amplifier but not initiator of LPS-induced differences in NF- κ B and MAPK activation as well as cytokine secretion in *Atg16l1*-deficient macrophages.

Despite pro-IL1 β in the spleen, untreated *Atg16l1LysM* mice showed significantly enhanced serum levels of the pro-inflammatory cytokine IL18, another component of the IL1 cytokine family. However, mRNA expression of *Il18* was significantly diminished in the spleen of *Atg16l1LysM* mice. One might speculate that decreased *Il18* mRNA expression reflects a compensatory effect of the hyper-inflammatory state in the spleen or that the loss of *Atg16l1* rather affects IL18 maturation and/or secretion than expression. Interestingly, maturation of IL1 β and IL18 is equally processed by caspase-1 [266]. In contrast, IL1 β - and IL18-initiated signaling is mediated by distinct receptors, namely IL1 receptor and IL18 receptor [270, 271]. This fact excludes IL18 as target for Anakinra [272]. Consistent with serum cytokine levels of untreated *Atg16l1LysM* mice, fetal liver-derived macrophages lacking *Atg16l1* secreted higher amounts of IL18 in response to LPS [22]. *In vivo* neutralization of IL1 β and IL18 using a combination of specific antibodies significantly ameliorated the severe dextran sodium sulfate (DSS)-induced colitis in *Atg16l1* chimeric mice. In agreement with these results, IL18 neutralizing antibodies prevented the spontaneous lung inflammation in adult *Atg7LysM* mice [252] pointing towards a role for IL1 cytokines in inflammatory processes of mice with defects in the autophagic machinery.

However in conclusion, the obtained *in vivo* and *ex vivo* results suppose a dispensable role for IL1 α and IL1 β in the development of the inflammatory phenotype of *Atg16l1LysM* mice and BMDMs whereas the role of IL18 in this scenario needs to be further elucidated.

5.2 AUTOPHAGY AS A NEGATIVE REGULATOR OF TLR4 SIGNALING

5.2.1 LOSS OF *ATG16L1* LEADS TO INCREASED TLR4-MEDIATED NF- κ B SIGNALING

Studies in *Atg16l1LysM* BMDMs provided first evidence that ATG16L1 might act as crucial regulator in TLR4-mediated signaling. An earlier, stronger and prolonged activation of canonical NF- κ B but also p38 MAPK signaling in response to LPS was observed. Specifically, differences in p65 and p38 MAPK activation at the early time points, in which no pro-inflammatory cytokines were yet produced, indicate that loss of *Atg16l1* in macrophages directly modulates the TLR4 signaling cascade which in turn causes the significant increase in secretion of pro-inflammatory cytokines. In line with this observation, LPS-stimulated macrophages deficient for the autophagy-related gene *Irgm1* display an elevated and prolonged p65 and p38 signaling coinciding with increased pro-inflammatory cytokine secretion [61] suggesting a general role for autophagy in the regulation of TLR4 signaling.

The described inflammatory characteristics of untreated *Atg16l1LysM* mice phenocopy in large parts the pathologic phenotype of mice with defects in essential regulators of NF- κ B signaling. Constitutive activation of NF- κ B in *IkBa*-deficient mice resulted in extensive granulopoiesis and pro-inflammatory cytokine production [209]. Mice lacking the NF- κ B negative feedback mediators *Cyld* or *A20* developed exacerbated lymphoid organ abnormalities and abnormal B cell responses as well as multi-organ inflammation, cachexia and premature lethality, respectively [208, 273, 274]. Hence, the inflammatory symptoms of *Atg16l1LysM* mice are another indication for a putative regulatory function of ATG16L1 in NF- κ B signaling. This presumption is further supported by the above discussed fact that *Atg16l1LysM* mice demonstrate a hyper-responsiveness towards the commensal microbiota which is a key player contributing to the host's immune homeostasis [275]. Similarly, the severe phenotype of *A20*-deficient mice was caused by homeostatic MyD88-dependent NF- κ B signaling triggered by the commensal microbiota [208]. It should be noted, however, that activation of NF- κ B is induced by an exceptionally large number of more than 150 stimuli including pathogens but also stress conditions and pro-inflammatory cytokines [276]. This fact complicates the interpretation of a potential molecular mechanism in which ATG16L1 might affect NF- κ B signaling *in vivo*.

However, in agreement with the *ex vivo* results presented in this thesis, *Atg16l1LysM* mice showed a severe susceptibility to a sublethal endotoxin-induced septic shock displaying more than 50 % mortality associated with remarkably increased serum levels of key acute phase cytokines like TNF α , IL1 β and IL12. Contributing to these findings, a recently published study reported an association of the T300A polymorphism in the human *ATG16L1* gene with septic shock in patients with ventilator-associated pneumonia [277]. Constitutive or tissue-specific

deletion of autophagy-related genes like *Atg7* [252], *Irgm1* [61], *Map1lc3b* and *Becn1* [222] caused a comparable severe phenotype in response to LPS which confirms the idea that an intact autophagic machinery serves as a protective factor in sepsis development [278, 279].

5.2.2 ATG16L1 ORCHESTRATES IN FIRST LINE MYD88- BUT NOT TRIF-MEDIATED SIGNALING

Corresponding to the increased canonical NF- κ B and p38 MAPK signaling detected in *Atg16l1LysM* BMDMs after LPS stimulation, the NF- κ B targets IL1 α and CXCL1 were significantly increased. Activation of transcription factors via TLR4-induced signaling is mediated by specific adaptor molecules. In contrast to NF- κ B signaling, which is initiated by both TLR4 adaptor molecules, MyD88 and TRIF, expression of type I interferons is tightly regulated by a TRIF-dependent activation of the transcription factors IRF3 and IRF7 [187, 280-282]. Precisely, internalization of the activated TLR4 complex to early endosomes represents an essential step which facilitates the recruitment of the TRIF-TRAM complex and results in the subsequent activation of IRF3/7 initiating the transcription of type I interferons like *Ifnb* [186, 283, 284]. Interestingly, mRNA and protein levels of IFN β in *Atg16l1LysM* BMDMs were comparable to *Atg16l1^{fl/fl}* control BMDMs in absence and presence of LPS. This leads to the hypothesis that ATG16L1 specifically regulates NF- κ B-mediated signal transduction but is not capable of modulating the type I interferon signaling pathways. In addition, unchanged IFN β levels also allow the conclusion to be drawn about a functional TLR4 internalization and ensuing endosomal TLR4 signaling which mediates a functional induction of the TRAM-TRIF pathway in absence of *Atg16l1*. Together with the observation that CD95 is functionally internalized in *Atg16l1LysM* BMDMs, the presented findings point to an intact TLR4 receptor internalization capacity in *Atg16l1*-deficient macrophages with only the MyD88-TRAF6 signaling downstream of the LPS-induced TLR4 activation being affected. It is known that TRIF-mediated signaling is able to orchestrate late NF- κ B signaling [187]. However, hyper-activation of NF- κ B and p38 MAPK signaling pathways occurred already within the first hour after TLR4 activation in *Atg16l1LysM* BMDMs. This finding indicates that loss of *Atg16l1* primarily affects the early MyD88-dependent NF- κ B response [285]. Peritoneal macrophages derived from *Irgm1*-deficient mice revealed a similar reaction pattern to LPS within the first 2 hours which was illustrated by elevated activation of NF- κ B and p38 MAPK but not IRF3 [61]. Interestingly, murine embryonic fibroblasts (MEFs) lacking either *Atg5* or *Atg16l1* also demonstrated an hyper-activated NF- κ B and MAPK signaling within the first 2 hours in response to IL1 β [60]. As MyD88 has a common function in the modulation of IL1R/TLR-mediated responses [286], this might point to a general regulatory mechanism for autophagy in MyD88-dependent signaling. Moreover, this might provide a

molecular explanation for the faster responsiveness to LPS observed in *Atg16l1LysM* mice as well as *Irgm1*-deficient mice [61] as both mouse models develop extraordinarily pro-inflammatory cytokine levels already one hour after injection.

5.2.3 CROSSTALK BETWEEN P38 MAPK AND NF-κB SIGNALING

Since TLR4 was described to be the only TLR acting via both, MyD88 and TRIF [141], crosstalks within individually activated downstream pathways are even more complex [287]. Recent studies implicated a role for p38 downstream kinases in the modulation of phosphorylation but also long-term nuclear retention of the NF-κB subunit p65 at least in TNF and IL1 receptor signaling [288-290]. However, analysis of the crosstalk between TLR4-activated p38 MAPK and NF-κB cascades in *Atg16l1LysM* BMDMs demonstrated only a weak effect of p38 activity on canonical NF-κB signaling. In contrast, diminished p38 activity substantially reduced CXCL1 secretion in both, LPS-treated *Atg16l1^{fl/fl}* and *Atg16l1LysM* macrophages, pointing to a general and indirect intervention of p38 MAPK in NF-κB signaling. Indeed, studies in the human monocyte cell line THP-1 as well as in the murine macrophage cell line RAW264.7 demonstrated a p38-dependent stabilization of LPS-induced transcripts containing adenylate/uridylate (AU)-rich elements like the human *Il8* and the murine *Cxcl1* [291, 292] which would also elucidate the increased mRNA level of *Cxcl1* in *Atg16l1LysM* macrophages.

Concluding, in absence of *Atg16l1*, p38 MAPK signaling serves as amplification factor for p65 phosphorylation and CXCL1 secretion. In this scenario, p38 might presumably enhance transcript stabilization but does not act as decisive initiator of NF-κB signaling.

5.2.4 THE AUTOPHAGY RECEPTOR P62 AS A PUTATIVE CENTRAL MEDIATOR OF NF-κB SIGNALING IN AUTOPHAGY-DEFICIENT CELLS

While Bihl and colleagues reported a positive correlation of *Tlr4* expression levels and LPS responsiveness using a *Tlr4* transgenic mouse model [293], *Atg16l1LysM* macrophages neither demonstrated augmented TLR4 protein levels nor cell surface expression. Similar observations were described for F4/80^{hi} macrophages from the spleen, kidney, and peritoneal cavity derived from *Atg7LysM^{cre/+}* mice [48]. These findings exclude TLR4 as key driver for the increased pro-inflammatory signaling in *Atg16l1LysM* BMDMs. Besides TLR4, regulation of LPS-mediated NF-κB activation can be provided by a second cell surface receptor, namely MSR1. MSR1 competitively binds LPS [196] and/or directly inhibits TRAF6 ubiquitination [294]. Thus, diminished levels of MSR1 would explain the hyper-activation seen in *Atg16l1LysM* BMDMs after LPS treatment. Disproving this suggestion, protein levels of

MSR1 were comparable between *Atg16l1^{fl/fl}* and *Atg16l1LysM* BMDMs indicating a MSR1-independent mechanism for ATG16L1 in the regulation of NF- κ B activation pathways. In contrast, deletion of *Atg3*, *Atg5* and *Atg7* was described to increase nuclear factor (erythroid-derived 2)-like 2 (NFE2L2)-dependent cell surface expression of MSR1 [47].

MyD88 [285], TRIF [187] and RIP1 [295] are crucial mediators of TLR4-induced NF- κ B activation and increased protein levels might elucidate the observed differences in LPS-mediated signaling [152]. However, loss of *Atg16l1* did not affect one of the mentioned molecules. This might be indicative for a regulatory mechanism in TLR4 signaling beside an impaired autophagic degradation of classical TLR4 key components.

Autophagy and innate immunity are strongly linked ancient processes, as TLR4-mediated signaling, is known to induce autophagy in a MyD88-dependent manner [31, 296]. Keeping this in mind, the observed LPS-induced levels of the autophagy receptor p62 in both, *Atg16l1^{fl/fl}* and *Atg16l1LysM* BMDMs, might simply be interpreted as a result of autophagy induction which is transient under physiological conditions [23]. However, a striking hallmark of *Atg16l1LysM* BMDMs was the cytoplasmic formation of p62 aggregates under basal conditions which increased even more in the presence of LPS. Interestingly, over-expression studies in HeLa cells and MEFs identified p62 as an essential component of so called cytoplasmic inclusion bodies targeting ubiquitinated proteins for their autophagic degradation [27, 297]. These observations might be a reasonable explanation for the observed cytoplasmic p62 aggregates in *Atg16l1LysM* BMDMs.

Ubiquitination is a decisive regulatory mechanism in NF- κ B signaling [298]. In this context, recent studies implicated an essential role for multimeric complexes of p62 and sequestered Lys⁶³ poly-ubiquitinated proteins in the activation of NF- κ B serving as stabilizing platform [60, 299]. Indeed, p62 was originally described as a substantial modulator of NF- κ B activity acting as a scaffolding protein [297, 300]. The recommended role of p62 as signaling-organizing node in NF- κ B signaling relies on its multifunctional domains [301] which result in a variety of interactions with signaling modulators. Besides its autophagy-related LC3 interaction region [27], p62 harbors a N-terminal PB1 domain mediating the binding of atypical protein kinases C (aPKCs) [302]. In addition, the N-terminus encodes for a ZZ finger domain interacting with RIP1 [300] as well as for a TRAF6 binding site [303]. Since on the one hand oligomerized p62, putatively provoked by impaired autophagy, is proposed to bind Lys⁶³ poly-ubiquitin chains with a higher affinity [304] and, on the other hand, TRAF6 and RIP1 are reported to undergo Lys⁶³-ubiquitination as a crucial step in NF- κ B activation [174, 295], this might lead to the idea of a p62 dose-dependent stabilization of TLR4-mediated signaling in *Atg16l1*-deficient macrophages.

Corroborating this hypothesis, a common feature of the above mentioned p62 interaction partners is the recruitment and activation of TAK1 [305-307]. Because it is known to be a key

modulator of both, NF- κ B and p38 signaling [175], TAK1 would be a promising candidate downstream of the observed p62 aggregates operating as key signal-transducer in TLR4-induced hyper-activation of *Atg16l1*-deficient macrophages (Figure 5-2).

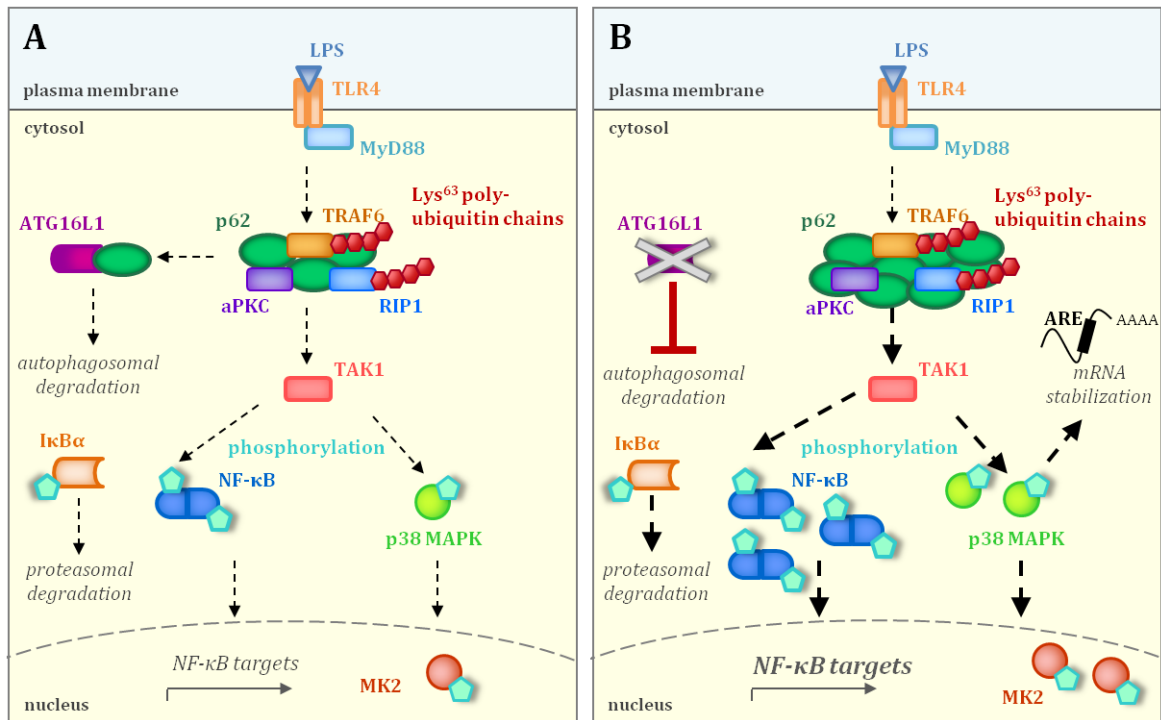


FIGURE 5-2: SUGGESTED EFFECT OF P62 AGGREGATES ON NF- κ B SIGNALING STABILIZATION IN *ATG16L1*-DEFICIENT BMDMS

(A) TLR4 signaling is initiated by LPS-induced dimerization of the receptor. Engagement of adaptor molecules including MyD88 stimulates downstream signaling pathways that involve the interaction between the scaffolding protein p62 and atypical PKCs (aPKCs), TRAF6 and RIP1 which results in the activation of TAK1. Following this, TAK1 facilitates the phosphorylation of I κ B α causing its subsequent degradation by the proteasome. These events allow for the phosphorylation of NF- κ B and its translocation into the nucleus consequentially activating gene transcription. On the other hand, TAK1 stimulates the activation of the canonical p38 MAPK signaling. In this scenario, ATG16L1 mediates the degradation of p62 via the autophagosomal-lysosomal pathway. **(B)** Absence of ATG16L1 and thus autophagy provokes the accumulation and oligomerization of p62 which presumably promotes the sustained formation of a signaling platform. As a major consequence, homeostatic p62 signaling might constitutively stimulates, probably via TAK1, on the one hand increased and prolonged degradation of I κ B α and thus NF- κ B activation and NF- κ B-dependent gene expression and on the other prolonged and increased p38 MAPK signaling facilitating augmented stabilization of transcript containing AU-rich elements (ARE) (see also chapter 5.2.3 for more detail).

On the other hand, the above mentioned model would also give an explanation for the increased number of activated CD11b⁺ macrophages in *Atg16l1LysM* mice. As seen in untreated *Atg16l1LysM* BMDMs, splenocytes of the red pulp, which mainly present myeloid cells [308], demonstrated large p62 accumulations in the cytoplasm. Similar observations were reported for hepatocytes and neurons of liver- and brain-specific *Atg7* knock-out mice as well as for various organs of mice bearing a mosaic deletion of *Atg5* [42, 309]. In addition, large p62 aggregates were determined in *Irgm1*-deficient MEFs [310]. Beside mammals, *Drosophila melanogaster* deficient in *atg8a*, the homologue of the vertebrate LC3A, showed comparable accumulations of the p62 orthologue Ref(2)P in the brain [311]. These findings

point towards a general phenomenon of p62 aggregate formation in case of impaired autophagy. Comparable to *Atg16l1LysM* mice, loss of *Atg7* in hepatocytes and neurons also resulted in hepatomegaly and fatal behavioral abnormalities, respectively [21, 44]. Thus, one might speculate about a pathophysiological association of p62 aggregates with the inflammatory phenotype of autophagy-deficient mice. In fact, deletion of *p62* in liver-specific *Atg7* knock-out mice rescued the liver injury [42]. However, the neuronal phenotype of mice bearing a brain-specific ablation of *Atg7* was not attenuated after additional ablation of *p62* [42]. This paradoxical finding was interpreted to depend on distinct tissue-dependent autophagic activities supporting the above declared suggestion of a positive correlation between the magnitude of p62 aggregates and NF- κ B signaling. For this reason, disrupted degradation of p62 multimeric complexes might already provoke a constitutive activation of NF- κ B signaling and thus increased activation of *Atg16l1*-deficient CD11b⁺ macrophages that in turn leads to chronic inflammatory conditions. Thus, *Atg16l1* and probably autophagy might represent crucial regulatory component for the temporal control of p62-mediated NF- κ B signaling.

Finally, it is worth mentioning that the initial stimulation experiment in the presented study also revealed increased CXCL1 production in response to Poly I:C, ssRNA, TNF α and MDP. Interactions of p62 with aPKCs, RIP1 and TRAF6 were originally identified in NF- κ B regulatory processes of TNFR- and IL1R-mediated signaling pathways [300, 303]. Later on, p62 was reported as scaffolding protein in numerous NF- κ B activating signaling cascades of cell surface receptors like TLR2/6 and TLR4 [32] but also receptor activator of nuclear factor κ B (RANK) [312]. Consequently, the in this study proposed regulatory function of p62 multimeric complexes might not be completely restricted to TLR4-mediated NF- κ B activation. In agreement with this suggestion, increased IL1 β -induced NF- κ B activation in *Atg16l1*-deficient MEFs was assumed to rely on a p62-promoted activation and oligomerization of TRAF6 [60]. Additionally, a recently published study identified p62 as positive regulator of NOD2-mediated NF- κ B and p38 MAPK activity based on its direct interaction with NOD2 [313]. Park and colleagues assumed in their study a similar mechanism for p62 in the formation and stabilization of large p62-NOD2 complexes. Based on a genomic and functional approach, a similar model of selective degradation for TLR adaptors via NDP52, another autophagy cargo receptor, was recommended which indicates a general role for selective autophagy in the modulation of TLR signaling [314, 315]. Studies in human HEK293T cells suggested a similar working model for NDP52 to mediate aggregation of MyD88-TRAF6 and TRIF-TRAF6 which are eliminated via the autophagosomal-lysosomal pathway under certain conditions [240].

Accumulation of p62 was not only associated with inflammatory phenotypes of autophagy-deficient mice but also with dysregulated protein levels in neurodegenerative disorders like

amyotrophic lateral sclerosis (ALS) [316] and huntingtin disease [297] as well as in tumorigenesis and tumor growth [317, 318]. Consequently, the results of the presented study might strengthen the focus on p62 and its targeted protein aggregates as new promising therapeutical targets in several human diseases.

Although, the determined accumulation of p62 in *Atg16l1*-deficient cells might be a reasonable explanation for the observed *in vivo* and *ex vivo* inflammatory phenotype, a detailed characterization of the nature and function of p62 aggregates and putatively p62 multimeric complexes in *Atg16l1LysM* BMDMs is necessary to advance the understanding of their presumable regulatory role in cellular pathology. This is subject of ongoing research.

5.2.5 IMPAIRED AUTOPHAGOSOMAL-LYSOSOMAL DEGRADATION OF A20 IS ASSOCIATED WITH SUSTAINED NF- κ B SIGNALING

Supporting the hypothesis that an autophagy-driven impaired proteostasis specifically modulates the maintenance of TLR4 signaling, a second protein, namely A20, showed increased levels in *Atg16l1LysM* BMDMs in response to LPS. Similarly, *Atg7*-deficient F4/80^{hi}-sorted macrophages showed elevated A20 levels in response to the TLR2 agonist Pam₃CSK₄ [48]. Contributing this idea, an additional treatment with BafA in LPS-stimulated *Atg16l1^{fl/fl}* control BMDMs, inhibiting the acidification and protein degradation in (autophago-)lysosomes [319], reproduced the observed A20 accumulation seen in LPS-treated *Atg16l1*-deficient BMDMs. Paradoxically, A20 is a well described protein ensuring the intrinsic termination of TLR4-mediated NF- κ B activity [201]. For this reason, decreased but not increased levels or an impaired functionality of the accumulated A20 would elucidate the constitutively activated TLR4-mediated signaling in *Atg16l1LysM* BMDMs.

Surprisingly, protein levels of CYLD, another protein belonging to the broad repertoire of NF- κ B-regulating negative feedback loops [204], are not affected by the ablation of *Atg16l1*. This points to a specific autophagy-dependent mechanism in the regulation of LPS-mediated A20 levels. Inhibition of the protein biosynthesis using CHX demonstrated a LPS-induced *de novo* synthesis of A20 in *Atg16l1LysM* macrophages corresponding to an NF- κ B-induced A20 synthesis after activation of the TNFR pathway [203]. As CYLD activity is not controlled by NF- κ B activity but either by its subcellular localization in perinuclear regions or by its phosphorylation [205, 320], it would be conceivable that the observed differences in A20 might occur from the increased activation of NF- κ B. However, mRNA levels of *A20* were neither increased in absence nor in presence of LPS in *Atg16l1*-deficient BMDMs which indicates a regulation of A20 on the post-translational level.

Besides A20, stimulation with LPS in combination with BafA also increased levels of phospho-p65 associated with an amplified secretion of CXCL1 in *Atg16l1^{fl/fl}* control macrophages. This phenotype reflects the increased inflammatory state of solely LPS-treated *Atg16l1LysM* BMDMs. Consequently, it seems reasonable to assume that the augmented inflammatory NF- κ B-mediated response in *Atg16l1LysM* BMDMs might occur independently of the magnitude of A20. With this in mind, a compromised functional activity of A20 would give a reason for the prolonged TLR4-mediated signaling in absence of *Atg16l1*.

Although both, A20 and CYLD attenuate canonical NF- κ B signaling by acting as deubiquitinase enzymes (DUBs), their molecular mechanisms depend on different domains. CYLD belongs to the DUB family of ubiquitin-specific proteases [321] whereas A20 harbors a deubiquitinating ovarian tumor (OTU) domain. Interestingly, the inhibitory capacity of A20 on NF- κ B was originally described to be mediated by its DUB activity on Lys⁶³ poly-ubiquitinated signaling intermediaries like TRAF6, NEMO and RIP1 [200-202]. However, a recently published study in *A20^{ΔOTU}* transgenic mice, lacking the OTU domain of A20, implicated a dispensable role for its DUB activity in TNF- and LPS-mediated NF- κ B activation [322]. Taking this into account, an NF- κ B-terminating molecular mechanism for A20 apart from its DUB activity might explain the differences in A20 and CYLD levels due to the loss of autophagy.

Unlike CYLD, A20 is able to add Lys⁴⁸ poly-ubiquitin chains via its C-terminal zinc finger domains targeting substrates like RIP1 for their proteolytic degradation [200]. Because *Atg16l1^{fl/fl}* and *Atg16l1LysM* BMDMs demonstrated comparable protein levels of RIP1 and the above mentioned mechanism was up to now only described in the TNFR pathway, an impaired E3 ubiquitin ligase activity is implausible. Accordingly, over-expression of A20 in aortic allografts showed stable protein levels of RIP1 and Enesa *et al.* consequentially suggested to uncouple the anti-inflammatory effects of A20 from its proposed role in RIP1 destabilization [323].

Besides its function as a dual ubiquitin-modifying enzyme, several non-catalytic mechanisms were identified by which A20 is capable to interrupt NF- κ B signaling and thus strictly controls inflammation. Inactivation of TRAF6 is achieved by an A20-dependent disruption of the TRAF6-Ubc13/UbcH5c interaction [324]. Inhibition of IKK phosphorylation is based on a poly-ubiquitin-dependent recruitment of A20 to NEMO [325]. Nevertheless, none of these functions gives reason for the contradictory finding of simultaneously augmented A20 levels and NF- κ B signaling in absence of *Atg16l1* and autophagosomal-lysosomal degradation.

However, in line with the above mentioned observations in BMDMs showing a deficient or inhibited autophagosomal-lysosomal degradation, another catalytic-independent mechanism for A20 in the modulation of NF- κ B signaling was described. Precisely, Li and colleagues discovered a membrane-associated localization of endogenous A20 in HeLa cells which was

even more apparent in response to TNF α [326]. Further studies elucidated an NF- κ B-regulating function for lysosome-associated A20 by capturing signaling components like TRAF2 for their lysosomal degradation [327]. Similarly, a study in human umbilical vein endothelial cells (HUVECs) developed a model in which A20 abolishes NF- κ B signaling by targeting Lys⁶³ poly-ubiquitinated signaling proteins like RIP1 for their transport to aggresomes [323]. Interestingly, recruitment of A20 to TNFR signaling complexes strictly depends on its binding capacity to Lys⁶³ poly-ubiquitin chains [328, 329]. Thus, an involvement of autophagosomal degradation might be possible. Supporting this hypothesis, a recently published study demonstrated a p62-mediated autophagic sequestration of A20 in cytoplasmic punctate structures [48]. However, in contrast to *Atg16l1LysM* BMDMs, loss of *Atg7* in F4/80^{hi} macrophages led to a reverse correlation between the amount of A20 and the activity of NF- κ B, at least in response to Pam₃CSK₄. Whether the change in A20 levels and/or localization contributes to the observed phenotype of sustained NF- κ B activation e.g. by sequestering A20 activity or whether A20 levels are simply overridden by other mechanisms needs to be further investigated.

5.3 FUTURE PROSPECTS

The presented work provides first insights into the sophisticated function of ATG16L1 in myeloid cells modulating tissue homeostasis and NF- κ B-mediated inflammatory responses. Based on these findings, a number of unresolved issues as well as new questions raised and will be discussed below.

Loss of *Atg16l1* in the myeloid lineage of mice resulted in far-reaching impacts on the basal phenotype of *Atg16l1LysM* mice. In the present thesis, the particular research focus was set on the impaired tissue homeostasis in hematopoietic organs and the peripheral blood. Although several facts implicate a MDSC-like phenotype of CD11b⁺/Ly6G⁺ cells in *Atg16l1LysM* mice, one has to be aware that all splenic experiments were performed on whole tissues. Thus, a quantitative comparison of MDSC-characteristic genes between isolated CD11b⁺/Ly6G⁺ cells of both genotypes as well as *ex vivo* co-culture experiments might probably confirm the proposed hypothesis of an immunosuppressive capability of *Atg16l1*-deficient CD11b⁺/Ly6G⁺ cells on T cell proliferation and activation.

Gross examination of the gastrointestinal tract further revealed an elongated small intestine in *Atg16l1LysM* mice. Thus, it would be interesting to investigate the morphology and cellular composition of the lamina propria in more detail. With regard to the described association of *ATG16L1* with Crohn's disease [64], the role of *Atg16l1*-deficient macrophages in the gastrointestinal tract under basal as well as challenging conditions like DSS need to be further elucidated.

Further studies might also include the observed bone differences in *Atg16l1LysM* mice. As the autophagy receptor p62 is also known to play a pivotal role in murine osteoclastogenesis [312] and increased expression of p62, due to a genetic mutation in the UBA domain, is associated with disordered bone formation in Paget's disease [330], it might be a conceivable explanation for the characteristically brighter bones of *Atg16l1LysM* mice. Histological examination of the bone formation as well as *ex vivo* differentiation experiments of osteoclasts might be a good starting point for the studies of osteogenesis in absence of *Atg16l1*.

On the other hand, the physiological relevance of p62 aggregates observed in the spleen as well as in BMDMs of *Atg16l1LysM* mice is still unclear. As proposed by Komatsu *et al.*, the impact of p62 inclusion bodies on the impaired tissue homeostasis and its related physiological abnormalities in autophagy-deficient mice seem to depend on the basal autophagic activity of the affected cell types [42]. For this reason, a double knock-out of *Atg16l1* and *p62* in myeloid cells could help to understand the suggested function of p62 aggregates in inflammatory response of *Atg16l1*-deficient macrophages. On the molecular

level, it needs to be further addressed whether p62 indeed stabilizes TLR4-mediated NF- κ B signaling and whether this occurs due to the interaction of one or more interaction partner. In this scenario, it would also be of interest to include autophagy inhibitors and other *Atg* knock out models to confirm a general role for autophagic degradation as NF- κ B-regulating mechanism. Moreover, stimulation of other NF- κ B-activating immune receptors like additional Toll-like receptors and NOD-like receptors but also the role of other autophagy receptors might facilitate the identification of common features and molecules, which might partially complete the yet insufficient understanding about the regulatory mechanisms by which ATG16L1 negatively controls immune responses.

An impaired NF- κ B-regulating function of A20 would explain the similar basal and LPS-induced phenotypes between *Atg1611LysM* mice and *A20*-deficient mice [208, 331]. Similarly, it would be a possible exemplification of the controversial findings in *Atg1611LysM* macrophages demonstrating simultaneously increased levels of phospho-p65 and its upstream negative regulator after TLR4 activation. However, a convincing proof is missing so far. This might be done by studying the localization of A20 as well as the binding capacity to its substrates/interaction partners like TRAF6.

Last but not least, one has to keep in mind that all experiments presented in this work were performed in mice and murine primary cells. Thus, the transferability of the obtained knowledge into the human (cell) system and in the long term into a therapeutic approach in patients would be the next important steps to elucidate the molecular mechanisms by which ATG16L1 modulates immunoregulatory processes.

6 SUMMARY

Eukaryotic cells adapt to changing nutrient conditions through an evolutionarily conserved catabolic mechanism called autophagy. During this “self-eating” process, cytoplasmic constituents and organelles are engulfed by a specialized double-membraned autophagosome, which delivers its cargo to degrading lysosomes. Recent studies also implicated a role for autophagy in immunological processes, such as the removal of intracellular pathogens and the secretion of cytokines. Contributing to these observations, impaired autophagy is associated with a wide range of human diseases like inflammatory bowel disease, asthma and cancer. Studies in mice and men demonstrated a multifunctional role of ATG16L1 not only as an essential component of the autophagic machinery but also as regulator of inflammatory signaling. However, the molecular mechanisms by which ATG16L1 and probably autophagy modulate inflammatory processes remains poorly understood. Thus, the aim of the presented study was to get deeper insights in the impact of ATG16L1 on inflammatory signaling pathways and cytokine production in myeloid cells.

The presented work shows for the first time that ablation of *Atg16l1* in murine myeloid cells has far-reaching consequences for immune homeostasis. Mice lacking *Atg16l1* specifically in myeloid cells (*Atg16l1LysM*) spontaneously develop a hepatosplenomegaly and lymphadenopathy associated with enhanced myeloproliferation in hematopoietic organs and the peripheral blood. Systemic inflammation in *Atg16l1LysM* mice is further typified by the upregulation of a variety of pro-inflammatory cytokines in spleen and serum coinciding with increased activation markers at the cell surface of CD11b⁺ macrophages. Despite increased numbers of CD11b⁺/Ly6G⁺ neutrophils in spleen and peripheral blood, diminished T cell numbers in *Atg16l1LysM* mice were observed. Molecular analysis of the spleen determined elevated markers of T cell-suppressing myeloid-derived suppressor cells (MDSCs), like the exclusive expression of *iNOS*, suggesting a MDSC-like phenotype of CD11b⁺/Ly6G⁺ cells in these mice. In addition, a recurring observation in *Atg16l1LysM* mice was the upregulation of interleukin-1 family members like pro-IL1 β in the spleen and IL1 α in the serum. Therapeutical treatment with Anakinra, a human interleukin-1 receptor (IL1R) antagonist, had no attenuating effect on the inflammatory symptoms of *Atg16l1LysM* mice indicating a dispensable role for IL1R signaling in the manifestation of the spontaneous phenotype. In contrast, prevention of the postnatal microbial colonization of the gastrointestinal tract using antibiotics restored the splenomegaly as well as the immunosuppressed T cell phenotype which points to a hyper-sensitivity of *Atg16l1LysM* mice towards the intestinal commensal microbiota.

Detailed studies in *Atg16l1LysM* bone marrow-derived macrophages (BMDMs) revealed an earlier, increased and prolonged activation of I κ B α -mediated NF- κ B signaling as well as canonical p38 MAPK signaling in response to LPS. These findings corresponded with an increased NF- κ B-dependent cytokine production suggesting a terminating role for ATG16L1 in the temporal control of NF- κ B signaling. Investigations of an impaired proteostasis due to the loss of autophagy determined the accumulation of p62 and A20. Whereas p62 acts as the autophagic cargo receptor and NF- κ B signaling modulator, A20 is a well-known TLR4 negative regulator. Whether the accumulation of p62 or A20 is causative for the increased TLR4-mediated signaling in *Atg16l1*-deficient macrophages needs to be further addressed.

In conclusion, the presented work provides strong evidence for a crucial role of ATG16L1 in inflammatory processes of myeloid cells. By regulating the proteostasis of TLR4 signaling components, ATG16L1 and presumably autophagy represents an important control mechanism in the termination of TLR4-mediated signaling. Thus, the loss of *Atg16l1* in the myeloid lineage *in vivo* results in a disrupted immune homeostasis leading to impaired host-microbe interactions.

7 ZUSAMMENFASSUNG

Eukaryotische Zellen besitzen einen evolutionär konservierten Mechanismus namens Autophagozytose, der es ermöglicht, sich an ändernde Nährstoffbedingungen anzupassen. Hierbei werden zytoplasmatische Bestandteile und Organellen von einer Doppelmembran umschlossen, die sich zu einem Autophagosom ausbildet, und ihren Inhalt anschließend für den Abbau zu Lysosomen transportiert. Neueste Studien implizieren jedoch auch einen Einfluss von Autophagie auf immunologischen Prozessen wie der Abwehr von intrazellulären Pathogenen und der Zytokinsekretion. Eine gestörte Autophagozytose ist mit einer Vielzahl humaner Krankheiten wie chronisch-entzündlichen Darmerkrankungen, Asthma und Krebs assoziiert. Humane und murine Studien konnten bereits eine multifunktionelle Rolle für das mit der Autophagozytose-assoziierte Protein ATG16L1 zeigen. Neben der essentiellen Rolle bei der Ausbildung des Autophagosoms, wird ATG16L1 auch mit der Regulation von inflammatorischen Signalkaskaden in Verbindung gebracht. Die molekularen Mechanismen sind dabei bisher nur unzulänglich aufgeklärt. Aus diesem Grund war das Ziel der vorliegenden Studie, detailliertere Erkenntnisse über den Einfluss von ATG16L1 auf inflammatorische Signalkaskaden und die Zytokinsekretion in myeloiden Zellen zu gewinnen.

In der vorliegenden Arbeit konnte zum ersten Mal gezeigt werden, dass die Deletion von *Atg16l1* in myeloiden Zellen weitreichende Konsequenzen für die Immunhomöostase hat. Mäuse mit einer gewebsspezifischen Deletion von *Atg16l1* in den myeloiden Zellen (*Atg16l1LysM*) entwickeln eine vermehrte Myeloproliferation in hämatopoetischen Organen und dem peripheren Blut, die mit einer spontanen Hepatosplenomegalie sowie eine Lymphadenopathie assoziiert ist. Die systemische Entzündung in *Atg16l1LysM* Mäusen wird außerdem von erhöhten Zytokinleveln in Milz und Serum sowie der vermehrte Expression von Aktivierungsmarkern auf der Zelloberfläche von CD11b⁺ Makrophagen geprägt. Die erhöhte Anzahl an CD11b⁺/Ly6G⁺ Neutrophilen in der Milz und dem peripheren Blut ist mit einer verminderten Anzahl von T-Zellen assoziiert. Es konnte gezeigt werden, dass die Milz vermehrt Charakteristika von T-Zell-supprimierenden myeloiden Suppressorzellen aufweist. Zusätzlich konnte in *Atg16l1LysM* Mäusen ein erhöhtes Auftreten von Komponenten der Interleukin-1 Zytokinfamilie, wie zum Beispiel pro-IL1 β in der Milz und IL1 α im Serum, festgestellt werden. Eine Therapie mit Anakinra, einem humanen Interleukin 1 Rezeptor (IL1R) Antagonisten, zeigte keinen Effekt auf die inflammatorischen Symptome der *Atg16l1LysM* Mäuse, so dass eine wesentliche Beteiligung dieser Signalkaskade in der Ausprägung des spontanen Phänotyps auszuschließen ist. Im Gegensatz dazu, konnte die Prävention der postnatalen mikrobiellen Kolonisierung des gastrointestinalen Trakts durch die Gabe von Antibiotika sowohl die Ausbildung der Splenomegalie als auch des Phänotyps

der T-Zellen in *Atg1611LysM* Mäusen verhindert werden. Dieser Befund weist auf eine erhöhte Sensitivität gegenüber der intestinalen kommensalen Mikroflora hin. Die vermehrte Anzahl sowie die erhöhten Aktivierungsmarker auf CD11b⁺ Makrophagen blieben jedoch auch nach der Depletion der intestinalen Mikrobiota bestehen.

Detailliertere Studien in *Atg1611LysM* Knochenmarksmakrophagen wiesen eine frühere, verstärkte und anhaltende Aktivierung des NF- κ B und p38 MAPK Signalweges nach LPS Stimulation auf. Diese Ergebnisse korrelierten mit einer NF- κ B-abhängigen Zytokinproduktion, was auf einen Einfluss von ATG16L1 auf die temporäre Kontrolle von NF- κ B Signalwegen deutet. Untersuchungen fehlregulierter Proteinlevel durch die gehemmte autophagosomale Degradation zeigten die Akkumulation von p62 und A20. Während p62 als Autophagie-Rezeptor sowie als Modulator von NF- κ B Signalwegen fungiert, agiert A20 als Negativregulator des TLR4 Signalweges. Ob die Akkumulation von p62 oder A20 jedoch ursächlich für die vermehrte TLR4-vermittelte Entzündungsreaktion in Makrophagen ist, müssen weitere Untersuchungen zeigen.

Zusammenfassend konnte in dieser Arbeit erstmals gezeigt werden, dass ATG16L1 eine entscheidende Rolle in entzündlichen Prozessen von myeloiden Zellen einnimmt. Durch die Regulation der Proteostase von Komponenten des TLR4 Signalweges, stellt ATG16L1 über die Autophagozytose einen wichtigen Kontrollmechanismus in der Terminierung des TLR4 Signalweges dar. Dadurch führt der Verlust von *Atg1611* in myeloiden Zellen *in vivo* vermutlich zu einer gestörten Immunhomöostase und Wirt-Mikrobiota-Interaktion.

8 APPENDIX

8.1 BUFFERS AND MEDIA

TABLE 21: LIST OF USED BUFFERS AND APPROPRIATE COMPOSITION

Buffer	Composition	Company
10 x TAE buffer	0.4 M Tris-acetate, 0.1 M EDTA	Roth (Karlsruhe, Germany)
10 x TBS	200 mM Tris (pH 7.6), 1,37 M NaCl	-
10 x TGS buffer	25 mM Tris (pH 8.3), 192 mM glycine, 0.1 % SDS	BioRad (Munich, Germany)
2 x DLB buffer	20 mM Tris (pH 7.4), 2 % (w/v) SDS	-
5 x SDS loading dye	250 mM Tris (pH 6.8), 10 % (w/v) SDS, 50 % (v/v) glycerol, 500 mM DTT	-
Anode buffer 1	30 mM Tris, 20 % (v/v) methanol	-
Anode buffer 2	300 mM Tris, 20 % (v/v) methanol	-
Cathode buffer	25 mM Tris , 40 mM 6-aminocaproic acid, 20 % (v/v) methanol	-
Citrate buffer	11 mM Citric acid (pH 6.0)	-
EMSA buffer 1	10 mM HEPES (pH 7.9), 10 mM KCl, 0. mM EDTA, 1 mM DTT	-
EMSA buffer 2	20 mM HEPES (pH 7.9), 0.4 M NaCl, 0.2 mM EDTA, 1 mM DTT	-
FACS washing buffer (FWP)	0.5 % (w/v) BSA in PBS	-
Phosphat-buffered saline (PBS)	1 mM KH ₂ PO ₄ , 155 mM NaCl, 3 mM Na ₂ HPO ₄ ·7H ₂ O	Gibco (Darmstadt, Germany)
Separation buffer	1.5 M Tris (pH 8.8), 0.4 % (w/v) SDS	-
Stacking buffer	0.5 M Tris (pH 6.8), 0.4 % (w/v)SDS	-
Stripping buffer	2 % (w/v) SDS, 62.5 mM Tris (pH 6.8)	-
TTBS	1 x TBS, 0.1 % (v/v) Tween20	-

TABLE 22: LIST OF USED MEDIA

Media	Company or composition
BMDM medium	DMEM and Macrophage SFM medium (1:1) supplemented with 10 % (v/v) FCS, 5 % (v/v) Penicillin/Streptomycin, 5 % (v/v) Fungizone
DMEM cell culture medium	Gibco (Darmstadt, Germany)
Hank's Balanced Salt Solution (HBSS)	Gibco (Darmstadt, Germany)
Macrophage SFM medium	Gibco (Darmstadt, Germany)

8.2 KITS

TABLE 23: LIST OF USED KITS

Kit	Company
ApopTag® Plus Peroxidase <i>In Situ</i> Apoptosis Detection Kit	Merck Millipore (Darmstadt, Germany)
Bio-Plex Pro™ Mouse Cytokine 23-plex Assay	Bio-Rad (Munich, Germany)
DC™ Protein Assay	Bio-Rad (Munich, Germany)
Lamina Propria Dissociation Kit for mouse	Miltenyi BioTec (Bergisch Gladbach, Germany)
Lineage Cell Depletion kit for mouse	Miltenyi BioTec (Bergisch Gladbach, Germany)
Maxima H Minus First Strand cDNA Synthesis kit	Thermo Scientific (Darmstadt, Germany)
MiSeq Reagent Kit v3 (2 x 300 bp)	Illumina (San Diego, USA)

PowerSoil® DNA Isolation Kit	MoBio (Carlsbad, USA)
QIAquick Gel Extraction Kit	Qiagen (Hilden, Germany)
Quant-iT™ PicoGreen® dsDNA Assay Kit	Invitrogen (Darmstadt, Germany)
RNeasy kit	Qiagen (Hilden, Germany)
SequalPrep™ Normalization Plate Kit	Invitrogen (Darmstadt, Germany)
Vectastain Elite ABC Kit Rabbit IgG	Vector Labs (Peterborough, United Kingdom)

8.3 REAGENTS

TABLE 24: LIST OF USED REAGENTS FOR ANIMAL EXPERIMENTS

Reagents for animal experiments	Company
0.9 % (w/v) NaCl	Fresenius Kabi Deutschland GmbH (Bad Homburg, Germany)
Ampicillin	Sigma Aldrich (Munich, Germany)
Anakinra (Kineret®)	Swedish Orphan Biovitrum AB (Stockholm, Sweden)
Ciprofloxacin	Fresenius Kabi Deutschland GmbH (Bad Homburg, Germany)
LPS (<i>Escherichia coli</i>, strain KPM53)	generous gift by Dr. Nicolas Gisch (Research Center Borstel, Borstel, Germany)
Metronidazole	Sigma Aldrich (Munich, Germany)
Neomycin	Sigma Aldrich (Munich, Germany)
Phosphat-buffered saline (PBS)	Gibco (Darmstadt, Germany)
Vancomycin	Hikma Pharma GmbH, Gräfelfing, Germany)

TABLE 25: LIST OF USED REAGENTS

Reagents	Company
1 % Eosin solution	Roth (Karlsruhe, Germany)
10 % Formalin	Sigma Aldrich (Munich, Germany)
10 x BD FACS Lysing Solution	BD Biosciences (Heidelberg, Germany)
10 x SYBR® Safe DNA gel stain	Life Technologies (Darmstadt, Germany)
30 % Bis-acrylamide (37.5:1)	Bio-Rad (Munich, Germany)
30 % Hydrogen peroxide (H₂O₂)	Sigma Aldrich (Munich, Germany)
5 x Green GoTaq® Reaction Buffer	Promega (Mannheim, Germany)
6-aminocaproic acid	Sigma Aldrich (Munich, Germany)
Agarose	Biozym (Hessisch Oldendorf, Germany)
Ammonium persulfate (APS)	Sigma Aldrich (Munich, Germany)
Bafilomycin A	Enzo Life Sciences GmbH (Lörrach, Germany)
Blotting grade blocker (non-fat dry milk)	Bio-Rad (Munich, Germany)
Bovine serum albumin (BSA)	Roth (Karlsruhe, Germany)
Brefeldin A	Sigma Aldrich (Munich, Germany)
CD11b MicroBeads (human and mouse)	Miltenyi BioTec (Bergisch Gladbach, Germany)
CD95L (Jo2)	BD Biosciences (Heidelberg, Germany)
CellROX Deep Red	Life Technologies (Darmstadt, Germany)
Citric acid	Roth (Karlsruhe, Germany)
Cycloheximide (CHX)	Sigma Aldrich (Munich, Germany)
Deoxynucleotide triphosphates (dNTPs)	Thermo Scientific (Darmstadt, Germany)
Dimethyl sulfoxide (DMSO)	Sigma Aldrich (Munich, Germany)
Diphenyleneiodonium (DPI)	Sigma Aldrich (Munich, Germany)

Dithiothreitol (DTT)	Sigma Aldrich (Munich, Germany)
DreamTaq DNA Polymerase	Thermo Scientific (Darmstadt, Germany)
ECL™ Western Blotting Detection Reagents	GE Healthcare (Hamburg, Germany)
Ethanol	Roth (Karlsruhe, Germany)
Ethylenediaminetetraacetic acid (EDTA)	Sigma Aldrich (Munich, Germany)
Fc-receptor block (anti-CD16/32)	BD Biosciences (Heidelberg, Germany)
Fetal calf serum (FCS)	Merck Millipore (Darmstadt, Germany)
FITC-Dextran	Sigma Aldrich (Munich, Germany)
FSL-1 (Pam₂CGDPKHPKSF)	Invivogen (Toulouse, France)
Glycerol	Roth (Karlsruhe, Germany)
Heat-killed <i>Listeria monocytogenes</i> (HKLM)	Invivogen (Toulouse, France)
Hematoxylin solution	Th Geyer (Renningen, Germany)
HEPES	Sigma Aldrich (Munich, Germany)
Interferon γ (IFNγ) (recombinant mouse)	Immunotools (Friesoythe, Germany)
Interleukin 1 β (IL1β) (recombinant mouse)	Peptotech (Hamburg, Germany)
Lipopolysaccharid (<i>Escherichia coli</i>, F515)	generous gift by Dr. Nicolas Gisch (Research Center Borstel, Borstel, Germany)
Macrophage colony-stimulating factor (mCSF)	Immunotools (Friesoythe, Germany)
Methanol	Roth (Karlsruhe, Germany)
Mitotracker Red	Life Technologies (Darmstadt, Germany)
Muramyl dipeptide (MDP)	Bachem (Bubendorf, Switzerland)
N,N,N',N'-Tetramethylethyldiamin (TEMED)	Sigma Aldrich (Munich, Germany)
Nuclease-free water	Qiagen (Hilden, Germany)
Pam₃CSK₄	Invivogen (Toulouse, France)

Paraffin	Thermo Scientific (Darmstadt, Germany)
Penicillin-Streptomycin (10,000 U/mL)	Life Technologies (Darmstadt, Germany)
Phusion HotStart Flex 2 Master Mix	New England Biolabs GmbH (Frankfurt a.M., Germany)
Pierce ECL™ Plus Western Blotting Substrate	Thermo Scientific (Darmstadt, Germany)
Polyinosinic:polycytidylic acid (Poly (I:C))	Invivogen (Toulouse, France)
Protease and phosphatase inhibitor	Thermo Scientific (Darmstadt, Germany)
Proteinase K	Thermo Scientific (Darmstadt, Germany)
Rapamycin (<i>Streptomyces hygroscopicus</i>)	Sigma Aldrich (Munich, Germany)
Roti-Histokitt mounting medium	Roth (Karlsruhe, Germany)
SB-202190(ip38)	Enzo Life Sciences GmbH (Lörrach, Germany)
Sodium chloride (NaCl)	Merck Millipore (Darmstadt, Germany)
Sodium dodecyl sulfate (SDS)	Roth (Karlsruhe, Germany)
Sodium hydroxide (NaOH)	Merck Millipore (Darmstadt, Germany)
ssRNA 40	Invivogen (Toulouse, France)
SYBR® Select Master Mix	Applied Biosystems (Darmstadt, Germany)
TaqMan Gene Expression Master	Applied Biosystems (Darmstadt, Germany)
Tris	Merck Millipore (Darmstadt, Germany)
Tumor necrosis factor α (TNFα) (recombinant mouse)	Peprtech (Hamburg, Germany)
Tween 20	Roth (Karlsruhe, Germany)
Xylene	Thermo Scientific (Darmstadt, Germany)
Z-Leu-Leu-Leu-CHO (MG132)	Enzo Life Sciences GmbH (Lörrach, Germany)
β-Mercaptoethanol	Sigma Aldrich (Munich, Germany)

8.4 DEVICES

TABLE 26: LIST OF USED DEVICES

Devices	Company
100-1000 μL pipette	Eppendorf (Hamburg, Germany)
10-100 μL pipette	Eppendorf (Hamburg, Germany)
10-200 μL multi-channel pipette	Eppendorf (Hamburg, Germany)
1-10 μL pipette	Eppendorf (Hamburg, Germany)
7900HT Fast Real Time PCR System	Applied Biosystems (Darmstadt, Germany)
Agarose gel chamber wide mini sub-cell GT	Bio-Rad (Munich, Germany)
Automatic developer machine Curix 60	Agfa (Mortsel, Belgium)
Axio Imager Z1	ZEISS (Oberkochen, Germany)
Balance	PeqLab (Erlangen, Germany)
Cell Counter (Cellometer Auto T4 Plus)	Heraeus (Hanau, Germany)
Centrifuge Fresco21 Centrifuge	Heraeus (Hanau, Germany)
Centrifuge Megafuge 16	Bio-Rad (Munich, Germany)
ChemiDoc XRS	Biometra (Göttingen, Germany)
Confocal laser scanning microscope TCS SP5	Leica (Wetzlar, Germany)
Electrophoresis chamber Multigel G44	Tecan (Männedorf, Switzerland)
ELISA plate shaker	Thermo Scientific (Darmstadt, Germany)
ELISA washer Columbus plus	BD Biosciences (Heidelberg, Germany)
Embedding station STP120	Applied Biosystems (Darmstadt, Germany)
FACSCalibur™	BD Biosciences (Heidelberg, Germany)
GeneAmp PCR System 9700	Sartorius (Göttingen, Germany)
Incubator	Tecan (Männedorf, Switzerland)

Magnetic stirring plate	Severin (Sundern, Germany)
Microplate reader Infinite M200 Pro	Illumina (San Diego, USA)
Microwave	PeqLab (Erlangen, Germany)
MiSeq sequencer	Miltenyi BioTec (Bergisch Gladbach, Germany)
NanoDrop spectrometer ND1000	Biometra (Göttingen, Germany)
OctoMACS	Leica (Wetzlar, Germany)
Power Supply PP 3000	Bandelin (Berlin, Germany)
RM2255 microtome	Heraeus (Hanau, Germany)
Sonificator Sonopuls	Eppendorf (Hamburg, Germany)
Sterile bench Herasafe KS12	Bio-Rad (Munich, Germany)
Thermomixer compact	ZEISS (Oberkochen, Germany)
TransBlot Turbo Transfer System	Stuart Scientific (Chelmsford, United Kingdom)
Tube rotator SRT6	GFL (Burgwedel, Germany)
Vortex Genie 2	Scientific Industries (New York, USA)
Water bath 1013	GFL (Burgwedel, Germany)

8.5 CONSUMABLES

TABLE 27: LIST OF USED CONSUMABLES

Consumables	Company
0.5 mL/1.5 mL/2.0 mL tubes	Sarstedt (Nümbrecht, Germany)
1.5 mL/2.0 mL safe seal tubes	Sarstedt (Nümbrecht, Germany)
10 mL syringe	BD Biosciences (Heidelberg, Germany)
1-10 µL/10-100 µL/100-1000 µL pipette (filter) tips	Sarstedt (Nümbrecht, Germany)
15 cm/10 mL petri dish	Sarstedt (Nümbrecht, Germany)

15 mL/50 mL tubes	Sarstedt (Nümbrecht, Germany)
18G/20G/26G needles	BD Biosciences (Heidelberg, Germany)
1 mL syringe	BD Biosciences (Heidelberg, Germany)
384-well plates	Life Technologies (Darmstadt, Germany)
40 µm/70 µm cell strainer	BD Biosciences (Heidelberg, Germany)
5 mL/10 mL/25 mL pipettes	Sarstedt (Nümbrecht, Germany)
6-well/12-well/96-well plate (flat bottom)	Sarstedt (Nümbrecht, Germany)
96-well V-bottom plate	BD Biosciences (Heidelberg, Germany)
cell scraper	Sarstedt (Nümbrecht, Germany)
coverslips (24x50mm)	Geyer (Renningen, Germany)
FACS tubes	Greiner (Frickenhausen, Germany)
EDTA tubes	Sarstedt (Nümbrecht, Germany)
Lithium-heparin tubes	Sarstedt (Nümbrecht, Germany)
MACS MS columns	Miltenyi BioTec (Bergisch Gladbach, Germany)
Nunc Lab-Tek II Chamber Slide 8-wells	Thermo Scientific (Darmstadt, Germany)

9 REFERENCES

1. Schrader, E.K., K.G. Harstad, and A. Matouschek, *Targeting proteins for degradation*. Nat Chem Biol, 2009. **5**(11): p. 815-822.
2. Kaur, J. and J. Debnath, *Autophagy at the crossroads of catabolism and anabolism*. Nat Rev Mol Cell Biol, 2015. **16**(8): p. 461-472.
3. Cuervo, A.M., *Chaperone-mediated autophagy: Dice's 'wild' idea about lysosomal selectivity*. Nat Rev Mol Cell Biol, 2011. **12**(8): p. 535-541.
4. Cuervo, A.M. and E. Wong, *Chaperone-mediated autophagy: roles in disease and aging*. Cell Res, 2014. **24**(1): p. 92-104.
5. Li, W.-w., J. Li, and J.-k. Bao, *Microautophagy: lesser-known self-eating*. Cellular and Molecular Life Sciences, 2012. **69**(7): p. 1125-1136.
6. Klionsky, D.J., *Autophagy: from phenomenology to molecular understanding in less than a decade*. Nat Rev Mol Cell Biol, 2007. **8**(11): p. 931-937.
7. Klionsky, D.J. and B.A. Schulman, *Dynamic regulation of macroautophagy by distinctive ubiquitin-like proteins*. Nat Struct Mol Biol, 2014. **21**(4): p. 336-345.
8. Xie, Z. and D.J. Klionsky, *Autophagosome formation: core machinery and adaptations*. Nat Cell Biol, 2007. **9**(10): p. 1102-1109.
9. Ganley, I.G., et al., *ULK1-ATG13-FIP200 Complex Mediates mTOR Signaling and Is Essential for Autophagy*. Journal of Biological Chemistry, 2009. **284**(18): p. 12297-12305.
10. Russell, R.C., et al., *ULK1 induces autophagy by phosphorylating Beclin-1 and activating Vps34 lipid kinase*. Nature cell biology, 2013. **15**(7): p. 741-750.
11. Ravikumar, B., et al., *Regulation of Mammalian Autophagy in Physiology and Pathophysiology*. Physiological Reviews, 2010. **90**(4): p. 1383-1435.
12. Mizushima, N., et al., *Mouse Apg16L, a novel WD-repeat protein, targets to the autophagic isolation membrane with the Apg12-Apg5 conjugate*. Journal of Cell Science, 2003. **116**(9): p. 1679-1688.
13. Mizushima, N., et al., *A protein conjugation system essential for autophagy*. Nature, 1998. **395**(6700): p. 395-398.
14. Mizushima, N., et al., *A New Protein Conjugation System in Human: THE COUNTERPART OF THE YEAST Apg12p CONJUGATION SYSTEM ESSENTIAL FOR AUTOPHAGY*. Journal of Biological Chemistry, 1998. **273**(51): p. 33889-33892.
15. Dooley, Hannah C., et al., *WIPI2 Links LC3 Conjugation with PI3P, Autophagosome Formation, and Pathogen Clearance by Recruiting Atg12 and Atg16L1*. Molecular Cell, 2014. **55**(2): p. 238-252.

16. Hanada, T., et al., *The Atg12-Atg5 Conjugate Has a Novel E3-like Activity for Protein Lipidation in Autophagy*. Journal of Biological Chemistry, 2007. **282**(52): p. 37298-37302.
17. Hemelaar, J., et al., *A Single Protease, Apg4B, Is Specific for the Autophagy-related Ubiquitin-like Proteins GATE-16, MAP1-LC3, GABARAP, and Apg8L*. Journal of Biological Chemistry, 2003. **278**(51): p. 51841-51850.
18. Tanida, I., T. Ueno, and E. Kominami, *LC3 conjugation system in mammalian autophagy*. The International Journal of Biochemistry & Cell Biology, 2004. **36**(12): p. 2503-2518.
19. Kabeya, Y., et al., *LC3, a mammalian homologue of yeast Apg8p, is localized in autophagosome membranes after processing*. The EMBO Journal, 2000. **19**(21): p. 5720-5728.
20. Kuma, A., et al., *The role of autophagy during the early neonatal starvation period*. Nature, 2004. **432**(7020): p. 1032-1036.
21. Komatsu, M., et al., *Impairment of starvation-induced and constitutive autophagy in Atg7-deficient mice*. The Journal of Cell Biology, 2005. **169**(3): p. 425-434.
22. Saitoh, T., et al., *Loss of the autophagy protein Atg16L1 enhances endotoxin-induced IL-1[bgr] production*. Nature, 2008. **456**(7219): p. 264-268.
23. Klionsky, D., et al., *Guidlines for the use and interpretation of assays for monitoring autophagy*. Autophagy, 2012. **8**: p. 445 - 544.
24. Stolz, A., A. Ernst, and I. Dikic, *Cargo recognition and trafficking in selective autophagy*. Nat Cell Biol, 2014. **16**(6): p. 495-501.
25. Zaffagnini, G. and S. Martens, *Mechanisms of Selective Autophagy*. Journal of Molecular Biology.
26. Tan, J.M.M., et al., *Lysine 63-linked ubiquitination promotes the formation and autophagic clearance of protein inclusions associated with neurodegenerative diseases*. Human Molecular Genetics, 2008. **17**(3): p. 431-439.
27. Pankiv, S., et al., *p62/SQSTM1 Binds Directly to Atg8/LC3 to Facilitate Degradation of Ubiquitinated Protein Aggregates by Autophagy*. Journal of Biological Chemistry, 2007. **282**(33): p. 24131-24145.
28. Kirkin, V., et al., *A Role for NBR1 in Autophagosomal Degradation of Ubiquitinated Substrates*. Molecular Cell, 2009. **33**(4): p. 505-516.
29. Thurston, T.L.M., et al., *The TBK1 adaptor and autophagy receptor NDP52 restricts the proliferation of ubiquitin-coated bacteria*. Nat Immunol, 2009. **10**(11): p. 1215-1221.
30. Wooten, M.W., et al., *Essential Role of Sequestosome 1/p62 in Regulating Accumulation of Lys63-ubiquitinated Proteins*. Journal of Biological Chemistry, 2008. **283**(11): p. 6783-6789.

31. Chen, C., et al., *Lipopolysaccharide Stimulates p62-Dependent Autophagy-Like Aggregate Clearance in Hepatocytes*. BioMed Research International, 2014. **2014**: p. 13.
32. Lee, H.-M., et al., *Autophagy Negatively Regulates Keratinocyte Inflammatory Responses via Scaffolding Protein p62/SQSTM1*. The Journal of Immunology, 2011. **186**(2): p. 1248-1258.
33. Itakura, E. and N. Mizushima, *p62 targeting to the autophagosome formation site requires self-oligomerization but not LC3 binding*. The Journal of Cell Biology, 2011. **192**(1): p. 17-27.
34. Jiang, P. and N. Mizushima, *Autophagy and human diseases*. Cell Res, 2014. **24**(1): p. 69-79.
35. Yue, Z., et al., *Beclin 1, an autophagy gene essential for early embryonic development, is a haploinsufficient tumor suppressor*. Proceedings of the National Academy of Sciences, 2003. **100**(25): p. 15077-15082.
36. Gan, B., et al., *Role of FIP200 in cardiac and liver development and its regulation of TNF α and TSC-mTOR signaling pathways*. The Journal of Cell Biology, 2006. **175**(1): p. 121-133.
37. Cann, G.M., et al., *Developmental expression of LC3 α and β : Absence of fibronectin or autophagy phenotype in LC3 β knockout mice*. Developmental Dynamics, 2008. **237**(1): p. 187-195.
38. Mortensen, M., et al., *The autophagy protein Atg7 is essential for hematopoietic stem cell maintenance*. The Journal of Experimental Medicine, 2011. **208**(3): p. 455-467.
39. Pua, H.H., et al., *A critical role for the autophagy gene Atg5 in T cell survival and proliferation*. The Journal of Experimental Medicine, 2007. **204**(1): p. 25-31.
40. Pua, H.H., et al., *Autophagy Is Essential for Mitochondrial Clearance in Mature T Lymphocytes*. The Journal of Immunology, 2009. **182**(7): p. 4046-4055.
41. Miller, B.C., et al., *The autophagy gene ATG5 plays an essential role in B lymphocyte development*. Autophagy, 2008. **4**(3): p. 309-314
42. Komatsu, M., et al., *Homeostatic Levels of p62 Control Cytoplasmic Inclusion Body Formation in Autophagy-Deficient Mice*. Cell, 2007. **131**(6): p. 1149-1163.
43. Hara, T., et al., *Suppression of basal autophagy in neural cells causes neurodegenerative disease in mice*. Nature, 2006. **441**(7095): p. 885-889.
44. Komatsu, M., et al., *Loss of autophagy in the central nervous system causes neurodegeneration in mice*. Nature, 2006. **441**(7095): p. 880-884.
45. Cadwell, K., et al., *A common role for Atg16L1, Atg5, and Atg7 in small intestinal Paneth cells and Crohn's disease*. Autophagy, 2009. **5**(2): p. 250-252.

46. Castillo, E.F., et al., *Autophagy protects against active tuberculosis by suppressing bacterial burden and inflammation*. Proceedings of the National Academy of Sciences, 2012. **109**(46): p. E3168–E3176.
47. Bonilla, Diana L., et al., *Autophagy Regulates Phagocytosis by Modulating the Expression of Scavenger Receptors*. Immunity, 2013. **39**(3): p. 537-547.
48. Kanayama, M., et al., *Autophagy enhances NFκB activity in specific tissue macrophages by sequestering A20 to boost antifungal immunity*. Nat Commun, 2015. **6**.
49. Zhao, Z., et al., *Atg5 is Essential for Cellular Immunity in vivo and recruitment of a p47 GTPase to the Toxoplasma gondii Parasitophorous Vacuole in Macrophages*. Cell Host & Microbe, 2008. **4**(5): p. 458-469.
50. Mizushima, N., T. Noda, and Y. Ohsumi, *Apg16p is required for the function of the Apg12p–Apg5p conjugate in the yeast autophagy pathway*. Vol. 18. 1999. 3888-3896.
51. Kuma, A., et al., *Formation of the 350-kDa Apg12-Apg5-Apg16 Multimeric Complex, Mediated by Apg16 Oligomerization, Is Essential for Autophagy in Yeast*. Journal of Biological Chemistry, 2002. **277**(21): p. 18619-18625.
52. Matsushita, M., et al., *Structure of Atg5-Atg16, a Complex Essential for Autophagy*. Journal of Biological Chemistry, 2007. **282**(9): p. 6763-6772.
53. Zheng, H., et al., *Cloning and Analysis of Human Apg16L*. DNA Sequence, 2004. **15**(4): p. 303-305.
54. Parkhouse, R., et al., *The N-Terminal Region of the Human Autophagy Protein ATG16L1 Contains a Domain That Folds into a Helical Structure Consistent with Formation of a Coiled-Coil*. PLoS ONE, 2013. **8**(9): p. e76237.
55. Stirnimann, C.U., et al., *WD40 proteins propel cellular networks*. Trends in Biochemical Sciences, 2010. **35**(10): p. 565-574.
56. Gammoh, N., et al., *Interaction Between FIP200 and ATG16L1 Distinguishes ULK1 Complex-Dependent and -Independent Autophagy*. Nature structural & molecular biology, 2013. **20**(2): p. 144-149.
57. Nishimura, T., et al., *FIP200 regulates targeting of Atg16L1 to the isolation membrane*. EMBO reports, 2013. **14**(3): p. 284-291.
58. Jiang, T., et al., *Three isoforms of the Atg16L1 protein contribute different autophagic properties*. Molecular and Cellular Biochemistry, 2013. **378**(1-2): p. 257-266.
59. Hwang, S., et al., *Nondegradative Role of Atg5-Atg12/ Atg16L1 Autophagy Protein Complex in Antiviral Activity of Interferon Gamma*. Cell Host & Microbe, 2012. **11**(4): p. 397-409.
60. Lee, J., et al., *Autophagy Suppresses Interleukin-1β (IL-1β) Signaling by Activation of p62 Degradation via Lysosomal and Proteasomal Pathways*. Journal of Biological Chemistry, 2012. **287**(6): p. 4033-4040.

61. Bafica, A., et al., *The IFN-Inducible GTPase LRG47 (Irgm1) Negatively Regulates TLR4-Triggered Proinflammatory Cytokine Production and Prevents Endotoxemia*. *The Journal of Immunology*, 2007. **179**(8): p. 5514-5522.
62. Dupont, N., et al., *Autophagy-based unconventional secretory pathway for extracellular delivery of IL-1[beta]*. *EMBO J*, 2011. **30**(23): p. 4701-4711.
63. Torisu, T., et al., *Autophagy regulates endothelial cell processing, maturation and secretion of von Willebrand factor*. *Nat Med*, 2013. **19**(10): p. 1281-1287.
64. Hampe, J., et al., *A genome-wide association scan of nonsynonymous SNPs identifies a susceptibility variant for Crohn disease in ATG16L1*. *Nat Genet*, 2007. **39**(2): p. 207-211.
65. Rioux, J.D., et al., *Genome-wide association study identifies new susceptibility loci for Crohn disease and implicates autophagy in disease pathogenesis*. *Nat Genet*, 2007. **39**(5): p. 596-604.
66. Cadwell, K., et al., *A key role for autophagy and the autophagy gene Atg16l1 in mouse and human intestinal Paneth cells*. *Nature*, 2008. **456**(7219): p. 259-263.
67. Adolph, T.E., et al., *Paneth cells as a site of origin for intestinal inflammation*. *Nature*, 2013. **503**(7475): p. 272-276.
68. Murthy, A., et al., *A Crohn's disease variant in Atg16l1 enhances its degradation by caspase 3*. *Nature*, 2014. **506**(7489): p. 456-462.
69. Lapaquette, P., et al., *Crohn's disease-associated adherent-invasive E. coli are selectively favoured by impaired autophagy to replicate intracellularly*. *Cellular Microbiology*, 2010. **12**(1): p. 99-113.
70. Plantinga, T.S., et al., *Crohn's disease-associated ATG16L1 polymorphism modulates pro-inflammatory cytokine responses selectively upon activation of NOD2*. *Gut*, 2011. **60**(9): p. 1229-1235.
71. Shi, C.-S., et al., *Activation of autophagy by inflammatory signals limits IL-1[beta] production by targeting ubiquitinated inflammasomes for destruction*. *Nat Immunol*, 2012. **13**(3): p. 255-263.
72. Zhou, R., et al., *A role for mitochondria in NLRP3 inflammasome activation*. *Nature*, 2011. **469**(7329): p. 221-225.
73. Conference, I.H., *Preamble of the Constitution of the World Health Organization*. *Official Records of the World Health Organization*, 1946. **2**: p. 100.
74. Amit, I., D.R. Winter, and S. Jung, *The role of the local environment and epigenetics in shaping macrophage identity and their effect on tissue homeostasis*. *Nat Immunol*, 2016. **17**(1): p. 18-25.
75. Medzhitov, R., *Origin and physiological roles of inflammation*. *Nature*, 2008. **454**(7203): p. 428-435.

76. Kumar V, A.A.K., Aster J C, *Robbins basic pathology*. Saunders, 2013. **9th Edition**.
77. Hotamisligil, G.S., *Inflammation and metabolic disorders*. Nature, 2006. **444**(7121): p. 860-867.
78. Libby, P., *Inflammation and cardiovascular disease mechanisms*. The American Journal of Clinical Nutrition, 2006. **83**(2): p. 456S-460S.
79. Amor, S., et al., *Inflammation in neurodegenerative diseases – an update*. Immunology, 2014. **142**(2): p. 151-166.
80. Wahren-Herlenius, M. and T. Dörner, *Immunopathogenic mechanisms of systemic autoimmune disease*. The Lancet. **382**(9894): p. 819-831.
81. Neurath, M.F., *Cytokines in inflammatory bowel disease*. Nat Rev Immunol, 2014. **14**(5): p. 329-342.
82. Grivennikov, S.I., F.R. Greten, and M. Karin, *Immunity, Inflammation, and Cancer*. Cell, 2010. **140**(6): p. 883-899.
83. Majno, G., *The Ancient Riddle of (Sepsis)*. The Journal of Infectious Diseases, 1991. **163**: p. 937-945.
84. Angus, D.C. and T. van der Poll, *Severe Sepsis and Septic Shock*. New England Journal of Medicine, 2013. **369**(9): p. 840-851.
85. Bone, R.C., W.J. Sibbald, and C.L. Sprung, *The accp-sccm consensus conference on sepsis and organ failure*. Chest, 1992. **101**(6): p. 1481-1483.
86. Levy, M.M.M., FCCP; Fink, Mitchell P. MD, FCCP; Marshall, John C. MD; Abraham, Edward MD; Angus, Derek MD, MPH, FCCP; Cook, Deborah MD, FCCP; Cohen, Jonathan MD; Opal, Steven M. MD; Vincent, Jean-Louis MD, FCCP, PhD; Ramsay, Graham MD, *2001 SCCM/ESICM/ACCP/ATS/SIS International Sepsis Definitions Conference*. Critical Care Medicine, 2003. **31** (**4**): p. 1250-1256.
87. Marshall, J.C., *Predisposition to Sepsis*, in *Anaesthesia, Pain, Intensive Care and Emergency A.P.I.C.E.*, A. Gullo, Editor. 2008, Springer Milan. p. 241-254.
88. Cohen, J., *The immunopathogenesis of sepsis*. Nature, 2002. **420**(6917): p. 885-891.
89. Engel, C., et al., *Epidemiology of sepsis in Germany: results from a national prospective multicenter study*. Intensive Care Medicine, 2007. **33**(4): p. 606-618.
90. Adhikari, N.K.J., et al., *Critical care and the global burden of critical illness in adults*. The Lancet. **376**(9749): p. 1339-1346.
91. Benjamim, C.F., C.M. Hogaboam, and S.L. Kunkel, *The chronic consequences of severe sepsis*. Journal of Leukocyte Biology, 2004. **75**(3): p. 408-412.
92. Yende, S., T.J. Iwashyna, and D.C. Angus, *Interplay between sepsis and chronic health*. Trends in Molecular Medicine, 2014. **20**(4): p. 234-238.

93. Ou, S.-M., et al., *Long-term Mortality and Major Adverse Cardiovascular Events in Sepsis Survivors: A Nationwide Population-based Study*. American Journal of Respiratory and Critical Care Medicine, 2016.
94. Jagannathan-Bogdan, M. and L.I. Zon, *Hematopoiesis*. Development (Cambridge, England), 2013. **140**(12): p. 2463-2467.
95. Kondo, M., I.L. Weissman, and K. Akashi, *Identification of Clonogenic Common Lymphoid Progenitors in Mouse Bone Marrow*. Cell. **91**(5): p. 661-672.
96. Akashi, K., et al., *A clonogenic common myeloid progenitor that gives rise to all myeloid lineages*. Nature, 2000. **404**(6774): p. 193-197.
97. De Kleer, I., et al., *Ontogeny of Myeloid Cells*. Frontiers in Immunology, 2014. **5**: p. 423.
98. Hotchkiss, R.S., G. Monneret, and D. Payen, *Sepsis-induced immunosuppression: from cellular dysfunctions to immunotherapy*. Nat Rev Immunol, 2013. **13**(12): p. 862-874.
99. Sankaran, V.G. and M.J. Weiss, *Anemia: progress in molecular mechanisms and therapies*. Nat Med, 2015. **21**(3): p. 221-230.
100. Kaufmann, S.H.E., *Immunology's foundation: the 100-year anniversary of the Nobel Prize to Paul Ehrlich and Elie Metchnikoff*. Nat Immunol, 2008. **9**(7): p. 705-712.
101. Kumar, V. and A. Sharma, *Neutrophils: Cinderella of innate immune system*. International Immunopharmacology, 2010. **10**(11): p. 1325-1334.
102. Hammond, M.E., et al., *IL-8 induces neutrophil chemotaxis predominantly via type I IL-8 receptors*. The Journal of Immunology, 1995. **155**(3): p. 1428-33.
103. Ribeiro, R.A., et al., *IL-8 causes in vivo neutrophil migration by a cell-dependent mechanism*. Immunology, 1991. **73**(4): p. 472-477.
104. Fleming, T.J., M.L. Fleming, and T.R. Malek, *Selective expression of Ly-6G on myeloid lineage cells in mouse bone marrow. RB6-8C5 mAb to granulocyte-differentiation antigen (Gr-1) detects members of the Ly-6 family*. The Journal of Immunology, 1993. **151**(5): p. 2399-408.
105. Mócsai, A., *Diverse novel functions of neutrophils in immunity, inflammation, and beyond*. The Journal of Experimental Medicine, 2013. **210**(7): p. 1283-1299.
106. Falloon, J. and J.I. Gallin, *Neutrophil granules in health and disease*. Journal of Allergy and Clinical Immunology, 1986. **77**(5): p. 653-662.
107. Dahlgren, C. and A. Karlsson, *Respiratory burst in human neutrophils*. Journal of Immunological Methods, 1999. **232**(1-2): p. 3-14.
108. Kasama, T., et al., *Expression and regulation of human neutrophil-derived macrophage inflammatory protein 1 alpha*. The Journal of Experimental Medicine, 1993. **178**(1): p. 63-72.
109. Nathan, C., *Neutrophils and immunity: challenges and opportunities*. Nat Rev Immunol, 2006. **6**(3): p. 173-182.

110. Ocuin, L.M., et al., *Neutrophil IL-10 suppresses peritoneal inflammatory monocytes during polymicrobial sepsis*. Journal of Leukocyte Biology, 2011. **89**(3): p. 423-432.
111. Pillay, J., et al., *A subset of neutrophils in human systemic inflammation inhibits T cell responses through Mac-1*. The Journal of Clinical Investigation, 2011. **122**(1): p. 327-336.
112. van Furth, R. and Z.A. Cohn, *THE ORIGIN AND KINETICS OF MONONUCLEAR PHAGOCYTES*. The Journal of Experimental Medicine, 1968. **128**(3): p. 415-435.
113. Passlick, B., D. Flieger, and H. Ziegler-Heitbrock, *Identification and characterization of a novel monocyte subpopulation in human peripheral blood*. Blood, 1989. **74**(7): p. 2527-2534.
114. Jakubzick, C., et al., *Minimal Differentiation of Classical Monocytes as They Survey Steady-State Tissues and Transport Antigen to Lymph Nodes*. Immunity, 2013. **39**(3): p. 599-610.
115. Geissmann, F., S. Jung, and D.R. Littman, *Blood Monocytes Consist of Two Principal Subsets with Distinct Migratory Properties*. Immunity, 2003. **19**(1): p. 71-82.
116. Schulz, C., et al., *A Lineage of Myeloid Cells Independent of Myb and Hematopoietic Stem Cells*. Science, 2012. **336**(6077): p. 86-90.
117. Alliot, F., I. Godin, and B. Pessac, *Microglia derive from progenitors, originating from the yolk sac, and which proliferate in the brain*. Developmental Brain Research, 1999. **117**(2): p. 145-152.
118. Ginhoux, F. and S. Jung, *Monocytes and macrophages: developmental pathways and tissue homeostasis*. Nat Rev Immunol, 2014. **14**(6): p. 392-404.
119. Denning, T.L., et al., *Lamina propria macrophages and dendritic cells differentially induce regulatory and interleukin 17-producing T cell responses*. Nat Immunol, 2007. **8**(10): p. 1086-1094.
120. Taylor, P.R., et al., *MACROPHAGE RECEPTORS AND IMMUNE RECOGNITION*. Annual Review of Immunology, 2005. **23**(1): p. 901-944.
121. Harding, C.H. and G.H. J., *Class II MHC Molecules Are Present in Macrophage Lysosomes and Phagolysosomes That Function in the Phagocytic Processing of Listeria Monocytogenes for Presentation of T Cells*. The Journal of Cell Biology, 1992. **119**(3): p. 531-542.
122. Giroir, B.P., et al., *The tissue distribution of tumor necrosis factor biosynthesis during endotoxemia*. The Journal of Clinical Investigation, 1992. **90**(3): p. 693-698.
123. D'Andrea, A., et al., *Production of natural killer cell stimulatory factor (interleukin 12) by peripheral blood mononuclear cells*. The Journal of Experimental Medicine, 1992. **176**(5): p. 1387-1398.

124. Yoshimura, T., et al., *Neutrophil chemotactic factor produced by lipopolysaccharide (LPS)-stimulated human blood mononuclear leukocytes: partial characterization and separation from interleukin 1 (IL 1)*. *The Journal of Immunology*, 1987. **139**(3): p. 788-93.
125. Walz, A., et al., *Purification and amino acid sequencing of NAF, a novel neutrophil-activating factor produced by monocytes*. *Biochemical and Biophysical Research Communications*, 1987. **149**(2): p. 755-761.
126. Harmsen, A.G. and E.A. Havell, *Roles of tumor necrosis factor and macrophages in lipopolysaccharide-induced accumulation of neutrophils in cutaneous air pouches*. *Infection and Immunity*, 1990. **58**(2): p. 297-302.
127. Edwards, J.P., et al., *Biochemical and functional characterization of three activated macrophage populations*. *Journal of Leukocyte Biology*, 2006. **80**(6): p. 1298-1307.
128. Altemeier, W.A., et al., *Fas (CD95) Induces Macrophage Pro-Inflammatory Chemokine Production via a MyD88-dependent, Caspase-independent Pathway*. *Journal of Leukocyte Biology*, 2007. **82**(3): p. 721-728.
129. Peter, M.E., et al., *The role of CD95 and CD95 ligand in cancer*. *Cell Death Differ*, 2015. **22**(4): p. 549-559.
130. Landmann, R., et al., *Human monocyte CD14 is upregulated by lipopolysaccharide*. *Infection and Immunity*, 1996. **64**(5): p. 1762-9.
131. Matsuura, K., et al., *Upregulation of mouse CD14 expression in Kupffer cells by lipopolysaccharide*. *The Journal of Experimental Medicine*, 1994. **179**(5): p. 1671-1676.
132. Fearn, C., et al., *Murine CD14 gene expression in vivo: extramyeloid synthesis and regulation by lipopolysaccharide*. *The Journal of Experimental Medicine*, 1995. **181**(3): p. 857-66.
133. Korn, D., et al., *Modulation of Macrophage Efferocytosis in Inflammation*. *Frontiers in Immunology*, 2011. **2**: p. 57.
134. Koh, T.J. and L.A. DiPietro, *Inflammation and wound healing: The role of the macrophage*. *Expert reviews in molecular medicine*, 2011. **13**: p. e23-e23.
135. Janeway, C.A., *Approaching the Asymptote? Evolution and Revolution in Immunology*. *Cold Spring Harbor Symposia on Quantitative Biology*, 1989. **54**: p. 1-13.
136. Anderson, K.V., G. Jürgens, and C. Nüsslein-Volhard, *Establishment of dorsal-ventral polarity in the Drosophila embryo: Genetic studies on the role of the Toll gene product*. *Cell*, 1985. **42**(3): p. 779-789.
137. Gay, N.J. and F.J. Keith, *Drosophila Toll and IL-1 receptor*. *Nature*, 1991. **351**(6325): p. 355-356.

138. Whitham, S., et al., *The product of the tobacco mosaic virus resistance gene N: Similarity to toll and the interleukin-1 receptor*. Cell, 1994. **78**(6): p. 1101-1115.
139. Rock, F.L., et al., *A family of human receptors structurally related to Drosophila Toll*. Proceedings of the National Academy of Sciences, 1998. **95**(2): p. 588-593.
140. Kawai, T. and S. Akira, *The roles of TLRs, RLRs and NLRs in pathogen recognition* ARTICLE. International Immunology, 2009. **21**(4): p. 317-337.
141. O'Neill, L.A.J., D. Golenbock, and A.G. Bowie, *The history of Toll-like receptors [mdash] redefining innate immunity*. Nat Rev Immunol, 2013. **13**(6): p. 453-460.
142. Gay, N.J., et al., *Assembly and localization of Toll-like receptor signalling complexes*. Nat Rev Immunol, 2014. **14**(8): p. 546-558.
143. Bell, J.K., et al., *Leucine-rich repeats and pathogen recognition in Toll-like receptors*. Trends in Immunology, 2003. **24**(10): p. 528-533.
144. Hayashi, F., et al., *The innate immune response to bacterial flagellin is mediated by Toll-like receptor 5*. Nature, 2001. **410**(6832): p. 1099-1103.
145. Takeuchi, O., et al., *Discrimination of bacterial lipoproteins by Toll-like receptor 6*. International Immunology, 2001. **13**(7): p. 933-940.
146. Takeuchi, O., et al., *Cutting Edge: Role of Toll-Like Receptor 1 in Mediating Immune Response to Microbial Lipoproteins*. The Journal of Immunology, 2002. **169**(1): p. 10-14.
147. Alexopoulou, L., et al., *Recognition of double-stranded RNA and activation of NF-[kappa]B by Toll-like receptor 3*. Nature, 2001. **413**(6857): p. 732-738.
148. Heil, F., et al., *Species-Specific Recognition of Single-Stranded RNA via Toll-like Receptor 7 and 8*. Science, 2004. **303**(5663): p. 1526-1529.
149. Hemmi, H., et al., *A Toll-like receptor recognizes bacterial DNA*. Nature, 2000. **408**(6813): p. 740-745.
150. Hasan, U., et al., *Human TLR10 Is a Functional Receptor, Expressed by B Cells and Plasmacytoid Dendritic Cells, Which Activates Gene Transcription through MyD88*. The Journal of Immunology, 2005. **174**(5): p. 2942-2950.
151. Ozinsky, A., et al., *The repertoire for pattern recognition of pathogens by the innate immune system is defined by cooperation between Toll-like receptors*. Proceedings of the National Academy of Sciences of the United States of America, 2000. **97**(25): p. 13766-13771.
152. Medzhitov, R., et al., *MyD88 Is an Adaptor Protein in the hToll/IL-1 Receptor Family Signaling Pathways*. Molecular Cell, 1998. **2**(2): p. 253-258.
153. Zhang, F.X., et al., *Bacterial Lipopolysaccharide Activates Nuclear Factor- κ B through Interleukin-1 Signaling Mediators in Cultured Human Dermal Endothelial Cells and*

- Mononuclear Phagocytes*. Journal of Biological Chemistry, 1999. **274**(12): p. 7611-7614.
154. Muzio, M., et al., *The Human Toll Signaling Pathway: Divergence of Nuclear Factor κ B and JNK/SAPK Activation Upstream of Tumor Necrosis Factor Receptor-associated Factor 6 (TRAF6)*. The Journal of Experimental Medicine, 1998. **187**(12): p. 2097-2101.
 155. Ogus, A.C., et al., *The Arg753Gln polymorphism of the human Toll-like receptor 2 gene in tuberculosis disease*. European Respiratory Journal, 2004. **23**(2): p. 219-223.
 156. Kiechl, S., et al., *Toll-like Receptor 4 Polymorphisms and Atherogenesis*. New England Journal of Medicine, 2002. **347**(3): p. 185-192.
 157. Cario, E., *Toll-like receptors in inflammatory bowel diseases: A decade later*. Inflammatory Bowel Diseases, 2010. **16**(9): p. 1583-1597.
 158. Lorenz, E., et al., *RElevance of mutations in the tlr4 receptor in patients with gram-negative septic shock*. Archives of Internal Medicine, 2002. **162**(9): p. 1028-1032.
 159. Agnese D.M., C.J.E., Hahm S.J., Coyle, S.M., Corbett, S.A., Calvano, S.E., Lowry, S.F., *HUMAN Toll-Like Receptor 4 Mutations but Not CD14 Polymorphisms Are Associated with an Increased Risk of Gram-Negative Infections*. The Journal of Infectious Diseases, 2002. **186**: p. 1522-5.
 160. Medzhitov, R., P. Preston-Hurlburt, and C.A. Janeway, *A human homologue of the Drosophila Toll protein signals activation of adaptive immunity*. Nature, 1997. **388**(6640): p. 394-397.
 161. Poltorak, A., et al., *Defective LPS Signaling in C3H/HeJ and C57BL/10ScCr Mice: Mutations in Tlr4 Gene*. Science, 1998. **282**(5396): p. 2085-2088.
 162. Qureshi, S.T., et al., *Endotoxin-tolerant Mice Have Mutations in Toll-like Receptor 4 (Tlr4)*. The Journal of Experimental Medicine, 1999. **189**(4): p. 615-625.
 163. Hoshino, K., et al., *Cutting Edge: Toll-Like Receptor 4 (TLR4)-Deficient Mice Are Hyporesponsive to Lipopolysaccharide: Evidence for TLR4 as the Lps Gene Product*. The Journal of Immunology, 1999. **162**(7): p. 3749-3752.
 164. Shimazu, R., et al., *MD-2, a Molecule that Confers Lipopolysaccharide Responsiveness on Toll-like Receptor 4*. The Journal of Experimental Medicine, 1999. **189**(11): p. 1777-1782.
 165. Park, B.S., et al., *The structural basis of lipopolysaccharide recognition by the TLR4-MD-2 complex*. Nature, 2009. **458**(7242): p. 1191-1195.
 166. Akashi, S., et al., *Lipopolysaccharide Interaction with Cell Surface Toll-like Receptor 4-MD-2: Higher Affinity than That with MD-2 or CD14*. The Journal of Experimental Medicine, 2003. **198**(7): p. 1035-1042.

167. Schumann, R., et al., *Structure and function of lipopolysaccharide binding protein*. Science, 1990. **249**(4975): p. 1429-1431.
168. Martin, T.R., et al., *Lipopolysaccharide binding protein enhances the responsiveness of alveolar macrophages to bacterial lipopolysaccharide. Implications for cytokine production in normal and injured lungs*. Journal of Clinical Investigation, 1992. **90**(6): p. 2209-2219.
169. Li, S., et al., *IRAK-4: A novel member of the IRAK family with the properties of an IRAK-kinase*. Proceedings of the National Academy of Sciences, 2002. **99**(8): p. 5567-5572.
170. Kawagoe, T., et al., *Essential role of IRAK-4 protein and its kinase activity in Toll-like receptor-mediated immune responses but not in TCR signaling*. The Journal of Experimental Medicine, 2007. **204**(5): p. 1013-1024.
171. Fitzgerald, K.A., et al., *Mal (MyD88-adaptor-like) is required for Toll-like receptor-4 signal transduction*. Nature, 2001. **413**(6851): p. 78-83.
172. Cao, Z., et al., *TRAF6 is a signal transducer for interleukin-1*. Nature, 1996. **383**(6599): p. 443-446.
173. Lomaga, M.A., et al., *TRAF6 deficiency results in osteopetrosis and defective interleukin-1, CD40, and LPS signaling*. Genes & Development, 1999. **13**(8): p. 1015-1024.
174. Deng, L., et al., *Activation of the I κ B Kinase Complex by TRAF6 Requires a Dimeric Ubiquitin-Conjugating Enzyme Complex and a Unique Polyubiquitin Chain*. Cell, 2000. **103**(2): p. 351-361.
175. Wang, C., et al., *TAK1 is a ubiquitin-dependent kinase of MKK and IKK*. Nature, 2001. **412**(6844): p. 346-351.
176. Kanayama, A., et al., *TAB2 and TAB3 Activate the NF- κ B Pathway through Binding to Polyubiquitin Chains*. Molecular Cell, 2004. **15**(4): p. 535-548.
177. Singhirunnusorn, P., et al., *Critical Roles of Threonine 187 Phosphorylation in Cellular Stress-induced Rapid and Transient Activation of Transforming Growth Factor- β -activated Kinase 1 (TAK1) in a Signaling Complex Containing TAK1-binding Protein TAB1 and TAB2*. Journal of Biological Chemistry, 2005. **280**(8): p. 7359-7368.
178. Mercurio, F., et al., *IKK-1 and IKK-2: Cytokine-Activated I κ B Kinases Essential for NF- κ B Activation*. Science, 1997. **278**(5339): p. 860-866.
179. Rothwarf, D.M., et al., *IKK- γ is an essential regulatory subunit of the I κ B kinase complex*. Nature, 1998. **395**(6699): p. 297-300.
180. Chen, Z., et al., *Signal-induced site-specific phosphorylation targets I κ B alpha to the ubiquitin-proteasome pathway*. Genes & Development, 1995. **9**(13): p. 1586-1597.
181. DiDonato, J.A., et al., *A cytokine-responsive I κ B kinase that activates the transcription factor NF- κ B*. Nature, 1997. **388**(6642): p. 548-554.

182. Baeuerle, P. and D. Baltimore, *I kappa B: a specific inhibitor of the NF-kappa B transcription factor*. Science, 1988. **242**(4878): p. 540-546.
183. Hayden, M.S. and S. Ghosh, *Shared Principles in NF-κB Signaling*. Cell, 2008. **132**(3): p. 344-362.
184. P A Baeuerle, a. and T. Henkel, *Function and Activation of NF-kappaB in the Immune System*. Annual Review of Immunology, 1994. **12**(1): p. 141-179.
185. Yang, F., et al., *IKKβ Plays an Essential Role in the Phosphorylation of RelA/p65 on Serine 536 Induced by Lipopolysaccharide*. The Journal of Immunology, 2003. **170**(11): p. 5630-5635.
186. Kagan, J.C., et al., *TRAM couples endocytosis of Toll-like receptor 4 to the induction of interferon-[beta]*. Nat Immunol, 2008. **9**(4): p. 361-368.
187. Yamamoto, M., et al., *Role of Adaptor TRIF in the MyD88-Independent Toll-Like Receptor Signaling Pathway*. Science, 2003. **301**(5633): p. 640-643.
188. Hacker, H., et al., *Specificity in Toll-like receptor signalling through distinct effector functions of TRAF3 and TRAF6*. Nature, 2006. **439**(7073): p. 204-207.
189. Tseng, P.-H., et al., *Different modes of ubiquitination of the adaptor TRAF3 selectively activate the expression of type I interferons and proinflammatory cytokines*. Nat Immunol, 2010. **11**(1): p. 70-75.
190. Fitzgerald, K.A., et al., *IKK[epsi] and TBK1 are essential components of the IRF3 signaling pathway*. Nat Immunol, 2003. **4**(5): p. 491-496.
191. Perry, A.K., et al., *Differential Requirement for TANK-binding Kinase-1 in Type I Interferon Responses to Toll-like Receptor Activation and Viral Infection*. The Journal of Experimental Medicine, 2004. **199**(12): p. 1651-1658.
192. Solis, M., et al., *Involvement of TBK1 and IKKε in lipopolysaccharide-induced activation of the interferon response in primary human macrophages*. European Journal of Immunology, 2007. **37**(2): p. 528-539.
193. Sato, S., et al., *Toll/IL-1 Receptor Domain-Containing Adaptor Inducing IFN-β (TRIF) Associates with TNF Receptor-Associated Factor 6 and TANK-Binding Kinase 1, and Activates Two Distinct Transcription Factors, NF-κB and IFN-Regulatory Factor-3, in the Toll-Like Receptor Signaling*. The Journal of Immunology, 2003. **171**(8): p. 4304-4310.
194. Iwami, K.-i., et al., *Cutting Edge: Naturally Occurring Soluble Form of Mouse Toll-Like Receptor 4 Inhibits Lipopolysaccharide Signaling*. The Journal of Immunology, 2000. **165**(12): p. 6682-6686.
195. Mitsuzawa, H., et al., *Recombinant Soluble Forms of Extracellular TLR4 Domain and MD-2 Inhibit Lipopolysaccharide Binding on Cell Surface and Dampen Lipopolysaccharide-Induced Pulmonary Inflammation in Mice*. The Journal of Immunology, 2006. **177**(11): p. 8133-8139.

196. Ohnishi, K., et al., *Suppression of TLR4-mediated inflammatory response by macrophage class A scavenger receptor (CD204)*. *Biochemical and Biophysical Research Communications*, 2011. **411**(3): p. 516-522.
197. Janssens, S., et al., *Regulation of Interleukin-1- and Lipopolysaccharide-Induced NF- κ B Activation by Alternative Splicing of MyD88*. *Current Biology*, 2002. **12**(6): p. 467-471.
198. Burns, K., et al., *Inhibition of Interleukin 1 Receptor/Toll-like Receptor Signaling through the Alternatively Spliced, Short Form of MyD88 Is Due to Its Failure to Recruit IRAK-4*. *The Journal of Experimental Medicine*, 2003. **197**(2): p. 263-268.
199. Kobayashi, K., et al., *IRAK-M Is a Negative Regulator of Toll-like Receptor Signaling*. *Cell*, 2002. **110**(2): p. 191-202.
200. Wertz, I.E., et al., *De-ubiquitination and ubiquitin ligase domains of A20 downregulate NF-[kappa]B signalling*. *Nature*, 2004. **430**(7000): p. 694-699.
201. Boone, D.L., et al., *The ubiquitin-modifying enzyme A20 is required for termination of Toll-like receptor responses*. *Nat Immunol*, 2004. **5**(10): p. 1052-1060.
202. Mauro, C., et al., *ABIN-1 Binds to NEMO/IKK γ and Co-operates with A20 in Inhibiting NF- κ B*. *Journal of Biological Chemistry*, 2006. **281**(27): p. 18482-18488.
203. Werner, S.L., et al., *Encoding NF- κ B temporal control in response to TNF: distinct roles for the negative regulators I κ B α and A20*. *Genes & Development*, 2008. **22**(15): p. 2093-2101.
204. Trompouki, E., et al., *CYLD is a deubiquitinating enzyme that negatively regulates NF-[kappa]B activation by TNFR family members*. *Nature*, 2003. **424**(6950): p. 793-796.
205. Reiley, W., et al., *Regulation of the Deubiquitinating Enzyme CYLD by I κ B Kinase Gamma-Dependent Phosphorylation*. *Molecular and Cellular Biology*, 2005. **25**(10): p. 3886-3895.
206. Sun, S., et al., *NF-kappa B controls expression of inhibitor I kappa B alpha: evidence for an inducible autoregulatory pathway*. *Science*, 1993. **259**(5103): p. 1912-1915.
207. Arenzana-Seisdedos, F., et al., *Nuclear localization of I kappa B alpha promotes active transport of NF-kappa B from the nucleus to the cytoplasm*. *Journal of Cell Science*, 1997. **110**(3): p. 369-378.
208. Turer, E.E., et al., *Homeostatic MyD88-dependent signals cause lethal inflammation in the absence of A20*. *The Journal of Experimental Medicine*, 2008. **205**(2): p. 451-464.
209. Beg, A.A., et al., *Constitutive NF-kappa B activation, enhanced granulopoiesis, and neonatal lethality in I kappa B alpha-deficient mice*. *Genes & Development*, 1995. **9**(22): p. 2736-2746.
210. Balaci, L., et al., *IRAK-M Is Involved in the Pathogenesis of Early-Onset Persistent Asthma*. *American Journal of Human Genetics*, 2007. **80**(6): p. 1103-1114.

211. Ma, A. and B.A. Malynn, *A20: linking a complex regulator of ubiquitylation to immunity and human disease*. Nature reviews. Immunology, 2012. **12**(11): p. 774-785.
212. Sternberg, N. and D. Hamilton, *Bacteriophage P1 site-specific recombination: I. Recombination between loxP sites*. Journal of Molecular Biology, 1981. **150**(4): p. 467-486.
213. Clausen, B.E., et al., *Conditional gene targeting in macrophages and granulocytes using LysMcre mice*. Transgenic Research, 1999. **8**(4): p. 265-277.
214. Petrasek, J., et al., *IL-1 receptor antagonist ameliorates inflammasome-dependent alcoholic steatohepatitis in mice*. The Journal of Clinical Investigation, 2012. **122**(10): p. 3476-3489.
215. Rakoff-Nahoum, S., et al., *Recognition of Commensal Microflora by Toll-Like Receptors Is Required for Intestinal Homeostasis*. Cell, 2004. **118**(2): p. 229-241.
216. Takahashi, N., et al., *RIPK1 ensures intestinal homeostasis by protecting the epithelium against apoptosis*. Nature, 2014. **513**(7516): p. 95-99.
217. Quast, C., et al., *The SILVA ribosomal RNA gene database project: improved data processing and web-based tools*. Nucleic acids research, 2013. **41**(Database issue): p. D590-6.
218. Lowry, O.H., et al., *PROTEIN MEASUREMENT WITH THE FOLIN PHENOL REAGENT*. Journal of Biological Chemistry, 1951. **193**(1): p. 265-275.
219. de Winter, J.C.F., *Using the Student's t-test with extremely small sample sizes*. Practical Assessment, Research & Evaluation, 2013. **18**(10).
220. Klionsky, D.J., et al., *Guidelines for the use and interpretation of assays for monitoring autophagy in higher eukaryotes*. Autophagy, 2008. **4**(2): p. 151-175.
221. Gabrilovich, D.I. and S. Nagaraj, *Myeloid-derived suppressor cells as regulators of the immune system*. Nat Rev Immunol, 2009. **9**(3): p. 162-174.
222. Nakahira, K., et al., *Autophagy proteins regulate innate immune responses by inhibiting the release of mitochondrial DNA mediated by the NALP3 inflammasome*. Nat Immunol, 2011. **12**: p. 222 - 230.
223. Köhler, C., *Allograft inflammatory factor-1/Ionized calcium-binding adapter molecule 1 is specifically expressed by most subpopulations of macrophages and spermatids in testis*. Cell and Tissue Research, 2007. **330**(2): p. 291-302.
224. McCuskey Robert S., M.P.A., *Fine structure and function of Kupffer cells*. Journal of Electron Microscopy Technique, 1990. **14**(3): p. 237-46.
225. Rieger, T., D. Merkler, and S. Günther, *Infection of Type I Interferon Receptor-Deficient Mice with Various Old World Arenaviruses: A Model for Studying Virulence and Host Species Barriers*. PLoS ONE, 2013. **8**(8): p. e72290.
226. Kettenmann, H., et al., *Physiology of Microglia*. Vol. 91. 2011. 461-553.

227. Nakahira, K., et al., *Autophagy proteins regulate innate immune responses by inhibiting the release of mitochondrial DNA mediated by the NALP3 inflammasome*. *Nat Immunol*, 2011. **12**(3): p. 222-230.
228. Ea, H.-K., et al., *Pathogenic Role of Basic Calcium Phosphate Crystals in Destructive Arthropathies*. *PLoS ONE*, 2013. **8**(2): p. e57352.
229. Ishibashi, K., et al., *Atg16L1, an essential factor for canonical autophagy, participates in hormone secretion from PC12 cells independently of autophagic activity*. *Molecular Biology of the Cell*, 2012. **23**(16): p. 3193-3202.
230. Mori, N. and D. Prager, *Transactivation of the interleukin-1alpha promoter by human T-cell leukemia virus type I and type II Tax proteins*. Vol. 87. 1996. 3410-3417.
231. Hiscott, J., et al., *Characterization of a functional NF-kappa B site in the human interleukin 1 beta promoter: evidence for a positive autoregulatory loop*. *Molecular and Cellular Biology*, 1993. **13**(10): p. 6231-6240.
232. Ohmori, Y., S. Fukumoto, and T.A. Hamilton, *Two structurally distinct kappa B sequence motifs cooperatively control LPS-induced KC gene transcription in mouse macrophages*. *The Journal of Immunology*, 1995. **155**(7): p. 3593-600.
233. Sica, A., et al., *The c-rel protooncogene product c-Rel but not NF-kappa B binds to the intronic region of the human interferon-gamma gene at a site related to an interferon-stimulable response element*. *Proceedings of the National Academy of Sciences of the United States of America*, 1992. **89**(5): p. 1740-1744.
234. Sica, A., et al., *Interaction of NF-kB and NFAT with the Interferon-gamma Promoter*. *Journal of Biological Chemistry*, 1997. **272**(48): p. 30412-30420.
235. Zarubin, T. and J. Han, *Activation and signaling of the p38 MAP kinase pathway*. *Cell Res*, 2005. **15**(1): p. 11-18.
236. Miyamoto, S., Maki, M., Schmitt, M.J., Hatanaka, M., Verma, I.M., *Tumor necrosis factor alpha-induced phosphorylation of Ikbalpha is a signal for its degradation but not dissociation from NF-kB*. *Proceedings of the National Academy of Sciences*, 1994. **91**: p. 12740-12744.
237. Baeza-Raja, B. and P. Muñoz-Cánoves, *p38 MAPK-induced Nuclear Factor-kB Activity Is Required for Skeletal Muscle Differentiation: Role of Interleukin-6*. *Molecular Biology of the Cell*, 2004. **15**(4): p. 2013-2026.
238. Jiang, S.-Y., Y.-Y. Zou, and J.-T. Wang, *p38 mitogen-activated protein kinase-induced nuclear factor kappa-light-chain-enhancer of activated B cell activity is required for neuroprotection in retinal ischemia/reperfusion injury*. *Molecular Vision*, 2012. **18**: p. 2096-2106.

239. Fujita, K.-i., et al., *Nrf2-mediated induction of p62 controls Toll-like receptor-4-driven aggresome-like induced structure formation and autophagic degradation*. Proceedings of the National Academy of Sciences, 2011. **108**(4): p. 1427-1432.
240. Inomata, M., et al., *Regulation of Toll-like receptor signaling by NDP52-mediated selective autophagy is normally inactivated by A20*. Cellular and Molecular Life Sciences, 2012. **69**(6): p. 963-979.
241. Kobayashi, M., et al., *Regulatory Roles for MD-2 and TLR4 in Ligand-Induced Receptor Clustering*. The Journal of Immunology, 2006. **176**(10): p. 6211-6218.
242. Harhaj, E.W. and V.M. Dixit, *Deubiquitinases in the regulation of NF- κ B signaling*. Cell Research, 2011. **21**(1): p. 22-39.
243. Li, Y. and M.A. Trush, *Diphenyleneiodonium, an NAD(P)H Oxidase Inhibitor, also Potently Inhibits Mitochondrial Reactive Oxygen Species Production*. Biochemical and Biophysical Research Communications, 1998. **253**(2): p. 295-299.
244. Reikvam, D.H., et al., *Depletion of Murine Intestinal Microbiota: Effects on Gut Mucosa and Epithelial Gene Expression*. PLoS ONE, 2011. **6**(3): p. e17996.
245. Poon, A., et al., *ATG5, autophagy and lung function in asthma*. Autophagy, 2012. **8**(4): p. 694-695.
246. Aita, V.M., et al., *Cloning and Genomic Organization of Beclin 1, a Candidate Tumor Suppressor Gene on Chromosome 17q21*. Genomics, 1999. **59**(1): p. 59-65.
247. Liang, X.H., et al., *Induction of autophagy and inhibition of tumorigenesis by beclin 1*. Nature, 1999. **402**(6762): p. 672-676.
248. Saito, H., et al., *Detailed Deletion Mapping of Chromosome 17q in Ovarian and Breast Cancers: 2-cM Region on 17q21.3 Often and Commonly Deleted in Tumors*. Cancer Research, 1993. **53**(14): p. 3382-3385.
249. Koukourakis, M.I., et al., *Beclin 1 over- and underexpression in colorectal cancer: distinct patterns relate to prognosis and tumour hypoxia*. Br J Cancer, 2010. **103**(8): p. 1209-1214.
250. Granatowicz, A., et al., *An Overview and Update of Chronic Myeloid Leukemia for Primary Care Physicians*. Korean Journal of Family Medicine, 2015. **36**(5): p. 197-202.
251. Kanayama, M., Y.-W. He, and M.L. Shinohara, *The Lung Is Protected from Spontaneous Inflammation by Autophagy in Myeloid Cells*. The Journal of Immunology, 2015. **194**(11): p. 5465-5471.
252. Abdel Fattah, E., et al., *Critical Role for IL-18 in Spontaneous Lung Inflammation Caused by Autophagy Deficiency*. The Journal of Immunology, 2015.
253. Sica, A. and V. Bronte, *Altered macrophage differentiation and immune dysfunction in tumor development*. Journal of Clinical Investigation, 2007. **117**(5): p. 1155-1166.

254. Kusmartsev, S., et al., *Antigen-Specific Inhibition of CD8+ T Cell Response by Immature Myeloid Cells in Cancer Is Mediated by Reactive Oxygen Species*. The Journal of Immunology, 2004. **172**(2): p. 989-999.
255. Bronte, V. and P. Zanovello, *Regulation of immune responses by L-arginine metabolism*. Nat Rev Immunol, 2005. **5**(8): p. 641-654.
256. Youn, J.-I., et al., *Characterization of the nature of granulocytic myeloid-derived suppressor cells in tumor-bearing mice*. Journal of Leukocyte Biology, 2012. **91**(1): p. 167-181.
257. Klebanoff, S.J., *Myeloperoxidase: friend and foe*. Journal of Leukocyte Biology, 2005. **77**(5): p. 598-625.
258. Elkabets, M., et al., *IL-1 β regulates a novel myeloid-derived suppressor cell subset that impairs NK cell development and function*. European Journal of Immunology, 2010. **40**(12): p. 3347-3357.
259. Sinha, P., et al., *Proinflammatory S100 Proteins Regulate the Accumulation of Myeloid-Derived Suppressor Cells*. The Journal of Immunology, 2008. **181**(7): p. 4666-4675.
260. Rutkowski, Melanie R., et al., *Microbially Driven TLR5-Dependent Signaling Governs Distal Malignant Progression through Tumor-Promoting Inflammation*. Cancer Cell, 2015. **27**(1): p. 27-40.
261. Subramani, S. and V. Malhotra, *Non-autophagic roles of autophagy-related proteins*. EMBO reports, 2013. **14**(2): p. 143-151.
262. Arora, M., et al., *TLR4/MyD88-induced CD11b+Gr-1intF4/80+ non-migratory myeloid cells suppress Th2 effector function in the lung*. Mucosal Immunol, 2010. **3**(6): p. 578-593.
263. Rieber, N., et al., *Flagellin Induces Myeloid-Derived Suppressor Cells: Implications for Pseudomonas aeruginosa Infection in Cystic Fibrosis Lung Disease*. The Journal of Immunology, 2013. **190**(3): p. 1276-1284.
264. Kirkham B, K.A., Plevy SE, Barker J, *The Handbook of Biological Therapy*. 2008: p. 89.
265. de Luca, A., et al., *IL-1 receptor blockade restores autophagy and reduces inflammation in chronic granulomatous disease in mice and in humans*. Proceedings of the National Academy of Sciences, 2014. **111**(9): p. 3526-3531.
266. Dinarello, C.A., *Interleukin-1 β , Interleukin-18, and the Interleukin-1 β Converting Enzyme*. Annals of the New York Academy of Sciences, 1998. **856**(1): p. 1-11.
267. Franchi, L., et al., *The inflammasome: a caspase-1-activation platform that regulates immune responses and disease pathogenesis*. Nat Immunol, 2009. **10**(3): p. 241-247.
268. Akira, S. and K. Takeda, *Toll-like receptor signalling*. Nat Rev Immunol, 2004. **4**(7): p. 499-511.

269. Inaba, K., et al., *Generation of large numbers of dendritic cells from mouse bone marrow cultures supplemented with granulocyte/macrophage colony-stimulating factor*. The Journal of Experimental Medicine, 1992. **176**(6): p. 1693-1702.
270. Arend, W.P., G. Palmer, and C. Gabay, *IL-1, IL-18, and IL-33 families of cytokines*. Immunological Reviews, 2008. **223**(1): p. 20-38.
271. Latz, E., T.S. Xiao, and A. Stutz, *Activation and regulation of the inflammasomes*. Nat Rev Immunol, 2013. **13**(6): p. 397-411.
272. Lee, J.-K., et al., *Differences in signaling pathways by IL-1 β and IL-18*. Proceedings of the National Academy of Sciences of the United States of America, 2004. **101**(23): p. 8815-8820.
273. Jin, W., et al., *Deubiquitinating Enzyme CYLD Regulates the Peripheral Development and Naive Phenotype Maintenance of B Cells*. Journal of Biological Chemistry, 2007. **282**(21): p. 15884-15893.
274. Lee, E.G., et al., *Failure to Regulate TNF-Induced NF- κ B and Cell Death Responses in A20-Deficient Mice*. Science, 2000. **289**(5488): p. 2350-2354.
275. Round, J.L. and S.K. Mazmanian, *The gut microbiota shapes intestinal immune responses during health and disease*. Nat Rev Immunol, 2009. **9**(5): p. 313-323.
276. Pahl, H., *Activators and target genes of Rel/NF- κ B transcription factors*. Oncogene, 1999. **18**: p. 6853-6866.
277. Savva, A., et al., *Association of autophagy-related 16-like 1 (ATG16L1) gene polymorphism with sepsis severity in patients with sepsis and ventilator-associated pneumonia*. European Journal of Clinical Microbiology & Infectious Diseases, 2014. **33**(9): p. 1609-1614.
278. Hsieh, C., et al., *Complete induction of autophagy is essential for cardioprotection in sepsis*. Ann Surg, 2011. **253**: p. 1190 - 1200.
279. Takahashi, W., et al., *Kinetics and protective role of autophagy in a mouse cecal ligation and puncture-induced sepsis*. Critical Care, 2013. **17**(4): p. R160.
280. Wathélet, M.G., et al., *Virus Infection Induces the Assembly of Coordinately Activated Transcription Factors on the IFN- β Enhancer In Vivo*. Molecular Cell, 1998. **1**(4): p. 507-518.
281. Sato, M., et al., *Distinct and Essential Roles of Transcription Factors IRF-3 and IRF-7 in Response to Viruses for IFN- α/β Gene Induction*. Immunity, 2000. **13**(4): p. 539-548.
282. Yamamoto, M., et al., *Cutting Edge: A Novel Toll/IL-1 Receptor Domain-Containing Adapter That Preferentially Activates the IFN- β Promoter in the Toll-Like Receptor Signaling*. The Journal of Immunology, 2002. **169**(12): p. 6668-6672.

283. Tanimura, N., et al., *Roles for LPS-dependent interaction and relocation of TLR4 and TRAM in TRIF-signaling*. Biochemical and Biophysical Research Communications, 2008. **368**(1): p. 94-99.
284. Oganessian, G., et al., *Critical role of TRAF3 in the Toll-like receptor-dependent and -independent antiviral response*. Nature, 2006. **439**(7073): p. 208-211.
285. Kawai, T., et al., *Unresponsiveness of MyD88-Deficient Mice to Endotoxin*. Immunity, 1999. **11**(1): p. 115-122.
286. Janssens, S. and R. Beyaert, *A universal role for MyD88 in TLR/IL-1R-mediated signaling*. Trends in Biochemical Sciences, 2002. **27**(9): p. 474-482.
287. Oeckinghaus, A., M.S. Hayden, and S. Ghosh, *Crosstalk in NF- κ B signaling pathways*. Nat Immunol, 2011. **12**(8): p. 695-708.
288. Olson, C.M., et al., *p38 Mitogen-Activated Protein Kinase Controls NF- κ B Transcriptional Activation and Tumor Necrosis Factor Alpha Production through RelA Phosphorylation Mediated by Mitogen- and Stress-Activated Protein Kinase 1 in Response to Borrelia burgdorferi Antigens*. Infection and Immunity, 2007. **75**(1): p. 270-277.
289. Reber, L., et al., *Ser276 Phosphorylation of NF- κ B p65 by MSK1 Controls SCF Expression in Inflammation*. PLoS ONE, 2009. **4**(2): p. e4393.
290. Gorska, M.M., et al., *MK2 controls the level of negative feedback in the NF- κ B pathway and is essential for vascular permeability and airway inflammation*. The Journal of Experimental Medicine, 2007. **204**(7): p. 1637-1652.
291. Frevel, M.A.E., et al., *p38 Mitogen-Activated Protein Kinase-Dependent and -Independent Signaling of mRNA Stability of AU-Rich Element-Containing Transcripts*. Molecular and Cellular Biology, 2003. **23**(2): p. 425-436.
292. Biswas, R., et al., *Regulation of Chemokine mRNA Stability by Lipopolysaccharide and IL-10*. The Journal of Immunology, 2003. **170**(12): p. 6202-6208.
293. Bihl, F., et al., *Overexpression of Toll-Like Receptor 4 Amplifies the Host Response to Lipopolysaccharide and Provides a Survival Advantage in Transgenic Mice*. The Journal of Immunology, 2003. **170**(12): p. 6141-6150.
294. Yu, X., et al., *Pattern Recognition Scavenger Receptor CD204 Attenuates Toll-like Receptor 4-induced NF- κ B Activation by Directly Inhibiting Ubiquitination of Tumor Necrosis Factor (TNF) Receptor-associated Factor 6*. Journal of Biological Chemistry, 2011. **286**(21): p. 18795-18806.
295. Cusson-Hermance, N., et al., *Rip1 Mediates the Trif-dependent Toll-like Receptor 3- and 4-induced NF- κ B Activation but Does Not Contribute to Interferon Regulatory Factor 3 Activation*. Journal of Biological Chemistry, 2005. **280**(44): p. 36560-36566.
296. Xu, Y., et al., *Toll-like Receptor 4 Is a Sensor for Autophagy Associated with Innate Immunity*. Immunity, 2007. **27**(1): p. 135-144.

297. Bjørkøy, G., et al., *p62/SQSTM1 forms protein aggregates degraded by autophagy and has a protective effect on huntingtin-induced cell death*. The Journal of Cell Biology, 2005. **171**(4): p. 603-614.
298. Liu, S. and Z.J. Chen, *Expanding role of ubiquitination in NF- κ B signaling*. Cell Res, 2011. **21**(1): p. 6-21.
299. Zotti, T., et al., *TRAF6-mediated ubiquitination of NEMO requires p62/sequestosome-1*. Molecular Immunology, 2014. **58**(1): p. 27-31.
300. Sanz, L., et al., *The interaction of p62 with RIP links the atypical PKCs to NF- κ B activation*. The EMBO Journal, 1999. **18**(11): p. 3044-3053.
301. Moscat, J., M.T. Diaz-Meco, and M.W. Wooten, *Signal integration and diversification through the p62 scaffold protein*. Trends in Biochemical Sciences, 2007. **32**(2): p. 95-100.
302. Sanchez, P., et al., *Localization of Atypical Protein Kinase C Isoforms into Lysosome-Targeted Endosomes through Interaction with p62*. Molecular and Cellular Biology, 1998. **18**(5): p. 3069-3080.
303. Sanz, L., et al., *The atypical PKC-interacting protein p62 channels NF- κ B activation by the IL-1-TRAF6 pathway*. Vol. 19. 2000. 1576-1586.
304. Long, J., et al., *Dimerisation of the UBA Domain of p62 Inhibits Ubiquitin Binding and Regulates NF- κ B Signalling*. Journal of Molecular Biology, 2010. **396**(1): p. 178-194.
305. Huang, X., et al., *An Atypical Protein Kinase C (PKC ζ) Plays a Critical Role in Lipopolysaccharide-Activated NF- κ B in Human Peripheral Blood Monocytes and Macrophages*. The Journal of Immunology, 2009. **182**(9): p. 5810-5815.
306. Yang, Y., et al., *A Cytosolic ATM/NEMO/RIP1 Complex Recruits TAK1 To Mediate the NF- κ B and p38 Mitogen-Activated Protein Kinase (MAPK)/MAPK-Activated Protein 2 Responses to DNA Damage*. Molecular and Cellular Biology, 2011. **31**(14): p. 2774-2786.
307. Ninomiya-Tsuji, J., et al., *The kinase TAK1 can activate the NIK-I κ B as well as the MAP kinase cascade in the IL-1 signalling pathway*. Nature, 1999. **398**(6724): p. 252-256.
308. Cesta, M.F., *Normal Structure, Function, and Histology of the Spleen*. Toxicologic Pathology, 2006. **34**(5): p. 455-465.
309. Takamura, A., et al., *Autophagy-deficient mice develop multiple liver tumors*. Genes & Development, 2011. **25**(8): p. 795-800.
310. Traver, M.K., et al., *Immunity-related GTPase M (IRGM) Proteins Influence the Localization of Guanylate-binding Protein 2 (GBP2) by Modulating Macroautophagy*. Journal of Biological Chemistry, 2011. **286**(35): p. 30471-30480.

311. Nezis, I.P., et al., *Ref(2)P, the Drosophila melanogaster homologue of mammalian p62, is required for the formation of protein aggregates in adult brain*. The Journal of Cell Biology, 2008. **180**(6): p. 1065-1071.
312. Durán, A., et al., *The Atypical PKC-Interacting Protein p62 Is an Important Mediator of RANK-Activated Osteoclastogenesis*. Developmental Cell, 2004. **6**(2): p. 303-309.
313. Park, S., et al., *p62/SQSTM1 Enhances NOD2-Mediated Signaling and Cytokine Production through Stabilizing NOD2 Oligomerization*. PLoS ONE, 2013. **8**(2): p. e57138.
314. Till, A., et al., *Autophagy receptor CALCOCO2/NDP52 takes center stage in Crohn disease*. Autophagy, 2013. **9**(8): p. 1256-1257.
315. Ellinghaus, D., et al., *Association Between Variants of PRDM1 and NDP52 and Crohn's Disease, Based on Exome Sequencing and Functional Studies*. Gastroenterology, 2013. **145**(2): p. 339-347.
316. Gal, J., et al., *p62 Accumulates and Enhances Aggregate Formation in Model Systems of Familial Amyotrophic Lateral Sclerosis*. Journal of Biological Chemistry, 2007. **282**(15): p. 11068-11077.
317. Wei, H., et al., *p62/SQSTM1 synergizes with autophagy for tumor growth in vivo*. Genes & Development, 2014. **28**(11): p. 1204-1216.
318. Duran, A., et al., *The Signaling Adaptor p62 Is an Important NF- κ B Mediator in Tumorigenesis*. Cancer Cell, 2008. **13**(4): p. 343-354.
319. Yoshimori, T., et al., *Bafilomycin A1, a specific inhibitor of vacuolar-type H(+)-ATPase, inhibits acidification and protein degradation in lysosomes of cultured cells*. Journal of Biological Chemistry, 1991. **266**(26): p. 17707-17712.
320. Massoumi, R., et al., *Cyld Inhibits Tumor Cell Proliferation by Blocking Bcl-3-Dependent NF- κ B Signaling*. Cell, 2006. **125**(4): p. 665-677.
321. Brummelkamp, T.R., et al., *Loss of the cylindromatosis tumour suppressor inhibits apoptosis by activating NF- κ B*. Nature, 2003. **424**(6950): p. 797-801.
322. De, A., et al., *The deubiquitinase activity of A20 is dispensable for NF- κ B signaling*. EMBO reports, 2014. **15**(7): p. 775-783.
323. Enesa, K., et al., *A20 suppresses vascular inflammation by recruiting proinflammatory signaling molecules to intracellular aggresomes*. The FASEB Journal, 2015. **29**(5): p. 1869-1878.
324. Shembade, N., A. Ma, and E.W. Harhaj, *Inhibition of NF- κ B Signaling by A20 Through Disruption of Ubiquitin Enzyme Complexes*. Science, 2010. **327**(5969): p. 1135-1139.
325. Skaug, B., et al., *Direct, Noncatalytic Mechanism of IKK Inhibition by A20*. Molecular Cell, 2011. **44**(4): p. 559-571.

326. Li, L., et al., *Localization of A20 to a lysosome-associated compartment and its role in NF κ B signaling*. *Biochimica et Biophysica Acta (BBA) - Molecular Cell Research*, 2008. **1783**(6): p. 1140-1149.
327. Li, L., et al., *The zinc finger protein A20 targets TRAF2 to the lysosomes for degradation*. *Biochimica et Biophysica Acta (BBA) - Molecular Cell Research*, 2009. **1793**(2): p. 346-353.
328. Bosanac, I., et al., *Ubiquitin Binding to A20 ZnF4 Is Required for Modulation of NF- κ B Signaling*. *Molecular Cell*, 2010. **40**(4): p. 548-557.
329. Tokunaga, F., et al., *Specific recognition of linear polyubiquitin by A20 zinc finger 7 is involved in NF- κ B regulation*. *The EMBO Journal*, 2012. **31**(19): p. 3856-3870.
330. Chamoux, E., et al., *The p62 P392L Mutation Linked to Paget's Disease Induces Activation of Human Osteoclasts*. *Molecular Endocrinology*, 2009. **23**(10): p. 1668-1680.
331. Matmati, M., et al., *A20 (TNFAIP3) deficiency in myeloid cells triggers erosive polyarthritis resembling rheumatoid arthritis*. *Nat Genet*, 2011. **43**(9): p. 908-912.

10 SUPPLEMENTS

10.1 LIST OF ABBREVIATIONS

(RT)-PCR	Reverse transcription PCR
ABx	antibiotics
ALS	amyotrophic lateral sclerosis
AP-1	activator protein-1
aPKC	atypical protein kinase C
APS	ammonium persulfate
ARE	AU-rich elements
ASC	pyrin domain of apoptosis-associated speck-like protein containing a CARD
ATG	autophagy-related
ATG16L1	autophagy-related protein 16 like 1 (<i>S. cerevisiae</i>)
AU	adenylate/uridylate
BafA	Bafilomycin A
BMDMs	bone marrow-derived macrophages
BrefA	Brefeldin A
BSA	bovine serum albumin
c	corona
CD	cluster of differentiation
CD95L	anti-CD95 ligand
cDNA	complementary DNA
CHX	cycloheximide
c-Kit	proto-oncogene c-Kit
CLP	common lymphoid progenitor
CMF	common myeloid progenitor
Ct	cycle threshold
CXCL1	(C-X-C motif) ligand 1
CYLD	cylindromatosis (turban tumor syndrome)
DAB	3,3'-Diaminobenzidine
DC	dendritic cell
DLB	denaturing lysis buffer
DNA	deoxyribonucleic acid
dNTPs	deoxynucleotide triphosphates
DPI	diphenyleneiodonium

DSS	dextran sodium sulfate
DTT	dithiothreitol
DUB	deubiquitinase enzyme
EDTA	ethylenediaminetetraacetic acid
ELISA	enzyme linked immunosorbent assay
ER	endoplasmic reticulum
ERK	extracellular signal-regulated protein kinase
FACS	fluorescence-activated cell sorting
FIP200	focal adhesion kinase-interacting protein of 200 kDa
FITC	Fluorescein isothiocyanate
for	forward
FSC	forward scatter
FSL-1	synthetic diacylated lipoprotein (Pam2CGDPKHPKSF)
FWB	FACS washing buffer
gc	germinal center
G-CSF	granulocyte-colony stimulating factor
GM-CSF	granulocyte-macrophage stimulating factor
H&E	hematoxylin and eosin
HKLM	heat-killed <i>Listeria monocytogenes</i>
HRP	horseradish peroxidase
Hsc70	heat shock-cognate protein of 70 kDa
HSCs	hematopoietic stem cells
IBA-1	ionized calcium-binding adapter molecule 1
IECs	intestinal epithelial cells
IFN	interferon
IKKα/β/γ	I κ B kinase α / β / γ
IL	interleukin
IL1R	interleukin-1 receptor
IL1Ra	interleukin-1 receptor antagonist
iNOS	inducible nitric oxide synthase
ip38	p38 activity inhibitor SB202190
IRAK1/2/4	interleukin 1 receptor-associated kinase 1/2/4
IRF3/7	interferon-regulatory transcription factor 3/7
IVCs	individual ventilated cages
IκB	inhibitor of nuclear factor of kappa light polypeptide gene enhancer in B-cells

JNK	c-Jun N-terminal kinase
LAMP-2A	lysosome-associated membrane protein type 2A
LBP	LPS-binding protein
LC3	microtubule-associated protein 1 light chain 3
lin⁻	lineage negative
LIR	LC3 interacting region
LPS	lipopolysaccharide
LRR	leucine-rich repeat
LysM	LysMcre
Lyz2	lysozyme 2
MACS	magnetic-activated cell sorting
MAPK	mitogen-activated protein kinase
MAPKAP2/MK2	MAP kinase-activated protein kinase 2
MCP1	monocyte chemotactic protein 1
mCSF	macrophage colony-stimulating factor
MD2	myeloid differentiation factor 2
MDP	muramyl dipeptide
MDSCs	myeloid derived-suppressor cells
MEFs	murine embryonic fibroblasts
MHC	major histocompatibility complex
MIP1α	macrophage inflammatory protein 1 alpha
MIP1β	macrophage inflammatory protein 1 beta
MKK3/6	MAPK kinase 3/6
MLNs	mesenteric lymph nodes
MPO	myeloperoxidase
mRNA	messenger Ribonucleic acid
MSR1	macrophage scavenger receptor 1
mTORC1	mammalian target of rapamycin complex 1
MyD88	myeloid differentiation primary-response protein 88
MyD88s	spliced MyD88
NaCl	sodium chloride
NADPH	nicotinamide adenine dinucleotide phosphate
NBR1	neighbor of BRCA1 gene 1 protein
NDP52	nuclear dot protein 52 kDa
NETs	neutrophil extracellular traps
NFE2L2	nuclear factor (erythroid-derived 2)-like 2

NF-κB	nuclear factor 'kappa-light-chain-enhancer' of activated B-cells
NK cell	natural killer cell
NLRP3	NOD-like receptor family, Pyrin domain containing 3
NO	nitric oxide
OTU domain	ovarian tumor domain
Pam₃	Pam3CSK4, synthetic triacylated lipopeptide
PAMP	pathogen-associated molecular pattern
PBS	phosphate-buffered saline
PCR	polymerase-chain reaction
PI3P	phosphatidylinositol 3-kinase
Poly I:C	polyinosinic:polycytidylic acid
pp	Peyer's patches
pro-Casp1	pro-Caspase-1
PRR	pattern recognition receptor
PVDF	polyvinylidene difluoride
qPCR	quantitative real-time PCR
RANK	receptor activator of nuclear factor κ B
RANTES	regulated on activation, normal T cell expressed and secreted
rev	reverse
RIP1	receptor-interacting serine/threonine-protein kinase 1
RNA	ribonucleic acid
ROS	reactive oxygen species
S.D.	standard deviation
S100A8	S100 calcium binding protein A8
S100A9	S100 calcium binding protein A9
Sca-1	stem cell antigen-1
SNP	single-nucleotide polymorphism
SPF	specific-pathogen-free
SQSTM1/p62	sequestosome-1
SSC	sideward scatter
ssRNA	single-stranded RNA
TAB1/2/3	TAK1 binding protein 1/2/3
TAE	Tris-acetate
TAK1	transforming growth factor β -activated kinase 1
TANK	TRAF-associated NF- κ B activator
TBK1	TANK-binding kinase-1

TBS	Tris-buffered saline
TEMED	<i>N,N,N',N'</i> -Tetramethylethane-1,2-diamine
temp	temperature
TGS	Tris/Glycine/SDS
TIR domain	Toll-IL1 receptor domain
TIRAP/Mal	TIR domain-containing adaptor protein
TLR	Toll-like receptor
TNFAIP3/A20	TNF α -induced protein 3
TNFα	tumor necrosis factor alpha
TRAF3/6	TNF receptor-associated factor 3/6
TRAM	TRIF-related adaptor molecule
TRIF	TIR-domain-containing adapter-inducing interferon- β
TTBS	TBS supplemented with 0.1 % (v/v) Tween 20
TUNEL	terminal deoxynucleotidyl transferase dUTP nick end labeling
UBD	ubiquitin-binding domain
ULK1/2	UNC51-like kinase 1/2
VPS15/34	vacuolar protein sorting 15/34
WD	tryptophan-aspartic acid
WIPI2b	WD-repeat phosphatidylinositol 3-phosphate effector protein 2b

10.2 LIST OF FIGURES

Figure 1-1: Schematic depiction of main types of autophagy (modified from [3])	9
Figure 1-2: Ubiquitin-like conjugation systems involved in autophagosome biogenesis (modified from [11])	11
Figure 1-3: Schematic steps of leukocyte differentiation (modified from [97, 98])	18
Figure 1-4: Mammalian Toll-like receptor (TLR) signaling [140]	22
Figure 3-1: Targeting strategy for the conditional <i>Atg16l1</i> mouse line	28
Figure 3-2: Agarose gel electrophoresis of genotyping PCRs for <i>Atg16l1^{fl/fl}</i> and <i>Atg16l1LysM</i>	29
Figure 4-1: Tissue-specific knock-out of ATG16L1 in CD11b ⁺ myeloid cells	47
Figure 4-2: CD11b expression on <i>ex vivo</i> differentiated BMDMs of <i>Atg16l1^{fl/fl}</i> and <i>Atg16l1LysM</i> mice	48
Figure 4-3: Successful knock-out of <i>Atg16l1</i> in <i>Atg16l1LysM</i> BMDMs	48
Figure 4-4: Impaired autophagy in <i>Atg16l1LysM</i> BMDMs	49
Figure 4-5: Basal phenotype of hematopoietic organs of the <i>Atg16l1LysM</i> mouse model	50
Figure 4-6: Basal phenotype of the gastrointestinal tract in the <i>Atg16l1LysM</i> mice	51
Figure 4-7: Spontaneous immune cell infiltration in various tissues of <i>Atg16l1LysM</i> mice	52
Figure 4-8: Increased number of hematopoietic stem cells in the spleen of <i>Atg16l1LysM</i> mice	53
Figure 4-9: Equal numbers of apoptotic TUNEL ⁺ cells in the spleen of <i>Atg16l1^{fl/fl}</i> and <i>Atg16l1LysM</i> mice	54
Figure 4-10: Intact hematopoiesis in Bone marrow of <i>Atg16l1LysM</i> mice	54
Figure 4-11: Gating strategy of immune cell populations in the spleen of <i>Atg16l1LysM</i> mice	55
Figure 4-12: Altered immune cell composition in the spleen of <i>Atg16l1LysM</i> mice	56
Figure 4-13: Changed expression of cell type-specific markers in the spleen of <i>Atg16l1LysM</i> mice	56
Figure 4-14: Increased number of activated myeloid cells but not T cells in <i>Atg16l1LysM</i> spleen	57
Figure 4-15: Identification of MDSC attributes in the spleen of <i>Atg16l1LysM</i> mice	58
Figure 4-16: Altered expression of myeloid- and T cell-specific cytokines and chemokines in the spleen of <i>Atg16l1LysM</i> mice	59
Figure 4-17: No bacterial invasion in the spleen of <i>Atg16l1LysM</i> mice	59
Figure 4-18: Pro-IL1 β but not TLR4 signaling molecules accumulate in the spleen of <i>Atg16l1LysM</i> mice	60
Figure 4-19: Unaltered expression on NLRP3 inflammasome components in <i>Atg16l1LysM</i> spleens	61
Figure 4-20: Increased number of MPO ⁺ cells in MLN, liver and lung of <i>Atg16l1LysM</i> mice	62

Figure 4-21: Elevated infiltration of IBA-1 ⁺ macrophages in MLN, liver and lung of <i>Atg16l1LysM</i> mice.....	63
Figure 4-22: Proportion of leukocytes in the blood of <i>Atg16l1LysM</i> mice.....	64
Figure 4-23: Increased cytokine and chemokine levels in the serum of <i>Atg16l1LysM</i> mice.....	65
Figure 4-24: Body and organ weight of <i>Atg16l1^{fl/fl}</i> and <i>Atg16l1LysM</i> mice after Anakinra therapy.....	66
Figure 4-25: Histological analysis of the splenic morphology in <i>Atg16l1LysM</i> mice after Anakinra treatment.....	66
Figure 4-26: Inhibition of IL1R signaling did not rescue the altered leukocyte composition in the spleen of <i>Atg16l1LysM</i> mice.....	67
Figure 4-27: Anakinra treatment did not alter differences in cytokine expression of <i>Atg16l1^{fl/fl}</i> and <i>Atg16l1LysM</i> mice.....	68
Figure 4-28: Unaltered cytokine concentrations in the serum after Anakinra treatment.....	68
Figure 4-29: Increased CXCL1 secretion in <i>Atg16l1LysM</i> BMDMs upon TLR4 stimulation.....	69
Figure 4-30: TLR4-mediated hyper-secretion of cytokines and chemokines in <i>Atg16l1LysM</i> BMDMs.....	70
Figure 4-31: <i>Atg16l1</i> -deficiency leads to an altered gene expression of cytokines and chemokines after LPS stimulation.....	71
Figure 4-32: Increased and prolonged phosphorylation of canonical p65 and p38 MAPK signaling in <i>Atg16l1LysM</i> macrophages upon LPS stimulation.....	72
Figure 4-33: Constitutive activation of p65 occurred independent of p38 MAPK activity.....	73
Figure 4-34: Protein levels of TLR4 signaling molecules in absence and presence of LPS.....	74
Figure 4-35: <i>In vitro</i> and <i>in vivo</i> aggregates of p62 in <i>Atg16l1</i> -deficient macrophages.....	75
Figure 4-36: Intact pinocytosis in <i>Atg16l1</i> -deficient BMDMs.....	76
Figure 4-37: Similar internalization capacity of CD95 on <i>Atg16l1^{fl/fl}</i> and <i>Atg16l1LysM</i> BMDMs.....	77
Figure 4-38: Equal expression of LPS-binding receptors in <i>Atg16l1^{fl/fl}</i> and <i>Atg16l1LysM</i> BMDMs.....	77
Figure 4-39: <i>Atg16l1</i> deficiency affects A20 but not CYLD levels.....	78
Figure 4-40: Similar mRNA expression of A20 upon LPS stimulation in <i>Atg16l1LysM</i> and <i>Atg16l1^{fl/fl}</i> macrophages.....	79
Figure 4-41: Inhibition of lysosomal degradation during LPS stimulation leads to A20 accumulation.....	79
Figure 4-42: <i>Atg16l1</i> deficiency does not alter mitochondrial membrane potential and ROS production in macrophages.....	80
Figure 4-43: Inhibition of LPS-induced production of reactive oxygen species in BMDMs.....	80

Figure 4-44: Inhibition of reactive oxygen species ameliorates the LPS-mediated phenotype in <i>Atg16l1LysM</i> BMDMs.....	81
Figure 4-45: Inhibition of IL1R signaling does not affect LPS-induced NF- κ B activation	82
Figure 4-46: Survival curve during sublethal endotoxin shock.....	83
Figure 4-47: Organ weight after 72 hours of an endotoxin-induced septic shock	83
Figure 4-48: Cytokine and chemokine levels during endotoxin-induced sepsis.....	84
Figure 4-49: Body weight loss during antibiotic treatment.....	85
Figure 4-50: Successful microbial depletion in the feces of antibiotic-treated mice.....	85
Figure 4-51: Spleen and caecum weight after Antibiotic treatment	86
Figure 4-52: Cytokine levels in serum of antibiotic-treated <i>Atg16l1LysM</i> and <i>Atg16l1^{f/f}</i> mice	86
Figure 4-53: Expression of cell type specific markers in the spleen after antibiotic treatment	87
Figure 4-54: Microbial depletion results in reduced numbers of splenic MPO ⁺ cells in <i>Atg16l1LysM</i> mice.....	88
Figure 4-55: Organ weight and length after preventive antibiotic treatment.....	89
Figure 4-56: Splenic cell composition after preventive antibiotic treatment.....	89
Figure 4-57: Activation status of splenic immune cells after preventive antibiotic treatment.....	90
Figure 4-58: Attenuated expression of MDSC-associated genes in the spleen of <i>Atg16l1LysM</i> mice after preventive antibiotic treatment.....	91
Figure 5-1: Proposed mechanism for the impact of the commensal microbiota on the manifestation of the <i>Atg16l1LysM</i> phenotype	95
Figure 5-2: Suggested effect of p62 aggregates on NF- κ B signaling stabilization in <i>Atg16l1</i> -deficient BMDMs.....	103

10.3 LIST OF TABLES

Table 1: Primer sequences for genotyping of <i>Atg16l1^{fl/fl}</i> and <i>Atg16l1ΔMφ</i> mice	28
Table 2: PCR programs for genotyping of <i>Atg16l1^{fl/fl}</i> and <i>Atg16l1ΔMφ</i> mice.....	29
Table 3: PCR Program for the amplification of the variable regions V3 and V4 of the <i>16S rRNA</i> gene	32
Table 4: Composition of stacking and separation gel for protein separation by SDS-PAGE	35
Table 5: List of primary antibodies used for immunoblotting.....	36
Table 6: List of horseradish peroxidase (HRP)-conjugated secondary antibodies used for immunoblotting.....	37
Table 7: Pipetting scheme for standard PCR reaction	38
Table 8: List of primers used for the semi-quantitative end-point PCR	38
Table 9: Standard PCR program Table 10: Touchdown PCR program	39
Table 11: List of primers used for the quantitative real-time PCR	39
Table 12: List of TaqMan Assays used for quantitative real-time PCR.....	40
Table 13: Designed TaqMan Assay used for eukaryotic bacterial DNA quantification by quantitative real-time PCR.....	40
Table 14: List of antibodies used for immunohistochemistry	42
Table 15: List of antibody pairs used for enzyme linked immunosorbent assays.....	43
Table 16: List of used fluorochrome-labeled antibodies for flow cytometry analysis.....	44
Table 17: List of isotype controls used for flow cytometry analysis	44
Table 18: List of unconjugated antibodies and isotype controls for flow cytometry analysis .	45
Table 19: List of secondary antibodies for flow cytometry analysis	45
Table 20: Number of mice of various genotypes obtained by the <i>ATG16L1^{fl/LysM}</i> intercross	50
Table 21: List of used Buffers and appropriate composition	114
Table 22: List of used media.....	115
Table 23: List of used kits.....	115
Table 24: List of used reagents for animal experiments	116
Table 25: List of used reagents	117
Table 26: List of used devices.....	120
Table 27: List of used consumables	121

10.4 ACKNOWLEDGEMENT

First of all, I would like to express my sincere appreciation to my principal supervisor, Prof. Dr. Philip Rosenstiel, for his continuous support of me and my studies, for his generous guidance and confidence, for his immense expertise and for his motivation. It was a great pleasure to work with you.

I would also like to thank Prof. Dr. Thomas Roeder for his interest in my studies and for kindly taking over the co-referat.

I am truly grateful to Dr. Maren Falk-Paulsen and Dr. Jan Kuiper for their unwavering support and their infectious enthusiasm. Thank you for all the innumerable discussions and precious advices and for instilling me the qualities of being a good scientist.

I would like to acknowledge Dr. Ateequr Rehman and Dr. Robert Häsler for their help with the microbiota analysis and the heat-map generation, respectively.

Thanks also go to the CRC877 “Proteolysis as a Regulatory Event in Pathophysiology” as well as the associated Integrated Research School who supported me and my project financially.

I would like to thank the colleagues of the animal facilities “Zentrale Tierhaltung” and “Tierhaus 1” for an excellent cooperation, for taking care of the mice and their support which enabled the experiments of this thesis.

I would like to express my heartfelt gratitude to our technicians Tanja, Katha, Sabine, Maren, Dorina, Tatjana, Karina, Manuela and Dina. This work would not have been successful without your profound knowledge, dedication and help. I would also like to take the opportunity to acknowledge all my colleagues past and present of the lab, especially Marlene, Helene, Steffi, Frauke, Matthias, Simone, Konrad and Anna for their help and valuable suggestions, for their understanding ears and their moral support which made my work during the last years much more enjoyable.

Last but not least, my deepest appreciation belongs to my family and my husband for their unconditional love, patience and understanding. Thank you for everything.

10.5 CURRICULUM VITAE

PERSONAL DATA

First and last name: Anne Luzius
Maiden name: Fischer
Date of birth: 25.12.1986
Place of birth: Berlin
Nationality: German
Contact: anne.luzius@web.de

RESEARCH EXPERIENCE

- 09/2011 – now **PhD student** at the Christian-Albrechts-University Kiel, Germany
Institute of Clinical Molecular Biology
Leading scientist: Prof. Dr. Philip Rosenstiel
Title: “Immunoregulatory function for the autophagy protein ATG16L1 in myeloid cells”
- 03/2011 – 09/2011 **Master thesis** at the Christian-Albrechts-University Kiel, Germany
Institute of Immunology
Leading scientist: Prof. Dr. Dieter Adam
Title: “Charakterisierung der Proteine Aftiphilin (AFTPH) und Retinoblastom-Bindeprotein 7 (RBBP7) als neue Interaktionspartner der neutralen Sphingomyelinase 2 (nSMase2)”
- 10/2009 – 09/2011 **Master studies** at the Christian-Albrechts-University Kiel, Germany
Course of studies: Biology
- 07/2009 – 10/2009 **Bachelor thesis** at the Christian-Albrechts-University Kiel, Germany
Institute of Human Biology
Leading scientist: Prof. Dr. Manuela Dittmar
Title: “Vergleichende Analyse der Polymorphismen des *AANAT*-Gens bei Morgen- und Abendmenschen “
- 10/2006 – 10/2009 **Bachelor studies** at the Christian-Albrechts-University Kiel, Germany
Course of studies: Biology

EDUCATION

08/1997 – 06/2006 **Secondary school** Heinrich-Schliemann-Oberschule, Berlin, Germany
– Higher education entrance qualification

POSTER PRESENTATION

Luzius A, Paulsen M, Oberg H, Schreiber S, Rosenstiel P.

Intestinal epithelial stem cell isolation from Atg16l1 Δ IEC mice for transcriptional profiling

35. Arbeitstagung der Norddeutschen Immunologen (*Abstract and Poster*)

Luzius A, Paulsen M, Boeck J, Billmann-Born S, Rosenstiel P.

A role for the autophagy protein Atg16l1 in secretory pathways

Signal Transduction 2013 (*Abstract and Poster*)

Luzius A, Paulsen M, Boeck J, Billmann-Born S, Rosenstiel P.

A role for the autophagy protein Atg16l1 in secretory pathways

Studierendentagung Kiel 2013 (*Abstract and Poster*)

Luzius A, Falk-Paulsen M, Kuiper J, Jentzsch M, Häsler R, Rosenstiel P.

An immunoregulatory function for ATG16L1 in TLR4 signaling

International 5th Annual Cluster Symposium 2015 „Inflammation at Interfaces“

(*Abstract und Poster*)

SCIENTIFIC PAPER

Barann M, Esser D, Klostermeier UC, Lappalainen T, **Luzius A**, Kuiper JW, Ammerpohl O, Vater I, Siebert R, Amstislavskiy V, Sudbrak R, Lehrach H, Schreiber S, Rosenstiel P.

Janus--a comprehensive tool investigating the two faces of transcription.

Bioinformatics. 2013 Jul 1;29(13):1600-6.

Anne Luzius, Maren Falk-Paulsen, Jan W. P. Kuiper, Stamatia Papoutsopoulou, Hang Thi Thu Nguyen, Marlene Jentzsch, Robert Häsler, Nicolas Gisch, Wolfram Klapper, Stefan Schreiber, Nicolas Barnich, Werner Müller, Philip Rosenstiel.

Autophagy is a critical mechanism for temporal control of NF- κ B signaling in myeloid cells.

Manuscript in preparation

10.6 EIDESSTATTLICHE ERKLÄRUNG

Hiermit erkläre ich, Anne Luzius geb. Fischer, an Eides statt, dass ich die vorliegende Arbeit unter der wissenschaftlichen Leitung von Prof. Dr. Philip Rosenstiel selbständig und ohne fremde Hilfe verfasst habe. Die Abhandlung stellt nach Form und Inhalt meine eigene Arbeit dar und ich habe außer der Beratung meiner Betreuer, Prof. Dr. Philip Rosenstiel und Dr. Maren Falk-Paulsen, keine weitere Hilfe in Anspruch genommen wurde.

Weiterhin habe ich keine anderen als die von mir angegebenen Quellen und Hilfsmittel benutzt und die den verwendeten Werken wörtlich und inhaltlich entnommenen Stellen als solche kenntlich gemacht. Die Arbeit wurde unter der Einhaltung der Regeln guter wissenschaftlicher Praxis der Deutschen Forschungsgemeinschaft erstellt. Auszüge der Dissertation wurden bereits bei Posterbeiträgen veröffentlicht.

Ich versichere, dass ich weder an der Christian-Albrechts-Universität zu Kiel noch anderweitig versucht habe, eine Dissertation einzureichen oder mich einer Promotionsprüfung zu unterziehen.

Kiel, den _____

Anne Luzius